

Alma Mater Studiorum – Università di Bologna

DOTTORATO DI RICERCA IN

Chimica

Ciclo XXX

Settore Concorsuale: 03/A1- CHIMICA ANALITICA

Settore Scientifico Disciplinare: CHIM/01-CHIMICA ANALITICA

**Investigation of the Thermochemiluminescent (TCL)
phenomenon as innovative detection technique for
(bio)analytical applications: from the synthesis of new TCL
candidates to the realization of TCL-based probes for
immunoassays**

Presentata da: Andronico Luca Alfio

Coordinatore Dottorato

Roda Aldo

Supervisore:

Roda Aldo

Co-supervisore:

Quintavalla Arianna

Esame finale anno 2018

Abstract:

Investigation of the Thermochemiluminescent (TCL) phenomenon as an innovative detection technique for (bio)analytical applications: from the synthesis of new TCL candidates to the realization of TCL-based probes for immunoassays

In the present PhD thesis, thermochemiluminescence (TCL) phenomenon as a new promising tool for development of innovative (bio)analytical detection methods has been investigated. The TCL process occurs when an increase in temperature triggers the decomposition of a thermolabile molecule (e.g. 1,2-dioxetane derivatives), generating a fragment in its electronic excited state, which relaxes to the ground state through the emission of a photon. The first part of this work was focused on the synthesis of new TCL candidates (acridin-based 1,2-dioxetanes), aiming the optimization of the TCL properties in terms of lower decomposition temperatures and higher fluorescence quantum yields of the generated excited fragments. Thus, a small library of acridin-based 1,2-dioxetanes were synthesized, introducing various electron withdrawing groups (EWG) on the acridin moiety. Then, more significant structural modifications were investigated, replacing the acridin portion with a different chromophoric unit. Moreover, through a chemometric approach, both the structural and electronic molecular descriptors for each molecule were analysed and used to elaborate a model able to predict the olefin photooxygenation outcome (a key step in the synthesis of 1,2-dioxetane derivative). Moving forward, the focus was shifted to the realization of TCL-based nanosensors for immunoassay applications. In particular, the fabrication of both molecular and nanometric-scale probes was performed, linking the TCL substrate (1,2-dioxetane) directly to universal biomarker or encapsulating it within a polymeric nanoshell.

Concerning the molecular probe, acridin 1,2-dioxetane was functionalized with biotin in order to create a TCL sensor for detection of streptavidin-based targets. However, the final molecule did not show enough stability to be employed in (bio)analytical applications. TCL process was, then, combined with the semiconductive polymer dots (Pdots) technology to realize ultrabright thermo-responsive nanoparticles able to detect biotinylated compounds of interest. In particular, the FRET mechanism occurring between the polymeric matrix of Pdots (CN-PPV, $\phi_F = 60\%$) and TCL substrate (1,2-dioxetane, $\phi_F = 11\%$), has been exploited to both enhance the light generation and shift the emission towards longer wavelengths (550 nm). Furthermore, TCL-Pdots were tested in a non-competitive sandwich-type immunoassay for detection of Immunoglobuline G (IgG), revealing a TCL signal proportional to the concentration of analyte and a limit of detection (LOD) in the nanomolar range. The last part of this work was focused on the realization of an home-made portable device to combine TCL-based detection technique with smartphone technology. All the different items constituting the apparatus have been fabricated exploiting a 3D printing process and acrylonitrile-butadiene-styrene (ABS), as starting material. The device was tailored to the 41-megapixel camera of a Nokia Lumia 1020 exploiting, thus, the performance of the complementary Metal Oxide Semiconductor (CMOS) sensor of the smartphone's camera (used as detector). Preliminary measurements exhibited a good reproducibility and a low limit of detection ($LOD = 2,58 \times 10^{-12} \text{ mol mm}^{-2}$), for the TCL-based smartphone device, suggesting its suitability for development of point-of-need analytical test.

Contents

1	The role of 1,2-dioxetane compounds in the luminescent processes	1
1.1	Introduction	1
1.2	Exergonicity of the 1,2-dioxetane thermal decomposition	3
1.3	Mechanism for the 1,2-dioxetane chemiexcitation	4
1.4	1,2-dioxetane and analogues as the common ingredient in luminescent phenomena	6
1.4.1	1,2-dioxetanes and analogues in Chemiluminescence (CL)	7
	Luminol and derivatives	8
	Lucigenin and Acridinium esters	10
	1,2-dioxetane compounds	11
	Coelenterazine and oxalate esters	11
1.4.2	1,2-dioxetanes in Bioluminescence (BL)	13
	Bioluminescent Bacteria	14
	Fireflies and Cnidaria	16
1.4.3	1,2-dioxetanes in Thermochemiluminescence (TCL)	17
1.4.4	1,2-dioxetanes in Mechanochemiluminescence (MCL)	19
2	Synthesis of 1,2-Dioxetanes as Thermochemiluminescent Labels for Ultrasensitive Bioassays: Rational Prediction of Olefin Photooxygenation Outcome by Using a Chemometric Approach	21
2.1	Introduction	21
2.2	Results and discussion	24
2.2.1	Synthesis	24
2.2.2	Photophysical and TCL properties	27
2.2.3	Chemometric analyses	31
2.3	Conclusion	41
2.4	Experimental Section	42
2.4.1	Representative procedure for the synthesis of alkenes 3	42
2.4.2	Representative procedure for the synthesis of 1,2-dioxetanes 4	42

3	Development of a molecular probe based on TCL phenomenon	43
3.1	Introduction	43
3.2	Results and discussion	44
3.3	Conclusion	48
4	Yellow-emitting thermochemiluminescent Semiconducting Polymer Dots functionalized with Streptavidin for immunoassay applications	49
4.1	Introduction	49
4.2	Results and discussion	54
4.2.1	Preparation of TCL-Pdots nanoprobe	54
4.2.2	TCL-emission and FRET experiments	56
4.2.3	Activation parameters of 1 and TCL-Pdots-SA stability .	58
4.2.4	Development of a TCL-Pdot-SA based immunoassay for IgG detection	60
4.2.5	Conclusion	60
5	Realization of a portable device for (bio)analytical analyses, combining the smartphone technology with TCL-based detection methods	63
5.1	Introduction	63
5.2	Materials and Methods	64
5.2.1	Device fabrication	64
5.2.2	Nokia Lumia 1020 for image capturing and processing .	65
5.3	Results and discussion	66
5.4	Conclusion	69
6	Supporting Information of Chapter 2	71
6.1	General Remarks	71
6.2	Optimization Study	72
6.3	Synthetic Procedures and Characterizations	73
6.3.1	General procedure for the synthesis of ketones 2h-l, 2y .	73
6.3.2	General procedure for the synthesis of compounds 2o-q .	83
6.3.3	General procedure for the synthesis of alkenes 3h-t, 3y-z, 3C-E, 3G-I:	86
6.3.4	General procedure for the synthesis of 1,2-dioxetanes 4h-t, 4H-I:	98
6.4	Thermochemiluminescence (TCL) Measurements	107
6.5	Molecular Descriptors	109
6.6	Multivariate Analyses (PCA and LDA)	112
6.7	Computational Details	114

7	Supporting Information of Chapter 3	115
7.1	General Remarks	115
7.2	Synthetic Procedures and Characterizations	116
8	Supporting Information of Chapter 4	123
8.1	General Remarks	123
8.2	Synthesis of Thermochemiluminescent Semiconductive Polymer dots (TCL-Pdots-SA)	124
8.3	Photophysical properties of CN-PPV polymer and 1,2-dioxetane 1	125
8.4	Synthesis of PS-NH ₂ - 2 derivative and FRET experiments	125
8.5	Influence of temperature upon the emission of CN-PPV polymer	127
8.6	TCL emission experiment and determination of activation param- eters (E _a and lnA)	128
8.7	TCL-based non-competitive sandwich-type immunoassay for de- tection of IgG	129
A	License	131
	Bibliography	137

Chapter1

The role of 1,2-dioxetane compounds in the luminescent processes

1.1 Introduction

The term luminescence was introduced for the first time in 1888 by the physicist and historian Eilhardt Wiedemann to describe all those phenomena in which the light production was not due to an increase in temperature. In this terms, luminescence or *cold light* represents the opposite of incandescence or *hot light*, which consists in the black-body radiation. During the luminescent phenomenon, an electronically excited molecule relaxes to its electronic ground state, releasing the excess of energy as an electromagnetic radiation (*EMR*). The wavelength of such EMR will depend on the energy gap between the electronic levels involved in the transition. The luminescence process can be distinguished in two main categories, according to the different ways of triggering the emission of photons:

Photoluminescence if the molecule is excited through a physical stimulus (*i.e.* an electromagnetic radiation). Typical photoluminescent phenomena are the *Fluorescence* and *Phosphorescence* processes;

Chemical luminescence if the excitation step does not require any interaction between the molecule and the EMR. On the contrary, the excitation energy is provided by a chemical reaction. The main luminescent processes of this category are:

- Bioluminescence (*BL*)
- Chemiluminescence (*CL*)
- Electrochemiluminescence (*ECL*)
- Thermochemiluminescence (*TCL*)
- Meccanochemiluminescence (*MCL*)

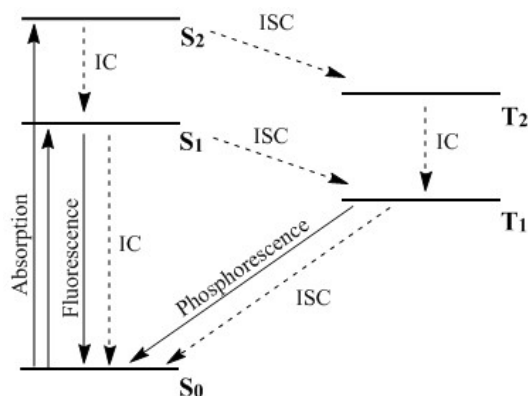
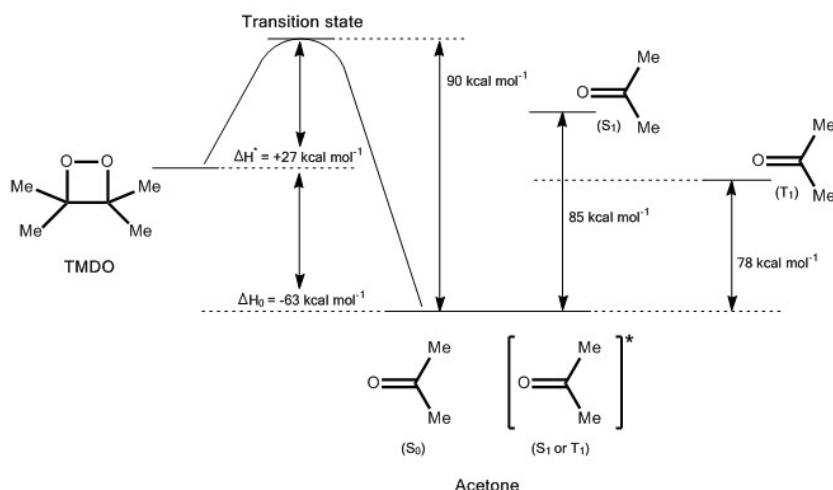


Figure 1.1: The Jablonski energy diagram. The radiative and non radiative process are represented by solid and dashed lines respectively.

Regardless of the nature of the triggering process, an electronically excited molecule will undergo the same fate. In fact, as soon as the molecule absorbs energy from the external environment, the electrons will be promoted from the ground state to an excited one. While the electronic ground-state is always a singlet one (S_0), the final state (just before the molecule relaxes emitting a photon) can be either a singlet ($S_1, S_2, S_2 \dots$) or a triplet (T_1) one, depending on the energy absorbed. Once the molecule is excited, it can relax back to the ground state following two different intramolecular pathways, as depicted by the Jablonski diagram [see Ref. 1] in Figure 1.1:

- **Non-radiative relaxation** if the excess of energy is dissipated as thermal energy towards the environment. Examples of this process are the *internal conversion* (IC) and the *intersystem crossing* (ISC). Both of them bring the excited molecule to its lower state S_1 or T_1 , respectively;
- **Radiative relaxation** if the excited molecule decays to its ground state emitting a photon. Examples of this pathway are the Fluorescence (corresponding to the transition $S_1 \rightarrow S_0$) and the Phosphorescence (corresponding to the transition $T_1 \rightarrow S_0$) processes.

Usually, a fluorophore needs to be excited to its S_1 or T_1 first, then it can relax to the ground state emitting a photon. In fact, common fluorescent or phosphorescent substrates have to absorb energy from an external source such as a Uv-vis lamp, a laser *etc.*, since they do not possess extra energy *per se*. However, 1,2-dioxetanes represent an uncommon class of fluorescent organic molecules, which have gained a great interest among the scientific community due to their peculiar properties. The endoperoxide unit, characteristic of 1,2-dioxetane derivatives, can undergo a fast triggered decomposition generating two fragments,



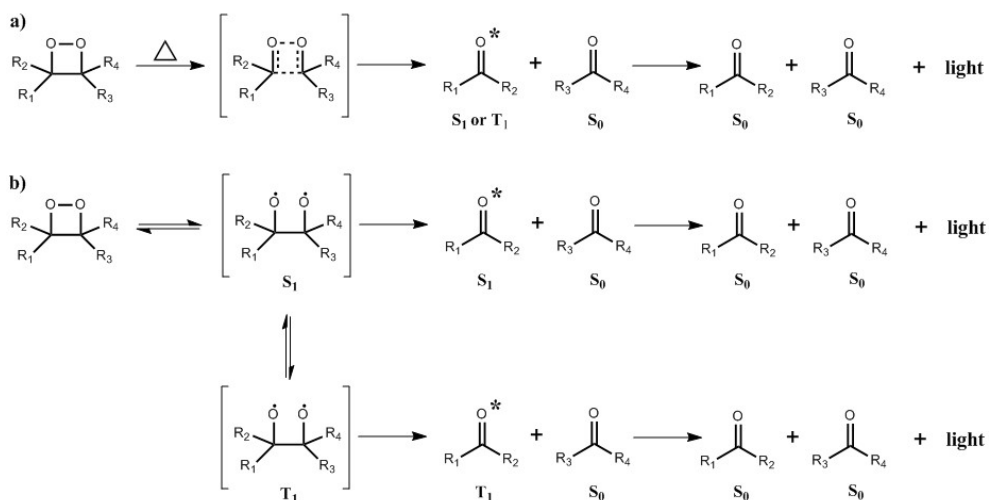
Scheme 1.1: The energy diagram relative to the thermal decomposition of *TMDO*.

one of which in its electronically excited state. The capacity of producing light, without any excitation source, have made this class of organic compounds very appealing for development of new (bio)analytical detection methods.

1.2 Exergonicity of the 1,2-dioxetane thermal decomposition

Using the proper trigger (*e.g.* a chemical reaction, an increase in temperature *etc.*), the 1,2-dioxetane can decompose generating two carbonyl fragments, one of which in its fundamental state (S_0) and the other one in its excited state (S_1 , from which the corresponding triplet state T_1 may be populated by ISC). The latter, then, relaxes to the ground state, releasing a photon with energy equal to the *HOMO-LUMO* gap. The generation of an electronic excited product can be explained considering the thermodynamic of the whole decomposition process. In particular, it could be helpful looking at the well-studied thermal decomposition of the tetramethyl 1,2-dioxetane (*TMDO*) [see Ref. 2], depicted in Scheme 1.1. *TMDO* undergoes a thermal decomposition, generating two molecules of acetone. The energy of the transition state is remarkably high in respect to the energy of final product ($\approx 90 \text{ kcal mol}^{-1}$ higher) and it can be calculated as the sum of the activation enthalpy ΔH^\ddagger ($\approx +27 \text{ kcal mol}^{-1}$) and the reaction enthalpy ΔH ($\approx -63 \text{ kcal mol}^{-1}$). Therefore, the exothermicity of the reaction insures the formation of the electronically excited fragment. Depending on the electronic and structural features, the 1,2-dioxetane derivatives can release energies ranging from 65 to 90 kcal mol^{-1} .

$$-\Delta G \geq \frac{hc}{\lambda_{\text{ex}}} = \frac{28600}{\lambda_{\text{ex}}} \quad (1.1)$$



Scheme 1.2: Mechanism *a*) concerted and *b*) biradical, proposed for the decomposition of 1,2-dioxetane.

Thus, using the formula for the free energy involved in the process (see Eq. 1.1), the thermal decomposition can produce photons in the range 320 - 440 nm.

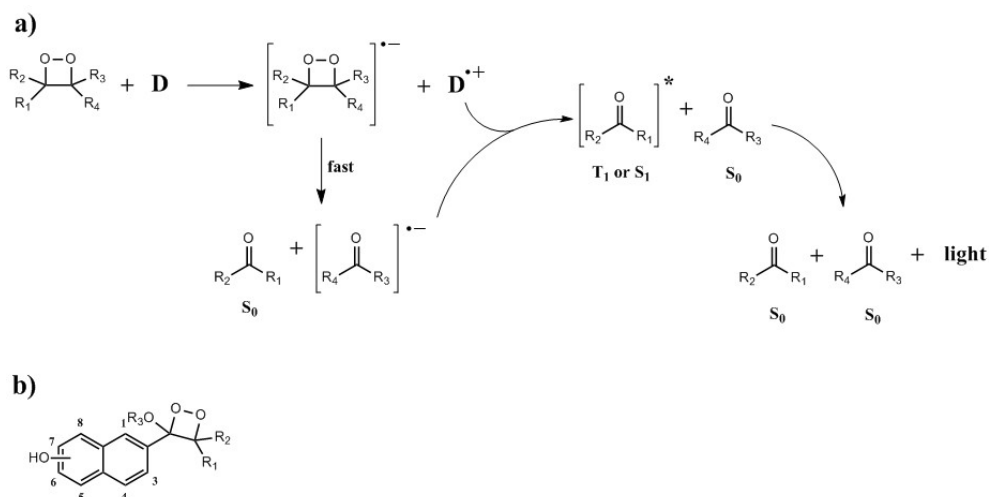
1.3 Mechanism for the 1,2-dioxetane chemiexcitation

Although the 1,2-dioxetanes have been known for a long time, the mechanism of their decomposition is still under debate. In fact, several hypothesis have been proposed to explain the process by which the endoperoxide group generates an electronically excited fragment, but none of them can be taken as a comprehensive theory for the chemiexcitation step. The first mechanism, known as the *synchronous* or concerted process, consists in a symmetry forbidden pericyclic rearrangement, and it was proposed by McCapra [see Ref. 3, 4] and Turro [see Ref. 5–7] at the end of the '60s (see Scheme 1.2 a). It suggests the simultaneous homolytic scission of the bonds between both the oxygen atoms (*O-O*) and the carbon ones (*C-C*). Besides the *synchronous*, concerted pathway, O'Neal [see Ref. 8, 9] and Richardson [see Ref. 10] have described a stepwise mechanism that proceeds *via* a biradical intermediate (see Scheme 1.2 b). They propose the formation of a biradical compound, after the homolytic cleavage of the *O-O* bond, as supported by kinetic [see Ref. 11] and *ab initio* calculation [see Ref. 12] results.

As depicted in Scheme 1.2, both the *synchronous* and the biradical mechanism lead to the formation of two carbonyl fragments, one of which in an electronically excited state that can be either a S_1 or a T_1 state. The excited fragment, then, relaxes, to its ground state emitting a photon. Quantum mechanic calculations have suggested the dependence of the decomposition pathway on the specific

1,2-dioxetane derivative: aliphatic compounds seem to follow the concerted process [see Ref. 13, 14], while substrates bearing aromatic rings or heteroatoms proceed along the biradical mechanism [see Ref. 12, 15–17]. A subsequent computational study on 1,2-dioxetane decomposition has proposed an alternative path for the chemiexcitation step. In particular, De Vico *et al.* [see Ref. 18] have described the thermal decomposition of the parent 1,2-dioxetane as a sequence of four different events: first, stretching of the $O-O'$ and $C-C'$ bonds, followed by the torsion of the dihedral angle $O-C-C'-O'$ and the asymmetric stretching of the $O-C$ and $O'-C'$ bonds. Lastly, the asymmetric pyramidalization of the C/C' atoms leads to the final products. According to this theory, the parent dioxetane would decompose through an *asynchronous* but somehow concerted mechanism, because, after the formation of the biradical intermediate, there is no energy barrier left for further fragmentation. Re-elaborating some previous theoretical studies about the isoelectronic 1,4-tetramethylene biradical [see Ref. 19], De Vico has proposed the existence of the so-called "entropic trapping" effect even in the decomposition mechanism of the 1,2-dioxetane. Basically, the potential energy surface (PES) for the ground-state S_0 of the parent dioxetane has been calculated, using a multistate multiconfigurational second-order perturbation level of theory and found a minimal energy path (MEP) that starts from the S_0 transition state and proceeds, almost flat, along the rotation of the dihedral angle $O-C-C'-O'$. During the time spent in the MEP, the biradical intermediate can explore different torsional configurations that are almost equivalent in energy. However, only specific dihedral angles allow the trajectories to escape from the MEP back to the ground-state PES, thus, the longer the intermediate remains in the entropic trap (*i.e.* the MEP) the longer it will take to dissociate into the products [see Ref. 20]. Furthermore, it was found that both the S_1 and T_1 become degenerate when the dioxetane is in the vicinity of the transition state ($O-O'$ bond cleavage) and they remain so along all the entropic trap region. This evidence seems to explain the effect of substituents upon the chemiexcitation efficiency for the dioxetane decomposition: increasing the number of substituents it will increase the degrees of freedom and, therefore, the time passed within the entropic trap, where state crossing is possible.

The influence of electron-donating substituents upon the chemiluminescence yield was highlighted by Schaap and Gagnon [see Ref. 21] who synthesized a phenol substituted dioxetane. Indeed, after removing the phenolic proton, they measured a remarkable increase in the decomposition rate along with the predominant formation of the singlet excited state S_1 . From that moment on, several chemically-triggered 1,2-dioxetanes have been synthesized, changing the nature of the protected functional group, thus the deprotecting reagent used for the



Scheme 1.3: a) CIEEL mechanism for the thermal decomposition of 1,2-dioxetane derivatives and b) Numbering of odd and even positions for a generic naphthalen-based 1,2-dioxetane.

chemiluminescence reaction. Furthermore, a new decomposition mechanism was proposed to explain this very efficient chemiexcitation: the *chemically initiated electron exchange luminescence* (CIEEL) [see Ref. 22–28]. According to the CIEEL mechanism (Scheme 1.3 a), the first step consists in a mono-electronic transfer from a donor compound (D) to the dioxetane ring, which decomposes generating a radical anion intermediate. The latter, then, reacts with the radical cation of the donor compound ($D^{\bullet+}$) within a solvent cage and the charge recombination process leads to the final excited product.

Another interesting result about triggerable 1,2-dioxetanes has been obtained by Edwards and Bronstein [see Ref. 29, 30], who synthesized several naphthalen-based dioxetanes, bearing a silylated hydroxyl group on the aromatic system. Exploiting different triggering reactions (*e.g.* base treatment or catalysis by fluorine), they noticed a relationship between the position of the functional group on the aromatic system, and the chemiluminescence yield. In particular, it was demonstrated that substituents in "odd" positions (*i.e.* 4, 5 or 7, as showed in Scheme 1.3 b) lead to a much more efficient chemiexcitation than dioxetane with a "even" pattern (*i.e.* substituents in 3, 6 or 8 position, in Scheme 1.3 b).

1.4 1,2-dioxetane and analogues as the common ingredient in luminescent phenomena

Since the '70s, the 1,2-dioxetane system has been attracting a great interest among the scientific community, due to the astounding ability to emit photons after its decomposition. An interesting aspect is the presence of this cyclic en-

doperoxide group in a variety of luminescent processes (*e.g.* chemiluminescence, bioluminescence *etc.* phenomena) where it can participate either as a reagent or an intermediate. In the following sections, a brief overview of the multiple analytical systems based on the 1,2-dioxetane unit will be provided.

1.4.1 1,2-dioxetanes and analogues in Chemiluminescence (CL)

The chemiluminescent phenomenon consists in the production of a *EMR* triggered by a chemical reaction. The light signal generates after mixing two or more reagents in the presence of a catalyst (usually an inorganic base or an enzyme). The exergonic reaction produce an electronically excited product which can relax to the ground-state through a radiative or non-radiative process. Two different types of chemiluminescent reactions can be distinguished: the *type I* (or direct) CL process and the *type II* (or indirect) CL reaction. The latter differs from the *type I* process since the product is not intrinsically fluorescent, thus, it has to transfer the energy to a second molecule (energy acceptor, *EA*) which will relax through the emission of a photon. A useful parameter to estimate the efficiency of a chemiluminescent process is the CL quantum yield (Φ_{CL}), defined as the number of photons generated divided by the number of molecules (*i.e.* substrates) reacted [see Ref. 31] (see Eq. 1.2).

$$\Phi_{CL} = \frac{\text{number of photons emitted}}{\text{number of molecules reacted}} \quad (1.2)$$

The CL quantum yield can also be expressed as the product of three distinct quantities (see Eq. 1.3): the quantum yield for the formation of the intermediate Φ_{Int} that depends on the efficiency of the chemical reaction; the quantum yield for the production of electronically excited products Φ_{SE} , correlated to the energy transfer efficiency, and the emission quantum yield Φ_{Em} .

$$\Phi_{CL} = \Phi_{Int} \cdot \Phi_{SE} \cdot \Phi_{Em} \quad (1.3)$$

The 1,2-dioxetane has assumed a pivotal role in the field of chemiluminescence-based analytical methods, since it represents the smallest CL active system and the most versatile one (*e.g.* it can be functionalized quite easily, insuring the tunability of CL properties). In particular, the dioxetane-based CL substrates can be gathered in five different classes:

Luminol and derivatives

The CL properties of 3-aminophthalhydrazide (luminol) have been described for the first time in 1928 by the German chemist H. O. Albrecht, when he noticed an enhancement of the luminescence of luminol dissolved in an alkaline solution of hydrogen peroxide in presence of blood [see Ref. 32]. Looking at the molecular structure of luminol (see Figure 1.2 for the structure of luminol and its main derivatives), it is noticeable the presence of the hydrazide group which is responsible for the chemiluminescent behaviour.

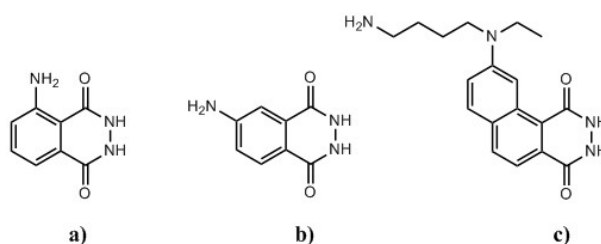
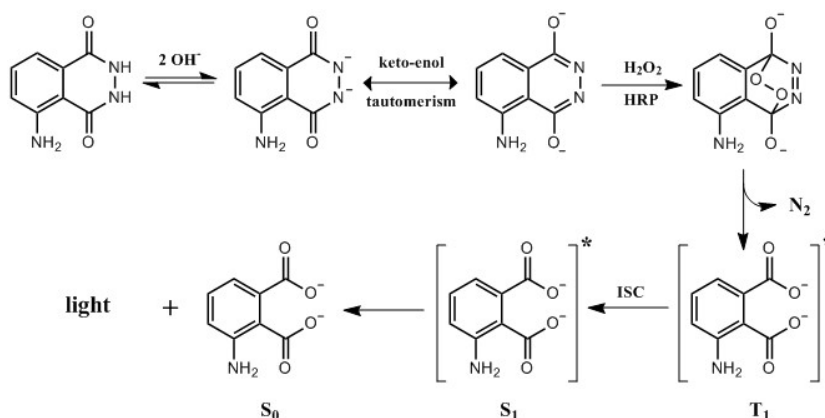


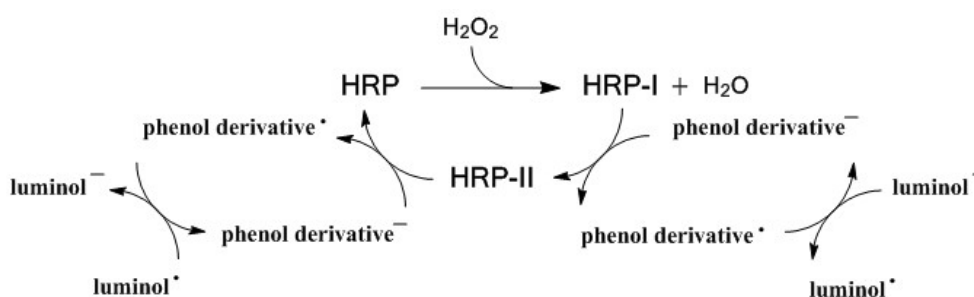
Figure 1.2: Molecular structure of *a*) luminol, and its derivatives *b*) isoluminol and *c*) ABEN.

The typical reaction mechanism of these substrates occurs in a basic environment and involves a Peroxidase enzyme, that operates as catalyst, and an oxidizing agent. The Horseradish peroxidase (HRP) and hydrogen peroxide (H_2O_2) are the most common reagents used in the luminol-based CL systems. As depicted in Scheme 1.4, the CL reaction starts with the deprotonation of the hydrazide group, generating a dianion species. The keto-enol tautomerism promotes the formation of the thermodynamically more stable intermediate which undergoes the oxidation by H_2O_2 and HRP, generating the key-compound dioxetane. The latter decomposes giving the final electronically excited product. Computational studies have showed the dependence of the oxidation step on the reaction environment [see Ref. 33]. In particular, aprotic solvents (DMSO or DMF) require strong oxidizing agents [see Ref. 34] while, in protic solvents (H_2O and alcohols), the CL reaction occurs even using mild oxidants. However, in both cases the use of an enzymatic and/or inorganic catalyst is required [see Ref. 35].

The main disadvantage of the luminol-based methods is the low fluorescence quantum yield (Φ_f) of the phthalhydrazide moiety, that is only 5% in DMSO [see Ref. 36] and 1-1.5 % in H_2O [see Ref. 34, 35]. For many years, several research groups have been introducing structural modifications on the luminol substrate, aiming to enhance the chemiluminescent signal. A noticeable relationship between the position of substituents and Φ_f has been revealed, showing a retention of chemiluminescence property, if the modifications affect the aromatic ring, or a complete loss of light production, when structural changes interest the cyclic



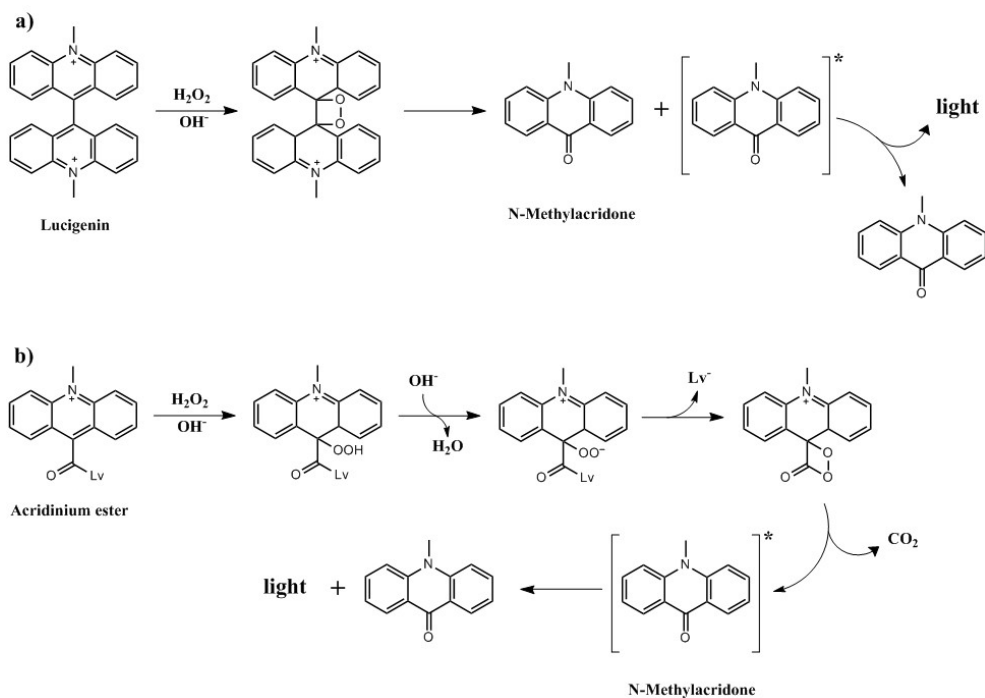
Scheme 1.4: Mechanism for the CL reaction of luminol.



Scheme 1.5: Mechanism for the oxidation of luminol, using phenol derivatives.

phtalhydrazide portion [see Ref. 35–37]. In addition to structural modifications, the use of *chemical enhancers* can improve further the CL response modulating the catalytic power of the used enzyme. For instance, Diaz *et al.* [see Ref. 38] have reported the use of phenol derivatives in HRP/H₂O₂/luminol systems, to enhance the HRP catalytic efficiency through a different reaction mechanism (see Scheme 1.5).

The first step consists in the oxidation of HRP by H₂O₂ to give the intermediate HRP-I; the latter, then, reacts with the dianion of luminol generating a partially reduced complex HRP-II and the luminol radical. At this point, the original oxidation state of HRP is restored after reacting with a second molecule of luminol. However, not all the phenol compounds are able to act as *chemical enhancer*, but only those which produce radicals with a similar or greater reduction potential than luminol at pH 8.5 (0.8 V) can accelerate the CL reaction, thus increase the light signal. Nowadays, luminol (and some of its derivatives) is one of the most widely used compound in CL-based methods, thanks to its availability and low cost. It has found applications in multiple fields of (bio)analytical chemistry. For instance, it is used in food and environmental monitoring, in clinical analysis and diagnostics, in forensic investigations *etcetera* [see Ref. 39, 40].

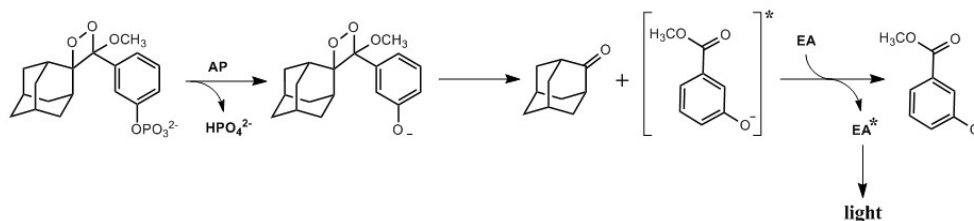


Scheme 1.6: Mechanism for the CL reaction of *a)* Lucigenin and *b)* acridinium ester.

Lucigenin and Acridinium esters

The CL properties of acridinium salt and its derivatives have been known since 1935, when Gleu and Petsch observed a blue (or green) light coming out from the oxidation of bis(*N*-methylacridinium) nitrate (Lucigenin) [see Ref. 41]. The Lucigenin dication undergoes an oxidation reaction by hydrogen peroxide in basic environment, generating the key-intermediate dioxetane, which decomposes instantaneously into the electronically excited 10-methyl-9(10*H*)-acridone (see Scheme 1.6 a). Around Thirty years later, a new class of acridin-based CL substrates were proposed, replacing one of the acrin moieties of Lucigenin with an ester unit [see Ref. 4, 42, 43]. The CL reaction mechanism for a generic acridinium ester is depicted in Scheme 1.6 b: firstly, the oxidation of the acridinium unit occurs, followed by a deprotonation and intramolecular cyclization of the hydroperoxide. The main difference between the decomposition mechanism of Lucigenin and an acridinium ester consists in the formation of a new high-energetic intermediate. In fact, rather than a 1,2-dioxetane, the intramolecular cyclization leads to a dioxetanone compound, which releases carbon dioxide (CO_2) and the final excited product.

Looking at the molecular structure of acridinium salt, two distinct portions can be identified: the acridin moiety and the leaving group ($-Lv$). Both of them play a crucial role in the modulation of CL properties. Indeed, introducing electron-donating or -withdrawing groups onto the aromatic system, as well as



Scheme 1.7: Mechanism for the CL decomposition of Alkaline Phosphatase substrate.

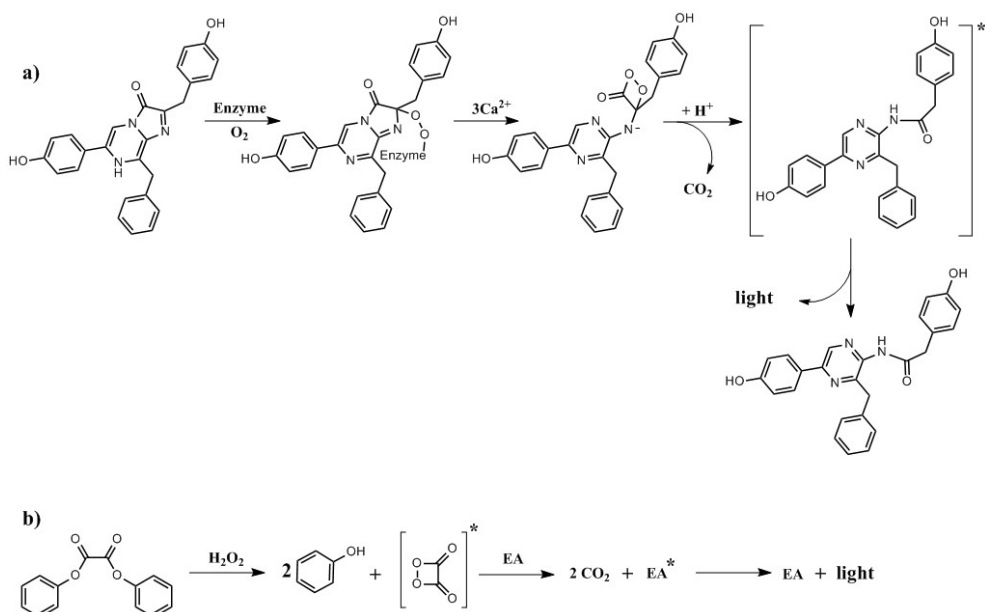
changing the $-L_v$ nature, it is possible to modulate both the chemical stability and the CL efficiency of these substrates [see Ref. 44]. Due to the strong interaction with single-strand DNAs, acridinium derivatives are mainly used in the development of CL-based probes for the analysis of pairing speed in hybridization processes, or to determine the thermodynamic affinity between oligonucleotidic fragments and their target molecules [see Ref. 45–47].

1,2-dioxetane derivatives

The above-cited acridinium esters have to be oxidized *in situ*, since the dioxetanone intermediate is quite unstable. However, introducing a proper stabilizing moiety and a protected functional group, it is possible to create a triggerable 1,2-dioxetane derivative that results stable enough to be handled and even stored. Therefore, the CL decomposition can be obtained using a chemical stimulus which removes the protecting group and triggers the dioxetane fragmentation. Among the myriad of chemically-triggered dioxetanes [see Ref. 48–51], the phosphoryl derivative represents the most common one, and it is used as substrate for the Alkaline Phosphatase (AP) enzyme. The CL mechanism (Scheme 1.7) expects a dephosphorylation of the substrate by the AP enzyme and the subsequent formation of a negative charge upon the aromatic ring. The latter causes a destabilization of the dioxetane which decomposes generating an electronically-excited methyl benzoate fragment. Due to the low Φ_f of the benzoate moiety, the presence of a fluorescent energy acceptor (EA) is required, in order to develop dioxetane-based analytical methods with high sensitivity.

Coelenterazine and oxalate esters

Coelenterazine is a light-emitting molecule (for the molecular structure see Scheme 1.8 a) present in many coelenterate and represents the typical substrate for luciferases, such as *Renilla reniformis luciferase* (Rluc), *Gaussia luciferase* (Gluc), and some photoproteins like *Aequorin*. Coelenterazine was simultaneously isolated by two groups during the characterization of the luminescent organisms sea pansy (*Renilla reniformis*) and the coelenterate *Aequorea victoria*, respectively



Scheme 1.8: a) Molecular structure of Coelenterazine and b) Mechanism for the CL decomposition of diphenyl oxalate.

[see Ref. 52, 53]. The BL reaction follows the mechanism typical of acridinium esters, but the intramolecular cyclization of hydroperoxide requires the presence of both the enzyme and calcium cations [see Ref. 54–56]. Coelenterazine and its derivatives have found several applications in the (bio)analytical field, especially to detect the concentration of superoxide anions and metallic species (*e.g.* Calcium and Barium) [see Ref. 57, 58].

A well-known class of dioxetane-based CL molecules are represented by the oxalate esters. These compounds were proposed, for the first time, in 1967 by Rauhut *et al.* [see Ref. 59], when he reported the chemiluminescent decomposition of diphenyl oxalate, induced by hydrogen peroxide. Differently from the compounds described so far, the oxidation of oxalate leads to a dioxetanedione intermediate (Scheme 1.8 b) which decomposes instantaneously into two molecules of CO₂ [see Ref. 60–62].

The three most famous oxalate derivatives are bis(2,4,6-trichlorophenyl)oxalate (TCPO), Bis(2,4,5-trichlorophenyl-6-carbopentoxyphenyl)oxalate (CPPO) and bis(2,4-dinitrophenyl) oxalate (DNPO), which are all used in glow sticks fabrications. Every oxalate-based system shows the presence of an EA, since the dioxetanedione intermediate is not able to emit light *per se*. Moreover, the low stability of oxalate esters has always represented the main disadvantage for this class of CL substrates, and it has prompted researchers to investigate the effect of different ester groups upon the oxalate stability [see Ref. 63–65]. Despite the above-cited disadvantages, oxalate esters have found several applications as CL

markers in immunoassay for hydrogen peroxide detection [see Ref. 66, 67].

1.4.2 1,2-dioxetanes in Bioluminescence (BL)

Bioluminescence is one of the most spectacular phenomena that occur in nature and it has been observed and admired since the ancient times. It consists in a particular form of chemiluminescence that occurs in living organisms, where an enzyme (luciferase) catalyzes the oxidation of a luminescent substrate (luciferin), causing the emission of a bright light (mostly in the blue region of visible spectrum).

Testimonies of BL manifestations have been reported by many academics of the classical era such as Aristotle and Plynny the Elder, who described an enchanting glow coming out from damp wood. Even the English naturalist Charles Darwin reports an encounter with the BL phenomenon in his *Journal and remarks* [see Ref. 68]:

While sailing in these latitudes on one very dark night, the sea presented a wonderful and most beautiful spectacle. There was a fresh breeze, and every part of the surface, which during the day is seen as foam, now glowed with a pale light. The vessel drove before her bows two billows of liquid phosphorus, and in her wake she was followed by a milky train. As far as the eye reached, the crest of every wave was bright, and the sky above the horizon, from the reflected glare of these livid flames, was not so utterly obscure, as over the rest of the heavens.

In 1920, a monograph about the theme of bioluminescence (*The Nature of Animal Light*) was published by the American zoologist E. Newton Harvey, who summarized all the previous work conducted until then [see Ref. 69]. He was also among the first to propose the causes for the evolution of BL systems, identifying in respiratory chain proteins that hold fluorescent groups, the origin of BL phenomenon [see Ref. 70]. Although his theory was disproven, Harvey prompted many scientists to start working on the subject, and the two main hypotheses about BL historical evolution, still prevailing today, were presented in 1993 and 1998 by Seliger and Rees *et al.*, respectively [see Ref. 71, 72]. Both theories concern the origin of marine bioluminescence but differ from each other in identifying the reason that led natural evolution to develop BL systems. Seliger suggests luciferases to be one of the oxygenase enzymes originally involved in the cleavage of pigment molecules. Therefore, when the early ancestors started moving down to deeper and darker waters, an increase in eye sensitivity and enhancement of visual signals occurred [see Ref. 73], provoking mutations in the oxygenase enzymes (luciferases) and the appearance of external luminescence in tissues.

On the other hand, Rees finds in the shift of luciferins functionality the origin of BL phenomenon. Indeed, he supports that luciferin was initially protecting marine organisms from deleterious reactive oxygen species (ROS), quenching the radical compounds generated by environmental stress condition. However, when early species moved down to the ocean depths, exposure to ROS decreased significantly and luciferin underwent a functional change from antioxidant agent to bioluminescent one.

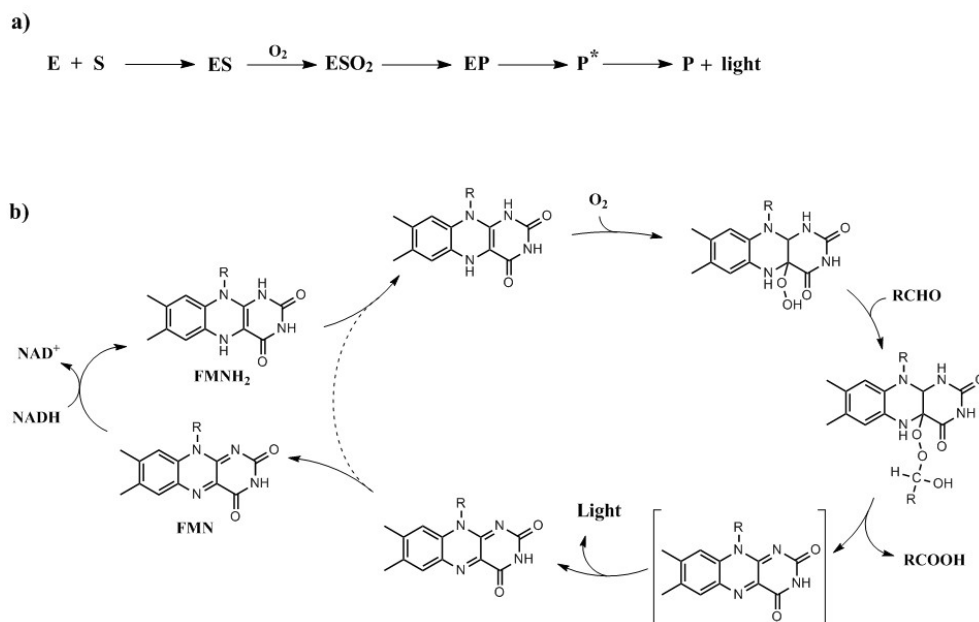
Bioluminescence phenomena are widely diffused among both the animal and vegetable kingdoms. In fact, it can be observed in several marine species, including fish, jellyfish, algae, crustaceans and cephalopod molluscs, or in terrestrial organisms, such as fireflies, glow-worms and fungi [see Ref. 74, 75]. Furthermore, BL process can assume a multitude of different functions, each one peculiar to the specific *taxa* [see Ref. 74]. For instance, it can appear during the courting phase to attract mates or repel contenders; it can participate in the hunting process luring, stunning or confusing the prey or it can play a defensive function like counterillumination camouflage, misdirection *etc.*

Regardless of the specific function or purpose of the BL event, the mechanism [see Ref. 76] always involves an oxidant enzyme (generally named Luciferase) and a substrate (known as Luciferin), which interact with each other forming an enzyme-substrate complex (ES). The latter forms a peroxy-luciferin-enzyme system (ESO₂) that undergoes an oxidation reaction, giving the complex product-enzyme (EP). The final step consists in the EP breakdown and the generation of the electronically excited product (see Scheme 1.9 a).

The chemical nature of both luciferin and luciferase can be profoundly different depending on the BL system analyzed, and this variations usually result in a different colour of the light emission. For instance, the substitution of a single amino acid along the peptide chain can strongly affect the wavelength of EMR [see Ref. 77, 78]. Furthermore, the BL spectrum not always overlaps the fluorescence one, since the species responsible for the light emission could be different from the final product (*i.e.* it could be the ESO₂ or the EP complex). The three main bioluminescent systems are described below, and they can be found in a multitude of BL-based methodologies [see Ref. 79–82]:

Bioluminescent Bacteria

Among the bioluminescent organisms, BL bacteria are the most diffused ones, especially in the marine environment such as on the surface of decomposing fish, in deep-water sediments and in the gut of aquatic animals. They can be found in coastal waters near the outflow of river and in all those places known as milky seas (such as Gulf of Trieste, coast of Africa and so on) [see Ref. 83].



Scheme 1.9: a) General mechanism for the bioluminescent process and b) Mechanism for the BL reaction occurring in bacteria.

Moreover, these BL creatures may live as independent organisms or in symbiosis with others, assimilating nutrients from hosts and providing bioluminescence, for camouflage, prey attraction *etc.*, in exchange. Although bioluminescent bacteria have been known and studied for centuries (folklores of ancient civilizations from Scandinavia, China and India are disseminated of encounters with "magical" luminescent small entities), the purpose for the light production is still under debate. A plausible explanation for the occurring of BL phenomenon can be found in the biochemistry of these organisms. Indeed, studies have suggested that BL process may be activated in conditions of low oxygen concentration, as an alternative pathway for electron flow [see Ref. 84]. Another hypothesis applies to enteric bacteria, assuming the dispersal of their colonies as the reason for bioluminescence [see Ref. 85]. In fact, once the bacteria have been digested and excreted in fecal pellets, they can exploit the luminescence to lure other organisms eating them, thus, they will insure a wider species distribution. An interesting aspect of bacterial bioluminescence is the role played in *quorum sensing*, namely, the particular communication process between cells, which controls and regulates gene expression in response to cell density [see Ref. 86]. When the bacterial population reaches high density levels, several extracellular signalling molecules (autoinducers) are released, which induce the over-expression of luciferase enzymes, thus, the increase in light production.

A luciferase characteristic of BL bacterial species consists in a two-units heterodimer enzyme. The subunit α (responsible for bioluminescence) is a 40

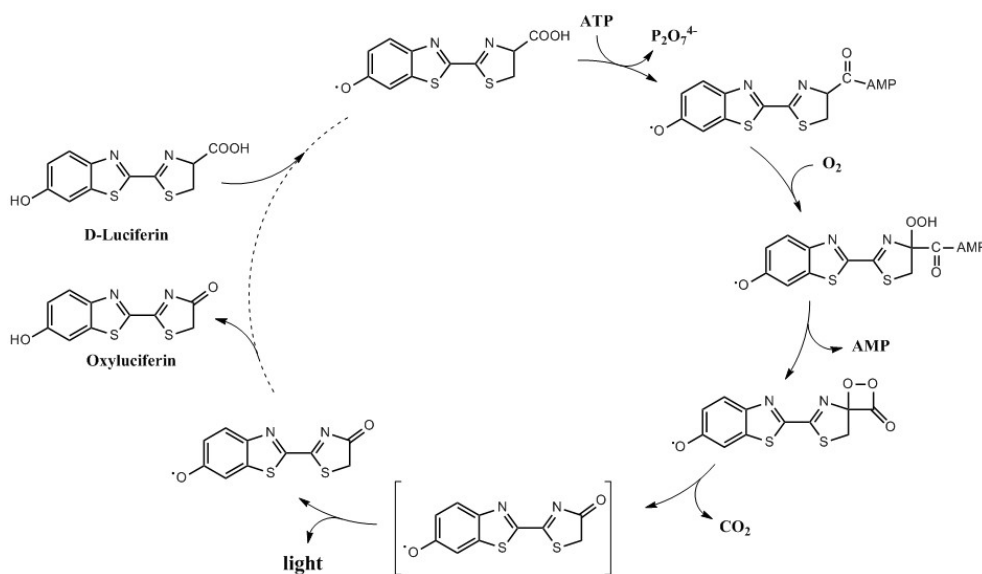
kDa peptide chain, while the subunit β is a 35 kDa protein fragment. A typical substrate (luciferin) is the flavin mononucleotide (FMN), which is produced from riboflavin (vitamin B₂) by the enzyme riboflavin kinase. Scheme 1.9 b shows the reaction mechanism occurring in bioluminescent bacteria: firstly, FMN is converted to its reduced form FMNH₂ by the coenzyme Nicotinamide Adenine Dinucleotide (NAD), followed by the formation of a luciferase-FMNH₂ complex. The latter reacts with molecular oxygen giving a quite stable peroxyde which forms an oxyhemiacetal intermediate, in presence of fatty aldehydes. Finally, the hydrolysis of hemiacetal leads to the hydroxyflavin-enzyme complex, responsible for the light emission[see Ref. 87, 88].

Bioluminescent bacteria have been mainly exploited in the field of biotechnology and environmental microbiology. In particular, several BL bacteria-based sensors have been developed for detection of contaminants in food or pollutants released into the environment [see Ref. 89–92].

Fireflies and Cnidaria

The term *Cnidaria* identifies a *phylum* containing over 10.000 species of aquatic animals which can be found in almost every marine environment (fresh-water and open ocean). *Cnidaria* members (sea anemones, true jellies, sea pens *etc.*) along with the *Ctenophora phylum* (comb jellies) are grouped under the *Coelenterate* class, since they all share the same physical characteristics. In fact, the term originates from the greek words *koilos* and *enteron* which mean "hollow" and "intestine" respectively, and it refers to the peculiar hollow body cavity that is typical of the two *phyla*. The bioluminescence for these organisms follows the above-described coelenterazine-based mechanism (see section 1.4.1), involving the formation of a 1,2-dioxetanone species, as key intermediate, and the following release of CO₂ and generation of an electronically excited product.

Fireflies are a family of insect in the beetle order *Coleoptera*, which are known for glowing during twilight to attract mates or to lure preies. These "lightning bugs" present specialized organs in the lower abdomen, where photons with wavelengths ranging from 545 to 595 nm can be produced through a peculiar bioluminescence reaction [see Ref. 93–95]. Luciferase from *Photinus pyralis* species (a fireflies variety hailing from the North America areas) is one of the most well-studied BL enzyme and it was the first employed in (bio)analytical applications. The mechanism for the bioluminescent reaction is depicted in Scheme 1.10, showing the chemical transformations occuring upon the benzothiazolyl thiazole derivative (D-Luciferin) [see Ref. 96, 97]. The first step consists in a condensation of D-Luciferin with adenosine triphosphate (ATP), catalyzed by luciferase and magnesium dication (Mg²⁺). In a second step, adenylate intermediate undergoes



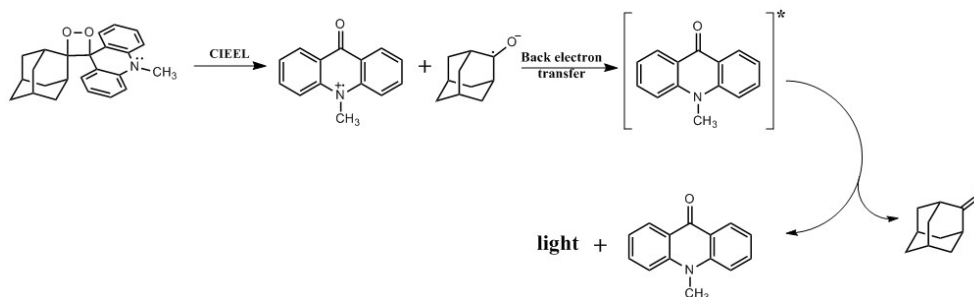
Scheme 1.10: Mechanism for the bioluminescent reaction occurring in *Photinus pyralis*.

an oxidation by molecular oxygen, generating a hydroperoxy compound which leads to the dioxetanone formation, after intramolecular cyclization. Lastly, the unstable endoperoxide follows the same fate of dioxetanes, decomposing in an electronically excited product.

Bioluminescence from fireflies have been widely exploited in a multitude of analytical methodologies, due to the remarkable sensibility (high BL efficiency and low matrix signal) and simplicity of the chemistry involved in this system. Several devices based on the *Bioluminescence Resonance Energy Transfer* (BRET) phenomenon have been used for monitoring the protein-protein interaction as well as to detect the presence of heavy metals or xenobiotics in cell cultures. Moreover, BL-based sensors have been utilized for *in vivo* imaging [see Ref. 98], in tracking tumoral cells or to determine the gene expression in living animals [see Ref. 99]. Other applications of fireflies-type BL systems can be found in drug-discovery, especially in the High Throughput Screening (HTS) processes [see Ref. 100], and environmental monitoring fields [see Ref. 101].

1.4.3 1,2-dioxetanes in Thermochemiluminescence (TCL)

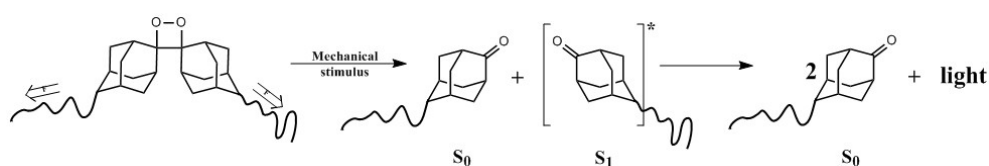
Among the luminescence processes that involve decomposition of a 1,2-dioxetane (or 1,2-dioxetanone) intermediate, Thermochemiluminescence (TCL) phenomenon represents the less explored one. In fact, first attempts to apply TCL as a detection method in (bio)analytical systems have been made in late '80s, when it was proposed for development of an immunoassay based on the adamantylidene adamantane 1,2-dioxetane [see Ref. 102]. Raising the temperature above 200-250 °C, the dioxetane decomposes into two identical fragments (2-adamantanone),



Scheme 1.12: CIEEL mechanism for the decomposition of acridin-based 1,2-dioxetanes.

O-O' breakdown (see Scheme 1.12). The first step consists in a electron transfer from nitrogen to the endoperoxide system and simultaneous ring fragmentation. Then, a back electron transfer occurs, leading to the formation of the electronically excited 9(10)-Acridanone. A small library of acridin-based dioxetanes have been synthesized [see Ref. 110, 111], and the influence of substituents (different electron withdrawing and donating groups on the aromatic system) upon TCL properties have been investigated. Furthermore, in order to obtain sensibilities comparable to those of classical CL methods, TCL-based nanometric probes have been developed [see Ref. 107], doping silica nanoparticles with a high number of both dioxetane derivatives and energy acceptors. The TCL probes have showed high Φ_F along with a quite low threshold for the decomposition temperature (emission start occurring when the temperature is raised above 100-120 °C) and good water solubility, all properties that make this system suitable for immunoassay applications.

1.4.4 1,2-dioxetanes in Mechanochemiluminescence (MCL)



Scheme 1.13: MCL process for the system dioxetane-poly methyl acrilate, occurring after a mechanical stress .

Recently, the luminescence properties of 1,2-dioxetanes have been combined with polymers technology, developing a rubber-like poly methyl acrilate system that is able to produce a bright light emission, after applying a mechanical stress upon the polymer chains [see Ref. 115]. Scheme 1.13 shows the mechanism involved in the MCL process. Polymer chains functionalized with adamantylidene

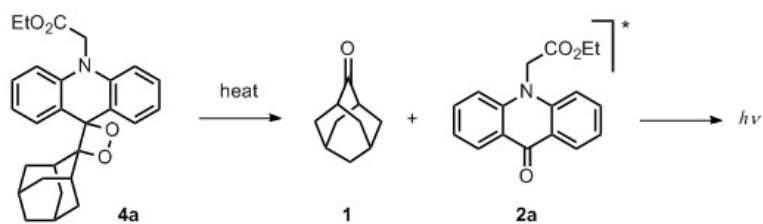
adamantane 1,2-dioxetanes demonstrated to be potentially useful in mapping the stress distribution in polymers, insuring high temporal resolution for real-time monitoring of chain-scission events.

Chapter 2

Synthesis of 1,2-Dioxetanes as Thermochemiluminescent Labels for Ultrasensitive Bioassays: Rational Prediction of Olefin Photooxygenation Outcome by Using a Chemometric Approach

2.1 Introduction

From the 1970s to date, the 1,2-dioxetane system [see Ref. 116–121] has continued to attract great interest due to its key role in chemiluminescence (CL) and bioluminescence (BL) reactions [see Ref. 122–125]. Its peculiar properties have stimulated and enabled the development of a wide array of applications. For example, recently, 1,2-dioxetanes have been exploited as luminescent mechanophores, namely, responsive units able to transduce mechanical stress into an optical response [see Ref. 126, 127]. Primarily, dioxetane analogues have proved to be potent tools in clinical diagnostics as chemiluminescent substrates for enzymes, such as alkaline phosphatase, used as labels in immunoassays and gene assays [see Ref. 128–138]. Indeed, CL, BL, and electrogenerated chemiluminescence (ECL) detection techniques are particularly well suited in applications in which high sensitivity is required, offering high detectability, even in low volumes, a wide linear range of responses, and a high signal to noise ratio. Nevertheless, CL, BL, and ECL detection requires the addition of reagents to induce light emission, thus decreasing assay rapidity and simplicity, which are crucial for on-field biosensor applications. The remarkable advantage of a thermochemiluminescence (TCL) label is that its light emission is simply produced by heating, and nothing else. In fact, the TCL phenomenon originates from heating a suitable thermodynamically relatively unstable molecule, which decomposes to yield a product mainly in the singlet excited state that decays with photon emission (see Scheme 2.1). Nowadays, TCL [see Ref. 139–149] offers challenging and unexplored opportunities for the development of reagentless and ultrasensitive detection methods exploitable, for example, in simple portable biosensors with



Scheme 2.1: Acridan-containing 1,2-dioxetane **4a**, which was employed by us as a TCL label.

TCL molecules as labels, as either single molecules or included in functionalized silica nanoparticles (SiNPs) [see Ref. 108, 109].

Thermochemiluminescent 1,2-dioxetanes, described for the first time in 1963, were proposed for analytical applications in the late 1980s with limited success due to the relatively high temperature of decomposition and very poor light emission efficiency [see Ref. 150–152]. Over the last four years, we have reinvestigated acridan-based 1,2-dioxetanes (for example **4a**; [see Ref. 153–158] Scheme 2.1) as TCL compounds. As an application, we incorporated **4a** into SiNPs with the aim of generating TCL probes for ultrasensitive immunoassays [see Ref. 107–110]. SiNPs doped with our acridan-based 1,2-dioxetane displayed remarkable advantages, compared to TCL labels proposed in the past, such as a lower trigger temperature (below 100 °C) and highly improved detectability, comparable with that obtained with enzyme-based CL detection.

In a preliminary stage, we studied the effect of weak electron-donating groups (EDGs), such as methyl substituents, on the acridan moiety of **4a** (**4b-4g**; see Figure 2.1). For example, we found that, with acridones as the emitting species, tri- and tetramethyl-substituted acridones showed the highest fluorescence quantum yields (Φ_F), in the range of 0.48-0.52. Accordingly, the corresponding 1,2-dioxetanes **4f** and **4g** (Figure 2.1) presented limit of detection (LOD) values more than one order of magnitude lower than that of the unsubstituted derivative **4a**, as determined by TCL imaging experiments. Moreover, we noticed that the impact of the substituent was greater in the 2-position (and/or 7-position). Methyl groups also caused a clear decrease in the activation energy (E_a) of the thermochemiluminescent reaction. Lastly, we observed that the rate of 1,2-dioxetane formation through photooxygenation of the corresponding alkene strongly depended on the substitution pattern of the acridan moiety.

Intrigued by the considerable effects of the acridan substituents on the properties of thermochemiluminescent 1,2-dioxetanes, we planned substantial structural modifications to the fluorophore moiety of the dioxetane with the purpose of 1) improving and modulating the photophysical characteristics and activation

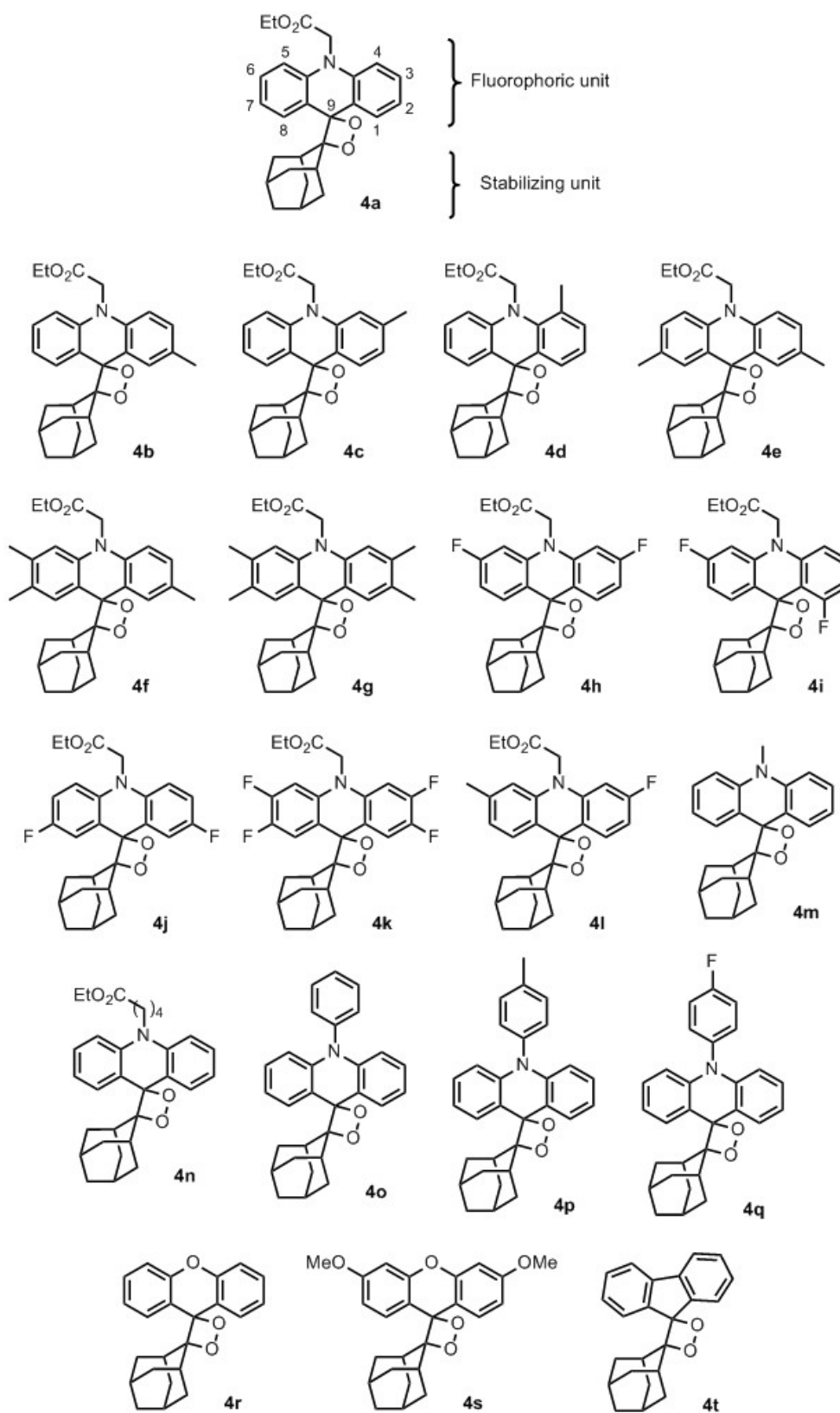
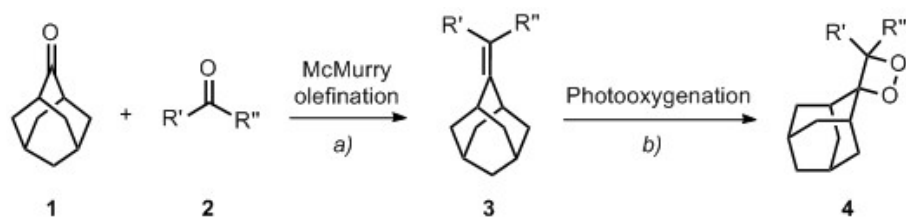


Figure 2.1: Library of 1,2-dioxetanes studied herein.



Scheme 2.2: Two-step synthetic approach to TCL 1,2-dioxetanes **4**.

parameters of the TCL labels, and 2) studying the impact of several structural features on a series of properties of the 1,2-dioxetanes, including the photooxygenation rate of the parent olefin with singlet oxygen (1O_2). The complete list of thermochemiluminescent 1,2-dioxetanes synthesized and investigated is shown in Figure 2.1. All members of this library were fully characterized in terms of TCL properties. The synthetic approach to thermochemiluminescent 1,2-dioxetanes **4** is depicted in Scheme 2.2. It consisted of two steps: a) reductive coupling of two properly selected ketones (**1** and **2**) under McMurry conditions [see Ref. 159–170], and b) photooxygenation [see Ref. 171–184] of the obtained tetrasubstituted alkene **3** to provide the desired 1,2-dioxetane **4**.

In a number of cases examined, however, photooxygenation did not occur. Thus, we decided to perform a chemometric investigation with the aim of correlating selected representative structural and electronic features of the olefin reagent with the success of the photooxygenation reaction.

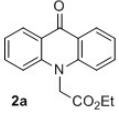
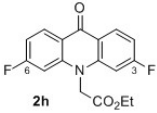
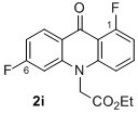
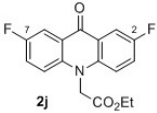
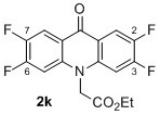
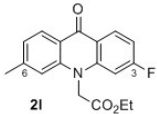
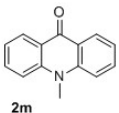
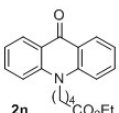
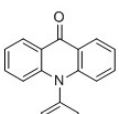
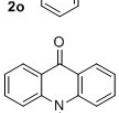
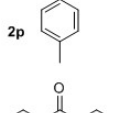
2.2 Results and discussion

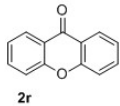
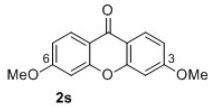
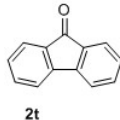
2.2.1 Synthesis

At the outset of this study, we optimized the reaction conditions of the two key steps that led to parent 1,2-dioxetane **4a**, which was selected as a model compound (see Table 6.1 in the Supporting Information. The optimized procedure is detailed in Table 2.1. The most relevant modifications concerning the photooxygenation step were the replacement of polymer-bound Bengal Rose with Methylene Blue as the sensitizer and an increased temperature; these conditions allowed us to achieve better yields in a shorter time.

By using the optimized synthetic protocol, we accomplished a series of modifications on the fluorophoric moiety of **4a** (Table 2.1), preserving unaltered the adamantyl unit that acts as a stabilizing framework [see Ref. 185, 186]. In fact, among substituents employed as stabilizing subunits in 1,2-dioxetane [see Ref. 187, 188], the adamantyl group is widely recognized as a rigid and sterically demanding framework able to significantly stabilize the endoperoxide unit.

Table 2.1: Synthesis of differently substituted 1,2-dioxetane **4a**, **4h-t**.^[a]

Entry	Ketone 2	Olefin 3 (yield [%]) ^[b]	1,2-Dioxetane 4 (time [h], yield [%]) ^[b]
1		3a (94)	4a (2, 92)
2		3h (86) ^[c]	4h (2, 95)
3		3i (88)	4i (7, 55) ^[d]
4		3j (76)	4j (4, 89)
5		3h (48) ^[e]	4k (4, 89)
6		3l (89)	4l (2, 80)
7		3m (95) ^[c]	4m (12, 80) ^[f]
8		3n (95)	4n (2, 91) ^[f]
9		3o (92) ^[c]	4o (2, 85)
10		3p (93) ^[c]	4p (2, 87) ^[f]
11		3q (91) ^[c]	4q (2, 92)

12		3r (90)	4r (5, 91)
13		3s (77)	4s (7, 82) ^[f]
14		3t (58)	4t (10, 50)

^[a]Reaction conditions: a) McMurry coupling: adamantanone **1** (0.28 mmol), ketone **2** (1 equiv), TiCl₄ (6.1 equiv), Zn (13.5 equiv), THF (6 mL), reflux, 45 min; b) photooxygenation: Methylene Blue (6.5 mol %), UV cutoff filter ($\lambda = 550$ nm), -20°C, CH₂Cl₂ (1 mL for 10 mg of olefin **3**), 500 W halogen lamp, O₂ (1 atm, balloon). ^[b]Determined after purification by flash chromatography. ^[c]Ketone **2** (3.2 equiv), 1.5 h. ^[d]-30°C. ^[e]Poor solubility of the starting ketone **2k**. ^[f]-40°C.

Three different structural modifications were examined on parent molecule **4a**. First, we decorated the acridone ring with fluorine substituents, as electron-withdrawing groups (EWGs), to obtain difluoro- or tetrafluoroacridan derivatives, as well as products containing both fluorine and a methyl substituent as EDG. McMurry olefination proceeded smoothly on acridones **2h-l**, regardless of the substitution pattern, to provide the corresponding alkenes **3h-l** in high yields (up to 89%).

Also, the photooxygenation step provided, in most cases, good results, but the reactivity of various olefins showed some differences. First, we observed that the formal [2+2] cycloaddition of singlet oxygen to acridane-derived alkenes strongly depended on steric hindrance. In fact, when a fluorine atom occupied the 1-position on the aromatic system (Table 2.1, entry 3), the reaction was significantly slower. On the other hand, the presence of EWGs (two or four fluorine atoms; Table 2.1, entries **2-4** and **5**, respectively) or a combination of an EWG and an EDG (Table 2.1, entry 6) did not affect 1,2-dioxetane formation.

In the second stage, we replaced the ethyl acetate on the nitrogen with alkyl or aryl substituents (Table 2.1, entries 7-11). The corresponding 1,2-dioxetanes **4m-q** were always accessible, but when the electron-donating effect was more pronounced (Table 2.1, entries 7, 8, and 10) we were forced to decrease the photooxygenation temperature to -40 °C to obtain good results, since at -20 °C partial degradation of the dioxetane **4** to the corresponding ketones **1** and **2** occurred.

We also focused our attention on the nature of the endocyclic heteroatom and replaced the nitrogen atom with oxygen (Table 2.1, entries 12 and 13). The oxygen-bearing xanthyl derivatives **2r** and **2s** smoothly underwent McMurry

olefination (**3r,s**) and subsequent photooxygenation; this allowed us to isolate the corresponding 1,2-dioxetanes **4r** and **4s** in high yields after chromatographic purification [see Ref. 189, 190]. The reaction with singlet oxygen was also acceptable (Table 2.1, entry 14) when a direct linkage between the two aromatic rings was created, as in fluorenone-derived olefin **3t** [see Ref. 191, 192].

2.2.2 Photophysical and TCL properties

The TCL properties of this series of 1,2-dioxetanes **4h-t** were investigated (Table 2.2), together with the photophysical properties of the corresponding ketones **2h-t**, which were the emitting species in the TCL process (Scheme 2.1). Specifically, we confirmed the nature of the emitting species for methyl-substituted acridan-1,2-dioxetanes ([see Ref. 110]) by comparing the TCL spectra of the 1,2-dioxetanes with the fluorescence spectra of the corresponding acridones. In all cases, the TCL spectra closely matched the fluorescence spectra of the corresponding acridones; thus demonstrating that the TCL emission was primarily due to the singlet excited state of acridone. The singlet excited state of 2-adamantanone could also be produced in the TCL process. However, its possible emission could not be detected due to overlap with the fluorescence emission of acridones and the weak intensity (for 2-adamantanone: $\Phi_F=0.015$ and $\lambda=425\text{nm}$) [see Ref. 193, 194]. For comparison, we also show data for previously reported 1,2-dioxetane **4a** and acridone **2a** (Table 2.2, entry 1).

When we measured the fluorescence quantum yields (Φ_F) of ketones **2a** and **2h-t** (Table 2.2), it appeared clear that the emission performances of the acridones (Table 2.2, entries 1-11) were strongly affected by the substitution pattern. In particular, compared to reference compound **2a** (Table 2.2, entry 1), fluorine atoms on the acridone aromatic rings significantly decreased the Φ_F values when present in the 3- and/or 6-positions (Table 2.2, entry 2) or in the 1-position (Table 2.2, entry 3). The ability of a *para*-fluorine to decrease the fluorescence quantum yield of the corresponding acridanone was further confirmed by comparing 3-F,6-Me derivative **2l** ($\Phi_F=0.04$) with 3-Me derivative ($\Phi_F=0.21$). Conversely, the insertion of fluorines in 2,7-positions enhanced the fluorescence quantum yield (**2j** cf. **2a**, **2k** cf. **2h**). These unexpected and intriguing results suggested that the emitting performances of F-substituted acridane-based ketones were mostly affected by the position rather than the electronic features of the substituents on the aromatic rings. As a further confirmation, by replacing a fluorine atom (EWG) in the 6-position with a methyl group (weak EDG), we obtained only a slight increase in the Φ_F value (**2l**, entry 6, cf. **2h**, entry 2, Table 2.2). The observed behavior also proved to be peculiar in comparison with the fluorescence quantum yield trend previously recorded for (poly)methylated acridones [see Ref. 110]. In

the presence of EDGs, the Φ_F values showed an increase for substitution at both the 2- and 3-positions. On the contrary, the insertion of fluorine atoms generated the opposite effect, depending on their location on the aromatic system.

Previous studies have already demonstrated a significant dependence of the CL quantum yield on the substitution pattern, for a specific class of 1,2-dioxetanes (aryl-substituted derivatives). A new rule, known as the "odd/even rationale" was defined to explain the outcome from the chemically-triggered decomposition of such compounds, which yield phenolate-like emitting species (strong EDG substitution). In particular, for chemically initiated electron exchange luminescence (CIEEL)-active spiroadamantane 1,2-dioxetanes, such as acetoxynaphthyl spiroadamantyl dioxetanes, it was observed empirically that extended conjugated (para substituted) carbonyl chromophores derived from dioxetanes triggered decomposition gave rise to low chemiexcitation efficiencies, whereas cross-conjugated (meta substituted) carbonyl compounds showed higher quantum yields. The odd/even rationale was proposed to explain this phenomenon: charge transfer from the donor (phenolate) to the acceptor (carbonyl group) occurs more effectively when the two groups are cross-conjugated (odd number of carbons between the interacting groups), and, presumably, the charge-transfer enhances the excited-state formation and ensures high chemiexcitation efficiency. On the contrary, extended conjugation (even number of carbons between the interacting groups) stabilizes the ground state through dipolar resonance, which disfavors excited-state formation and, consequently, provides low efficiency [see Ref. 195–198]. However, since the different molecular structure, it is not possible to apply the above-cited odd/even rationale to our 1,2-dioxetane derivatives (**4a**, **4h-t**). Furthermore, very few examples are present in the literature that describe the behavior of EWG-substituted 1,2-dioxetanes [see Ref. 199–206], and no studies have been reported on fluorine-bearing aryl dioxetanes or concerning the dependence of 1,2-dioxetanes properties on the EWG distribution on the acridan system. In particular, opposite effects on fluorescence quantum yield as a function of the substituent position have never been observed.

After examining the photophysical properties of ketones **2h-l**, we turned our attention to the activation parameters of the thermal decomposition of the fluorinated 1,2-dioxetanes **4h-l**. In particular, the activation parameters for the thermal decomposition of 1,2-dioxetanes **4a** and **4h-t** were determined by a standard isothermal kinetic method, which measured the emission decay kinetics at different temperatures and gave the kinetic constants of the TCL process (see the Supporting Information for details). The trend shown by acridane 1,2-dioxetanes containing EDGs consists of lowered activation energies (E_a) and pre-exponential coefficients (A) and increased fluorescence quantum yields Φ_F

Table 2.2: Photophysical properties of ketones **2a** and **2h-t** and activation parameters for the thermal decomposition of the corresponding 1,2-dioxetanes **4a** and **4h-t**.

Entry	2	$\Phi_F^{[a]}$	4	E_a (kcal mol ⁻¹) ^[b]	lnA (s ⁻¹) ^[b]	$t_{1/2}$ (months) ^[c]
1	2a	0.11	4a	31.5 ± 0.8	35.6 ± 1.0	11
2	2h	0.01	4h	41.7 ± 4.4	48.0 ± 5.6	1400 (117 y)
3	2i	4 × 10 ⁻³	4i	36.1 ± 4.3	41.8 ± 5.6	55
4	2j	0.65	4j	27.9 ± 1.2	30.6 ± 1.5	3.9
5	2k	0.11	4k	25.8 ± 1.1	28.6 ± 1.4	1.0
6	2l	0.04	4l	35.1 ± 2.7	42.9 ± 3.5	3.4
7	2m	0.61	4m	30.9 ± 1.5	37.3 ± 2.0	0.76
8	2n	0.44	4n	23.7 ± 1.6	27.2 ± 2.2	0.097
9	2o	0.28	4o	27.7 ± 0.7	31.0 ± 0.9	1.9
10	2p	0.43	4p	26.2 ± 2.4	29.5 ± 3.3	0.66
11	2q	4 × 10 ⁻⁴	4q	32.0 ± 1.4	37.4 ± 1.9	4.4
12	2r	1 × 10 ⁻⁴	4r	46.4 ± 3.4	58.0 ± 4.7	180 (15 y)
13	2s	2 × 10 ⁻⁴	4s	27.0 ± 1.1	29.5 ± 1.5	2.6
14	2t	0.025	4t	33.8 ± 1.4	40.8 ± 1.9	3.1

^[a]Determined in acetonitrile by using quinine sulfate as standard ($\Phi_F = 0.53$ in H₂SO₄ 0.05 mol L⁻¹).^[b]Mean ± SD of three independent measurements.^[c]Calculated for the solid compound at 25°C. **Note:** The variations of activation energy due to the presence of different substituents are very often paralleled by an analogous change in the pre-exponential coefficient. As a result, the trend in the activation energies often does not reflect the behavior of the kinetic rate constants of the TCL reaction, and thus, the $t_{1/2}$ values.

[see Ref. 110]. The significant increase in the fluorescence quantum yields of acridones containing EDGs could be due to a decrease in the intersystem crossing rate constant, and thus, to a lower efficiency of nonradiative deactivation processes, as reported for aromatic compounds, such as anthracene [207]. We reasoned that the introduction of fluorine atoms as EWGs should give more stable and easy to handle 1,2-dioxetanes, without causing an excessive impairment of the fluorescence quantum yield. The activation parameters recorded for the fluorinated 1,2-dioxetanes confirmed our hypothesis, but they also revealed some unexpected results. The 3,6-difluorodioxetane **4h** (Table 2.2, entry 2) was characterized by the highest activation energy ($E_a=41.7$ kcal mol⁻¹) and showed an outstanding and unprecedented calculated half-life ($t_{1/2}$) of 117 years, if stored as a solid at 25°C [see Ref. 208–211]. Increased stability compared with unsubstituted dioxetane **4a** was also recorded for compound **4i** (Table 2.2, entry 3; $E_a=36.1$ kcal mol⁻¹, $t_{1/2}=55$ months), whereas the remaining fluorinated dioxetanes **4j-l**

(Table 2.2, entries 4-6) proved to be less thermally stable. The results obtained from this family of compounds confirmed that there was a correlation between acridone fluorescence quantum yield and thermal stability of the corresponding 1,2-dioxetane. The substituents on the aromatic system that enhance the Φ_F value, such as fluorine atoms in the 2,7-positions (**2j-k**), facilitate dioxetane thermal decomposition (**4j-k**) at the same time. Conversely, 3,6-difluoro- (**2h**) and 1,6-difluoro-substituted (**2i**) acridones showed decreased fluorescence quantum yields, but the corresponding dioxetanes **4h-i** displayed significantly longer half-life values. A comparison of these data with those recorded for methyl-substituted acridan-based dioxetanes confirmed that the introduction of weak EDGs increased the ketone fluorescence quantum yield and lowered the dioxetane activation energy, regardless of the position on the aromatic ring. On the contrary, the impact of fluorine atoms depended dramatically on the substituent position.

The second structural feature we studied was the nature of the substituent on the acridan nitrogen (Table 2.2, entries 7-11). In fact, during the excitation step of the acridone system, charge is transferred from the donor N atom to the carbonyl group. The charge-transfer character of the excited acridone chromophore, as expected for a vinylogous amide, is its main electronic characteristic. Thus, it is reasonable that modifications on the nitrogen substituent affect the fluorescence quantum yield much more than the introduction of substituents on the aromatic rings. Furthermore, the position of the aromatic rings substituents perturbs this charge-transfer transition significantly less in acridan-based systems than in benzoate-based systems [see Ref. 212, 213].

Removing (**2m, 4m**) or elongating (**2n, 4n**) the ester group present in the parent compounds (**2a, 4a**) provided the expected enhancement of Φ_F and decrease in E_a values (Table 2.2, entries 7 and 8, respectively). This finding further confirmed the stabilizing effect postulated for the acetate moiety, due to its electron-withdrawing character. Then, we investigated N-aryl derivatives (**2o-q, 4o-q**; Table 2.2, entries 9-11) and observed, in general, a lower thermal stability of the dioxetanes with respect to the reference compound **4a**, even if the decrease was more pronounced for the EDG-substituted compound **4p** than that for the *para*-fluorophenyl derivative **4q**. The results obtained for N-aryl acridan 1,2-dioxetanes are in agreement with the data reported by other authors [see Ref. 153–158]. Considering the possible conformations of N-aryl acridan 1,2-dioxetanes, a steric repulsion between the peri-hydrogen atoms of the acridan system and the aryl group might be generated. Therefore, the two rings would not be able to conjugate each other sufficiently and the electronic effects of the aryl group would be largely reduced.

Thus, for acridane-based 1,2-dioxetanes, we conclude that 1) the introduction

of fluorine atoms onto the aromatic rings represents a remarkable tool to stabilize the dioxetane derivatives, in particular, when they are located at the 3- and/or 6- position, or to enhance their emitting performances, when located at the 2,7-positions; 2) the acetate moiety proves to be the best performing N-substituent, ensuring a good balance between ketone fluorescence quantum yield and dioxetane stability. As far as the activation parameters for the thermal decomposition of xanthyl-derived 1,2-dioxetanes (**4r**, **s**) and the photophysical properties of the corresponding emitting species **2r** and **2s** are concerned, we observed that the replacement of the endocyclic nitrogen with an oxygen provided a very stable dioxetane (**4r**), but also strongly decreased the fluorescence quantum yield (cf. Table 2.2, entries 1 and 12). Moreover, EDGs on the xanthyl scaffold (3,6-positions) dramatically decreased the activation parameters without a perceptible benefit in the Φ_F value (cf. Table 2.2, entries 12 and 13). Lastly, fluorenyl dioxetane **4t**, which featured a direct linkage between the aromatic rings, afforded acceptable emitting properties ($\Phi_F=0.025$) accompanied by moderate thermal stability (Table 2.2, entry 14).

2.2.3 Chemometric analyses

To widen our library of TCL 1,2-dioxetanes and to learn more about the structure–property relationships of this class of compounds, we also synthesized a series of olefins that, unexpectedly, did not undergo the photooxygenation step (Figure 2.2).

Previously investigated acridane-based alkenes **3u-x** [see Ref. 110] and the 1-Me, 6-F derivative **3y** are all characterized by the presence of a methyl group at the 1-position of the aromatic system. Such results suggest that steric crowding in this region disfavors the addition of singlet oxygen. The slow photooxygenation rate observed for 1,6-difluoro compound **3i** (Table 2.1, entry 3) supports this hypothesis.

The sulfur-containing olefins **3z-B** did not react with singlet oxygen, regardless of the sulfur oxidation state [see Ref. 214–217]. We tested other reaction temperatures (namely, 0 and -20°C) and extended the reaction times up to 7 h, but only the starting olefin was recovered. Finally, when we replaced the endocyclic heteroatom with a sp^3 - or sp^2 -hybridized carbon (**3C-E**), in all cases, photooxygenation did not occur.

These findings reveal that the reactivity of an olefin in the photooxygenation process strongly depends on its substitution pattern. It is known that the formal [2+2] cycloaddition of singlet oxygen to alkenes takes place efficiently on electronrich systems [see Ref. 218–225]. However, the mechanism of this process has been extensively debated in the literature (Scheme 2.3) [see Ref. 226–237], and

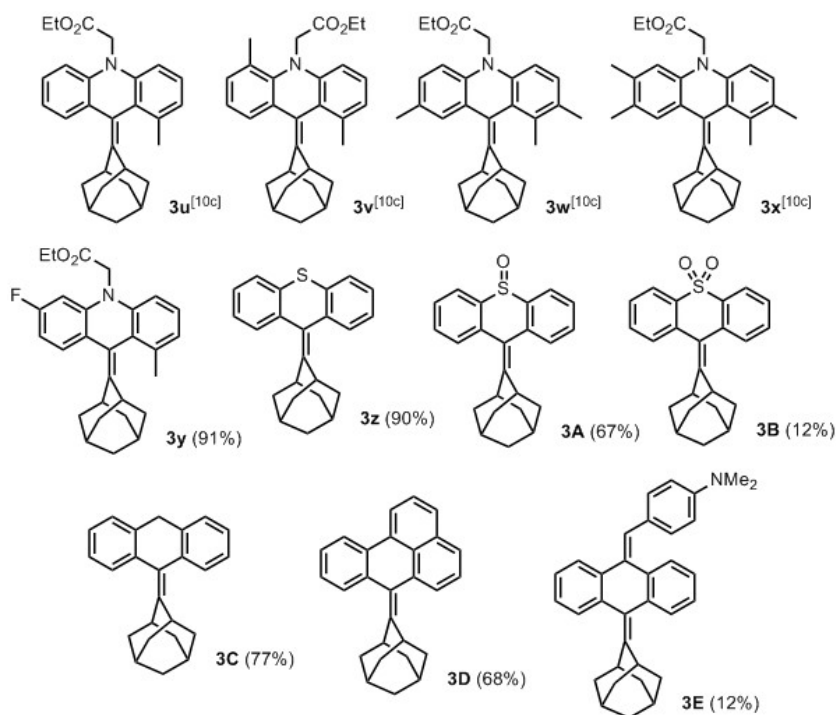
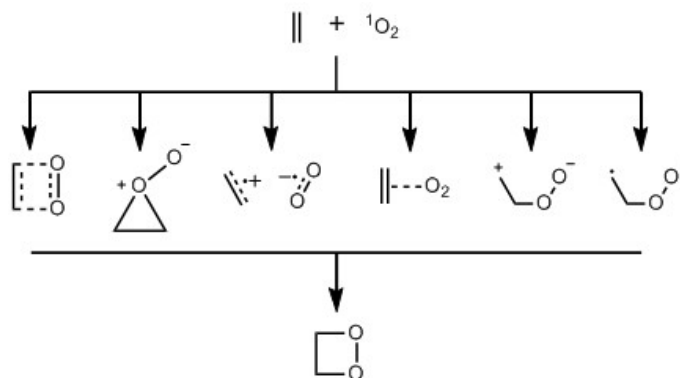


Figure 2.2: Differently substituted alkenes unreactive under photooxygenation conditions (the yields of olefin formation are given in parentheses; for synthetic details, see the Supporting Information).

the most reliable one can vary case by case, depending on the molecular structure of the substrate, the solvation energy, and also the sensitizer employed. As a consequence, the nature of the olefin substituents (electron-donating ability, presence of hydrogen-bond acceptors and/or donors, geometry, and steric hindrance) not only affects the success of singlet oxygen addition, but it also determines the reaction pathway.

The mechanism of singlet oxygen addition to double bonds has been studied computationally several times, but the rigorous approach to this diradical system requires expensive treatments of multireference states and it has been applied exclusively on very simple systems [see Ref. 238–240]. Moreover, the prediction of the mechanism of singlet oxygen reactions has proven a challenging task for many reasons [see Ref. 241, 242], including because different possible reaction pathways (Scheme 2.3) are often predicted depending on the level of theory employed [see Ref. 243].

To rationalize all of our results, we decided to avoid an extremely demanding and time-consuming quantum mechanical approach, considering that both excited and radical states are involved in the reaction. Rather, we envisioned a chemometric approach as a more practical tool to identify which structural and electronic properties of starting olefins, or combination of them, determine the success of



Scheme 2.3: A representation of the various hypothesized mechanisms for the formation of 1,2-dioxetanes through singlet oxygen addition to olefins.

the photooxygenation step.

At the outset, we adopted principal component analysis (PCA) [see Ref. 244–247] of the structural and electronic molecular descriptors obtained by DFT optimizations of olefins **3** [see Ref. 248]. After an initial conformational screening by using a molecular mechanics (MM) force field on the data set of molecules, the conformers obtained in a 8 kcal mol⁻¹ window were optimized by using DFT at the B3LYP/6-31G(d) level of theory (see the Supporting Information for details). Among the different calculated electronic descriptors, we selected the energy of the HOMO, the energy of the LUMO, the Mulliken charges on the olefin carbon terminals Ca-Mul and C9-Mul (Figure 2.3) and the coefficients of the atomic contribution of the alkene carbon atoms to the HOMO and LUMO orbitals, calculated by using the Mulliken decomposition method (Ca-HOMO, Ca-LUMO, C9-HOMO, and C9-LUMO). Moreover, we selected a few structural parameters that reflect the geometry of the molecules in close proximity to the double-bond reaction site.

In particular, we chose the two dihedral angles, ϕ_1 and ϕ_2 , which represent the deviation from planarity of the aromatic rings with respect to the plane defined by the carbon-carbon double bond, and the four interatomic distances d_1 - d_4 as an index of steric crowding of the aromatic ring substituents around the Ca-C9 double bond (Figure 2.3). Specifically, when a substituent was present in the C1 position of the aromatic system, d_2 and d_4 were taken as the interatomic distances between the double-bond carbon atoms Ca and C9 and the closest atom of the substituent group, as shown in Figure 2.3.

We analyzed first a set of 23 similar molecules that possessed a common acridane skeleton (**3a-q**, **3u-y**, and **3F**; Figure 2.4), the molecular descriptors of which are collected in Table 6.3 in the Supporting Information (see Chapter 6). Data were meancentered before analysis and were autoscaled by dividing them by

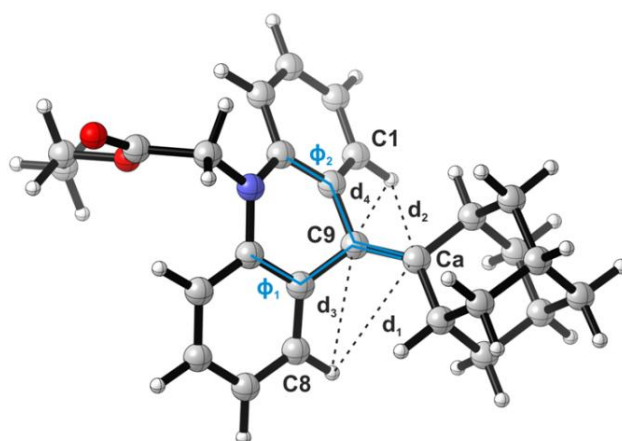


Figure 2.3: DFT-optimized structure of **3a** and structural molecular descriptors employed in the PCA.

the standard deviation of each column sample variable. The first four eigenvalues greater than 1 obtained by PCA of the 23x14 data matrix and the explained variances relative to each component are reported in Table 2.3. The model obtained is able to explain 84.9 % of the total variance by using only three PCs, whereas two PCs explain 64.7 % of the variance.

Table 2.3: Eigenvalues and percentage of explained variance relative to the first four principal components (PCs) of the model used for the description of olefins **3a-q**, **3u-y**, and **3F**.

PC	Eigenvalue	Variance (%)	Cumulative Eigenvalue	Cumulative Variance (%)
PC1	5.96	42.5	5.96	42.5
PC2	3.11	22.2	9.07	64.7
PC3	2.82	20.1	11.89	84.9
PC4	1.16	8.3	13.05	93.1

The score plot representing the projections of the data points in the plane defined by the two first PCs is reported in Figure 2.5 A. A clustering of data is apparent, with the alkenes that undergo photooxygenation grouped in the right side of the plot (blue triangles) and the unreactive molecules clustered on the left (red dots), mainly discriminated by the first PC. The loading plot, reported in Figure 2.5 B with the variables colored by relative contributions, shows that the variables mainly composing the first PC are the Mulliken charge C9-Mul ($\cos^2 = 0.834$), the dihedral angles ϕ_1 and ϕ_2 ($\cos^2 = 0.808$ and 0.807 , respectively),

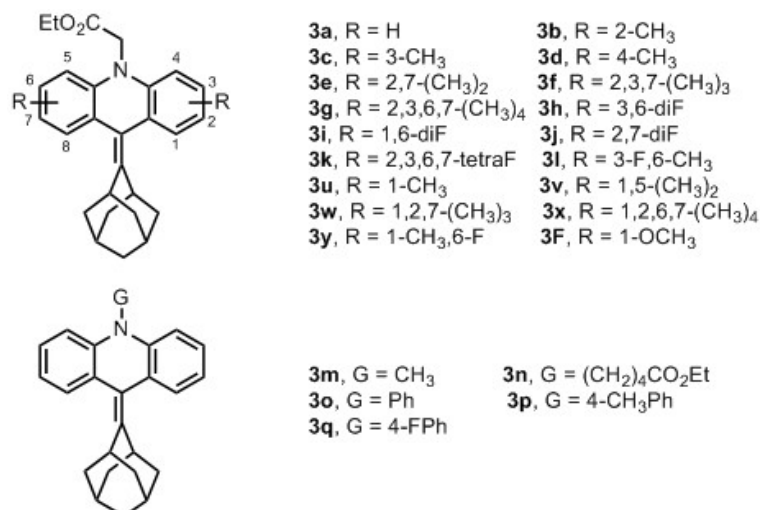


Figure 2.4: Initial set of acridan-containing alkenes analyzed with the chemometric approach.

the interatomic distances d_2 and d_4 ($\cos^2 = 0.815$ and 0.669 , respectively), and, to a lesser extent, the interatomic distance d_1 ($\cos^2 = 0.541$) and the Mulliken charge Ca-Mul ($\cos^2 = 0.582$). The only variables significantly contributing to the second PC are the interatomic distance d_3 ($\cos^2 = 0.641$) and, to a lesser extent, the interatomic distance d_1 ($\cos^2 = 0.413$) and the energies of the HOMO and LUMO orbitals ($\cos^2 = 0.461$ and 0.483 , respectively). PCA results seem to suggest that the difference in reactivity in the photooxygenation reaction between the two groups of alkenes is mainly due to steric effects and not to electronic ones. In particular, the presence of a bulky methyl group in the 1-position of the acridan skeleton results in a significantly larger deviation from planarity for compounds **3u-y**, with respect to all other reactive alkenes (see Table 6.3). This geometrical distortion has the overall effect of making the Ca-C9 double bond more sterically crowded and less accessible to singlet oxygen, as also evidenced by the shorter interatomic distances d_1 and d_2 in the unreactive compounds.

The same analysis was repeated on the expanded data set comprising the oxygen-bearing xanthyl derivatives **3r-s** (XAN family), the sulfur-containing olefins **3z**, **3A**, and **3B** (THI family), and the anthrone-derived alkenes **3C-E** (ANT family), in addition to the previously analyzed acridane derivatives **3a-q**, **3u-y**, and **3F** (ACR family). The eigenvalues greater than 1 derived from PCA of the as-obtained 31x14 data matrix are reported in Table 2.4, while the corresponding molecular descriptors employed are collected in Table 6.4 in the Supporting Information (see Chapter 6). By using the first three PCs, the model can be used to explain 73.8 % of the total variance, whereas 56 % of the variance is accounted for by using only the first two PCs.

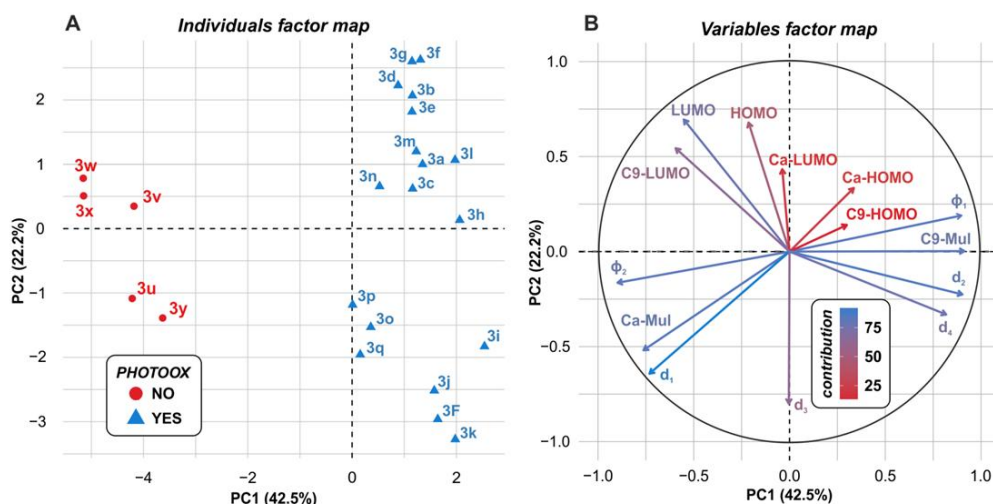


Figure 2.5: PCA results for the data matrix descriptors of olefins **3a-q**, **3u-y**, and **3F**: A) PCA score plot relative to the first two PCs (blue triangles: reactive compounds; red dots: unreactive compounds). B) PCA loading plot relative to the first two PCs (variables are colored according to their relative contribution).

Table 2.4: Eigenvalues and percentage of explained variance relative to the first five PCs of the model used for the description of olefins **3a-s**, **3u-z**, and **3A-F**.

PC	Eigenvalue	Variance (%)	Cumulative Eigenvalue	Cumulative Variance (%)
PC1	4.45	31.8	4.45	31.8
PC2	3.39	24.2	7.84	56.0
PC3	2.49	17.8	10.33	73.8
PC4	1.42	10.1	11.75	83.9
PC5	1.09	7.8	12.84	91.6

The score plot representing the projections of the data points in the plane defined by the two first PCs is reported in Figure 2.6 A and the corresponding loading plot with the variables colored by relative contributions is shown in Figure 2.6 B. Again, a quite marked separation in the score plot is apparent between the reactive and unreactive olefins, which in this expanded data set is discriminated by both the first and second PCs.

The relative loading plot (Figure 2.6 B) reveals that the variables contributing to the first PC are mainly the steric parameters, similarly to what is obtained for the previously analyzed **ACR** family. In particular, the highest contributing variables are mainly the dihedral angles ϕ_1 and ϕ_2 ($\cos^2 = 0.906$ and 0.915 , respectively) and, to a lesser extent, the interatomic distances d_2 and d_4 ($\cos^2 =$

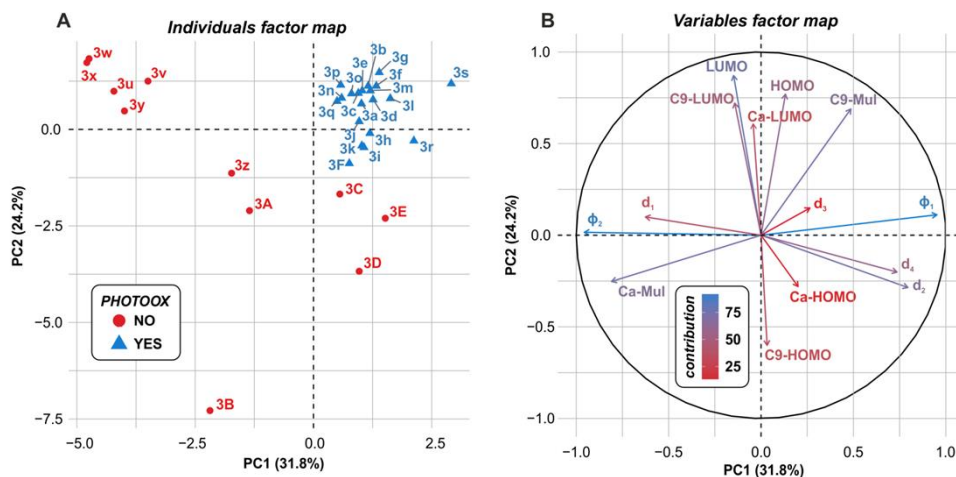


Figure 2.6: PCA results for the data matrix descriptors of olefins **3a-s**, **3u-z**, and **3A-F**: A) PCA score plot relative to the first two PCs (blue triangles: reactive compounds; red dots: unreactive compounds); B) PCA loading plot relative to the first two PCs (variables are colored according to their relative contribution).

0.632 and 0.542, respectively) and the Mulliken charge Ca-Mul ($\cos^2 = 0.654$). On the other hand, the variables significantly contributing to the second PC are mainly electronic parameters, namely, the energies of the HOMO and LUMO ($\cos^2 = 0.592$ and 0.759 , respectively) and, to a lesser extent, the Mulliken charge C9-Mul ($\cos^2 = 0.475$).

For this expanded data set, the PCA results suggest that both steric and electronic effects play a role in determining the reactivity under photooxygenation conditions; both factors are necessary, but not sufficient to trigger reactivity. The score plot of the data projections (Figure 2.6 A) is apparently divided into four quadrants, with the reactive olefins in the top-right sector, where both steric and electronic parameters cooperate in the same positive direction. The acridane-containing unreactive olefins (**3u-y**) are positioned in the top-left quadrant, in a region where electronic effects alone would allow the photooxygenation reaction, which is hampered solely by steric hindrance around the Ca-C9 double bond exerted by the methyl group present at the 1-position ($121\text{-}124^\circ$ versus 130° mean ϕ_1/ϕ_2 values for all compounds). On the other hand, the anthrone-derived alkenes **3C-E** are grouped in the bottom-right sector of the score plot, with the same coordinates of the reactive olefins along the first PC. Although photooxygenation should not be disallowed for steric reasons for these alkenes, the overall linear combination of their electronic descriptors renders them unreactive. The sulfur-containing olefins **3z** and **3A** are located in a borderline central region of the plot, where both steric and electronic factors are not ideal for promoting the photooxygenation reaction, whereas the sulfone analogue **3B** is projected farther

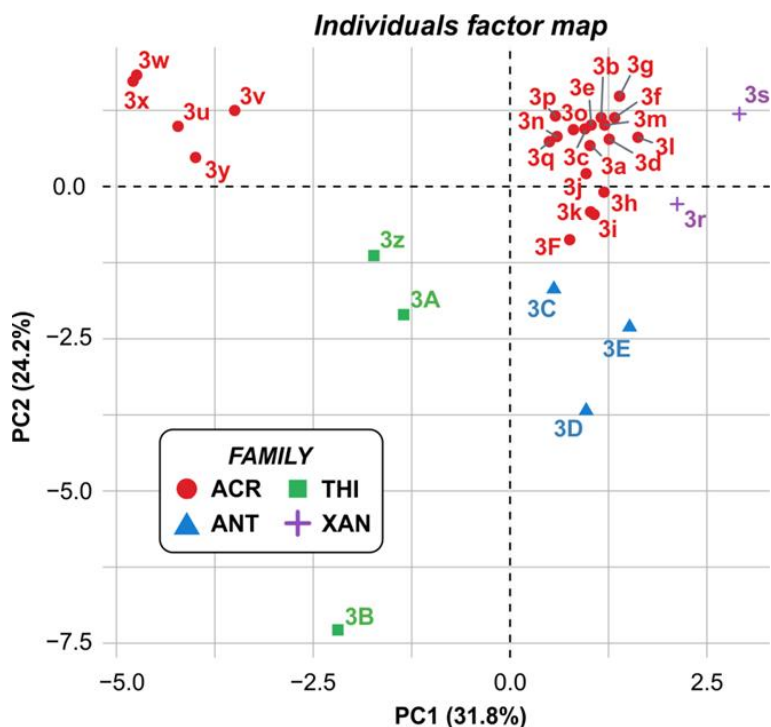


Figure 2.7: PCA results for the data matrix descriptors of olefins **3a–q**, **3u–y**, and **3F** (ACR); **3r–s** (XAN); **3z**, **3A–B** (THI); and **3C–E** (ANT). PCA score plot relative to the first two PCs, colored according to the structural features of the analyzed alkenes.

away along the negative PC2 axis. Finally, the reactive xanthyl derivatives **3r** and **3s** are correctly projected in the same top-right quadrant of the previously examined reactive acridane-based olefins, which possess both steric and electronic properties that allow the photooxygenation reaction to proceed smoothly. The score plot of the expanded data set relative to the first two PCs is again reported in Figure 2.7, with the projected data points now colored according to the common structural features of the employed alkenes (XAN: **3r,s**; THI: **3z**, **3A,B**; ANT: **3C–E**, and ACR: **3a–q**, **3u–y**, **3F**). The marked clustering obtained in this plot clearly shows the capability of the PCA model to discriminate between different alkenes on the basis of their common structural features.

To further validate our chemometric approach, a supervised linear discriminant analysis (LDA) was performed on the expanded 31x14 data set. Using the previously chosen parameters, we obtained a highly statistically significant model (Wilks' lambda = 0.0121, canonical correlation = 0.9939), showing perfect discrimination between the two classes of reactive (mean of canonical variables=6.48) and unreactive olefins (mean of canonical variables = -11.8). The corresponding raw and standardized coefficients of the obtained linear discriminant are reported in Table 2.5, whereas the canonical scores are plotted in Figure 2.8 for all compounds.

Table 2.5: Raw and standardized coefficients of the linear discriminant obtained in the LDA model used for the description of olefins **3a-s**, **3u-z**, and **3A-F**.

Variable	Raw coefficient	Standardized coefficient
HOMO	9.549	3.176
LUMO	-4.564	-1.216
Ca-Mul	865.7	6.167
C9-Mul	83.51	1.631
ϕ_1	0.8260	1.664
ϕ_2	-1.319	-3.620
d_1	-84.28	-2.000
d_2	32.63	2.630
d_3	-3.254	-0.05056
d_4	-6.801	-0.3888
Ca-HOMO	31.76	1.629
C9-HOMO	-40.83	-1.979
Ca-LUMO	23.65	0.7734
C9-LUMO	154.1	2.684
Constant	-194.9	-

It is interesting to note that, when LDA was performed by using a stepwise forward variable selection, only 8 of the 14 variables were used to obtain a statistically significant model (Wilks' lambda = 0.0191). Moreover, the most contributing variables were almost exactly the same as those that composed the main PCs of the corresponding PCA, namely, the dihedral angle ϕ_1 , the interatomic distances d_2 and d_4 , and the Mulliken charges Ca-Mul and C9-Mul.

To verify the capability of the LDA model to predict the reactivity of new compounds with singlet oxygen, the fluorenyl alkene **3t** (central five-membered ring) and the specially designed new olefin **3G** (central seven-membered ring; Figure 2.9) were projected onto the linear discriminant.

The fluorenyl-derived alkene **3t** was predicted to be reactive with a raw canonical score of 30.8; a particularly high value due to an almost completely planar arrangement of the aromatic rings with respect to the plane defined by the carbon-carbon double bond (ϕ_1 , $\phi_1 = 159.8^\circ$). As already mentioned in Table 2.1, entry 14, when **3t** was subjected to the photooxygenation conditions, the corresponding 1,2-dioxetane **4t** was isolated in 50% yield overall. On the contrary, 5-dibenzosuberone-derived alkene **3G** was predicted to be unreactive with a raw canonical score of -39.9, again a particularly low value, mainly due

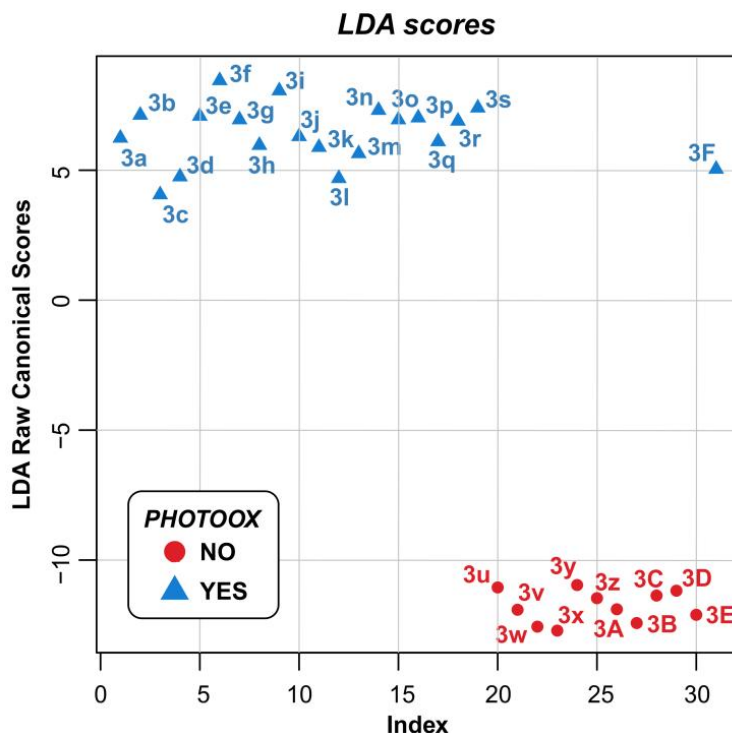


Figure 2.8: Canonical scores relative to the LDA model for alkenes **3a-s**, **3u-z** and **3A-F**.

to its significantly smaller dihedral angles ϕ_1 and ϕ_2 (113.3°) and to the greater negative Mulliken charge on C9 (-0.165 versus -0.09 mean C9-Mul charge). When subjected to the photooxygenation conditions, olefin **3G** did not react and only the starting material was observed in the reaction mixture.

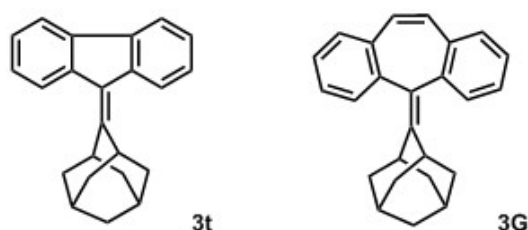
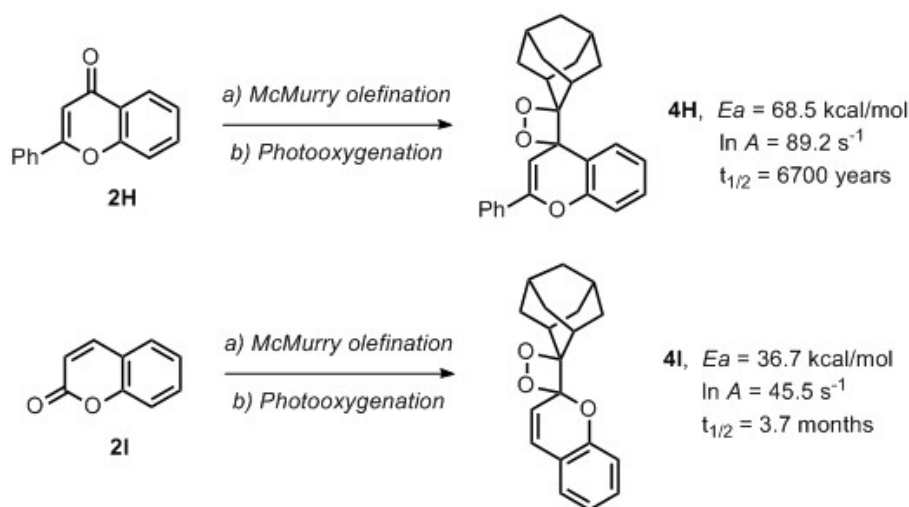


Figure 2.9: Olefins selected to verify the capability of the model to predict reactivity with singlet oxygen.

The experimental findings obtained for the supplementary alkenes **3t** and **3G** validate the developed chemometric model, which is able to anticipate the outcome of a photooxygenation reaction carried out on structurally different tetrasubstituted olefins, as characterized by an adamantyl unit coupled to a tricyclic aromatic scaffold (regardless of the nature of the central ring).

2.3 Conclusion

A small library of more than 30 olefins of general structure **3** have been subjected to photooxygenation, with the aim of synthesizing new dioxetane-based thermochemiluminescent labels with optimized light emission efficiency and CL temperature triggering. Among them, 20 starting olefins provided the corresponding 1,2-dioxetanes, whereas no traces of product were observed with the other members of the series. To anticipate the feasibility of the photooxygenation step leading to new potentially thermochemiluminescent dioxetanes, we sought a rationale. A complete DFT analysis of the transition states for the formation of all dioxetanes was not possible for us, given the heavy and time-consuming computational effort required by the multiconfigurational treatment of both closedshell and free-radical excited states at a rigorous level. Thus, we adopted a chemometric approach by exploiting PCA and LDA of the structural and electronic molecular descriptors obtained by DFT optimizations of olefins **3**. This approach allowed us to determine steric and electronic parameters that govern dioxetane formation. Great interest in new thermochemiluminescent molecules, for example, in bioanalytical assays, was the driving force of this study, which allowed us to discover that fluorine atoms on the acridan system remarkably stabilized 1,2-dioxetanes when located in the 3- and/or 6-position (**4h** and **4i**). On the other hand, 2,7-difluorinated acridane dioxetane **4j** showed a significantly enhanced fluorescence quantum yield with respect to the unsubstituted dioxetane **4a**. Our investigations for the development of original and enhanced dioxetane-based TCL labels are still ongoing. For instance, flavone- and coumarin-containing [see Ref. 249–259] derivatives **4H** and **4I** (Scheme 2.4) are of interest.



Scheme 2.4: Preliminary results concerning flavone- (**4H**) and coumarin-based (**4I**) 1,2-dioxetanes.

Indeed, even if their synthesis still requires some optimization, 1,2-dioxetanes **4H** and **4I** have been isolated and characterized as TCL compounds. Unexpectedly high values of the activation parameters for thermal decomposition were recorded for flavone-derived 1,2-dioxetane **4H**, which resulted in a remarkable calculated half-life at 25°C (more than 6000 years); this offers the opportunity of useful applications in diagnostics and bioanalysis. On the other hand, coumarin-based 1,2-dioxetane **4I** showed limited thermal stability. An analogous chemometric approach will be reported in due course for flavones and coumarins once a significant number of compounds has been synthesized.

2.4 Experimental Section

2.4.1 Representative procedure for the synthesis of alkenes **3**

Under a nitrogen atmosphere, TiCl₄ (1 M in dichloromethane, 6.1 equiv) was added to a suspension of zinc powder (13.5 equiv) in anhydrous THF (8 mL/0.5 mmol of **1**) at 0°C, and the suspension was stirred for 10 min under reflux. A solution of ketone **2** (1 equiv) and 2-adamantanone **1** (1 equiv) in dry THF (2 mL/0.5 mmol of **1**) was added dropwise over a period of 30 min. The reaction mixture was heated at reflux for 45 min. Then, it was cooled to room temperature, quenched with water, and extracted with AcOEt (3x10 mL). The combined organic layers were dried over sodium sulfate and evaporated under vacuum. The crude product was purified by flash chromatography on silica gel.

2.4.2 Representative procedure for the synthesis of 1,2-dioxetanes **4**

Alkene **3** (16 equiv) and Methylene Blue (1 equiv) were dissolved in CH₂Cl₂ (1 mL/10 mg of alkene **3**). The solution was cooled (usually at -20 °C) and subjected to an oxygen atmosphere (1 atm, balloon). The solution was stirred at the same temperature under irradiation by using a 500W halogen lamp equipped with an UV cutoff filter (0.5% transmission at $\lambda = 550$ nm). Irradiation was continued until the starting material disappeared (usually 2 h of irradiation), and the conversion was monitored by ¹H NMR spectroscopy. Product **4** was purified by rapid filtration on a 5 mm layer of silica gel, by using cooled (-40°C) CH₂Cl₂ as the eluent, and the filtered solution was evaporated under vacuum at 0°C.

For further details about the synthesis and characterization of all the substrates above-reported see the corresponding Supporting Information (Chapte **6**).

Chapter3

Development of a molecular probe based on TCL phenomenon

3.1 Introduction

In a previous work, Roda *et al.* have reported the development of a new class of TCL organically modified silica nanoparticles (TCL-ORMOSIL NPs), doping the nanometric system with different acridin-based 1,2-dioxetanes [see Ref. 109]. Despite the enhanced emission efficiency (due to the high number of dioxetanes physically entrapped in the silica matrix), and the ease of (bio)functionalization, TCL-ORMOSIL NPs have showed a poor stability in water solution. In particular, it was observed a loss in TCL signal caused by the slow degradation of acridin-dioxetanes during the synthesis. A plausible explanation lies on the capacity of amino groups (necessary for the bioconjugation of NPs) to catalyze the decomposition of cyclic endoperoxides through both an electron transfer mechanism or nucleophilic attack [see Ref. 260, 261]. Furthermore, TCL compounds inside NPs have showed different activation parameters for thermal decomposition, in comparison with those of solid state. In fact, shorter half-life times have been observed for the TCL signal generating from nanometric system, suggesting that silica matrix may promote the decomposition of the endoperoxide unit [see Ref. 262]. In addition to the disadvantages above-cited, silica nanoparticles normally require a great effort during the designing step, since their tendency to aggregate in aqueous solution and give non-specific binding [see Ref. 263, 264]. In fact, a proper and case-specific functionalization of nanoparticles surface proves to be necessary in order to keep the colloidal suspension stable in time. Moreover, the optimization of surface concentrations for both inert and active functional groups ensure high selectivity, reducing the non-specific binding [see Ref. 265, 266].

Aiming to develop a robust, universal and easy-to-handle TCL-based immunoassay, we investigated the possibility to create a molecular probe through the direct derivatization of a 1,2-dioxetane substrate with a bioactive portion. The molecular structure for the designed TCL-probe (**8**) is depicted in Figure 3.1.

The molecular probe consists of three different portions: the thermochemi-

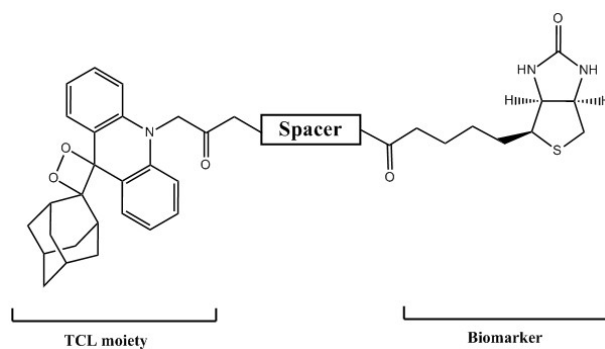
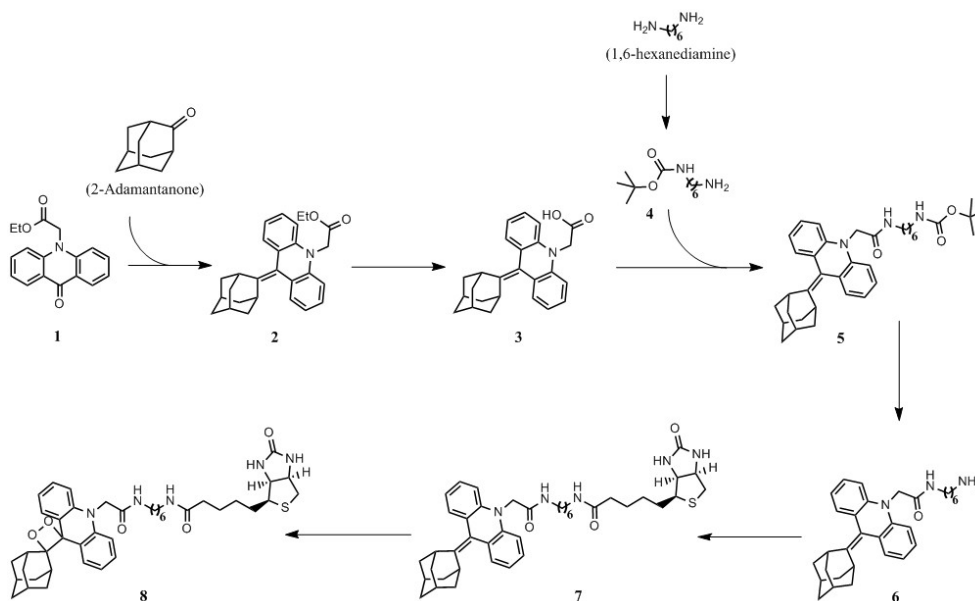


Figure 3.1: Molecular structure of TCL probe.

luminescent substrate, the biomarker unit and a connecting spacer. We chose the parent dioxetane **4a** (see Chapter 2) as TCL unit since it has been extensively studied by our group and it possess good TCL properties, in terms of low decomposition temperature and high fluorescence quantum yield. Concerning the bioactive unit, we decided to exploit the Biotin-Streptavidin interaction for enzyme recognition, functionalizing the TCL substrate with Biotin (Bt). In fact, although a multitude of ligand-binder systems have been described in literature [see Ref. 267], the affinity between the small molecule Biotin and Streptavidin (St) is known to be one of the highest among the enzyme-substrate non-covalent interactions, with a dissociation constant in the femtomolar range [see Ref. 268] and it can resist to very harsh experimental conditions (*i.e.* changes in pH values, high temperatures and so on). Furthermore, the numerous streptavidinated enzymes commercially available, along with the low cost of biotinylation reagents, make the use of Bt-St technology suitable for development of universal immunoassays. Regarding the spacer unit, a six-carbon atoms chain was chosen to preserve the Biotin-Streptavidin interaction, since the binding site is pocket buried about 9 Angstrom beneath the surface of Streptavidin [see Ref. 269].

3.2 Results and discussion

The synthetic strategy followed to obtain the molecular TCL-probe **8** is depicted in Scheme 3.1. Briefly, compound **1** [see Ref. 110], reacts with 2-adamantanone through a McMurry reductive coupling, giving the intermediate **2**, which then hydrolyzes under basic conditions to generate the free carboxylic acid **3**. The condensation reaction between **3** and the mono-protected amine derivative **4** leads to the formation of compound **5**. The latter undergoes a deprotection step, generating the intermediate **6**, followed by the conjugation with the biomarker Biotin to produce the corresponding olefin **7**. Lastly, the alkene precursor **7** reacts with singlet oxygen under irradiation, giving the final product **8**.



Scheme 3.1: Synthetic pathway followed to obtain compound **8**.

Before starting the synthesis of **8**, we insured about the stability of the olefin precursor **7** under oxidative conditions (typical of the photo-oxygenation step). In fact, the tendency of Biotin to generate the corresponding sulfone and sulfoxide byproducts in presence of oxidative species, has been reported in literature [see Ref. 270]. The unwanted oxidation of Biotin could disrupt the interaction with Streptavidin, making the TCL-probe unusable for immunoassay applications. Thus, a known amount of Biotin was tested under photo-oxygenation experimental conditions (O_2 atmosphere and irradiation) [see Ref. 110], and both 1H NMR and HPLC-MS analyses of the crude have confirmed the stability of the bioactive moiety.

During the synthesis of compound **8** we faced a few difficulties that eventually prompted us to change synthetic strategy. In fact, the partial degradation of some intermediates along with solubility-related issues during the purification steps, caused a drop-down in the overall yield obtained for compound **6**. Following, a brief description of the main problems encountered in each synthetic step is provided:

Synthesis of compound 3: While compound **2** was obtained in high yield (around 90%), it was not possible to isolate intermediate **3** from its byproducts. In fact, both 1H NMR and HPLC-MS analyses of the crude have showed the presence of several degradation products such as, 9(10)-acridone, 2-adamantanone and a few other unidentified compounds. Although we did not investigate the cause for degradation of **3**, the long reaction times (around three days) and the harsh experimental conditions might be responsible for the low stability of substrate **3**.

Synthesis of compound 4: As showed in Scheme 3.1, we chose the 1,6-hexanediamine to connect the TCL moiety to the biomarker. Although the mono-protection reaction occurred in high yield, it was not possible to completely purify compound **4** from its precursor. In fact, after testing several experimental parameters for the flash chromatography (*i.e.* different elution phases and amount of silica), we were not able to separate **4** from the starting material 1,6-hexanediamine, which kept co-eluting with the former.

Synthesis of compound 5: Condensation between **3** and the mono-protected 1,6-hexanediamine was carried out under the classical peptide coupling conditions, using 1-cyano-2-ethoxy-2-oxoethylidenedimethylamino-morpholinocarbenium hexafluorophosphate (COMU) as the coupling agent. COMU represents the third generation of uronium-type coupling reagent [see Ref. 271], and it has been recognized as one of the most efficient, especially for solution-phase peptide synthesis, since its by-products are water soluble, and thus, easy to remove. Although the coupling reaction showed high conversion of **3** to **5**, the final yield did not exceed 44%. In fact, the low solubility of **5** in almost all the organic solvents tested during the extraction phase, prevent us to recover it quantitatively.

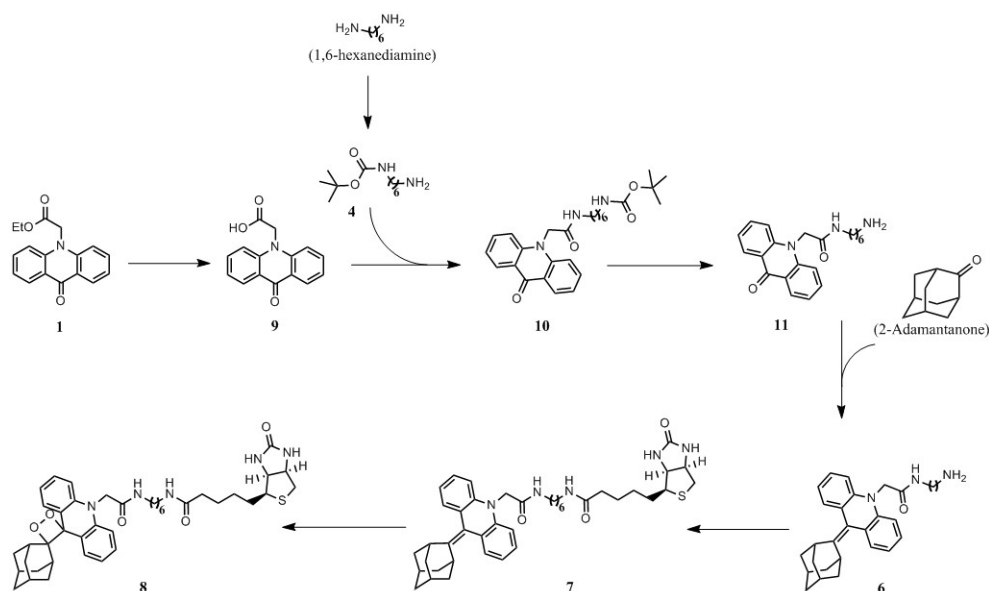
Synthesis of compound 6: The deprotection of **5** was carried out under extreme acid conditions, and the product was purified through multiple liquid-liquid extractions, using basic aqueous solution to deprotonate the quaternary ammonium cation, making it more organic-phase soluble. However, we were not able to isolate **6** from the byproducts already formed in the previous step.

Following the synthetic procedure described in Scheme 3.1, it was not possible to obtain compound **6** with overall yield higher than 30%. This result can be ascribed to the low stability of compound **3** and the solubility-related problems for the further intermediates. Thus, we designed an alternative synthetic strategy depicted in Scheme 3.2.

In the second strategy, we avoided the formation of **3** (unstable), conducting the hydrolysis of the ester unit upon the ketone **1**, rather than the olefin **2**. By this way, we were able to obtain **9** quantitatively, shortening the reaction time from three days down to two hours. Thus, we moved forward linking the acridin moiety to the spacer hexanediamine to obtain compound **10** and, after a deprotection step, intermediate **11**. Then, a McMurry reaction between 2-adamantanone and the already functionalized acridin portion yielded intermediate **6**. From this point on, the synthetic pathway was identical to the previous one.

Following the second strategy, we were not able to raise the yield for compound **6** above 45%. In fact, some of the new intermediates still showed a very low solubility in almost all the organic solvents (during the purification step

through liquid-liquid extraction), preventing us to further optimize the synthetic pathway. However, the second strategy was chosen as the best one, due to the remarkable shorter reaction time and higher yield for the hydrolysis step.



Scheme 3.2: Alternative synthetic pathway followed to obtain compound **8**.

After many synthetic efforts, we finally conducted the photo-oxygenation of precursor **7** to give the final product **8**. Following the classical procedure [see Ref. 111] we noticed a slowing down in the kinetic of oxygen addition, confirmed by ^1H NMR analysis of crude. In fact, the NMR spectrum acquired after 5 hours of irradiation, showed a very low conversion of starting material (SM) into **8**. We explained this result considering the low solubility of precursor **7** in the reaction environment (CH_2Cl_2). Thus, we added a few drops of methanol to better solubilize the starting material, and acquired the ^1H NMR after 5 hours of further irradiation. The second NMR spectrum showed the presence of several byproducts, which were identified through HPLC-MS analysis. In particular, after 10 hours of irradiation we found the crude to be constituted by a mixture of ketone **12**, its sulfoxide derivative (**13**) and the oxidation by-products of **7** and **8** (compound **14** and **15** respectively) (see Figure 3.2). The oxidation of Biotin moiety may be attributed to the enhanced solubility of **7** after methanol addition. Furthermore, this hypothesis might explain why we did not see any sulfoxide derivative during the preliminary test (Biotin dissolved in CH_2Cl_2 under irradiation), since the poor solubility of Biotin in organic solvents.

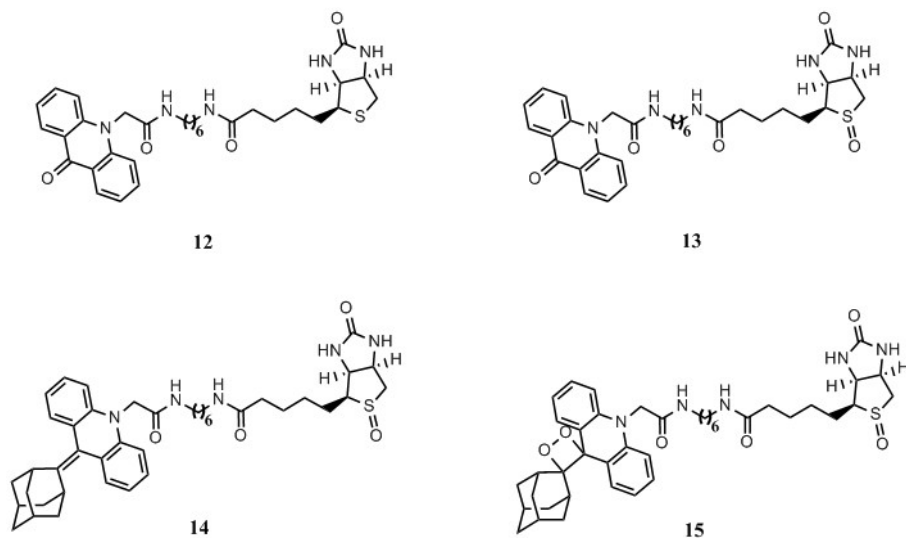


Figure 3.2: Molecular structures of byproducts obtained after the photo-oxygenation of **7**.

3.3 Conclusion

We investigated the development of a TCL-based molecular probe, linking the parent acridin 1,2-dioxetane **4a** to the biomarker Biotin through a 1,6-hexanediamine as spacer. Aiming to synthesize of product **8** in high yield, we explored two different synthetic approaches (see Scheme 3.1 and Scheme 3.2). The main limitations were represented by the poor solubility of almost all the intermediates in organic solvents. This prevented us to quantitatively recover each compound during the purification step (through a liquid-liquid extraction procedure). Moreover, we found product **8** to be unstable under the experimental conditions typical for the photo-oxygenation step. In fact, we confirmed by ^1H NMR and HPLC-MS analyses the presence of both the corresponding degradation products (2-adamantanone and ketone **12**) and the sulfoxide derivatives of **7**, **8** and **12** (see Figure 3.2). For the above-cited reasons, we decided to abandon further investigations upon the molecular TCL probe **8**.

More details about the experimental procedures followed for the synthesis of compounds **1-11** can be found in the Supporting Information (see Chapter 7).

Chapter4

Yellow-emitting thermochemiluminescent Semiconducting Polymer Dots functionalized with Streptavidin for immunoassay applications

4.1 Introduction

A definition for "biosensor" was introduced by IUPAC in 1992, describing it as an analytical device able to detect chemical compounds usually by electrical, thermal or optical signals [see Ref. 272]. The first biosensor was proposed by Clark and Lyons in 1962, who presented an electrochemical system for glucose measuring in biological samples [see Ref. 273]. Since then, thousands of papers have been published on the subject, describing an astonishing variety of biosensors for many types of application: from quality-control in food industry and environmental monitoring to clinical analysis, drug discovery and defence. In the last 40 years, the world market for biosensors has witnessed an apparently endless exponential growth, and predictions for the future estimate a turnover higher than US\$15 billions [see Ref. 274].

Classification of biosensor types can be made considering the different transduction principle behind the generation of analytical signal, along with the specific analyte determination mechanism. The response can be revealed either as an optical (fluorescence, color-changing *etc.*) or (electro)chemical signal, and the detection can rely on enzyme-substrate recognition, DNA-single strand pairing and so on [see Ref. 275, 276].

Regardless the specific technology which is based on, a good biosensor must possess some common characteristics, in order to be suitable for (bio)analytical applications. It should show high sensitivity and linearity within the operational concentrations range, it should be selective towards one or a few target molecules and it should display both a low limit of detection (LOD) and an almost absent background signal [see Ref. 277]. From a practical perspective, a worthy biosensor need to be both affordable and easy-to-handle, limiting the dependence of analysis success on the operator expertise. Furthermore, it should guarantee short analysis times along with automation compatibility, required for high-throughput screening.

The majority of biosensors, currently employed worldwide both in research laboratories and industries, is based on optical detection methods. In particular, fluorescence-based (FL) sensors have been used for detection of small organic molecules, enzymes and gas particles [see Ref. 278], in clinical analysis, diagnostic and environmental control [see Ref. 279, 280]. Furthermore, a multitude of homogeneous and heterogeneous FL-immunoassays have been developed so far [see Ref. 281, 282], exploiting FL-related phenomena such as light-polarization [see Ref. 283], quenching effect and Förster Resonance Energy Transfer (FRET) process [see Ref. 284]. Encapsulation of fluorescent dyes within nanometric biocompatible systems led to the realization of FL-sensors suitable for imaging applications. Thus, silica nanoparticles [see Ref. 285], hydrogels, carbon dots, semiconductive polymers *etc.*, have represented a common matrix for FL-sensors in bioimaging experiments [see Ref. 286]. Recent studies on FL sensors, have proposed their application in cell-sorting process [see Ref. 287] and lateral flow immunochromatography [see Ref. 288]. Despite its popularity, FL-based detection method still suffers of several practical limitations, observable mainly in biological fluids analysis [see Ref. 289]. The scattering of light as well as self-quenching phenomena due to aggregation in solution [see Ref. 290], can affect the outcome fluorescent signal. Besides, the presence of endogenous fluorophores can interfere with either the absorption (inner filter effect) or emission step. Improvements in FL sensors have been achieved through "Time-resolved" fluorescence technique, which relies on the long-lived luminescence exhibited by lanthanide complexes to reduce background interferences [see Ref. 291–293].

Alongside FL-based systems, a widespread class of luminescent sensors involve a chemical reaction for the light generation step. Chemiluminescence (CL) methods have been used for organic/inorganic molecules sensing [see Ref. 294], in determination of volatile species [see Ref. 295] and for bio-active agents measurement. In particular, Chemiluminescent Immunoassay (CLIA) technique have represented the direct descendent of Radio Immunoassay (RIA) method [see Ref. 296], and CL-biosensors have gradually replaced radioactive probes in biological and clinical analyses [see Ref. 297, 298]. Well-established CL biosensors utilize Luminol or Acridinium salts as CL substrates either for direct or indirect labelling, to reach very low limit of detection (down to attomoles of analyte). However, the CL efficiency for both systems do not exceed a few percentage points, due to the poor fluorescence of Luminol and derivatives or the low CL reaction yield for Acridinium salts in neutral or basic solutions [see Ref. 299]. The wide dynamic range, the high sensitivity (further increased by the use of CL enhancers [see Ref. 300]) and specificity towards the target analyte and the good compatibility with almost all the immunology assay protocols, have

made CL-based sensors particularly suitable for automation [see Ref. 301] and integration in on-site testing devices and microfluidic platforms [see Ref. 302, 303]. Although the many advantages of CLIA, the high cost and complexity of CL- apparatus along with the not-always linear and easy-to-understand analytical response still represent important limitations in CL-biosensors applicability.

Similarly to CL systems, Bioluminescent (BL) sensors exploit the emission signal generated by an enzyme-catalyzed chemical reaction for analyte measuring. BL-based methods have been largely employed in biochemistry and biotechnology fields to better understand the molecular mechanism behind a specific physiological process [see Ref. 304]. Applications of BL phenomenon can be found in assay for microbial viability [see Ref. 305–307] as well as bacterial detection [see Ref. 308]. Furthermore, scientific literature is disseminated of examples concerning *in vivo* experiments which rely on BL process for viral pathogenesis investigation, tumor growth monitoring and studies about the interaction between cellular transmembrane receptors and new potential drugs [see Ref. 309, 310]. Although many research groups have been trying to improve the properties of both enzymes [see Ref. 311–314] and substrates [see Ref. 315] involved in the biochemical reaction, BL-based detection techniques still present drawbacks related to difficulty of method standardization, poor stability and oxygen-sensitivity of the enzymatic catalyst and a limited number of Luciferase and Luciferin commercially available [see Ref. 316].

Another main category of sensors for (bio)analyses exploits the Electro-Chemiluminescent (ECL) phenomenon as transduction principle [see Ref. 317, 318]. Electrogenerated chemiluminescence have represented a powerful analytical tool for both *in vitro* and *in vivo* applications. In fact, It has been used in immuno- and DNA-assays development [see Ref. 319], for detection of peptides and nucleic acids, pathogenic bacterial, single cells *etc.* [see Ref. 320, 321]. The first class of ECL-based sensors used to employ polycyclic aromatic hydrocarbons (PAHs) as electro-active species [see Ref. 322]. Although the very interesting redox properties of PAHs, many of these organic molecules presented low solubility in aqueous solution along with a poor stability in presence of molecular oxygen. Thus, a well-established class of ECL biosensors have been utilizing the Ruthenium complex $\text{Ru}(\text{bpy})_3^{2+}$ as emitting specie, exploiting its electrochemical and photophysical properties for high-sensitive analytical measuring [see Ref. 323, 324]. Further improvements of ECL-based technique have been achieved exploring new electro-active luminescent nanomaterials such as semiconductor quantum dots (QDs), metal nanocluster (MCs) and upconversion nanoparticles (UCNPs) [see Ref. 325]. Despite the high sensitivity and robustness of electrochemiluminescent biosensors, the applicability of ECL methods is still limited by the often

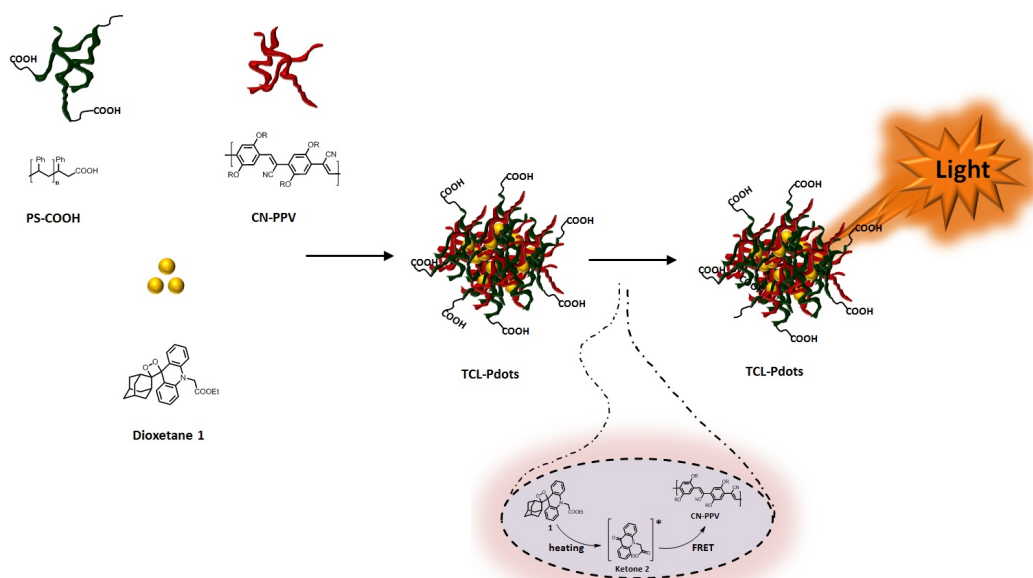
prohibitive cost and complexity of apparatus [see Ref. 326].

In recent years, semiconducting polymer dots (Pdots) have affirmed themselves as a new class of highly fluorescent nanomaterials, which have found application especially in bioimaging. Pdots-based probes have been successfully used for *in vivo* dynamic monitoring of small molecules such as HNO and HClO [see Ref. 327–329], in cell sorting [see Ref. 330] and for high-resolution fluorescence imaging [see Ref. 331–333]. In comparison with classical organic fluorophores, Pdots are characterized by some remarkable photophysical properties which make them particularly suitable for biological and medical applications [see Ref. 334, 335]. For instance, they possess enhanced photostability, high fluorescence quantum yield, fast radiative rates and very narrow band emission. Moreover, by changing the polymer matrix, it is possible to easily tune the wavelength of emitted light, thus creating a wide panel of Pdots-based sensors able to cover the entire visible spectrum (from blue light to NIR emission) [see Ref. 336–341].

Thermochemiluminescence (TCL) technique has been recently re-proposed by our group, as innovative detection method for immunoassay applications [see Ref. 107–109]. TCL process consists in the light production which occurs when a thermally unstable substrate (typically 1,2-dioxetane derivatives) is heated above a threshold temperature. Indeed, the energy released during the thermal decomposition of the endoperoxide unit [see Ref. 2] is high enough to bring one of the two fragments to its electronically excited state, from which it can relax emitting a photon (see Chapter 1). TCL-based methods benefit from several advantages particularly related to the reagentless nature of the process itself, such as short times of analyses and simplicity of the apparatus employed. Furthermore, the absence of an excitation source strongly reduce the matrix effect (due to endogenous fluorescent species or light scattering), allowing to reach high sensitivity and reproducibility. In addition, by changing the molecular structure of 1,2-dioxetane it is possible to finely tune the TCL properties in terms of higher fluorescence quantum yield and lower decomposition temperatures [see Ref. 110, 111].

Herein, we describe, for the first time, the synthesis of a TCL-based Pdot probe as innovative thermoresponsive biosensor for immunoassay applications. Following a nanoscale co-precipitation technique [see Ref. 342] we obtained cyano-polyphenylene vinylene (CN-PPV)-based Pdots doped with acridin 1,2-dioxetane derivative **1** (Scheme 4.1). The latter can undergo a fast thermal decomposition at temperatures above 100 °C generating two fragments, one of which (ketone **2**) in its electronically excited state. Exploiting a FRET mechanism occurring between the 1,2-dioxetane inside the nanoparticles (more precisely the ketone derivative) and the surrounding polymer matrix (Scheme 4.1), these

nanoprobes are able to emit yellow light (550 nm wavelength) after heating the solution above the threshold temperature. Furthermore, the overall efficiency of light generation has been enhanced thanks to the higher fluorescence quantum yield (Φ_F) of CN-PPV [60%, see Ref. 343], in comparison with Φ_F of ketone **2** [11%, see Ref. 107]. Besides, life-time measurements for the excited ketone **2** have confirmed an efficiency for the FRET mechanism of 90%.



Scheme 4.1: Synthesis of 1,2-dioxetane **1**-doped semiconductive polymer dots (TCL-Pdots) through the nanoprecipitation method.

The synthetic procedure for TCL-Pdots was optimized in order to maximize both the load of 1,2-dioxetane inside the NPs (*i.e.* the TCL signal) and the nanoparticles size. Furthermore, TCL-Pdots have been conjugated with the biomarker Streptavidin to make them suitable for detection of biotinylated analytical species. The analysis of TCL-Pdots stability at 4 °C (storage conditions) and 37 °C (typical temperature for the immunoassay incubation step) was assessed, revealing a loss in TCL signal lower than 30 or 20 % after 20 days or 4 hours respectively. The applicability of our nanoprobes as labelling agent was tested in a proof-of-concept non-competitive immunoassay for detection of Immunoglobuline G (IgG), which has shown a TCL signal proportional to the IgG concentration and a limit of detection (LOD) for the enzyme in the nanomolar range.

4.2 Results and discussion

4.2.1 Preparation of TCL-Pdots nanoprobe

The 1,2-dioxetane-doped Pdots were obtained following a nanoprecipitation method (Scheme 4.1) [see Ref. 342] where CN-PPV, substrate **1** and carboxylic acid functionalized polystyrene (PS-COOH) were blended together in anhydrous THF and then quickly injected into Milli-Q water under sonication. We obtained a quite monodispersed nanometric particles with an average diameter of 34 nm, as calculated from dynamic light scattering (DLS) analysis. Differently from a previously reported procedure [see Ref. 344], we chose PS-COOH polymer, rather than PS-PEG-COOH, to cover the particles surface with carboxylic acid units. The absence of the hydrophilic polyethylene glycol block should be able to limit the swelling of Pdots during the heating phase, thus ensuring more temperature-stable nanoparticles and preventing the potential leaking of **1** outside the nanoshell at high temperatures [see Ref. 345–347]. First attempts to make Pdots have shown a dependence of both the particle size and the amount of entrapped 1,2-dioxetane from the experimental conditions used in the nanoprecipitation step.

Thus, aiming at the optimization of Pdots dimension as well as their loading capacity of **1**, we conducted a stepwise screening of the three variables selected: volume of THF injected, percentage of PS-COOH and amount of 1,2-dioxetane. In particular, we investigated changes in the hydrodynamic diameter (by DLS analyses) and TCL emission signal (using a CCD camera) of Pdots for each optimization step (Table 4.1).

As reported in Table 4.1, the screening of both THF volumes and PS-COOH % (v/v) have shown a similar trend in diameter changing, with an initial increase in Pdots size and a subsequent reduction in particles dimensions for THF volume higher than 9 mL and PS-COOH % (v/v) greater than 7%. On the other hand, only a slight increase in TCL signal was observed for bigger nanoparticles, suggesting that the loading capacity of 1,2-dioxetane **1** might not be strongly influenced by Pdots size. An opposite tendency in the variation of particles size was observed during the screening of compound **1** % (v/v). Indeed, the diameter of Pdots was, generally, inversely proportional to the amount of doping substrate. With the goal to maximize the loading of 1,2-dioxetane **1**, but still keeping particles dimensions to relatively low values, we chose the best compromise among the variables investigated, namely 7 mL of THF injected, 7.1 and 3.6 % (v/v) of PS-COOH and 1,2-dioxetane respectively. The selected experimental conditions allowed us to obtain quite monodisperse nanoparticles with an average diameter of 42 nm, as confirmed by both DLS experiments and TEM images (Figure 4.1 a and b, respectively).

Table 4.1: Diameter and loading capacity of Pdots obtained in each step of the optimization screening.

Step I: screening of THF volume injected, keeping constant the amount of compound 1 , CN-PPV and PS-COOH.			
Entry	Volume of THF (mL)	Diameter (nm)	TCL signal \pm SD (u.a) ^{a,b}
1	1	16,2	415,44 \pm 141,70
2	3	13,1	461,82 \pm 37,80
3	5	12,7	309,54 \pm 20,14
4	7	21,1	522,13 \pm 37,71
5	8	40,5	659,44 \pm 54,88
6	9	52,3	610,29 \pm 9,92
7	10	33,8	621,48 \pm 4,32
Step II: screening of PS-COOH % (v/v), keeping constant the volume of THF (7 mL) and the amount of compound 1 and CN-PPV.			
Entry	PS-COOH % (v/v)	Diameter (nm)	TCL signal (u.a) ^a
1	0.7	21.3	778,13 \pm 43,62
2	1.4	21.1	558,73 \pm 68,78
3	4.3	25.0	834,3 \pm 8,34
4	7.1	32.4	1103,17 \pm 50,4
5	10.0	20.2	972,94 \pm 41,3
Step III: screening of compound 1 % (v/v), keeping constant the volume of THF (7 mL) and the amount of PS-COOH and CN-PPV.			
Entry	Compound 1 % (v/v)	Diameter (nm)	TCL signal (u.a) ^a
1	1.4	43.5	829,46 \pm 43,3
2	3.6	42.0	1103,17 \pm 50,4
3	5.7	28.5	1046,78 \pm 52,18
4	8.6	36.5	1086,1 \pm 51,67

^aTCL signal was measured through a CCD camera, acquiring images for 30 min at 110°C. ^bTCL emission as mean \pm SD of three independent measurements.

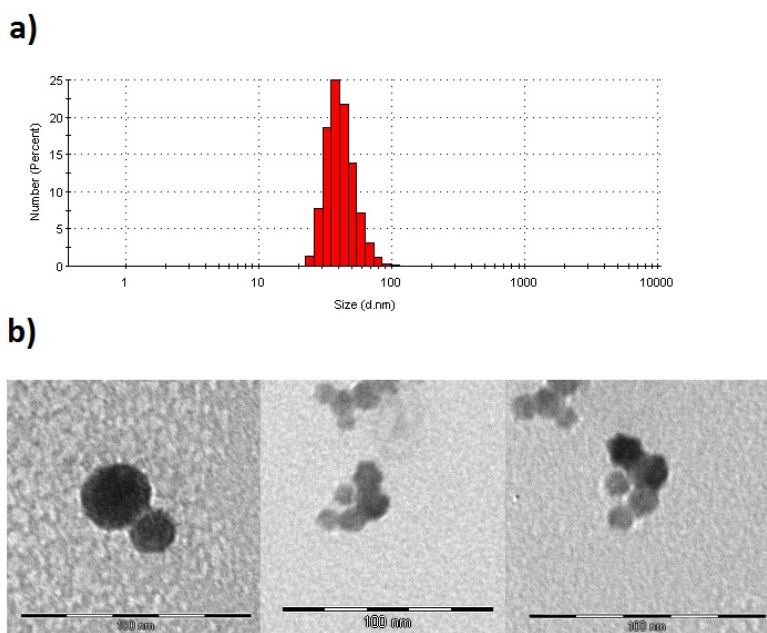


Figure 4.1: a) Dynamic light scattering analysis and b) TEM image of TCL-Pdots.

Then, TCL-Pdots were bioconjugated to Streptavidin (SA), following a previously reported procedure [see Ref. 339]. In particular, we performed a EDC-catalyzed codensation reaction between the carboxylic units of PS-COOH chains and amino groups of SA, to make a strong amide bond. In order to remove all the free enzyme as well as EDC byproducts, TCL-Pdots-SA were filtered with a 100 Da cutoff centrifugal membrane first, then purified by size exclusion chromatography. The absence of 1,2-dioxetane absorption in the UV-vis of filtrate, along with the TCL emission from Pdots-SA after chromatography (see Figure 8.1 of Supporting Information) confirmed the successful encapsulation of **1** inside the polymer nanoparticles.

4.2.2 TCL-emission and FRET experiments

To the best of our knowledge, Pdots have been largely used either as direct fluorescent sensors or as donor species in organic dye-coupled systems [see Ref. 348]. Here, we took advantage of the excellent light-harvesting ability of CN-PPV to collect the light produced by decomposition of 1,2-dioxetane within the polymeric nanoshell. Thus, the nanoparticle did not represent only a water-soluble carrier for **1**, but it actively participated in the light enhancement process.

Considering the extended overlap between the emission of dioxetane **1** (*i.e.* ketone **2**, which is the electronically excited fragment generated after thermal decomposition of **1**) and the absorption of CN-PPV-based Pdots (see Figure 8.2

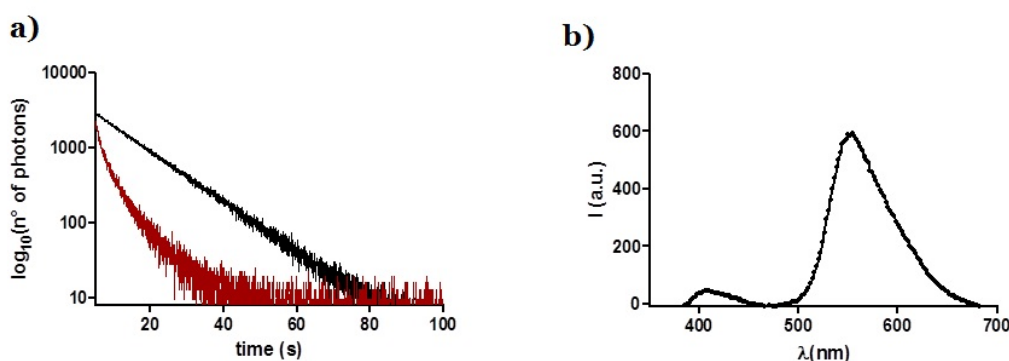


Figure 4.2: a) Lifetime measurements showing the fluorescence decay of ketone **2** (red line) and **2** in presence of quencher CN-PPV (black line); b) TCL emission spectrum for a solution of dioxetane **1** and CN-PPV polymer in THF.

of Supporting Information), we were expecting 1,2-dioxetane **1** to be able to efficiently transfer its energy to the polymer chains through a Förster resonance energy transfer. Therefore, we performed fluorescence life-time measurements of nanoparticles containing either ketone **2** alone or blended with CN-PPV to estimate the efficiency of FRET mechanism. Specifically, we conjugated compound **2** with amino-functionalized polystyrene (PS-NH₂), and then, we synthesized two different types of NPs according to the above-reported procedure (see Supporting Information), injecting PS-NH₂-**2** in H₂O with or without CN-PPV polymer.

The analysis of emission decays (Figure 4.2 a) has shown a remarkable decrease for the lifetime of excited ketone **2** in presence of CN-PPV. In fact, for nanoparticles containing only acridanone **2** we measured a lifetime of 12.9 ns (τ_0), which dropped down to 1.3 ns (τ_1) when the semiconductive polymer was blended together. Using the equation 4.1 [see Ref. 349], we calculated an efficiency for the quenching process (ϕ_{FRET}) of 90%.

$$\phi_{FRET} = 1 - \frac{\tau_1}{\tau_0} \quad (4.1)$$

Although the high efficiency of the FRET process, we noticed the fluorescence of CN-PPV to be interestingly dependent on the temperature, in terms of both the intensity and position of emission maximum (see Figure 8.5 of Supporting Information). Raising the temperature from 25 to 110°C (typically used during TCL signal acquisition), we observed a decrease in emission intensity of about 45% along with a shift of λ_{max} towards shorter wavelengths (from 600 to 550 nm). Assuming the same percentage decrease for ϕ_F of CN-PPV, Pdots system still represented a valid enhancer of light emission, ensuring a TCL signal about three times higher than 1,2-dioxetane **1** itself.

The occurrence of FRET mechanism was further confirmed by TCL emission experiment, in which compound **1** was thermally decomposed in presence of CN-PPV polymer and the emission spectrum was recorded. We dissolved both 1,2-dioxetane and semiconductive polymer together in THF first, then we raised the temperature up to 110 °C and started acquiring the emission. We did not analyze a solution of TCL-Pdots directly because it was not possible to let the solvent evaporate completely within the acquisition time. On the other hand, the high temperature ensured a quick evaporation of THF, allowing us to observe the TCL emission from a dry state sample, which is what we believe might be the actual system during TCL signal acquisitions. As shown in Figure 4.2 b, heating a solution of 1,2-dioxetane **1** and CN-PPV polymer above 100 °C generated a strong emission at 550 nm, ascribing to the excited polymer chains against a poor signal from ketone **2**.

4.2.3 Activation parameters of **1** and TCL-Pdots-SA stability

The thermal decomposition of 1,2-dioxetane substrates is known to follow a first-order kinetic and it can be analyzed according to a standard Arrhenius equation 8.1, to evaluate the activation parameters of the TCL reaction itself. k represents the kinetic constant while A and E_a are the preexponential factor and the activation energy, respectively. T represents the temperature in Kelvin and R the gas constant.

$$k = Ae^{-\frac{E_a}{RT}} \quad (4.2)$$

In a previous study addressed to the encapsulation of acridin-based 1,2-dioxetanes inside silica particles [see Ref. 107, 109, 110], we noticed a quite strong dependence of both the activation energy (E_a) and preexponential coefficient (A) of **1** from the surrounding environment. Thus, we investigated which effect the polymeric shell of NPs might have upon the thermal decomposition of 1,2-dioxetane substrate. By acquiring the emission decay at different temperatures, we obtained the kinetic constants k (*i.e.* the inverse of the decay time in seconds) of TCL process and then, we calculated both E_a and $\ln A$ of **1** from the Arrhenius plot (see Figure 4.3 a).

We found the E_a and $\ln A$ of substrate **1** to be $21.12 \pm 2.4 \text{ kcal mol}^{-1} \text{ K}^{-1}$ and 21.42 ± 3.11 respectively, which were lower than the activation parameters of 1,2-dioxetane **1** in its dry state [see Ref. 111]. However, using these results to extrapolate the life-time of TCL substrate at different temperatures, we calculated a remarkable delay in thermal decomposition of **1** occurring for high values of T (°C), which was confirmed by kinetic experiments. For instance, as shown in

Figure 4.3 b, extinction of TCL signal at 110 °C fully occurred in a period of time longer than 30 minutes, suggesting a shielding effect of the polymeric matrix towards the increase in temperature.

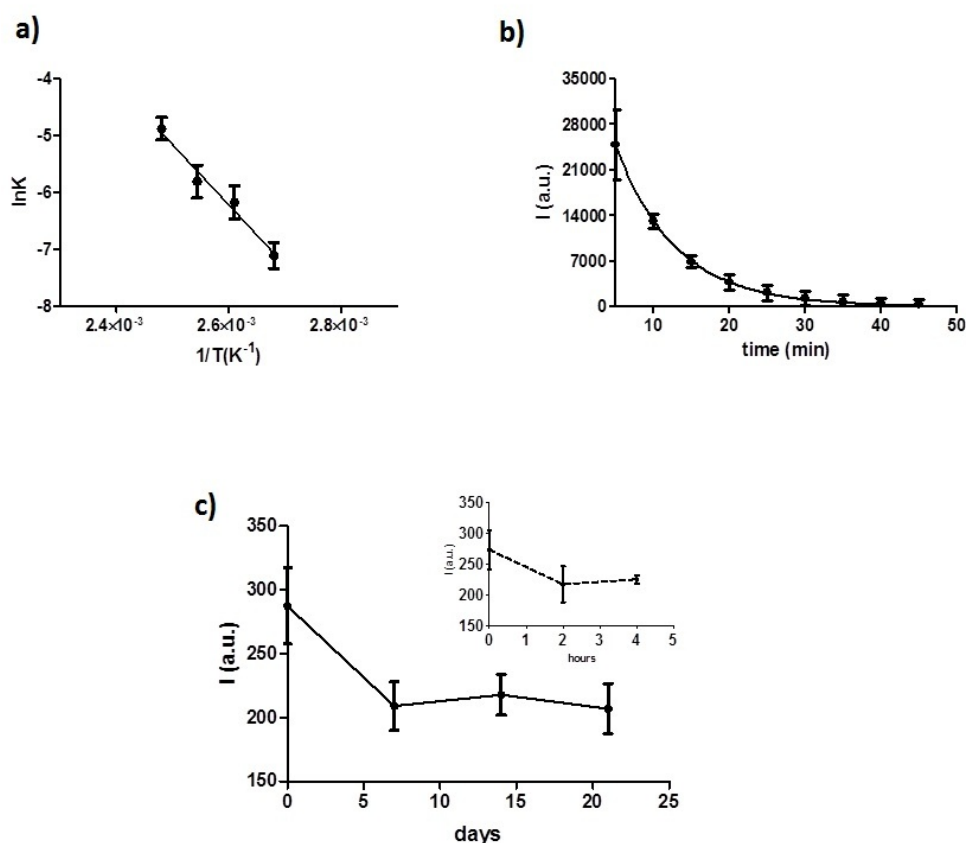


Figure 4.3: a) Arrhenius plot obtained from thermal decomposition studies of dioxetane **1**, displaying the logarithm of kinetic constants at different temperatures against the inverse of temperature; b) TCL emission decay of substrate **1**, occurring at 110 °C; c) TCL signal acquired to assess the stability of TCL-Pdots-SA over time, showing the emission of nanoparticles solution kept at 4 °C (solid line) or 37 °C (dashed line).

In order to be suitable for immunoassay applications, TCL-Pdots-SA should demonstrate a good stability throughout all the operational steps. We therefore monitored the TCL signal over the storage conditions (in refrigerator at 4 °C) as well as during incubation at 37 °C. In Figure 4.3 c, we show the plots TCL signal vs time of different aliquots of NP solutions kept at 4 (solid line) or 37 °C (dashed line). It can be clearly seen how TCL-Pdots-SA were particularly stable over time, giving a loss in TCL signal lower than 30%, at storage conditions, or 20% at 4 °C. Comparing these results with the stability of a previously reported silica-based TCL nanoparticles [see Ref. 109], we concluded that 1,2-dioxetane **1** was much more stable when encapsulated into a polymeric matrix rather than

in presence of silica atoms. This evidence could be explained considering the high light-harvesting capacity of CN-PPV-based Pdots, which might act as filter for the external ambient light. In fact, it has been already demonstrated how benzoate-based 1,2-dioxetanes, bearing an aromatic ring as chromophore unit, can undergo a light-induced decomposition under normal room illumination [see Ref. 350]. This photo-catalyzed degradation would be even more evident for compound **1**, due to the higher molar extinction coefficient of acridin unit. We therefore hypothesize that polymeric shell could prevent substrate **1** to absorb the light from the outside very efficiently.

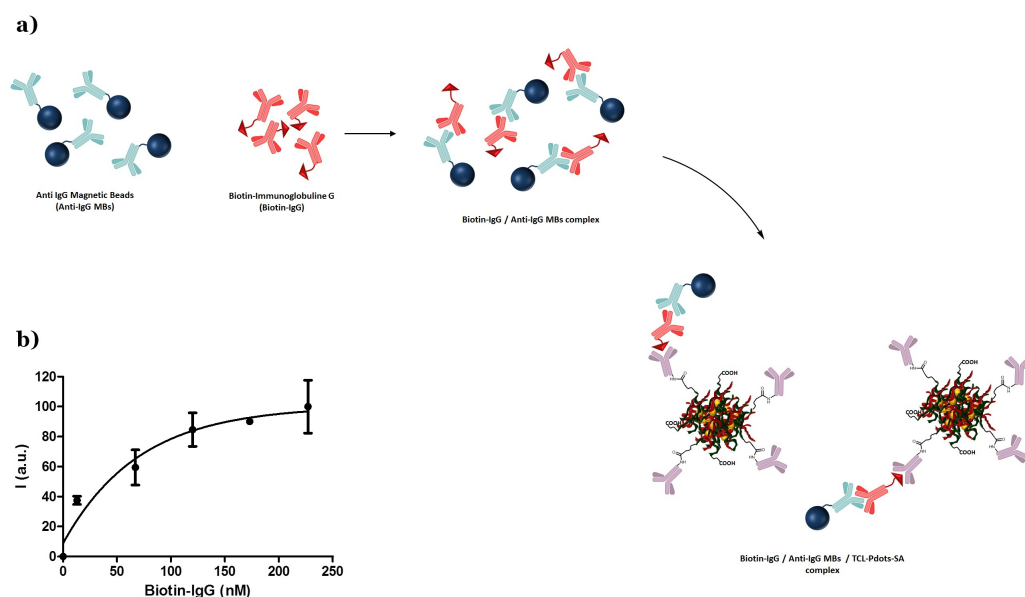
4.2.4 Development of a TCL-Pdot-SA based immunoassay for IgG detection

The applicability of TCL-Pdots-SA was tested in a proof-of-concept immunoassay for determination of Immunoglobuline G (IgG) (Scheme 4.2 a). In particular, we combined the biofunctionalized magnetic bead (MB) technology with TCL-based detection method to build up a non-competitive sandwich-type assay for detection of Biotinylated targets (Scheme 4.2a). In details, equal volumes of Anti-IgG magnetic beads (Anti-IgG MBs) were incubated with a solution of Biotinylated IgG (Biotin-IgG) at different concentrations. After the washing steps, same volumes of Streptavidinated TCL nanoprobe were added to the solutions to selectively interact only with the bounded Biotin-IgG. An additional washing step followed by elution of Pdots from MBs allowed us to effectively recover TCL-Pdots-SA/Biotin-IgG complex in basic aqueous solutions, which were analyzed by a CCD camera in a classical TCL experiment. The entire immunoassay analysis was performed in less than 5 hours, which is a quite short time, in comparison with classical CL- or BL-based assays.

The sandwich-like immunoassay developed for detection of IgG has shown a good sensibility and a TCL signal proportional to the analyte concentration (Scheme 4.2 b) in the nanomolar range. Furthermore, although it was just a proof of the applicability of TCL-Pdots-SA nanoprobe as labeling agents in (bio)analyses, the TCL immunoassay allowed us to reach a quite low limit of detection (LOD), namely 13 nM of Biotin-IgG.

4.2.5 Conclusion

Herein, we described the synthesis of the first thermochemiluminescent Pdot-based (TCL-Pdots-SA) nanoprobe suitable for immunoassay applications. Following a nanoprecipitation method, we easily obtained quite monodisperse TCL-Pdots, employing CN-PPV as the polymer matrix and 1,2-dioxetane **1** as TCL



Scheme 4.2: a) Representation of the proof-of-concept non-competitive sandwich-type immunoassay for detection of IgG, b) Calibration curve obtained from the TCL-Pdots based immunoassay. TCL signal was calculated as mean of three independent measurements

substrate. The NPs were successfully functionalized with Streptavidin to generate TCL nanolabels specific for Biotinylated-target detection. Furthermore, TCL-Pdots-SA have shown a remarkable stability over time, giving a minimal loss in TCL signal under storage conditions as well as during the immunoassay incubation phase. Exploiting a highly efficient ($\phi_{FRET} = 90\%$) FRET mechanism occurring between dioxetane **1** and the surrounding polymer matrix, we were able to shift the emission of TCL substrates from blue to yellow wavelengths. Besides, TCL signal from Pdots was further amplified thanks to the higher fluorescence of CN-PPV polymer. Lastly, we tested our TCL-nanoprobes in a proof-of-concept non-competitive immunoassay for detection of IgG, which showed a good sensibility in the nanomolar range and a LOD for IgG of about 10 nM. We firmly believe TCL-Pdots based systems to represent a new valid alternative to the classical luminescent probes used so far in (bio)analytical analyses. In fact, combining the advantages of Pdots (*i.e.* high ϕ_F and light-harvesting capacity, biocompatibility, tunability *etc.*) with the inherent characteristics of TCL-based detection methods (no further reagents required for luminescent reaction, thermally-triggered light generation *etc.*) a broad panel of ultrabright TCL nanoprobes could be designed for development of high sensitive ultra-fast immunoassays.

Chapter 5

Realization of a portable device for (bio)analytical analyses, combining the smartphone technology with TCL-based detection methods

5.1 Introduction

In recent years, smartphone technologies have been gaining several attentions by the scientific community, especially among researchers actively involved in development of new (bio)analytical methods suitable for implementation in Point-of-Care (POC) test [see Ref. 351–357]. In fact, the inherent characteristics of a smartphone-based detection methodology perfectly match some crucial requirements that a robust and user-friendly diagnostic device should possess for POC applications, namely a reduced dimensions and weight of detector (smartphone's camera) and autonomous power supply system (phone's battery) which make it portable and easy-to-handle, even by unskilled operators. Furthermore, the increasing computing capabilities of latest smartphones, the multitude of built-in applications (apps) available and the possibility to quickly diffuse a lot of data into the worldwide network through direct internet connection, have made smartphones almost self-sufficient in development of analytical portable devices. In principle, using a smartphone-based detection method it can be possible to acquire the analytical signal *in situ*, to perform data analyses and to communicate the results to a specialized laboratory or a physician all at once, for almost real-time diagnosis.

Herein, we describe the realization of a home-made portable device to combine TCL-based detection techniques with smartphone technology. All the different items constituting the apparatus (Figure 5.1) have been fabricated exploiting a 3D printing process [see Ref. 358] and acrylonitrile-butadiene-styrene (ABS) as starting material. The device was tailored to the 41-megapixel camera of a Nokia Lumia 1020 (used as detector) and 1,2-dioxetane **1** was chosen as TCL substrate because of its good TCL stability and high fluorescence quantum



Figure 5.1: Different 3D-printed items which constitute the TCL-based portable device.

yield [see Ref. 111]. Preliminary experiments have been conducted to evaluate the performances of our portable TCL-based device for future immunoassay applications. In particular, we obtained a calibration curve for thermal decomposition of **1**, which has shown a good linearity of TCL signal along with quite low limit of detections. In addition, we tested the feasibility of FRET mechanism occurring between our TCL substrate and two different energy acceptors, in order to modulate the emission signal towards longer wavelengths.

5.2 Materials and Methods

5.2.1 Device fabrication

The analytical device (Figure 5.1) was designed using an open-source software for 3D images (Schetckup 2016) first, then it was easily obtained employing a low-cost commercial 3D printer (Replicator 2X Desktop 3D Printer, MakerBot Industries, New York, NY). The project files were exported as .stl files and MakerWare v.2.4 software, an algorithm that slices digital into thin layers for 3D printing, was used to define printing options and settings. As shown in Figure 5.1, the device consists of three main components:

- a disposable analytical cartridge, in which a defined area (0.6 x 0.4 cm) for sample loading was created exploiting the wax printing method [see Ref. 359]. Specifically, the rectangular-shape region for solution spotting (white region) was obtained through a negative printing approach, injecting a wax-based solid ink all around the selected area and heating the paper cartridge up to 120°C for a few minutes, in order to let the wax ink penetrate in between cellulose fibers. The surrounding hydrophobic walls, thus, can

prevent the spotted solutions from leaking out during acquisition of TCL emission.

- a cubic-like dark box (2 x 2 x 1.5 cm), comprising both a 0.2 cm thick channel, for cartridge insertion and holding, and a mini-heater element (0.8 x 1.2 cm) for TCL signal generation. The latter was obtained encasing a serpentine nickel/chrome thin-film resistance between two kapton layers. Besides, the dark box is encapsulate within an additional round-shape unit to better fit the smartphone adapter. A USB wire and a on-off type switch were used to connect the mini-heater to the power supply, represented by a common portable power bank.
- an external smartphone adapter, specific for Nokia Lumia 1020 model, required for the correct positioning of sample under the phone's camera. Moreover, the adapter includes a plano-convex plastic lens (diameter 0.6 cm, focus 0.12 cm), which focuses the image of the analyzed area directly onto the camera's sensor.

5.2.2 Nokia Lumia 1020 for image capturing and processing

We chose the Nokia Lumia 1020, as smartphone to be integrated in our portable device, since it possesses a 41-megapixel camera which can ensure outstanding high-resolution images acquisition. Moreover, the 1020's dual-core Snapdragon processor and 2GB of RAM allows to both capture and process pictures in very short times. As for the majority of smartphones, Lumia 1020's camera exploits the complementary metal-oxide semiconductor (CMOS) technology [see Ref. 360].

A CMOS circuit consists of an array of identical photo sensors organized within a grid. Once the light reaches the photo sensor, it is transformed into a digital signal [see Ref. 361] which is proportional to the incident light intensity. A three colour (red, green and blue) filter array (CFA) with a Bayer pattern is placed over the CMOS grid [see Ref. 360], causing each photo sensor to detect only one colour band of the UV-vis spectrum. Thus, images are represented by the sum of distinct signals according to a RGB pattern.

In order to decide what delay in time acquisition would have ensured the highest intensity for TCL signal, we followed the thermal decomposition of compound **1** over time (5 μL of **1** 4 mM in ACN), acquiring 10s images through a CCD camera (see Figure 5.2b). To obtain the calibration curve (Figure 5.3), 10 μL of **1** in ACN at different concentrations (ranging from 21 μM to 2 mM) were spotted onto the paper-based cartridge, and the solutions were heated up using the embedded mini-heater element. After a 90s time delay, we took a photo

using the Nokia Lumia's camera with the following default parameters for image acquisition: a 4s shutter opening, ISO value of 4000 and brightness of 14. The on-paper FRET experiments (Figure 5.4 a) were performed spotting a solution of **1** (10 μ L, 0.1 mM) together with 9,10-Bis(phenylethynyl)anthracene (BPEA, 10 μ L, 4 mM) or BPEA and Kiton red-620 dye (10 μ L, 4 mM), and following the above-reported setting for images acquisition. For evaluation of the signal-to-noise (S/N) ratios of the images, signals (S) were calculated by averaging the pixel intensity over the analyzed area, while noise (N) was taken as the standard deviation of the mean pixel intensity in a dark image area.

5.3 Results and discussion

In order to ensure fast and easy-to-perform analyses, we designed our portable device in such a way that it could employ cartridges made of simple cellulose. In fact, paper-based sensors have recently gained increasingly attentions since they represent a new alternative technology in the fabrication of simple, low-cost, user-friendly disposable apparatuses for (bio)analyses. Cellulose material have been largely used in sensors fabrication, to develop analytical devices for food quality control, environmental monitoring and assessment and clinical diagnosis [see Ref. 362–364].

Despite its versatility and low cost, a paper-based platform usually requires specific chemical or physical treatments to make it suitable for bio-applications. In addition to surface functionalization and derivatization, great efforts have been made trying to confine the liquid to a specific region of paper cartridge, such as photolithography [see Ref. 365], analogue plotting [see Ref. 366], inkjet printing [see Ref. 367] and etching [see Ref. 368], plasma treatment [see Ref. 369], paper cutting [see Ref. 370], flexography printing [see Ref. 371], screen printing [see Ref. 372], and laser treatment [see Ref. 373]. Here, we employed the wax-printing technology [see Ref. 359] to create a well-defined spot for sample loading on the cellulose cartridge, avoiding the potential diffusion of solution out from the analyzed area. Furthermore, since the fabrication of our paper-based cartridges required the use of a normal inkjet printer, it can be accomplished with simplicity even by unskilled operators.

TCL-based detection methods should be able to ensure high light detectability *per se*, due to the inherent reagentless nature and thermally-triggered signal of TCL process, which can prevent, in principle, any background interferences from the matrix. The use of a dark box (Figure 5.1) to hold both the mini-heater element and the cartridge, allowed us to further enhance the device's sensibility avoiding the external environmental light to be detected by the phone's camera, thus,

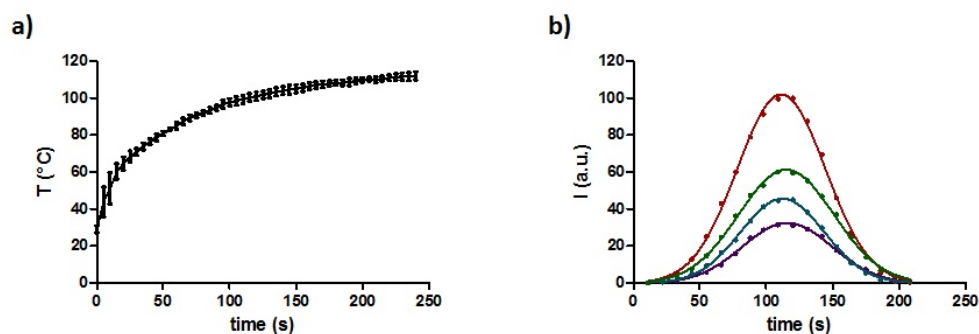


Figure 5.2: a) Thermal response of the resistance employed for the mini-heater fabrication; b) TCL signal generated by different concentrations of dioxetane **1** in ACN over time, using a CCD camera as detector and our portable device for sample heating.

lowering the background noise.

We designed and created the mini-heater element to perfectly fit into the dark box, ensuring a quick and homogeneous heating of cartridge (*i. e.* the loaded sample). However, we needed to assess the performance of our mini-heater first, in order to use it for reproducible analyses. We therefore measured the thermal response of the resistance, using a Type K thermocouple to detect the increase in temperature of the mini-heater surface, over time (Figure 5.2 a). We noticed the thermal profile of the resistance to be very reproducible over several heating experiments, giving a fast increase in temperatures up to 100 - 110 °C within 3 minutes. In addition, using a CCD camera as detector and our portable device for sample heating, we measured the TCL signal generated by different concentrations of dioxetane **1** in ACN, over time. As shown in Figure 5.2 b, TCL signal has followed a Gaussian-shape distribution for each concentration analyzed, with a maximum emission pick centered around 120 seconds. The atypical decomposition profile of **1** showed in Figure 5.2 b could be explained considering it as the overlap of two different kinetic processes: from one hand, decomposition of **1** keep speeding up along with the increase in temperature upon the heater's surface, then, once the temperature stays constant, decomposition of substrate **1** follows the usual first-order decay.

Aiming our portable device to allow very fast analyses, still ensuring high sensitivity, we decided to reduce the initial time delay (before each acquisitions) of about 30 sec. Thus, we started acquiring TCL emission after 90 sec from the device switching-on, rather than 2 minutes. Doing so, we were able to remarkably shorten the total time acquisition of TCL signal, saving about 30 sec for each image, versus a minimal loss in emission intensity (less than 10%).

Figure 5.3 shows the calibration curve we obtained from TCL experiments, using our portable device and the smartphone's camera. We found TCL signal

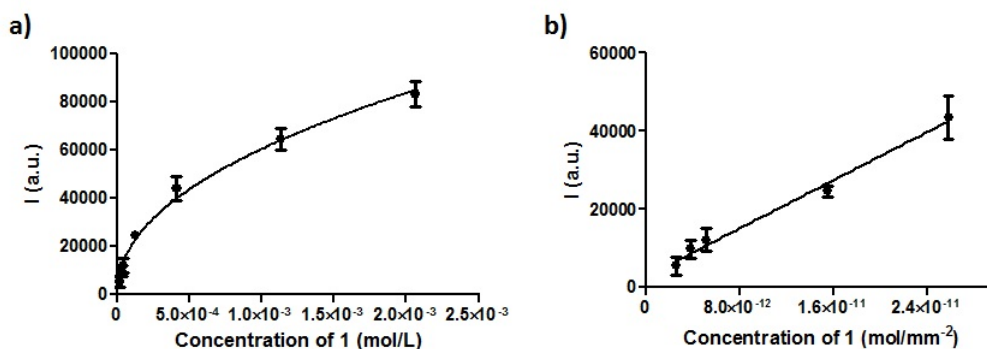


Figure 5.3: a) Calibration curve obtained measuring the TCL signal generated by solutions of **1** at different concentration; b) Linear response of TCL-based portable device for lower concentrations of **1**.

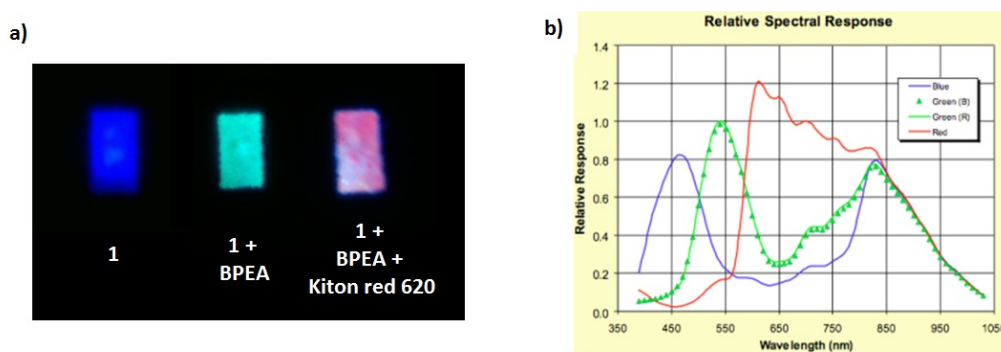


Figure 5.4: a) TCL images of solutions containing dioxetane **1** alone or together with energy acceptors BPEA (green light) and Kiton red-620 (red light); b) Spectral response for a CMOS-based camera.

to be proportional to the amount of substrate **1** within the entire concentrations range explored. Specifically, TCL signal has shown a different trend for low and higher concentrations of **1**, giving a linear or exponential tendency, respectively. We, then, measured the lowest amount of dioxetane **1** detectable by our device, which corresponded to a LOD of $2.6 \text{ picomol mm}^{-2}$.

Finally, we tested the feasibility of employing our TCL-based portable device in multiplex biosensing systems based on FRET mechanism. Thus, we analyzed solutions of substrate **1** in presence of two different energy acceptors, namely BPEA and Kiton red-620. The first one emits around 500 nm, while Kiton red-620 produces a photon in the red region of Uv-vis spectrum. As shown in Figure 5.4 a, FRET process occurred even for the solid state-like sample (mixed solution absorbed onto the paper-based cartridge), generating images of different colours. The possibility to shift the TCL emission towards longer wavelengths represents a great advantage of our system, since it could further increase both the performance

(CMOS are more sensible to red light, see Figure 5.4 b) and applications range (*e.g.* for immunoassay and *in vivo* experiments) of our portable device.

5.4 Conclusion

Here we described the fabrication of an homemade portable device for TCL-based (bio)analyses, exploiting the low-cost 3D printing technology and the performance of a CMOS camera, integrated in Nokia Lumia 1020 smartphone. Although the development of our analytical device is still in its early stage, we conducted some preliminary experiments which supported the suitability of our system for applications in the (bio)analytical field. Our portable device has shown a remarkable sensibility in detection of TCL signal along with a great reproducibility of experiments. Exploiting the thermal decomposition of dioxetane **1**, we have been able to reach a very low limit of detection, with the lowest detectable concentration of analyte in the picomolar range. Furthermore, our system potentially leads itself to simple or "cascade" type FRET experiments, usually necessary for immunoassay or *in vivo* applications, in which the red-shifted emission signal is required to reduce the background noise as well as matrix interference.

Chapter 6

Supporting Information of Chapter 2

6.1 General Remarks

All of the commercial chemicals were purchased from Sigma Aldrich, Alfa Aesar or TCI Chemicals, and used without additional purifications.

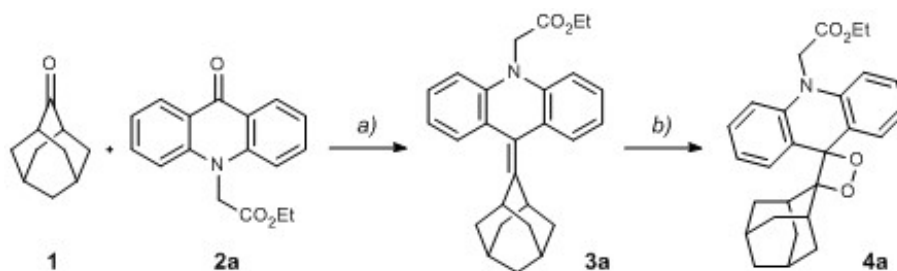
- The ^1H and ^{13}C NMR spectra were recorded on a 200 or 400 NMR instrument with a 5 mm probe. All chemical shifts have been quoted relative to deuterated solvent signals; chemical shifts (δ) are reported in ppm, and coupling constants (J) are reported in hertz. Protons and carbons are assigned as follows: (Ar) for aromatic protons, (Ad) for protons and carbons of the adamantyl portion, (H1, H2, H3...) for protons expressly labeled in the molecule picture, ($\text{H}\alpha$) for allylic protons of the adamantyl moiety in the alkenes (the same notation was used for the corresponding 1,2-dioxetanes), (CO) for carbonyl carbons, (COO) for carboxyl carbons, (CF) for carbons bearing a fluorine atom, (CHAr) for aromatic tertiary carbons, (Cq) for quaternary alkenyl and aromatic carbons, (C*) for carbons of the 1,2-dioxetane and (C1, C2, C3...) for carbons expressly labeled in the molecule picture.
- HPLC-MS analyses were performed on an Agilent Technologies HP1100 instrument coupled with an Agilent Technologies MSD1100 single-quadrupole mass spectrometer. A Phenomenex Gemini C18 3 μm (100 x 3 mm) column was employed for the chromatographic separation and two different analytical methods were used: method A: mobile phase $\text{H}_2\text{O}/\text{CH}_3\text{CN}$, gradient from 30% to 80% of CH_3CN in 8 min, 80% of CH_3CN until 22 min, then up to 90% of CH_3CN in 2 min, stop time at 25 min; flow rate 0.4 mL min^{-1} ; method B: gradient analogous to method A employing a mobile phase ($\text{H}_2\text{O}/\text{CH}_3\text{CN}$) containing 0.2% of formic acid. Mass spectrometric detection was performed in full-scan mode from m/z 50 to 2500, scan time 0.1 s in positive ion mode, ESI spray voltage 4500 V, nitrogen gas 35 psi, drying gas flow rate 11.5 mL min^{-1} , fragmentor voltage 30 V. Almost all the

synthesized compounds were analyzed employing method A; compounds analyzed with method B are specified.

- High-resolution MS (HRMS) ESI analyses were performed on a LTQ Orbitrap XL (Thermo Scientific) mass spectrometer.
- Melting point (mp) measurements were performed on a Bibby Stuart Scientific SMP3 apparatus.
- Flash chromatography purifications were carried out using VWR silica gel (40-63 μm particle size). Thin-layer chromatography was performed on Merck 60 F254 plates.
- Spectroscopic properties, in terms of maxima absorption and emission wavelengths (λ_{abs} and λ_{em}) and fluorescence quantum yields (ϕ_F) were recorded using a UV-Vis spectrophotometer (Varian Cary 50) and a Uv-Vis spectrofluorimeter (Carian Cary Eclipse). Fluorescent quantum yields were measured in acetonitrile, using quinine sulfate as standard ($\phi_F = 0.53$ in H_2SO_4 0.05 mol L^{-1}) [see Ref. 374].

6.2 Optimization Study

We selected the ketone **2a** as model compound for the optimization of the reaction conditions (Table 6.1) regarding the two key steps leading to the corresponding 1,2-dioxetane **4a** (Scheme 6.1).



Scheme 6.1

Concerning the McMurry coupling, we originally employed equimolar amounts of the two ketones (**1** and **2a**) and of the couple Zn/TiCl_3 , using three equivalents of the metal species with respect to the carbonyl substrates (entry 1) [see Ref. 107]. Although we obtained a good yield (87%), we tried to improve it and simultaneously to reduce the reaction time. Inspired by the work of other authors [see Ref. 375–380], we increased the excess of the metal species and replaced $\text{TiCl}_3 \times 3\text{THF}$ with the cheaper and easier to handle TiCl_4 (entry 2). Under these

Table 6.1: Optimization of the reaction conditions for the synthesis of the acridan-derived 1,2-dioxetane **4a**.

Entry	Substrate (eq.)	Reagents (eq.) and conditions	Time	Product	Yield (%) ^c
1 ^a	2a (1)	TiCl ₃ 3THF (3), Zn (3)	4 h	3a	87
2 ^a	2a (1)	TiCl ₄ (6.1) , Zn (13.5)	45 min	3a	94
3 ^a	2a (3.2)	TiCl ₄ (6.1), Zn (13.5)	30 min	3a	90
4 ^b	3a (1)	P-BR (0.05 g), -78 °C, UV cutoff filter (400 nm)	8 h	4a	64 ^d
5 ^b	3a (1)	MB (6.5 mol%), 0 °C UV cutoff filter (400 nm)	1.5 h	4a	81 ^d
6 ^b	3a (1)	MB (6.5 mol%), -20 °C UV cutoff filter (550 nm)	2 h	4a	92

^aReaction conditions: adamantanone **1** (0.28 mmol), tetrahydrofuran (THF, 7 mL), reflux. ^bReaction conditions: dichloromethane (DCM, 1 mL for 10 mg of **3a**), 500 W halogen lamp, O₂ (1 atm, balloon). ^cDetermined after purification by flash chromatography. ^dA partial decomposition of 1,2-dioxetane **4a** was observed. Eq. = equivalents, h = hours, min = minutes, P-BR = Polymer-bound Bengal Rose, MB = Methylene blue.

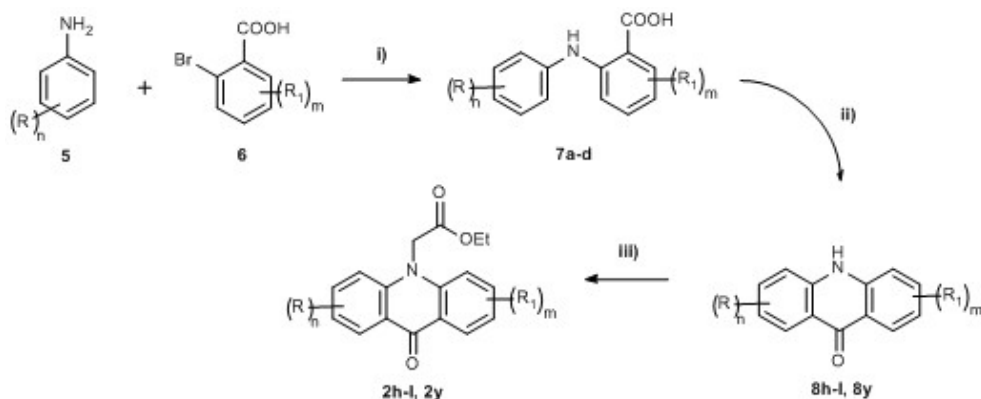
conditions the best yield (94%) of olefin **3a** was achieved after only 45 minutes. Increasing the amount of aromatic ketone **2a** we did not obtain further improvements (entry 3), therefore the subsequent McMurry couplings were carried out employing an equimolar amount of the two ketones (unless otherwise specified). The photooxygenation reaction was originally carried out at -78 °C with polymer-bound Bengal Rose as sensitizer and a 400 nm UV cutoff filter (entry 4). However, we found that, using Methylene Blue as sensitizer and increasing the temperature, better yields and shortened reaction times were achieved (entries 5 and 6).

6.3 Synthetic Procedures and Characterizations

6.3.1 General procedure for the synthesis of ketones **2h-l**, **2y**

Ketones **2h-l**, **2y** were synthesized following a previously reported three-steps synthetic pathway [see Ref. 110] (Scheme 6.2): i) Ullmann-type reaction between a substituted aniline (**5**) and a substituted 2-bromo benzoic acid (**6**) gave the intermediates **7a-d**; ii) intramolecular cyclization of intermediates **7a-d** to compounds **8h-l**, **8y**; iii) alkylation of the endocyclic nitrogen atom provided the desired ketones **2h-l**, **2y**.

Step i): A solution of substituted aniline **5** (1.4 eq.), substituted 2-bromobenzoic



Scheme 6.2

acid **6** (1 eq.), anhydrous K_2CO_3 (1.4 eq.), and copper (0.19 eq.) in anhydrous 1-pentanol (1 mL/1 mmol of **6**) was heated under reflux for 3 h. The solvent was evaporated under reduced pressure, and the residue was dissolved in hot H_2O and then filtered through Celite. The Celite was washed with H_2O and the filtrate was acidified with concentrated HCl to pH 6. The precipitate was isolated by filtration and washed with H_2O . The solid was purified by flash chromatography to give compounds **7a-d**.

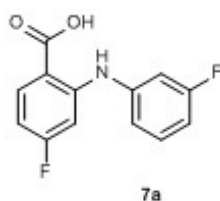


Figure 6.1

4-fluoro-2-((3-fluorophenyl)amino)benzoic acid (7a): 3-fluoroaniline (625 μL , 6.5 mmol) was coupled with 2-bromo-4-fluorobenzoic acid (1.03 g, 4.7 mmol), following the procedure described above (*step i*, Scheme 6.2). The chromatographic purification (eluent: cyclohexane/EtOAc = 80:20) provided product **7a** (710 mg, 61%) as pale yellow crystals (mp = 185 - 187 $^{\circ}\text{C}$). $^1\text{H NMR}$ (400 MHz, CD_3OD) δ 8.04 (dd, $J = 8.9, 6.9$ Hz, 1H, Ar), 7.39 - 7.33 (m, 1H, Ar), 7.05 (d, $J = 8.8$ Hz, 1H, Ar), 6.98 (dd, $J = 10.6, 2.4$ Hz, 1H, Ar), 6.91, (dd, $J = 11.9, 2.4$ Hz, 1H, Ar), 6.84 (dt, $J = 9.2, 2.4$ Hz, 1H, Ar), 6.51 (dt, $J = 8.0, 2.4$ Hz, 1H, Ar). $^{13}\text{C NMR}$ (100 MHz, CD_3OD) δ 170.9 (COO), 167.9 (d, $J = 248.5$ Hz, CF), 164.9 (d, $J = 242.8$ Hz, CF), 150.7 (d, $J = 12.2$ Hz, Cq), 143.4 (d, $J = 10.1$ Hz, Cq), 136.1 (d, $J = 11.4$ Hz, CHAr), 132.0 (d, $J = 9.8$ Hz, CHAr), 118.7 (d, $J = 2.9$ Hz, CHAr), 111.4 (d, $J = 21.7$ Hz, CHAr), 110.6 (Cq), 109.7 (d, $J = 23.8$ Hz, CHAr), 106.1 (d, $J = 22.7$ Hz, CHAr), 100.9 (d, $J = 26.5$ Hz, CHAr).

HPLC-MS (ESI, method B) $t_r = 10.0$ min; $[M+H]^+ = 250.0$ m/z . **HRMS** (ESI) $[M+H]^+$ calcd for $C_{13}H_{10}F_2NO_2$ 250.0680 found 250.0683.

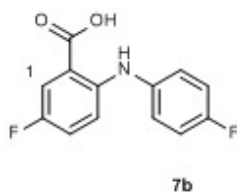


Figure 6.2

5-fluoro-2-((4-fluorophenyl)amino)benzoic acid (7b): 4-fluoroaniline (606 μ L, 6.39 mmol) was coupled with 2-bromo-5-fluorobenzoic acid (1 g, 4.57 mmol) following the procedure described above (*step i*, Scheme 6.2). The chromatographic purification (eluent: cyclohexane/EtOAc = 80:20) provided product **7b** (609 mg, 54%) as a pale yellow solid (mp = 222 - 224 $^{\circ}$ C). $^1\text{H NMR}$ (400 MHz, CD_3OD) δ 7.63 (dd, $J = 12.5, 3.0$ Hz, 1H, H1), 7.21 - 7.16 (m, 2H, Ar), 7.13 - 7.04 (m, 4H, Ar). $^{13}\text{C NMR}$ (100 MHz, CD_3OD) δ 170.7 (COO), 160.7 (d, $J = 239.4$ Hz, CF), 155.5 (d, $J = 233.4$ Hz, CF), 146.5 (Cq), 138.6 (Cq), 125.5 (d, $J = 8.0$ Hz, CHAr), 122.5 (d, $J = 18.0$ Hz, CHAr), 118.1 (d, $J = 23.3$ Hz, CHAr), 117.0 (d, $J = 22.7$ Hz, CHAr), 116.2 (d, $J = 6.9$ Hz, CHAr), 113.9 (Cq). **HPLC-MS** (ESI, method B) $t_r = 9.3$ min; $[M+H]^+ = 250.0$ m/z . **HRMS** (ESI) $[M+H]^+$ calcd for $C_{13}H_{10}F_2NO_2$ 250.0680 found 250.0684.

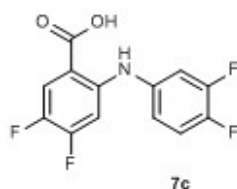


Figure 6.3

2-((3,4-difluorophenyl)amino)-4,5-difluorobenzoic acid (7c): 3,4-difluoroaniline (1.17 mL, 11.81 mmol) was coupled with 2-bromo-4,5-difluorobenzoic acid (2 g, 8.44 mmol) following the procedure described above (*step i*, Scheme 6.2). The crude product **7c** (1.7 g) was directly used in the next step without additional purification. $^1\text{H NMR}$ (400 MHz, DMSO-d_6) δ 7.83 (dd, $J = 11.2, 9.2$ Hz, 1H, Ar), 7.44 - 7.36 (m, 2H, Ar), 7.12 - 7.06 (m, 2H, Ar). **HPLC-MS** (ESI, method B) $t_r = 10.1$ min; $[M]^+ = 286.0$ m/z .

4-fluoro-2-(m-tolylamino)benzoic acid (7d): m-toluidine (697 μ L, 6.5 mmol) was coupled with 2-bromo-4-fluorobenzoic acid (1.03 g, 4.7 mmol) following the procedure described above (*step i*, Scheme 6.2). The chromatographic purification (eluent: cyclohexane/EtOAc = 70:30) provided product **7d** (615 mg, 53%) as pale

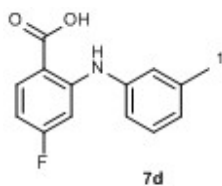


Figure 6.4

brown crystals (mp = 153 - 155 °C). $^1\text{H NMR}$ (400 MHz, CDCl_3) δ 9.42 (br s, 1H, NH), 8.06 (dd, J = 9.2, 6.8 Hz, 1H, Ar), 7.29 (t, J = 8.0 Hz, 1H, Ar) 7.09 - 7.08 (m, 2H, Ar), 7.02 (d, J = 7.6 Hz, 1H, Ar), 6.82 (dd, J = 12.4, 2.4 Hz, 1H, Ar), 6.44 (dt, J = 9.0, 2.4 Hz, 1H, Ar), 2.39 (s, 3H, H1). $^{13}\text{C NMR}$ (100 MHz, CDCl_3) δ 172.9 (COO), 167.6 (d, J = 251.0 Hz, CF), 151.6 (d, J = 13.2 Hz, Cq), 139.6 (Cq), 139.4 (Cq), 135.3 (d, J = 12.0 Hz, CHAr), 129.4 (CHAr), 125.8 (CHAr), 124.5 (CHAr), 120.8 (CHAr), 106.5 (Cq), 104.9 (d, J = 23.4 Hz, CHAr), 99.9 (d, J = 26.1 Hz, CHAr), 21.4 (C2). **HPLC-MS** (ESI, method B) t_r = 10.6 min; $[\text{M}+\text{H}]^+ = 246.2$ m/z . **HRMS** (ESI) $[\text{M}+\text{H}]^+$ calcd for $\text{C}_{14}\text{H}_{13}\text{FNO}_2$ 246.0930 found 246.0929.

Step ii): Compounds **8h-l**, **8y** were synthesized by adapting previously reported procedure. ([see Ref. 110]) Typically, the starting material (**7a-d**) (1 eq.) was dissolved in CH_3CN (2.25 mL/1 mmol of limiting reagent) and heated to reflux. Phosphorus (V) oxychloride (2.2 eq.) was added over 1 h. The solution was refluxed for further 2 h and then cooled to 10-15 °C. H_2O (1.25 mL/1 mmol of limiting reagent) was added, and the mixture was heated to reflux for 2.5 h. The suspension was cooled to 10 °C and filtered. The solid was washed with H_2O and CH_3CN and then dried under vacuum to obtain compounds **8h-l**, **8y**. The crude product was purified by flash chromatography on silica gel or directly used in the next step, without additional purifications.

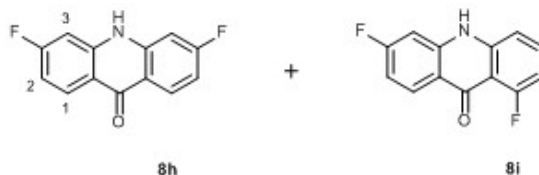


Figure 6.5

3,6-difluoroacridin-9(10H)-one (8h) and 1,6-difluoroacridin-9(10H)-one (8i): compound **7a** (498 mg, 2 mmol) was cyclized following the procedure described above (*step ii*, Scheme 6.2), to give a mixture of products **8h** and **8i** (326 mg of a mixture **8h/8i** = 60/40, calculated from the $^1\text{H NMR}$ spectrum in DMSO-d_6). The mixture was used without additional purification in the *step iii*

(Scheme 6.2).

Ketone 8h: $^1\text{H NMR}$ (400 MHz, DMSO- d_6) δ 11.89 (NH), 8.26 (dd, $J = 8.8, 6.4$ Hz, 2H, H1), 7.21 (dd, $J = 10.4, 2.4$ Hz, 2H, H3), 7.12 (dt, $J = 8.8, 2.4$ Hz, 2H, H2). **HPLC-MS** (ESI) $t_r = 7.1$ min; $[\text{M}+\text{H}]^+ = 232.1$ m/z , $[\text{2M}+\text{Na}]^+ = 485.0$ m/z .

Ketone 8i: $^1\text{H NMR}$ (400 MHz, DMSO- d_6) δ 11.87 (NH), 8.21 (dd, $J = 9.2, 6.8$ Hz, 1H, Ar), 7.69 - 7.64 (m, 1H, Ar), 7.28 (d, $J = 8.4$ Hz, 1H, Ar), 7.17 - 7.06 (m, 2H, Ar), 6.94 (dd, $J = 12.4, 8.4$ Hz, 1H, Ar). **HPLC-MS** (ESI) $t_r = 6.2$ min; $[\text{M}+\text{H}]^+ = 232.1$ m/z , $[\text{2M}+\text{Na}]^+ = 485.0$ m/z .

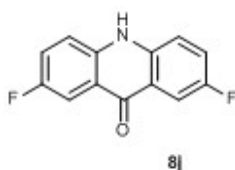


Figure 6.6

2,7-difluoroacridin-9(10H)-one (8j): compound **7b** (550 mg, 2.21 mmol) was cyclized following the procedure described above (*step ii*, Scheme 6.2). The crude product was purified by flash chromatography on silica gel (eluent: cyclohexane/EtOAc = 85:15) providing product **8j** (299 mg, 59%). The obtained spectroscopic data were in agreement with the literature data [see Ref. 381].

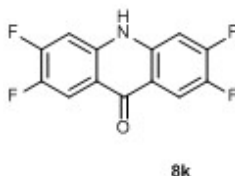


Figure 6.7

2,3,6,7-tetrafluoroacridin-9(10H)-one (8k): compound **7c** (1.5 g, 5.26 mmol) was cyclized following the procedure described above (*step ii*, Scheme 6.2), to give a mixture of products **8k** and its constitutional isomer 1,2,6,7-tetrafluoroacridin-9(10H)-one (901 mg of a mixture **8k**/constitutional isomer = 50/50, calculated from the $^1\text{H NMR}$ spectrum in CDCl_3). The mixture was used without additional purification in the following *step iii* (Scheme 6.2).

Ketone 8k: $^1\text{H NMR}$ (400 MHz, CDCl_3) δ 8.09 (dd, $J = 10.4, 8.8$ Hz, 2H, Ar), 7.15 (dd, $J = 10.8, 6.4$ Hz, 2H, Ar). **HPLC-MS** (ESI) $t_r = 8.7$ min; $[\text{M}+\text{H}]^+ = 268.0$ m/z .

1,2,6,7-tetrafluoroacridin-9(10H)-one: $^1\text{H NMR}$ (400 MHz, CDCl_3) δ 7.78 (dd, $J = 11.2, 9.2$ Hz, 1H, Ar), 7.02 - 6.97 (m, 1H, Ar), 6.89 - 6.87 (m, 1H, Ar),

6.81 (dd, $J = 13.2, 6.5$ Hz, 1H, Ar). **HPLC-MS** (ESI) $t_r = 7.9$ min; $[M+H]^+ = 268.0$ m/z , $[2M+Na]^+ = 557.0$ m/z .

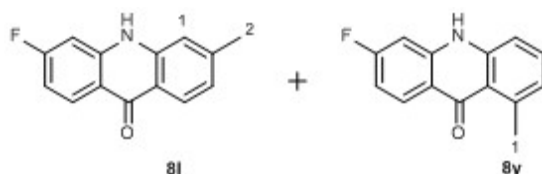


Figure 6.8

3-fluoro-6-methylacridin-9(10H)-one (8l) and 6-fluoro-1-methylacridin-9(10H)-one (8y): compound **7d** (490 mg, 2 mmol) was cyclized following the procedure described above (*step ii*, Scheme 6.2), to give a mixture of products **8l** and **8y** (536 mg of a mixture **8l/8y** = 40/60, calculated from the ^1H NMR spectrum in DMSO- d_6). The mixture was used without additional purification in the following *step iii* (Scheme 6.2).

Ketone 8l: ^1H NMR (400 MHz, DMSO- d_6) δ 11.78 (NH), 8.26 (dd, $J = 8.8, 6.4$ Hz, 1H, Ar), 8.10 (d, $J = 8.4$ Hz, 1H, Ar), 7.32 (d, $J = 8.0$ Hz, 1H, Ar), 7.28 (s, 1H, H1), 7.23 (dd, $J = 10.0, 2.8$ Hz, 1H, Ar), 7.12 - 7.08 (m, 1H, Ar), 2.50 (s, 3H, H2). **HPLC-MS** (ESI) $t_r = 7.1$ min; $[M+H]^+ = 228.1$ m/z , $[2M+Na]^+ = 477.0$ m/z .

Ketone 8y: ^1H NMR (400 MHz, DMSO- d_6) δ 11.66 (NH), 8.21 (dd, $J = 8.8, 6.8$ Hz, 1H, Ar), 7.54 (t, $J = 8.0$ Hz, 1H, Ar), 7.16 (dd, $J = 10.8, 2.4$ Hz, 1H, Ar), 7.07 - 7.02 (m, 2H, Ar), 6.98 (d, $J = 6.8$ Hz, 1H, Ar), 2.50 (s, 3H, H1). **HPLC-MS** (ESI) $t_r = 8.2$ min; $[M+H]^+ = 228.1$ m/z , $[2M+Na]^+ = 477.0$ m/z .

Step iii): According to the reported procedure,(...) a solution of the cyclic intermediate **8** (1 eq.) in anhydrous DMF (5 mL/1 mmol **8**) was added to a suspension of NaH (1.2 eq.) in anhydrous DMF (1.6 mL/1 mmol **8**). The mixture was stirred for 30 min at room temperature, and then, after the mixture was cooled to 0 °C, ethyl 2-bromoacetate (1.5 eq.) and tetrabutylammonium iodide (0.01 eq.) were added. The solution was stirred for further 24 h at room temperature and then poured into cold water. The precipitate was collected by filtration, dried under vacuum, and purified by flash chromatography on silica gel.

Ethyl 2-(3,6-difluoro-9-oxoacridin-10(9H)-yl)acetate (2h) and ethyl 2-(1,6-difluoro-9-oxoacridin-10(9H)-yl)acetate (2i): the mixture of compounds **8h** and **8i** (358 mg, 1.55 mmol) was alkylated following the procedure described above (*step iii*, Scheme 6.2) to give an overall 92% yield. The chromatographic purification (eluent: cyclohexane/EtOAc = 80:20) provided products **2h** (370 mg) and **2i** (83 mg).

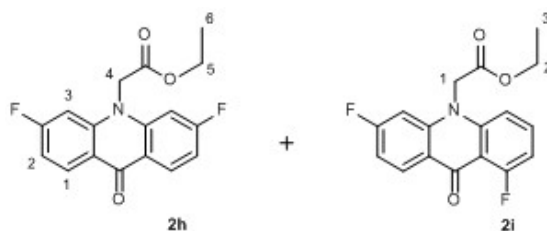


Figure 6.9

Ketone 2h: white solid, mp = 198 - 200 °C ; λ_{abs} = 355, 371 nm, λ_{em} = 386, 403 nm, ϕ_F = 0.01; $^1\text{H NMR}$ (400 MHz, CDCl_3) δ 8.58 (dd, J = 8.9, 6.8 Hz, 2H, H1), 7.05 (dt, J = 10.1, 2.4 Hz, 2H, H2), 6.97 (dd, J = 11.5, 2.4 Hz, 2H, H3), 4.94 (s, 2H, H4), 4.36 (q, J = 7.1 Hz, 2H, H5), 1.35 (t, J = 7.1 Hz, 3H, H6). $^{13}\text{C NMR}$ (100 MHz, CDCl_3) δ 176.2 (CO), 167.4 (COO), 166.4 (d, J = 251.5 Hz, CF), 144.1 (d, J = 11.5 Hz, Cq), 131.1 (d, J = 11.1 Hz, C1), 119.4 (d, J = 1.6 Hz, Cq), 110.9 (d, J = 22.6 Hz, CHAr), 100.9 (d, J = 27.1 Hz, CHAr), 62.5 (C5), 48.7 (C4), 14.1 (C6). **HPLC-MS** (ESI) t_r = 9.0 min; $[\text{M}+\text{H}]^+$ = 318.0 m/z , $[\text{2M}+\text{Na}]^+$ = 657.0 m/z . **HRMS** (ESI) $[\text{M}+\text{H}]^+$ calcd for $\text{C}_{17}\text{H}_{14}\text{F}_2\text{NO}_3$ 318.0942 found 318.0943.

Ketone 2i: white solid, mp = 176 - 178 °C; λ_{abs} = 363, 378 nm, λ_{em} = 395 nm, ϕ_F = 4×10^{-3} ; $^1\text{H NMR}$ (400 MHz, CDCl_3) δ 8.51 (dd, J = 8.8, 6.8 Hz, 1H, Ar), 7.64 - 7.59 (m, 1H, Ar), 7.04 (d, J = 8.6 Hz, 2H, Ar), 7.01 - 6.90 (m, 2H, Ar), 4.95 (s, 2H, H1), 4.35 (q, J = 7.1 Hz, 2H, H2), 1.34 (t, J = 7.1 Hz, 3H, H3). $^{13}\text{C NMR}$ (100 MHz, CDCl_3) δ 175.7 (CO), 167.7 (COO), 166.4 (d, J = 251.3 Hz, CF), 162.8 (d, J = 263.3 Hz, CF), 144.3 (d, J = 2.7 Hz, Cq), 143.5 (d, J = 11.4 Hz, Cq), 134.2 (d, J = 11.7 Hz, CHAr), 130.9 (d, J = 11.1 Hz, CHAr), 120.4 (d, J = 1.4 Hz, Cq), 112.7 (d, J = 8.1 Hz, Cq), 110.7 (d, J = 22.6 Hz, CHAr), 110.0 (d, J = 4.2 Hz, CHAr), 109.3 (d, J = 21.5 Hz, CHAr), 100.7 (d, J = 27.0 Hz, CHAr), 62.4 (C2), 49.5 (C1), 14.1 (C3). **HPLC-MS** (ESI) t_r = 8.2 min; $[\text{M}+\text{H}]^+$ = 318.0 m/z , $[\text{2M}+\text{Na}]^+$ = 657.0 m/z . **HRMS** (ESI) $[\text{M}+\text{H}]^+$ calcd for $\text{C}_{17}\text{H}_{14}\text{F}_2\text{NO}_3$ 318.0942 found 318.0944.

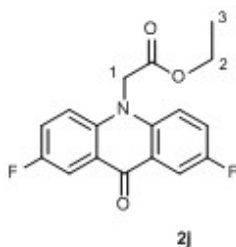


Figure 6.10

Ethyl 2-(2,7-difluoro-9-oxoacridin-10(9H)-yl)acetate (2j): compound 8j

(98 mg, 0.42 mmol) was alkylated following the procedure described above (*step iii*, Scheme 6.2). The crude product was purified by flash chromatography on silica gel (eluent: cyclohexane/EtOAc = 80:20) providing compound **2j** (82 mg, 62%) as a yellow solid, mp = 221 - 223 °C; λ_{abs} = 387, 408 nm, λ_{em} = 421, 444 nm, ϕ_F = 0.65; $^1\text{H NMR}$ (400 MHz, CDCl_3) δ 8.17 (dd, J = 8.6, 3.0 Hz, 2H, Ar), 7.50 - 7.45 (m, 2H, Ar), 7.32 (dd, J = 9.2, 3.9 Hz, 2H, Ar), 5.06 (s, 2H, H1), 4.33 (q, J = 7.1 Hz, 2H, H2), 1.32 (t, J = 7.2 Hz, 3H, H3). $^{13}\text{C NMR}$ (100 MHz, CDCl_3) δ 176.6 (CO), 167.9 (COO), 157.9 (d, J = 242.4 Hz, CF), 138.7 (d, J = 1.4 Hz, Cq), 122.9 (Cq), 122.7 (d, J = 24.8 Hz, CHAr), 116.4 (d, J = 7.4 Hz, CHAr), 112.3 (d, J = 22.5 Hz, CHAr), 62.4 (C2), 49.0 (C1), 14.2 (C3). **HPLC-MS** (ESI) t_r = 9.1 min; $[\text{M}+\text{H}]^+$ = 318.0 m/z , $[\text{M}+\text{K}]^+$ = 356.0 m/z . **HRMS** (ESI) $[\text{M}+\text{H}]^+$ calcd for $\text{C}_{17}\text{H}_{14}\text{F}_2\text{NO}_3$ 318.0942 found 318.0942.

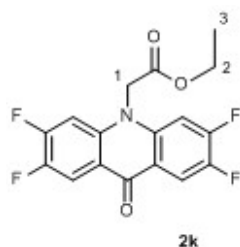


Figure 6.11

Ethyl 2-(2,3,6,7-tetrafluoro-9-oxoacridin-10(9H)-yl)acetate (2k): the mixture of compounds **8k** and its constitutional isomer 1,2,6,7-tetrafluoroacridin-9(10H)-one (800 mg, 2.99 mmol) was alkylated following the procedure described above (*step iii*, Scheme 6.2). From the chromatographic purification (eluent: cyclohexane/EtOAc = 90:10) only compound **2k** was isolated as brown crystals (633 mg, 60%), mp = 211 - 213 °C; λ_{abs} = 368, 386 nm, λ_{em} = 399, 419 nm, ϕ_F = 0.11; $^1\text{H NMR}$ (400 MHz, DMSO-d_6) δ 8.13 (dd, J = 10.0, 9.2 Hz, 2H, Ar), 7.87 (dd, J = 13.6, 6.4 Hz, 2H, Ar), 5.42 (s, 2H, H1), 4.21 (q, J = 7.2 Hz, 2H, H2), 1.24 (t, J = 7.2 Hz, 3H, H3). $^{13}\text{C NMR}$ (100 MHz, DMSO-d_6) δ 173.7 (CO), 167.8 (COO), 153.7 (dd, J = 250.7, 14.5 Hz, CF), 145.7 (d, J = 243.8, 14.0 Hz, CF), 139.8 (d, J = 10.3 Hz, Cq), 117.7 (d, J = 5.1 Hz, Cq), 113.8 (dd, J = 17.6, 2.6 Hz, CHAr), 105.5 (d, J = 23.3 Hz, CHAr), 61.5 (C2), 48.4 (C1), 13.9 (C3). **HPLC-MS** (ESI) t_r = 10.6 min; $[\text{M}+\text{H}]^+$ = 354.0 m/z , $[\text{2M}+\text{Na}]^+$ = 729.0 m/z . **HRMS** (ESI) $[\text{M}+\text{H}]^+$ calcd for $\text{C}_{17}\text{H}_{12}\text{F}_4\text{NO}_3$ 354.0753 found 354.0752.

Ethyl 2-(3-fluoro-6-methyl-9-oxoacridin-10(9H)-yl)acetate (2l) and ethyl 2-(6-fluoro-1-methyl-9-oxoacridin-10(9H)-yl)acetate (2y): the mixture of compounds **8l** and **8y** (485 mg, 2.14 mmol, **8l/8y** = 40/60) was alkylated following the procedure described above (*step iii*, Scheme 6.2) to give an overall 59% yield. The chromatographic purification (eluent: cyclohexane/EtOAc = 80:20) provided

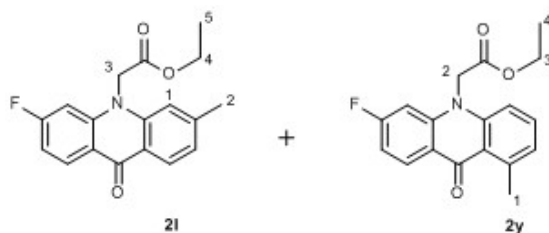


Figure 6.12

products **2l** (173 mg) and **2y** (219 mg).

Ketone 2l: pale yellow solid, mp = 138 - 140 °C; λ_{abs} = 361, 378 nm, λ_{em} = 394 nm, ϕ_F = 0.04; $^1\text{H NMR}$ (400 MHz, CDCl_3) δ 8.47 (dd, J = 8.80, 6.76 Hz, 1H, Ar), 8.33 (d, J = 8.12 Hz, 1H, Ar), 7.11 (d, J = 8.12 Hz, 1H, Ar), 7.03 (s, 1H, H1), 6.98 (dt, J = 9.2, 2.1 Hz, 1H, Ar), 6.93 (dd, J = 11.4, 1.9 Hz, 1H, Ar), 4.96 (s, 2H, H3), 4.29 (q, J = 7.08 Hz, 2H, H4), 2.47 (s, 3H, H2), 1.28 (t, J = 7.12 Hz, 3H, H5). $^{13}\text{C NMR}$ (100 MHz, CDCl_3 with a few drops of CD_3OD to enhance the solubility) δ 177.3 (CO), 168.0 (COO), 166.4 (d, J = 251.0 Hz, CF), 145.6 (Cq), 143.9 (d, J = 11.8 Hz, Cq), 130.8 (d, J = 11.1 Hz, CHAr), 127.7 (CHAr), 124.3 (Cq), 124.1 (CHAr), 120.3 (Cq), 119.1 (Cq), 114.1 (CHAr), 110.5 (d, J = 22.8 Hz, CHAr), 100.7 (d, J = 26.9 Hz, CHAr), 62.3 (C4), 48.4 (C3), 22.4 (C2), 14.0 (C5). **HPLC-MS** (ESI) t_r = 9.2 min; $[\text{M}+\text{H}]^+$ = 314.2 m/z , $[\text{2M}+\text{Na}]^+$ = 649.2 m/z . **HRMS** (ESI) $[\text{M}+\text{H}]^+$ calcd for $\text{C}_{18}\text{H}_{17}\text{FNO}_3$ 314.1192 found 314.1191.

Ketone 2y: pale brown crystals, mp = 166 - 168 °C; $^1\text{H NMR}$ (400 MHz, CDCl_3) δ 8.50 (dd, J = 8.80, 6.72 Hz, 1H, Ar), 7.54 (dd, J = 8.5, 7.3 Hz, 1H, Ar), 7.12 - 7.10 (m, 2H, Ar), 7.00 (dt, J = 8.9, 2.0 Hz, 1H, Ar), 6.90 (dd, J = 11.24, 2.20 Hz, 1H, Ar), 4.94 (s, 2H, H2), 4.35 (q, J = 7.12 Hz, 2H, H3), 2.99 (s, 3H, H1), 1.34 (t, J = 7.12 Hz, 3H, H4). $^{13}\text{C NMR}$ (100 MHz, CDCl_3) δ 179.0 (CO), 168.05 (COO), 166.0 (d, J = 249.9 Hz, CF), 143.9 (Cq), 143.3 (d, J = 11.3 Hz, Cq), 142.9 (Cq), 132.8 (CHAr), 130.8 (d, J = 10.8 Hz, CHAr), 125.6 (CHAr), 121.2 (Cq), 120.6 (Cq), 112.3 (CHAr), 110.0 (d, J = 22.7 Hz, CHAr), 100.3 (d, J = 26.9 Hz, CHAr), 62.2 (C2), 49.3 (C3), 24.4 (C1), 14.1 (C4). **HPLC-MS** (ESI) t_r = 10.2 min; $[\text{M}+\text{H}]^+$ = 314.2 m/z , $[\text{2M}+\text{Na}]^+$ = 649.2 m/z . **HRMS** (ESI) $[\text{M}+\text{H}]^+$ calcd for $\text{C}_{18}\text{H}_{17}\text{FNO}_3$ 314.1192 found 314.1195.

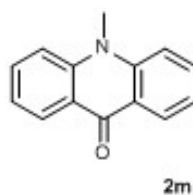


Figure 6.13

10-methylacridin-9(10H)-one (2m) was synthesized by adapting a reported procedure [see Ref. 382]: to a suspension of NaH (60% oil dispersion, 316 mg, 7.9 mmol) in anhydrous DMF (20 mL) was added 9(10H)-acridone (500 mg, 2.56 mmol) at 0 °C. The reaction mixture was stirred at 60 °C for 30 min, then iodomethane (560 μ L, 8.96 mmol) was added, and stirring was continued at 60 °C for 14 h. The reaction mixture was quenched with H₂O. The resulting solid was collected by filtration and thoroughly washed with ethanol to give product **2m** as light-yellow solid. A further amount of product was recovered by extracting the filtered water phase with CH₂Cl₂. Then, the combined organic layers were washed with brine, dried over sodium sulfate, and concentrated. 508 mg of compound **2m** was obtained (95% yield). The obtained spectroscopic data were in agreement with the literature data [see Ref. 382].

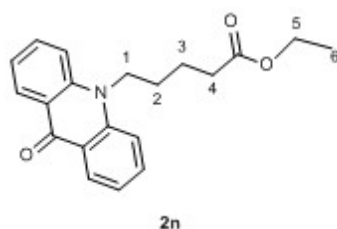
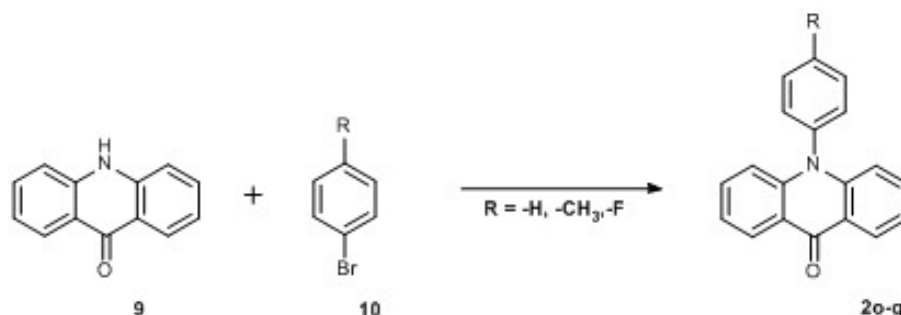


Figure 6.14

Ethyl 5-(9-oxoacridin-10(9H)-yl)pentanoate (2n) was synthesized following the reported procedure [see Ref. 110]: a solution of 9(10H)-acridone (500 mg, 2.56 mmol) in anhydrous DMF (10 mL) was added to a suspension of NaH (123 mg, 3.07 mmol) in anhydrous DMF (5 mL). The mixture was stirred for 30 min at room temperature, and then, after the mixture was cooled to 0 °C, ethyl 5-bromovalerate (610 μ L, 3.84 mmol) and tetrabutylammonium iodide (10 mg, 0.027 mmol) were added. The solution was stirred for further 24 h at room temperature and then poured into cold water. The precipitate was collected by filtration, dried under vacuum, and purified by flash chromatography on silica gel (eluent: cyclohexane/EtOAc = 90:10) providing compound **2n** (323 mg, 40%), as pale yellow solid; mp = 92 - 94 °C; λ_{abs} = 399 nm, λ_{em} = 413 nm, ϕ_F = 0.44; **¹H NMR** (400 MHz, CDCl₃) δ 8.60 (dd, J = 8.0, 1.2 Hz, 2H, Ar), 7.76 (t, J = 7.4 Hz, 2H, Ar), 7.51 (d, J = 8.7 Hz, 2H, Ar), 7.31 (t, J = 7.4 Hz, 2H, Ar), 4.39 (t, J = 7.6 Hz, 2H, H1), 4.17 (q, J = 7.1 Hz, 2H, H5), 2.47 (t, J = 6.8 Hz, 2H, H4), 2.05 - 1.88 (m, 4H, H2 and H3), 1.27 (t, J = 7.1 Hz, 3H, H6). **¹³C NMR** (100 MHz, CDCl₃) δ 177.9 (CO), 173.0 (COO), 141.7 (Cq), 133.9 (CHAr), 128.0 (CHAr), 122.5 (Cq), 121.3 (CHAr), 114.4 (CHAr), 60.6 (C5), 45.8 (C1), 33.7 (C4), 26.6 and 22.2 (C2 and C3), 14.2 (C6). **HPLC-MS** (ESI) t_r = 9.6 min; [M+H]⁺ = 324.2 m/z , [M+Na]⁺ = 346.3 m/z . **HRMS** (ESI) [M+H]⁺ calcd for C₂₀H₂₂NO₃ 324.1600

found 324.160.

6.3.2 General procedure for the synthesis of compounds 2o-q



Scheme 6.3

Compounds **2o-q** were synthesized by adapting a previously reported procedure (Scheme 6.3) [see Ref. 383]: 1-bromobenzene derivative 10 (1.1 eq.), acridin-9(10H)-one (**9**) (1 eq.), K₂CO₃ (1.1 eq.), CuI (0.1 eq.), 2,2,6,6-tetramethyl-3,5-heptanedione (0.19 eq.) were dissolved in anhydrous DMF (6 mL/1 mmol of **9**), into a three-necked round flask. The mixture was degassed and refluxed under nitrogen atmosphere for 24 h. After cooling to room temperature, the reaction mixture was quenched with H₂O and extracted with ethyl acetate (3 X 10 mL). The combined organic layers were collected, dried over sodium sulfate and evaporated under vacuum. Then, the crude product was purified by flash chromatography on silica gel.

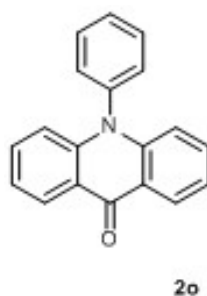
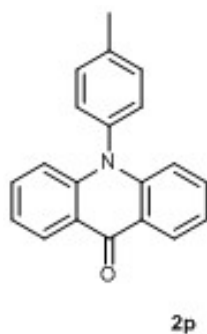


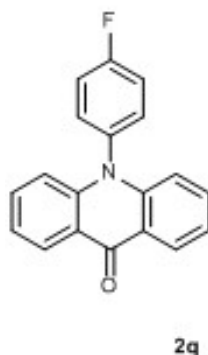
Figure 6.15

10-phenylacridin-9(10H)-one (2o): compound **9** (300 mg, 1.54 mmol) was coupled with bromobenzene (180 μ L, 1.71 mmol) following the above-mentioned procedure (Scheme 6.3). The chromatographic purification (eluent: cyclohexane/EtOAc = 95:5) provided compound **2o** (362 mg, 87%). The obtained spectroscopic data were in agreement with the literature data [see Ref. 384].

10-(p-tolyl)acridin-9(10H)-one (2p): compound **9** (300 mg, 1.54 mmol) was coupled with 1-bromo-4-methylbenzene (210 μ L, 1.71 mmol) following

**Figure 6.16**

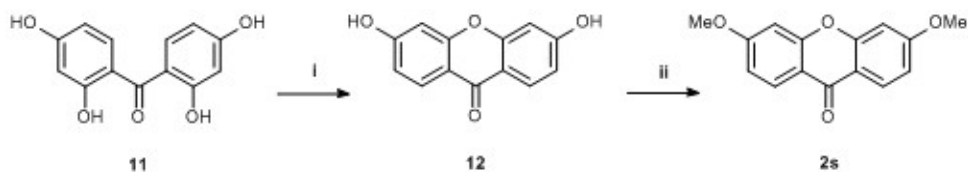
the above-mentioned procedure (Scheme 6.3). The chromatographic purification (eluent: cyclohexane) provided compound **2p** (89 mg, 20%). The obtained spectroscopic data were in agreement with the literature data [see Ref. 385].

**Figure 6.17**

10-(4-fluorophenyl)acridin-9(10H)-one (2q): compound **9** (300 mg, 1.54 mmol) was coupled with 1-bromo-4-fluorobenzene (253 μ L, 2.31 mmol) following the above-mentioned procedure (Scheme 6.3). The chromatographic purification (eluent: cyclohexane/EtOAc = 80:20) provided compound **2q** (107 mg, 24%). The obtained spectroscopic data were in agreement with the literature data [see Ref. 384].

Procedure for the synthesis of compound 2s: a previously reported two-steps synthetic pathway (Scheme 6.4) [see Ref. 386], was followed to synthesize ketone**2s**: i) intramolecular cyclization of 2,2',4,4'-tetrahydroxybenzophenone (**11**) gave the intermediate **12**; ii) di-methylation of compound **12** yielded the desired product **2s**.

Step i): 2,2',4,4'-Tetrahydroxybenzophenone (**11**) (1 g, 4.07 mmol) was heated at 210-220 °C (sand bath) for 4 h. The yellow powder in the reaction mixture changed to a brown solid. The crude product was purified by flash chromatography on silica gel (eluent: cyclohexane/EtOAc = 50:50) to give ketone

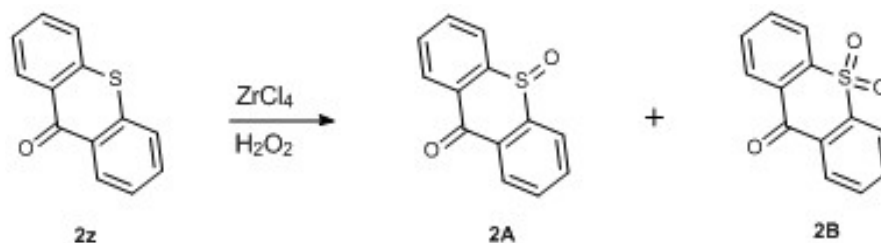


Scheme 6.4

12 (790 mg, 85%). The obtained spectroscopic data were in agreement with the literature data [see Ref. 386].

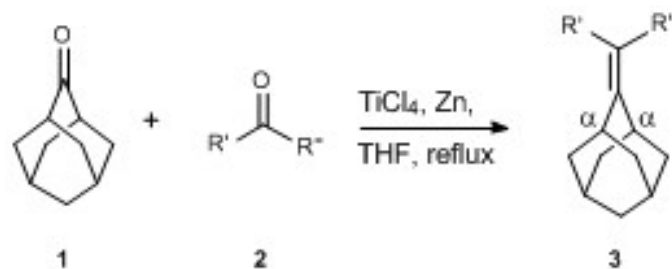
Step ii): ketone **12** (250 mg, 1.10 mmol), K_2CO_3 (227 mg, 1.64 mmol), MeI (273 μ L, 4.39 mmol) and acetone (15 mL) were mixed, and the reaction mixture was stirred under reflux for 3 h. The reaction mixture was then filtered and washed with ethyl acetate (3 X 10 mL). The organic layer was evaporated under vacuum and purified by flash chromatography on silica gel (eluent: cyclohexane/EtOAc = 80:20) to give compound **2s** (126 mg, 45% yield). The obtained spectroscopic data were in agreement with the literature data [see Ref. 386].

Procedure for the synthesis of ketones **2A** and **2B**:



Scheme 6.5

9H-thioxanthen-9-one 10-oxide (2A) and **9H-thioxanthen-9-one 10,10-dioxide (2B)** were synthesized by adapting a reported procedure (Scheme 6.5) [see Ref. 387]: 11 9H-thioxanthen-9-one (**2z**) (400 mg, 1.88 mmol) was dissolved in MeOH (8 mL). Then, H_2O_2 (30% in H_2O , 563 μ L, 4.97 mmol) and $ZrCl_4$ (1.1 g, 4.7 mmol) were added and the mixture was stirred at room temperature for 10 minutes. After that, the solution was evaporated under vacuum and the crude product was purified by flash chromatography on silica gel (eluent: cyclohexane/EtOAc = 90:10) to give compounds **2A** (135 mg, 31%) and **2B** (59 mg, 13%). The obtained spectroscopic data were in agreement with the literature data [see Ref. 388].



Scheme 6.6

6.3.3 General procedure for the synthesis of alkenes 3h-t, 3y-z, 3C-E, 3G-I:

All the synthesized olefins (except for **3A** and **3B**) were obtained by a reductive coupling under McMurry conditions (Scheme 6.6). Three different synthetic methods were followed:

Method A: Under a nitrogen atmosphere, TiCl₄ (1M in dichloromethane, 6.1 eq.) was added to a suspension of zinc powder (13.5 eq.) in anhydrous THF (8mL/0.5 mmol of 1) at 0 °C, and the suspension was stirred for 10 min under reflux. A solution of ketone **2** (1 eq.) and 2-adamantanone **1** (1 eq.) in dry THF (2 mL/0.5 mmol of 1) was added dropwise over a period of 30 min. The reaction mixture was refluxed for 45 minutes. Then, it was cooled to room temperature, quenched with water and extracted with AcOEt (3 x 10 mL). The combined organic layers were dried over sodium sulfate and evaporated under vacuum. The crude product was purified by flash chromatography on silica gel.

Method B: the same experimental procedure of method A was followed, except for the ratio between the starting materials **1** and **2** and the reaction time. In particular, 1 eq. of 2-adamantanone **1** and 3.2 eq. of aromatic ketone **2** were employed, and the reaction was stirred under reflux for 1.5 h.

Method C: compound **3I** was synthesized by adapting a reported procedure [see Ref. 389]: under a nitrogen atmosphere, LiAlH₄ (598 mg, 15.75 mmol) was added to a suspension of TiCl₄ 2THF (4.57 g, 13.70 mmol) in anhydrous THF (18 mL) at 0 °C, and the mixture was stirred for 10 min. After addition of triethylamine (4.1 mL, 30 mmol) at room temperature, the reaction mixture was refluxed for 1 h. A solution of lactone 2I (100 mg, 0.68 mmol) and 2-adamantanone **1** (1.54 g, 10.27 mmol) in dry THF (11 mL) was added dropwise over a period of 30 min. The reaction mixture was refluxed for 2 h and then, it was cooled to room temperature, quenched with water and extracted with AcOEt (3 x 12 mL). The combined organic layers were dried over sodium sulfate and evaporated under vacuum. The crude product was purified by flash chromatography on silica gel.

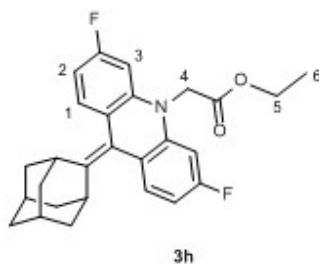


Figure 6.18

Compound 3h: 2-adamantanone **1** (18 mg, 0.12 mmol) and ketone **2h** were coupled following the above-mentioned procedure (method B, Scheme 6.6). The chromatographic purification (eluent: cyclohexane/EtOAc = 95:5) provided compound **3h** (45 mg, 86%) as a yellow solid (mp = 213 - 215 °C). $^1\text{H NMR}$ (400 MHz, CDCl_3) δ 7.14 (dd, $J = 8.4, 6.6$ Hz, 2H, H1), 6.76 (dt, $J = 8.4, 2.4$ Hz, 2H, H2), 6.50 (dd, $J = 10.9, 2.4$ Hz, 2H, H3), 4.57 (s, 2H, H4), 4.32 (q, $J = 7.1$ Hz, 2H, H5), 3.36 (br s, 2H, H_α), 2.28 - 1.57 (m, 12H, Ad), 1.33 (t, $J = 7.1$ Hz, 3H, H6). $^{13}\text{C NMR}$ (100 MHz, CDCl_3) δ 168.9 (COO), 161.6 (d, $J = 241.2$ Hz, CF), 144.9 (Cq), 144.3 (d, $J = 9.9$ Hz, Cq), 128.3 (d, $J = 26.9$ Hz, CHAr), 121.9 (d, $J = 2.7$ Hz, Cq), 118.3 (Cq), 107.5 (d, $J = 21.4$ Hz, CHAr), 100.3 (d, $J = 26.9$ Hz, CHAr), 61.7 (C5), 48.9 (C4), 36.9 (Ad), 32.2 (Ad), 14.2 (C6). **HPLC-MS** (ESI) $t_r = 21.1$ min; $[\text{M}+\text{H}]^+ = 436.1$. **HRMS** (ESI) $[\text{M}+\text{H}]^+$ calcd for $\text{C}_{27}\text{H}_{28}\text{F}_2\text{NO}_2$ 436.2088 found 436.2091.

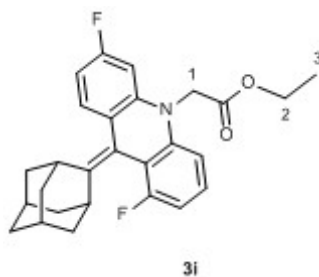


Figure 6.19

Compound 3i: 2-adamantanone **1** (20.4 mg, 0.14 mmol) and ketone **2i** were coupled following the above-mentioned procedure (method A, Scheme 6.6). The chromatographic purification (eluent: cyclohexane/EtOAc = 95:5) provided compound **3i** (52 mg, 88%) as a sticky solid. $^1\text{H NMR}$ (400 MHz, CDCl_3) δ 7.18 (dd, $J = 8.3, 6.5$ Hz, 1H, Ar), 7.15 - 7.09 (m, 1H, Ar), 6.80 - 6.72 (m, 2H, Ar), 6.56 (d, $J = 8.2$ Hz, 1H, Ar), 6.51 (dd, $J = 10.9, 2.3$ Hz, 1H, Ar), 4.64 (d, $J = 18.2$ Hz, 1H, H1a), 4.58 (d, $J = 18.2$ Hz, 1H, H1b), 4.30 (q, $J = 7.1$ Hz, 2H, H2), 3.34 (s, 1H, H_α), 2.73 (s, 1H, H_α), 2.22 - 2.03 (m, 5H, Ad), 1.85 (m, 3H, Ad), 1.76 - 1.66 (m, 2H, Ad), 1.60 - 1.53 (m, 2H, Ad), 1.30 (t, $J = 7.1$ Hz, 3H, H3). ^{13}C

NMR (100 MHz, CDCl₃) δ 169.0 (COO), 161.6 (d, J = 241.0 Hz, CF), 157.8 (d, J = 241.7 Hz, CF) 147.9 (Cq), 145.3 (d, J = 7.1 Hz, Cq), 144.6 (d, J = 10.0 Hz, Cq), 128.5 (d, J = 9.4 Hz, CHAr), 126.9 (d, J = 9.6 Hz, CHAr), 122.1 (d, J = 2.7 Hz, Cq), 114.4 (d, J = 21.1 Hz, Cq), 113.0 (Cq), 108.8 (d, J = 23.5 Hz, CHAr), 108.1 (d, J = 2.7 Hz, CHAr), 107.5 (d, J = 21.5 Hz, CHAr), 100.4 (d, J = 26.0 Hz, CHAr), 61.6 (C2), 49.1 (C1), 39.8 (Ad), 39.4 (Ad), 39.1 (Ad), 38.7 (Ad), 38.66 (Ad), 36.9 (Ad), 34.8 (Ad), 34.3 (Ad), 32.6 (Ad), 28.2 (Ad), 27.6 (Ad), 14.2 (C3). **HPLC-MS** (ESI) t_r = 18.2 min; [M+H]⁺ = 436.1 *m/z*. **HRMS** (ESI) [M+H]⁺ calcd for C₂₇H₂₈F₂NO₂ 436.2088 found 436.2088.

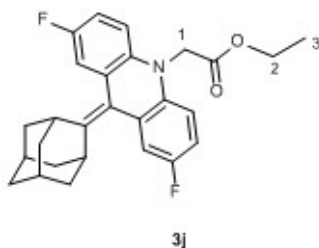


Figure 6.20

Compound 3j: 2-adamantanone **1** (42 mg, 0.27 mmol) and ketone **2j** were coupled following the above-mentioned procedure (method A, Scheme 6.6). The chromatographic purification (eluent: cyclohexane) provided compound **3j** (91 mg, 76%) as pale yellow crystals (mp = 209 - 211 °C). **¹H NMR** (400 MHz, CDCl₃) δ 6.95 - 6.86 (m, 4H, Ar), 6.69 (dd, J = 8.9, 4.6 Hz, 2H, Ar), 4.60 (s, 2H, C1), 4.29 (q, J = 7.1 Hz, 2H, C2), 3.43 (br s, 2H, H _{α}), 2.25 - 1.61 (m, 12H, Ad), 1.30 (t, J = 7.1 Hz, 3H, C3). **¹³C NMR** (100 MHz, CDCl₃) δ 169.5 (COO), 157.7 (d, J = 236.5 Hz, CF), 146.9 (Cq), 139.7 (d, J = 1.9 Hz, Cq), 127.1 (d, J = 7.6 Hz, Cq), 118.9 (Cq), 113.9 (d, J = 22.8 Hz, CHAr), 113.0 (d, J = 8.4 Hz, CHAr), 112.7 (d, J = 22.7 Hz, CHAr), 61.4 (C2), 49.1 (C1), 36.9 (Ad), 32.3 (Ad), 14.2 (C3). **HPLC-MS** (ESI) t_r = 19.4 min; [M+H]⁺ = 436.2 *m/z*. **HRMS** (ESI) [M+H]⁺ calcd for C₂₇H₂₈F₂NO₂ 436.2088 found 436.2089.

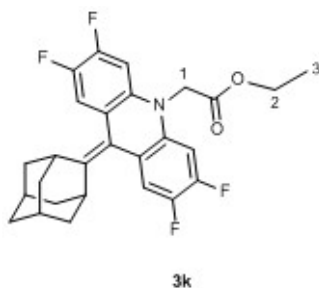


Figure 6.21

Compound 3k: 2-adamantanone **1** (61 mg, 0.41 mmol) and ketone **2k** were

coupled following the abovementioned procedure (method A, Scheme 6.6). The chromatographic purification (eluent: cyclohexane) provided compound **3k** (93 mg, Y = 48%) as pink solid (mp = 175 - 177 °C). $^1\text{H NMR}$ (400 MHz, CDCl_3) δ 6.98 (dd, J = 10.7, 8.6 Hz, 2H, Ar), 6.57 (dd, J = 12.0, 6.8 Hz, 2H, Ar), 4.51 (s, 2H, C1), 4.33 (q, J = 7.1 Hz, 2H, C2), 3.33 (br s, 2H, H_α), 2.20 - 1.59 (m, 12H, Ad), 1.34 (t, J = 7.1 Hz, 3H, C3). $^{13}\text{C NMR}$ (100 MHz, CDCl_3) δ 168.7 (COO), 148.6 (dd, J = 243.7, 13.6 Hz, CF), 146.8 (Cq), 145.2 (dd, J = 239.3, 12.9 Hz, CF), 139.6 (dd, J = 7.7, 2.1 Hz, Cq), 121.5 (dd, J = 5.5, 3.2 Hz, Cq), 117.1 (Cq), 115.6 (dd, J = 18.8, 1.3 Hz, CHAr), 102.1 (d, J = 21.4 Hz CHAr), 61.9 (C2), 49.2 (C1), 36.8 (Ad), 32.3 (Ad), 14.2 (C3). **HPLC-MS** (ESI) t_r = 19.9 min; $[\text{M}+\text{H}]^+ = 472.1$ m/z , $[\text{M}+\text{Na}]^+ = 494.0$ m/z . **HRMS** (ESI) $[\text{M}+\text{H}]^+$ calcd for $\text{C}_{27}\text{H}_{26}\text{F}_4\text{NO}_2$ 472.1900 found 472.1899.

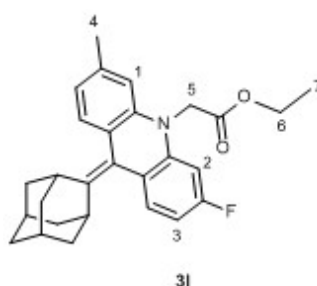


Figure 6.22

Compound 3l: 2-adamantanone **1** (63 mg, 0.42 mmol) and ketone **2l** were coupled following the above-mentioned procedure (method A, Scheme 6.6). The chromatographic purification (eluent: cyclohexane) provided compound **3l** (161 mg, 89%) as a yellow solid (mp = 195 - 197 °C). $^1\text{H NMR}$ (400 MHz, CDCl_3) δ 7.15 - 7.10 (m, 2H, Ar), 6.84 (d, J = 7.6 Hz, 1H, Ar), 6.70 (dt, J = 8.4, 2.2 Hz, 1H, H3), 6.58 (s, 1H, H1), 6.49 (dd, J = 11.1, 2.2 Hz, 1H, H2), 4.59 (s, 2H, H5), 4.30 (q, J = 7.1 Hz, 2H, H6), 3.42 (s, 1H, H_α), 3.36 (s, 1H, H_α), 2.34 (s, 3H, H4), 2.21 - 1.61 (m, 12H, Ad), 1.31 (t, J = 7.1 Hz, 3H, H7). $^{13}\text{C NMR}$ (100 MHz, CDCl_3) δ 169.5 (COO), 161.6 (d, J = 240.7 Hz, CF), 144.7 (d, J = 10.0 Hz, Cq), 144.1 (Cq), 142.7 (Cq), 135.9 (Cq), 128.2 (d, J = 9.4 Hz, CHAr), 127.2 (CHAr), 123.5 (Cq), 122.1 (d, J = 2.6 Hz, Cq), 121.7 (CHAr), 118.9 (Cq), 113.2 (CHAr), 106.8 (d, J = 21.4 Hz, CHAr), 100.1 (d, J = 25.9 Hz, CHAr), 61.4 (C6), 48.8 (C5), 37.1 (Ad), 32.2 (Ad), 21.6 (C4), 14.2 (C7). **HPLC-MS** (ESI) t_r = 20.9 min; $[\text{M}+\text{H}]^+ = 432.2$ m/z , $[\text{M}+\text{Na}]^+ = 454.2$ m/z . **HRMS** (ESI) $[\text{M}+\text{H}]^+$ calcd for $\text{C}_{28}\text{H}_{31}\text{FNO}_2$ 432.2339 found 432.2342.

Compound 3m: 2-adamantanone **1** (45 mg, 0.3 mmol) and ketone **2m** were coupled following the above-mentioned procedure (method B, Scheme 6.6). The chromatographic purification (eluent: cyclohexane/EtOAc = 95:5) provided com-

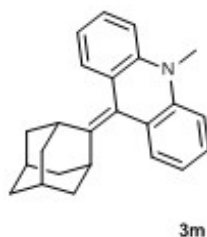


Figure 6.23

pound **3m** (93 mg, 95%). The obtained spectroscopic data were in agreement with the literature data [see Ref. 390].

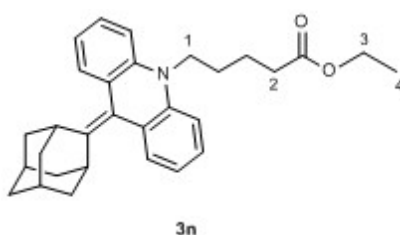


Figure 6.24

Compound 3n: 2-adamantanone **1** (69 mg, 0.46 mmol) and ketone **2n** were coupled following the above-mentioned procedure (method A, Scheme 6.6). The chromatographic purification (eluent: cyclohexane/EtOAc = 90:10) provided compound **3n** (193 mg, 95%) as a yellow oil. $^1\text{H NMR}$ (400 MHz, CDCl_3) δ 7.21 - 7.15 (m, 4H, Ar), 7.01 (d, $J = 8.0$ Hz, 2H, Ar), 6.96 (t, $J = 7.4$ Hz, 2H, Ar), 4.08 (q, $J = 7.1$ Hz, 2H, C3), 3.99 (t, $J = 6.8$ Hz, 2H, C1), 3.41 (s, 2H, H_α), 2.30 (t, $J = 7.4$ Hz, 2H, C2), 2.21 - 1.84 (m, 12H), 1.74 - 1.66 (m, 4H), 1.21 (t, $J = 7.1$ Hz, 3H, C4). $^{13}\text{C NMR}$ (100 MHz, CDCl_3) δ 173.3 (COO), 143.9 (Cq), 143.4 (Cq), 127.3 (CHAr), 126.8 (Cq), 126.0 (CHAr), 120.5 (Cq), 119.9 (CHAr), 112.9 (CHAr), 60.2 (C3), 44.8 (C1), 37.1, 33.9, 32.1, 25.7, 22.2, 14.1 (C4). **HPLC-MS** (ESI) $t_r = 28.5$ min; $[\text{M}+\text{H}]^+ = 442.3$ m/z . **HRMS** (ESI) $[\text{M}+\text{H}]^+$ calcd for $\text{C}_{30}\text{H}_{36}\text{NO}_2$ 442.2746 found 442.2748.

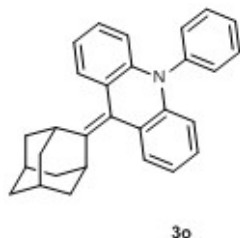


Figure 6.25

Compound 3o: 2-adamantanone **1** (14.7 mg, 0.1 mmol) and ketone **2o** were

coupled following the above-mentioned procedure (method B, Scheme 6.6). The chromatographic purification (eluent: cyclohexane/EtOAc = 95:5) provided compound **3o** (35 mg, 92%). The obtained spectroscopic data were in agreement with the literature data [see Ref. 390].

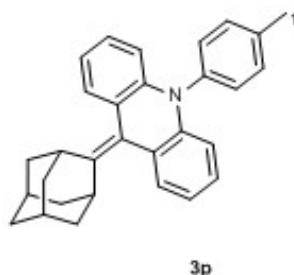


Figure 6.26

compound 3p: 2-adamantanone **1** (14 mg, 0.095 mmol) and ketone **2p** were coupled following the above-mentioned procedure (method B, Scheme 6.6). The chromatographic purification (eluent: cyclohexane/EtOAc = 90:10) provided compound **3p** (35.6 mg, 93%) as a sticky solid. $^1\text{H NMR}$ (400 MHz, CDCl_3) δ 7.42 (d, $J = 8.0$ Hz, 2H, Ar), 7.28 - 7.25 (m, 4H, Ar), 7.02 - 6.93 (m, 4H, Ar), 6.48 (dd, $J = 8.1, 1.3$ Hz, 2H, Ar), 3.51 (s, 2H, H_α), 2.50 (s, 3H, H_1), 2.04 - 1.89 (m, 12H, Ad). $^{13}\text{C NMR}$ (100 MHz, CDCl_3) δ 144.7 (Cq), 144.5 (Cq), 138.0 (Cq), 137.9 (Cq), 131.0 (CHAr), 130.9 (CHAr), 127.2 (CHAr), 125.8 (CHAr), 124.0 (Cq), 119.9 (CHAr), 119.8 (Cq), 113.7 (CHAr), 39.7 (Ad), 37.2 (Ad), 32.1 (Ad), 28.2 (Ad), 21.3 (C1). **HPLC-MS** (ESI) $t_r = 37.1$ min; $[\text{M}+\text{H}]^+ = 404.1$ m/z . **HRMS** (ESI) $[\text{M}+\text{H}]^+$ calcd for $\text{C}_{30}\text{H}_{30}\text{N}$ 404.2378 found 404.2381.

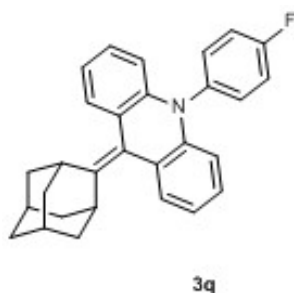


Figure 6.27

Compound 3q: 2-adamantanone **1** (18 mg, 0.12 mmol) and ketone **2q** were coupled following the above-mentioned procedure (method B, Scheme 6.6). The chromatographic purification (eluent: cyclohexane) provided compound **3q** (45 mg, 91%) as a sticky solid. $^1\text{H NMR}$ (400 MHz, CDCl_3) δ 7.38 - 7.34 (m, 2H, Ar), 7.31 - 7.24 (m, 4H, Ar), 7.03 - 6.95 (m, 4H, Ar), 6.43 (d, $J = 7.7$ Hz, 2H, Ar), 3.49 (s, 2H, H_α), 2.04 - 1.89 (m, 12H, Ad). $^{13}\text{C NMR}$ (100 MHz, CDCl_3) δ

162.1 (d, $J = 245.9$ Hz, CF), 145.0 (Cq), 144.4 (Cq), 136.6 (d, $J = 3.3$ Hz, Cq), 133.0 (d, $J = 8.5$ Hz, CHAr), 127.3 (CHAr), 125.9 (CHAr), 124.2 (Cq), 120.2 (CHAr), 119.6 (Cq), 117.3 (d, $J = 22.3$ Hz, CHAr), 113.6 (CHAr), 39.7 (Ad), 37.1 (Ad), 32.2 (Ad), 28.1 (Ad). **HPLC-MS** (ESI) $t_r = 34.2$ min; $[M+H]^+ = 408.2$ m/z . **HRMS** (ESI) $[M+H]^+$ calcd for $C_{29}H_{27}FN$ 408.2128 found 408.2126.

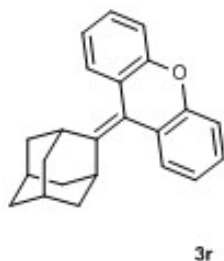


Figure 6.28

Compound 3r: 2-adamantanone **1** (230 mg, 1.53 mmol) and ketone **2r** were coupled following the above-mentioned procedure (method A, Scheme 6.6). The chromatographic purification (eluent: cyclohexane) provided compound **3r** (434 mg, 90%) as a yellow solid (mp = 217 - 219 °C). **1H NMR** (400 MHz, $CDCl_3$) δ 7.29 (d, $J = 8.0$ Hz, 2H, Ar), 7.23 - 7.18 (m, 4H, Ar), 7.12 - 7.08 (m, 2H, Ar), 3.53 (br s, 2H, H_α), 2.04 (br s, 2H, Ad), 1.97 - 1.90 (m, 10H, Ad). **^{13}C NMR** (100 MHz, $CDCl_3$) δ 155.0 (Cq), 146.6 (Cq), 127.5 (CHAr), 126.9 (CHAr), 126.7 (Cq), 122.6 (CHAr), 116.4 (CHAr), 116.38 (Cq), 39.5 (Ad), 37.0 (Ad), 32.5 (Ad), 27.9 (Ad). **HPLC-MS** (ESI, method B) $t_r = 22.5$ min; $[M+H]^+ = 315.2$ m/z . **HRMS** (ESI) $[M+H]^+$ calcd for $C_{23}H_{23}O$ 315.1749 found 315.1749.

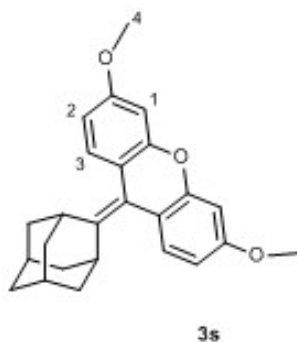


Figure 6.29

Compound 3s: 2-adamantanone **1** (46.3 mg, 0.31 mmol) and ketone **2s** were coupled following the above-mentioned procedure (method A, Scheme 6.6). The chromatographic purification (eluent: cyclohexane/EtOAc = 95:5) provided compound **3s** (89 mg, 77%) as orange crystals (mp = 182 - 184 °C). **1H NMR** (400 MHz, $CDCl_3$) δ 7.19 (d, $J = 8.5$ Hz, 2H, H3), 6.76 (d, $J = 2.4$ Hz, 2H, H1),

6.68 (dd, $J = 8.5, 2.4$ Hz, 2H, H2), 3.83 (s, 6H, H4), 3.48 (s, 2H, H $_{\alpha}$), 2.03 (s, 2H, Ad), 1.96 - 1.91 (m, 10H, Ad). ^{13}C NMR (100 MHz, CDCl_3) δ 158.6 (Cq), 155.9 (Cq), 144.0 (Cq), 127.9 (CHAr), 119.5 (Cq), 115.4 (Cq), 109.0 (CHAr), 101.7 (CHAr), 55.4 (C4), 39.4 (Ad), 37.1 (Ad), 32.5 (Ad), 27.9 (Ad). HPLC-MS (ESI) $t_r = 20.6$ min; $[\text{M}+\text{H}]^+ = 375.2$ m/z , $[\text{M}+\text{Na}]^+ = 397.1$ m/z . HRMS (ESI) $[\text{M}+\text{H}]^+$ calcd for $\text{C}_{25}\text{H}_{27}\text{O}_3$ 375.1960 found 375.1959.

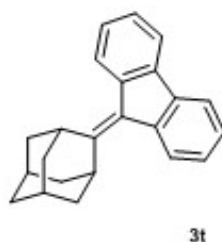


Figure 6.30

Compound 3t: 2-adamantanone **1** (166.5 mg, 1.11 mmol) and ketone **2t** were coupled following the above-mentioned procedure (method A, Scheme 6.6). The chromatographic purification (eluent: cyclohexane) provided compound **3t** (191 mg, 58%). The obtained spectroscopic data were in agreement with the literature data [see Ref. 390].

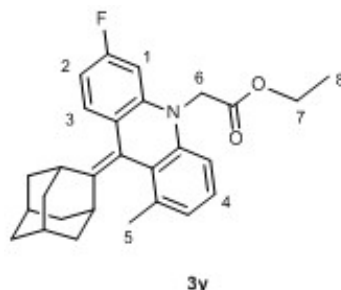


Figure 6.31

Compound 3y: 2-adamantanone **1** (28.5 mg, 0.19 mmol) and ketone **2y** were coupled following the above-mentioned procedure (method B, Scheme 6.6). The chromatographic purification (eluent: cyclohexane/EtOAc = 95:5) provided compound **3y** (75 mg, 91%) as yellow crystals (mp = 134 - 136 °C). ^1H NMR (400 MHz, CDCl_3) δ 7.16 (dd, $J = 8.4, 6.6$ Hz, 1H, H3), 7.09 (t, $J = 7.8$ Hz, 1H, H4), 6.94 (d, $J = 7.5$ Hz, 1H, Ar), 6.73 (dt, $J = 8.4, 2.2$ Hz, 1H, H2), 6.65 (d, $J = 8.1$ Hz, 1H, Ar), 6.55 (dd, $J = 11.1, 2.2$ Hz, 1H, H1), 4.65 (d, $J = 17.6$ Hz, 1H, H6a), 4.59 (d, $J = 17.6$ Hz, 1H, H6b), 4.29 (q, $J = 7.1$ Hz, 2H, H7), 3.26 (s, 1H, H $_{\alpha}$), 2.63 (s, 1H, H $_{\alpha}$), 2.38 (s, 3H, H5), 2.20 - 1.97 (m, 5H, Ad), 1.83 (br s, 3H, Ad), 1.69 - 1.59 (m, 2H, Ad), 1.45 (m, 2H, Ad), 1.30 (t, $J = 7.1$ Hz, 3H, H8). ^{13}C

NMR (100 MHz, CDCl₃) δ 169.3 (COO), 161.5 (d, $J = 240.0$ Hz, CF), 146.1 (Cq), 144.5 (d, $J = 10.2$ Hz, Cq), 143.2 (Cq), 134.7 (Cq), 127.8 (d, $J = 9.4$ Hz, CHAr), 125.7 (Cq), 125.5 (CHAr), 123.5 (CHAr), 123.2 (d, $J = 2.6$ Hz, Cq), 118.9 (Cq), 109.4 (CHAr), 106.9 (d, $J = 21.6$ Hz, CHAr), 100.0 (d, $J = 25.9$ Hz, CHAr), 61.4 (C7), 48.9 (C6), 40.0 (Ad), 39.6 (Ad), 39.0 (Ad), 37.3 (Ad), 36.8 (Ad), 33.4 (Ad), 32.6 (Ad), 27.9 (Ad), 27.7 (Ad), 20.2 (C5), 14.2 (C8). **HPLC-MS** (ESI) $t_r = 23.1$ min; $[M+H]^+ = 432.2$ m/z , $[M+Na]^+ = 454.1$ m/z . **HRMS** (ESI) $[M+H]^+$ calcd for C₂₈H₃₁FNO₂ 432.2339 found 432.2338.

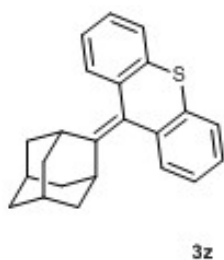
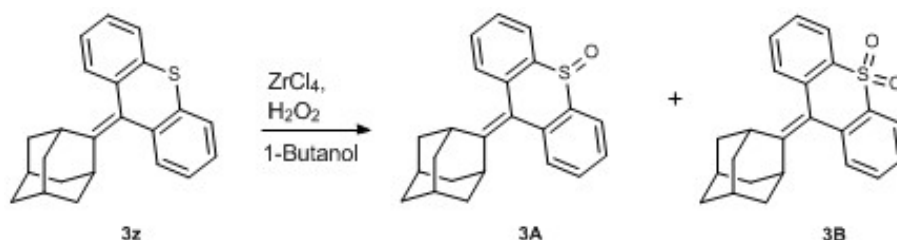


Figure 6.32

Compound 3z: 2-adamantanone **1** (60 mg, 0.4 mmol) and ketone **2z** were coupled following the above-mentioned procedure (method B, Scheme 6.6). The chromatographic purification (eluent: cyclohexane/EtOAc = 98:2) provided compound **3z** (119 mg, 90%) as a white solid (mp = 220 - 222 °C). **¹H NMR** (400 MHz, CDCl₃) δ 7.50 (dd, $J = 7.6, 1.1$ Hz, 2H, Ar), 7.30 (dd, $J = 7.6, 1.4$ Hz, 2H, Ar), 7.23 (dt, $J = 7.3, 1.2$ Hz, 2H, Ar), 7.16 (dt, $J = 7.5, 1.7$ Hz, 2H, Ar), 3.25 (s, 2H, H_α), 2.18 - 2.10 (m, 5H, Ad), 1.87 (s, 3H, Ad), 1.75 - 1.59 (m, 4H, Ad). **¹³C NMR** (100 MHz, CDCl₃) δ 147.2 (Cq), 137.6 (Cq), 135.6 (Cq), 128.1 (CHAr), 127.3 (CHAr), 125.8 (CHAr), 125.7 (CHAr), 39.9 (Ad), 39.4 (Ad), 37.0 (Ad), 33.0 (Ad), 28.4 (Ad), 27.6 (Ad). **HPLC-MS** (ESI) $t_r = 24.4$ min; $[M+H]^+ = 331.2$ m/z . **HRMS** (ESI) $[M+H]^+$ calcd for C₂₃H₂₃S 331.1520 found 331.1522.

Procedure for the synthesis of alkenes **3A** and **3B**:



Scheme 6.7

Compound 3A and **3B** were synthesized by the direct oxidation of alkene **3z** (Scheme 6.7), by adapting a reported synthetic procedure [see Ref. 387]. Alkene

3z (40.3 mg, 0.122 mmol) was dissolved in 1-butanol (4.5 mL). Then, H₂O₂ (30% in H₂O, 122 μL, 1.08 mmol) and ZrCl₄ (71.1 mg, 0.31 mmol) were added and the mixture was stirred at room temperature for 15 minutes. After that, the solution was evaporated under vacuum and the crude product was purified by flash chromatography on silica gel (eluent: cyclohexane/EtOAc = 90:10). However, it was not possible to isolate compounds **3A** and **3B** from the starting material **3z**. Both the ¹H NMR spectrum and the HPLC-MS analysis showed a 78% conversion of alkene **3z** to a mixture of alkenes **3A** and **3B** (**3A/3B** = 85/15). The mixture of the three olefins (**3z**, **3A** and **3B**) was subjected to photooxygenation reaction, but no traces of the corresponding 1,2-dioxetanes were observed.

Alkene 3A: ¹H NMR (400 MHz, CDCl₃) δ 7.93 - 7.90 (m, 2H, Ar), 7.42 - 7.36 (m, 6H, Ar), 3.30 (br s, 2H, H_α), 2.18 - 2.09 (m, 5H, Ad), 1.90 (br s, 3H, Ad), 1.80 (d, J = 11.2 Hz, 2H, Ad), 1.61 (d, J = 11.6 Hz, 2H, Ad). HPLC-MS (ESI) t_r = 14.0 min; [M+H]⁺ = 347.0 m/z, [M+Na]⁺ = 369.0 m/z, [2M+Na]⁺ = 715.1 m/z.

Alkene 3B: ¹H NMR (400 MHz, CDCl₃) δ 8.04 (d, J = 7.6 Hz, 2H, Ar), 7.45 - 7.36 (m, 6H, Ar), 3.30 (br s, 2H, H_α), 2.18 - 2.09 (m, 5H, Ad), 1.90 (br s, 3H, Ad), 1.80 (d, J = 11.2 Hz, 2H, Ad), 1.61 (d, J = 11.6 Hz, 2H, Ad). HPLC-MS (ESI) t_r = 13.5 min; [M+H]⁺ = 363.0 m/z, [M+Na]⁺ = 385.0 m/z, [2M+Na]⁺ = 747.0 m/z.

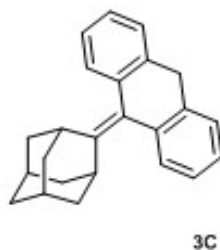


Figure 6.33

Compound 3C: 2-adamantanone **1** (45 mg, 0.3 mmol) and ketone **2C** were coupled following the above-mentioned procedure (method B, Scheme 6.6). The chromatographic purification (eluent: cyclohexane) provided compound **3C** (72 mg, 77%). The obtained spectroscopic data were in agreement with the literature data [see Ref. 390].

Compound 3D: 2-adamantanone **1** (90 mg, 0.6 mmol) and ketone **2D** were coupled following the above-mentioned procedure (method B, Scheme 6.6). The chromatographic purification (eluent: cyclohexane) provided compound **3D** (142 mg, 68%) as a colorless oil. ¹H NMR (400 MHz, CDCl₃) δ 8.09 (d, J = 7.2 Hz, 1H, Ar), 7.90 (d, J = 7.6 Hz, 1H, Ar), 7.79 (d, J = 8.4 Hz, 1H, Ar), 7.70 (dd, J = 7.2, 1.6 Hz, 1H, Ar), 7.56 (t, J = 7.6 Hz, 1H, Ar), 7.49 - 7.43 (m, 3H,

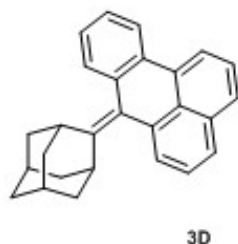


Figure 6.34

Ar), 7.34 (dt, $J = 7.6, 1.6$ Hz, 1H, Ar), 7.27 (dt, $J = 7.4, 1.2$ Hz, 1H, Ar), 3.63 (s, 1H, H_α), 3.58 (s, 1H, H_α), 2.00 - 1.82 (m, 12H, Ad). ^{13}C NMR (100 MHz, CDCl_3) δ 148.5 (Cq), 135.3 (Cq), 134.3 (Cq), 133.6 (Cq), 132.9 (Cq), 132.0 (Cq), 130.0 (Cq), 128.2 (CHAr), 127.2 (CHAr), 126.3 (CHAr), 125.9 (CHAr), 125.7 (CHAr), 125.5 (CHAr), 124.9 (CHAr), 124.9 (CHAr), 124.5 (CHAr), 123.7 (Cq), 119.1 (CHAr), 39.7 (Ad), 39.6 (Ad), 37.0 (Ad), 33.5 (Ad), 31.2 (Ad), 30.3 (Ad), 27.9 (Ad). **HPLC-MS** (ESI) $t_r = 29.7$ min; $[\text{M}+\text{H}]^+ = 349.1$ m/z . **HRMS** (ESI) $[\text{M}+\text{H}]^+$ calcd for $\text{C}_{27}\text{H}_{25}$ 349.1956 found 349.1955.

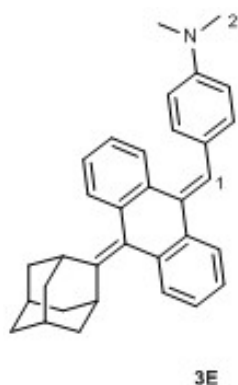


Figure 6.35

Compound 3E: 2-adamantanone **1** (70 mg, 0.46 mmol) and ketone **2E** were coupled following the above-mentioned procedure (method A, Scheme 6.6). The crude was purified by flash chromatography on silica gel (eluent: cyclohexane), however, it was not possible to perfectly purify compound **3E** (24 mg, 12% yield, calculated from the ^1H NMR spectrum). Because of the small amount of not perfectly purified alkene **3E**, ^{13}C NMR spectrum was not acquired. Both the ^1H NMR spectrum and the **HPLC-MS** analysis confirmed the presence of **3E**. The photooxygenation was carried out on the contaminated sample of **3E** and we observed no traces of the corresponding 1,2-dioxetane. ^1H NMR (400 MHz, CDCl_3) δ 7.69, (d, $J = 8.8$ Hz, 2H, Ar), 7.37 - 7.32 (m, 4H, Ar), 7.25 - 7.13 (m, 4H, Ar), 6.92 (s, 1H, H1), 6.45 (d, $J = 8.8$ Hz, 2H, Ar), 3.59 (br s, 1H, H_α), 3.44 (br s, 1H, H_α), 2.97 (s, 6H, H2), 2.51 (d, $J = 12.8$ Hz, 2H, Ad), 2.24 - 2.13 (m,

10H, Ad). **HPLC-MS** (ESI) $t_r = 35.4$ min; $[M+H]^+ = 444.2$ m/z .

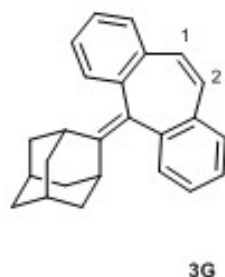


Figure 6.36

Compound 3G: 2-adamantanone **1** (146 mg, 0.97 mmol) and ketone **2G** were coupled following the above-mentioned procedure (method A, Scheme 6.6). The chromatographic purification (eluent: cyclohexane) provided compound **3G** (10 mg, 3%) as a sticky solid. $^1\text{H NMR}$ (400 MHz, CDCl_3) δ 7.34 - 7.30 (m, 4H, Ar), 7.24 - 7.02 (m, 4H, Ar), 6.92 (s, 2H, H1 and H2), 2.65 (br s, 2H, H_α), 2.09 - 1.93 (m, 6H, Ad), 1.82 - 1.80 (m, 3H, Ad), 1.65 - 1.62 (m, 3H, Ad). $^{13}\text{C NMR}$ (100 MHz, CDCl_3) δ 146.6 (Cq), 139.6 (Cq), 134.9 (Cq), 131.0 (CHAr), 128.2 (Cq), 121.1 (CHAr), 127.9 (CHAr), 127.7 (CHAr), 125.9 (CHAr), 39.5 (Ad), 39.3 (Ad), 37.1 (Ad), 32.8 (Ad), 28.4 (Ad), 27.9 (Ad). **HPLC-MS** (ESI) $t_r = 25.6$ min; $[M+H]^+ = 325.1$ m/z , $[M+Na]^+ = 347.1$ m/z . **HRMS** (ESI) $[M+H]^+$ calcd for $\text{C}_{25}\text{H}_{25}$ 325.1956 found 325.1956.

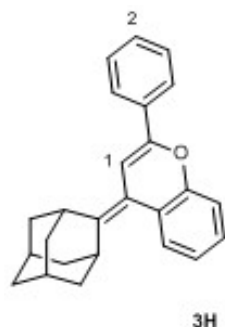


Figure 6.37

Compound 3H: 2-adamantanone **1** (45 mg, 0.3 mmol) and ketone **2H** were coupled following the above-mentioned procedure (method B, Scheme 6.6). The chromatographic purification (eluent: cyclohexane) provided compound **3H** (68 mg, 67%) as a pale yellow solid (mp = 124 -126 °C). $^1\text{H NMR}$ (400 MHz, CDCl_3) δ 7.74 (d, $J = 7.2$ Hz, 2H, Ar), 7.42 - 7.36 (m, 4H, Ar), 7.34 - 7.30 (m, 2H, Ar), 7.07 (t, $J = 8.4$ Hz, 1H, H2), 6.62 (s, 1H, H1), 3.55 (s, 1H, H_α), 3.19 (s, 1H, H_α), 2.05 - 1.88 (m, 12H, Ad). $^{13}\text{C NMR}$ (100 MHz, CDCl_3) δ 154.3 (Cq), 148.9 (Cq), 141.2 (Cq), 134.1 (Cq), 128.3 (CHAr), 128.1 (CHAr), 127.41 (CHAr),

127.40 (CHAr), 124.4 (CHAr), 124.1 (Cq), 122.8 (CHAr), 116.9 (CHAr), 115.9 (Cq), 102.6 (C1), 39.4 (Ad), 39.2 (Ad), 37.1 (Ad), 33.5 (Ad), 28.2 (Ad). **HPLC-MS** (ESI) t_r = 35.3 min; $[M+H]^+$ = 341.3 m/z . **HRMS** (ESI) $[M+H]^+$ calcd for $C_{25}H_{25}O$ 341.1905 found 341.1908.

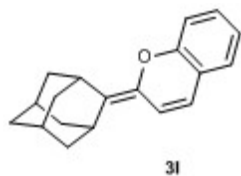
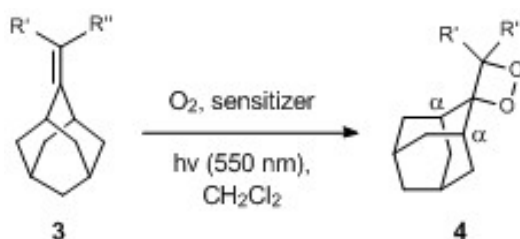


Figure 6.38

Compound 3I: 2-adamantanone **1** (1.54 g, 10.27 mmol) and lactone **2I** were coupled following the above-mentioned procedure (method C, Scheme 6.6). The chromatographic purification (eluent: cyclohexane/EtOAc = 90:10) provided compound **3I** (33 mg, 18%) as a yellow sticky solid. 1H NMR (400 MHz, $CDCl_3$) δ 7.05 (dt, J = 9.2, 1.6 Hz, 1H, Ar), 6.87 (dd, J = 7.3, 1.5 Hz, 1H, Ar), 6.80 (t, J = 7.2 Hz, 1H, Ar), 6.71 (d, J = 8.1 Hz, 1H, Ar), 6.37 (d, J = 10.1 Hz, 1H), 6.17 (d, J = 10.1 Hz, 1H), 3.30 (s, 1H, H_α), 2.23 (s, 1H, H_α), 1.99 (br s, 2H, Ad), 1.9 - 1.74 (m, 10H, Ad). ^{13}C NMR (100 MHz, $CDCl_3$) δ 154.5 (Cq), 138.2 (Cq), 128.9 (CHAr), 125.7 (CHAr), 124.1 (Cq), 121.8 (Cq), 121.77 (CHAr), 121.5 (CHAr), 119.2 (CHAr), 114.5 (CHAr), 39.3 (Ad), 38.6 (Ad), 37.2 (Ad), 31.2 (Ad), 29.2 (Ad), 28.4 (Ad). **HPLC-MS** (ESI) t_r = 21.8 min; $[M+H]^+$ = 265.1 m/z . **HRMS** (ESI) $[M+H]^+$ calcd for $C_{19}H_{21}O$ 265.1592 found 265.1596.

6.3.4 General procedure for the synthesis of 1,2-dioxetanes 4h-t, 4H-I:



Scheme 6.8

The 1,2-dioxetane derivatives **4** were synthesized by photooxygenation of the corresponding olefin **3** (Scheme 6.8): Alkene **3** (16 eq.) and Methylene Blue (1 eq.) were dissolved in CH_2Cl_2 (1 mL/10 mg of alkene **3**). The solution was cooled (usually at -20 °C) and subjected to an oxygen atmosphere (1 atm, balloon). The solution was stirred at the same temperature under irradiation using a 500 W

halogen lamp equipped with an UV cut-off filter (0.5% transmission at 550 nm). The irradiation was continued until the starting material disappeared (usually 2 h of irradiation), and the conversion was monitored by ^1H NMR. The product **4** was purified by a rapid filtration on a 5 mm layer of silica gel, using cooled (-40 °C) CH_2Cl_2 as eluent, and the filtered solution was evaporated under vacuum at 0 °C. The ^1H NMR spectrum was acquired immediately after stopping the reaction, whereas the ^{13}C NMR spectrum acquisition was carried out overnight. During the ^{13}C NMR spectrum acquisition, some 1,2-dioxetanes **4** partially decomposed into the corresponding ketones **1** and **2**. For this reason, the peaks referring to the dioxetane **4** are marked with a star in the ^{13}C NMR spectra. Due to the thermo-lability of the synthesized 1,2-dioxetanes **4**, it was not possible to obtain the corresponding HRMS analyses.

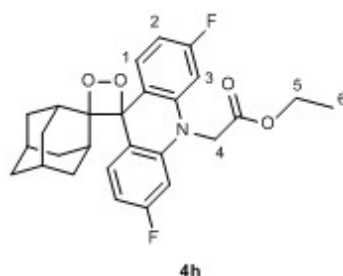


Figure 6.39

Compound 4h: alkene **3h** (21 mg, 0.048 mmol) was photooxygenated following the above-mentioned procedure (Scheme 6.8). The solution was irradiated at -20 °C for 2h to give compound **4h** (21.3 mg, 95%), as a yellow sticky solid. ^1H NMR (400 MHz, CDCl_3) δ 8.18 (dd, $J = 8.6, 6.4$ Hz, 2H, H1), 6.94 (dt, $J = 8.6, 2.4$ Hz, 2H, H2), 6.55 (dd, $J = 10.8, 2.4$ Hz, 2H, H3), 4.57 (s, 2H, H4), 4.32 (q, $J = 7.2$ Hz, 2H, H5), 2.25 (s, 2H, H_α), 1.81 (d, $J = 13.8$ Hz, 2H, Ad), 1.66 (br s, 1H, Ad), 1.49 - 1.42 (m, 5H, Ad), 1.32, (t, $J = 7.2$ Hz, 3H, H6), 1.21 (d, $J = 12.3$ Hz, 2H, Ad), 0.59 (d, $J = 15.0$ Hz, 2H, Ad). ^{13}C NMR (100 MHz, CDCl_3) δ 168.3 (COO), 163.4 (d, $J = 244.4$ Hz, CF), 140.5 (d, $J = 10.6$ Hz, Cq), 130.2 (d, $J = 9.8$ Hz, CHAr), 117.5 (d, $J = 2.5$ Hz, Cq), 108.4 (d, $J = 21.6$ Hz, CHAr), 99.7 (d, $J = 26.7$ Hz, CHAr), 97.7 (C*), 86.3 (C*), 62.0 (C5), 48.6 (C4), 36.0 (Ad), 32.9 (Ad), 32.8 (Ad), 31.6 (Ad), 25.6 (Ad), 25.4 (Ad), 14.2 (C6). HPLC-MS (ESI) $t_r = 15.3$ min; $[\text{M}+\text{H}]^+ = 468.2$ m/z .

Compound 4i: alkene **3i** (18 mg, 0.041 mmol) was photooxygenated following the above-mentioned procedure (Scheme 6.8). The solution was irradiated at -30 °C for 7h to give compound **4i** (10.6 mg, 55%), as a yellow sticky solid. ^1H NMR (400 MHz, CDCl_3) δ 8.27 (dd, $J = 8.8, 6.4$ Hz, 1H, Ar), 7.37 - 7.31 (m, 1H, Ar), 6.97 - 6.90 (m, 2H, Ar), 6.61 (d, $J = 8.4$ Hz, 1H, Ar), 6.54 (dd, $J = 10.8,$

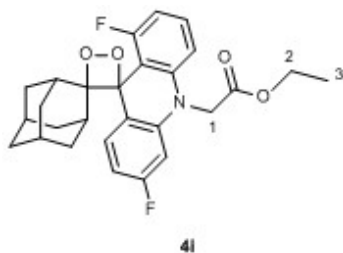


Figure 6.40

2.4 Hz, 1H, Ar), 4.62 (d, $J = 18.4$ Hz, 1H, H1a), 4.56 (d, $J = 18.4$ Hz, 1H, H1b), 4.32 (q, $J = 7.2$ Hz, 2H, H2), 2.51 (br s, 1H, H_{α}), 2.14 (br s, 1H, H_{α}), 1.94 (br d, $J = 13.6$ Hz, 1H, Ad), 1.83 (br d, $J = 16.4$ Hz, 1H, Ad), 1.66 (br s, 2H, Ad), 1.53 - 1.42 (m, 4H, Ad), 1.31 (t, $J = 7.2$ Hz, 3H, H3), 1.23 - 1.19 (m, 2H, Ad), 0.64 (br t, $J = 13.2$ Hz, 2H, Ad). $^{13}\text{C NMR}$ (100 MHz, CDCl_3) δ 168.5 (COO), 164.5 (d, $J = 117.9$ Hz, CF), 161.2 (d, $J = 126.4$ Hz, CF), 141.2 (d, $J = 7.5$ Hz, Cq), 140.2 (d, $J = 13.9$ Hz, Cq), 130.5 (d, $J = 13.1$ Hz, CHAr), 130.2 (d, $J = 14.8$ Hz, CHAr), 117.5 (Cq), 110.4 (d, $J = 32.1$ Hz, CHAr), 108.4 (d, $J = 12.6$ Hz, CHAr), 108.2 (d, $J = 12.2$ Hz, CHAr), 99.6 (d, $J = 35.6$ Hz, CHAr), 97.7 (C*), 91.2 (Cq), 86.9 (C*), 62.0 (C2), 49.4 (C1), 36.0 (Ad), 33.7 (Ad), 33.5 (Ad), 33.2 (Ad), 33.0 (Ad), 31.8 (Ad), 31.4 (Ad), 25.6 (Ad), 25.4 (Ad), 14.2 (C3). **HPLC-MS** (ESI) $t_r = 14.1$ min; $[\text{M}+\text{H}]^+ = 468.0$ m/z .

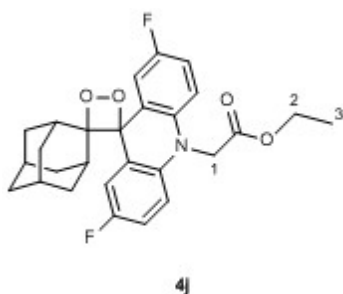


Figure 6.41

Compound 4j: alkene **3j** (20 mg, 0.046 mmol) was photooxygenated following the above-mentioned procedure (Scheme 6.8). The solution was irradiated at -20 °C for 4h to give compound **4j** (19 mg, 89%), as a yellow sticky solid. $^1\text{H NMR}$ (400 MHz, CDCl_3) δ 7.92 (dd, $J = 9.1, 2.9$ Hz, 2H, Ar), 7.12 - 7.07 (m, 2H, Ar), 6.76 (dd, $J = 8.9, 4.1$ Hz, 2H, Ar), 4.60 (s, 2H, H1), 4.30 (q, $J = 7.1$ Hz, 2H, H2), 2.31 (s, 2H, H_{α}), 1.83 (d, $J = 18.4$ Hz, 2H, Ad), 1.67 (br s, 1H, Ad), 1.50 - 1.42 (m, 5H, Ad), 1.29 (t, $J = 7.1$ Hz, 3H, H3), 1.23 (d, $J = 12.3$ Hz, 2H, Ad), 0.63 (d, $J = 13.1$ Hz, 2H, Ad). $^{13}\text{C NMR}$ (100 MHz, CDCl_3) δ 168.9 (COO), 157.9 (d, $J = 238.4$ Hz, CF), 135.8 (d, $J = 2.1$ Hz, Cq), 122.7 (d, $J = 7.1$ Hz, Cq), 116.2 (d,

$J = 23.1$ Hz, CHAr), 114.8 (d, $J = 24.2$ Hz, CHAr), 113.0 (d, $J = 7.8$ Hz, CHAr), 97.8 (C*), 86.6 (C*), 61.8 (C2), 48.8 (C1), 36.0 (Ad), 32.9 (Ad), 32.9 (Ad), 31.6 (Ad), 25.6 (Ad), 25.4 (Ad), 14.2 (C3). **HPLC-MS** (ESI) $t_r = 16.2$ min; $[M+H]^+ = 468.2$ m/z .

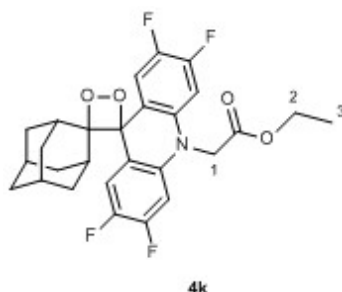


Figure 6.42

Compound 4k: alkene **3k** (25 mg, 0.053 mmol) was photooxygenated following the above-mentioned procedure (Scheme 6.8). The solution was irradiated at -20 °C for 4h to give compound **4k** (23.8 mg, 89%), as a yellow sticky solid. $^1\text{H NMR}$ (400 MHz, CDCl_3) δ 8.01 (dd, $J = 10.6, 8.7$ Hz, 2H, Ar), 6.65 (dd, $J = 11.8, 6.3$ Hz, 2H, Ar), 4.52 (s, 2H, H1), 4.33 (q, $J = 7.1$ Hz, 2H, H2), 2.26 (s, 2H, H_α), 1.82 (d, $J = 13.8$ Hz, 2H, Ad), 1.68 (br s, 1H, Ad), 1.51 - 1.44 (m, 5H, Ad), 1.33 (t, $J = 7.1$ Hz, 3H, H3), 1.26 (d, $J = 7.1$ Hz, 2H, Ad), 0.59 (d, $J = 12.9$ Hz, 2H, Ad). $^{13}\text{C NMR}$ (100 MHz, CDCl_3) δ 168.0 (COO), 150.3 (dd, $J = 247.3, 13.7$ Hz, CF), 145.7 (dd, $J = 241.7, 12.9$ Hz, CF), 135.9 (m, Cq), 117.3 (m, Cq), 117.1 (dd, $J = 21.2, 1.8$ Hz, CHAr), 101.8 (d, $J = 22.3$ Hz, CHAr), 97.8 (C*), 85.8 (C*), 62.2 (C2), 49.0 (C1), 35.9 (Ad), 33.0 (Ad), 32.9 (Ad), 31.6 (Ad), 25.5 (Ad), 25.4 (Ad), 14.2 (C3). **HPLC-MS** (ESI) $t_r = 17.5$ min; $[M+H]^+ = 504.0$ m/z .

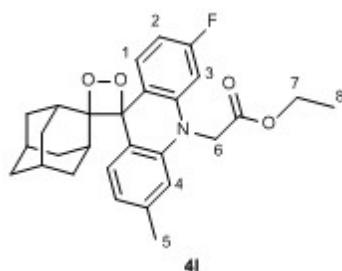


Figure 6.43

Compound 4l: alkene **3l** (20 mg, 0.046 mmol) was photooxygenated following the above-mentioned procedure (Scheme 6.8). The solution was irradiated at -20 °C for 2h to give compound **4l** (17 mg, 80%), as a sticky solid. $^1\text{H NMR}$ (400 MHz, CDCl_3) δ 8.17 (dd, $J = 8.2, 6.6$ Hz, 1H, H1), 8.08 (d, $J = 7.9$ Hz, 1H, Ar), 7.04 (d, $J = 7.9$ Hz, 1H, Ar), 6.89 (dt, $J = 8.2, 2.3$ Hz, 1H, H2), 6.62 (s, 1H,

H4), 6.54 (dd, $J = 11.0, 2.3$ Hz, 1H, H3), 4.63 (d, $J = 18.2$ Hz, 1H, H6a), 4.56 (d, $J = 18.2$ Hz, 1H, H6b), 4.31 (q, $J = 7.1$ Hz, 2H, H7), 2.41 (s, 3H, H5), 2.31 (s, 1H, H $_{\alpha}$), 2.24 (s, 1H, H $_{\alpha}$), 1.84 - 1.77 (m, 2H, Ad), 1.65 (s, 1H, Ad), 1.48 - 1.40 (m, 5H, Ad), 1.30 (t, $J = 7.1$ Hz, 3H, H8), 1.22 - 1.16 (m, 2H, Ad), 0.65 - 0.60 (m, 2H, Ad). ^{13}C NMR(100 MHz, CDCl_3) δ 168.8 (COO), 163.4 (d, $J = 243.8$ Hz, CF), 140.9 (d, $J = 10.5$ Hz, Cq), 139.3 (Cq), 138.9 (Cq), 130.1 (d, $J = 10.0$ Hz, CHAr), 128.3 (CHAr), 122.4 (CHAr), 118.9 (Cq), 117.7 (Cq), 112.6 (CHAr), 107.7 (d, $J = 21.6$ Hz, CHAr), 99.5 (d, $J = 26.4$ Hz, CHAr), 97.8 (C*), 86.6 (C*), 61.7 (C7), 48.5 (C6), 36.1 (Ad), 32.94 (Ad), 32.9 (Ad), 32.8 (Ad), 31.7 (Ad), 31.69 (Ad), 25.6 (Ad), 25.5 (Ad), 21.8 (C5), 14.2 (C8). **HPLC-MS** (ESI) $t_r = 15.9$ min; $[\text{M}+\text{H}]^+ = 464.2$ m/z .

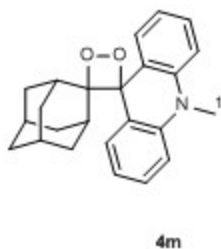


Figure 6.44

Compound 4m: alkene **3m** (21.7 mg, 0.066 mmol) was photooxygenated following the above-mentioned procedure (Scheme 6.8). The solution was irradiated at -40 °C for 12 h to give compound **4m** (19 mg, 80%), as a sticky solid. ^1H NMR (400 MHz, CDCl_3) δ 8.19 (d, $J = 8.8$ Hz, 2H, Ar), 7.41 (t, $J = 8.4$ Hz, 2H, Ar), 7.18 (t, $J = 7.6$ Hz, 2H, Ar), 7.02 (d, $J = 8.4$ Hz, 2H, Ar), 3.49 (s, 3H, H1), 2.29 (br s, 2H, H $_{\alpha}$), 1.84 (d, $J = 15.2$ Hz, 2H, Ad), 1.64 (br s, 1H, Ad), 1.47 - 1.38 (m, 5H, Ad), 1.18 (d, $J = 15.2$ Hz, 2H, Ad), 0.67 (d, $J = 13.6$ Hz, 2H, Ad). ^{13}C NMR(100 MHz, CDCl_3) δ 140.3 (Cq), 129.0 (CHAr), 127.9 (CHAr), 121.6 (Cq), 120.3 (CHAr), 111.7 (CHAr), 97.8 (C*), 87.0 (C*), 36.2, 33.1, 33.0, 32.9, 31.7, 29.7, 25.8, 25.5 (among the last unassigned 8 signals, 7 refer to adamantyl carbons and 1 refers to C1). **HPLC-MS** (ESI) $t_r = 16.7$ min; $[\text{M}+\text{H}]^+ = 360.0$ m/z .

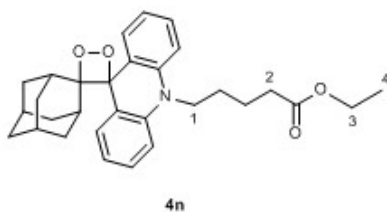


Figure 6.45

Compound 4n: alkene **3n** (12 mg, 0.027 mmol) was photooxygenated following the abovementioned procedure (Scheme 6.8). The solution was irradiated at $-40\text{ }^{\circ}\text{C}$ for 2 h to give compound **4n** (11.6 mg, 91%), as a sticky solid. The ^1H NMR spectrum showed a partial degradation of the product **4n** into the corresponding ketones **1** and **2n**. It was not possible to obtain the ^{13}C NMR spectrum because the 1,2-dioxetane **4n** totally decomposed during the overnight acquisition. ^1H NMR (400 MHz, CDCl_3) δ 8.22 (dd, $J = 8.0, 1.6$ Hz, 2H, Ar), 7.41 (dt, $J = 7.6, 1.6$ Hz, 2H, Ar), 7.16 (t, $J = 7.6$ Hz, 2H, Ar), 7.04 (d, $J = 8.0$ Hz, 2H, Ar), 4.17 (q, $J = 7.2$ Hz, 2H, H3), 4.01 - 3.98 (m, 2H, H1), 2.43 (t, $J = 7.2$ Hz, 2H, H2), 2.26 (br s, 2H, H_α), 1.92 - 1.79 (m, 6H), 1.63 (br s, 1H), 1.46 - 1.42 (m, 4H), 1.36 - 1.35 (m, 1H), 1.27 (t, $J = 7.2$ Hz, 3H, H4), 1.14 (br d, $J = 12.0$ Hz, 2H, Ad), 0.59 (br d, $J = 13.2$ Hz, 2H, Ad). HPLC-MS (ESI) $t_r = 20.8$ min; $[\text{M}+\text{H}]^+ = 474.2$ m/z .

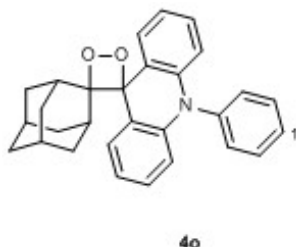


Figure 6.46

Compound 4o: alkene **3o** (30 mg, 0.077 mmol) was photooxygenated following the above-mentioned procedure (Scheme 6.8). The solution was irradiated at $-20\text{ }^{\circ}\text{C}$ for 2 h to give compound **4o** (27.5 mg, 85%), as a brown sticky solid. ^1H NMR (400 MHz, CDCl_3) δ 8.27 (dd, $J = 7.2, 2.2$ Hz, 2H, Ar), 7.65 (t, $J = 7.4$ Hz, 2H, Ar), 7.57 - 7.53 (m, 1H, H1), 7.25 (d, $J = 7.8$ Hz, 2H, Ar), 7.21 - 7.13 (m, 4H, Ar), 6.42 (dd, $J = 8.1, 1.6$ Hz, 2H, Ar), 2.35 (br s, 2H, H_α), 1.86 (d, $J = 12.5$ Hz, 2H, Ad), 1.67 (br s, 1H, Ad), 1.53 - 1.47 (m, 5H, Ad), 1.26 - 1.24 (m, 2H, Ad), 0.88 (d, $J = 13.7$ Hz, 2H, Ad). ^{13}C NMR (100 MHz, CDCl_3) δ 140.5 (Cq), 139.9 (Cq), 130.9 (CHAr), 130.8 (CHAr), 128.8 (CHAr), 128.7 (CHAr), 128.4 (CHAr), 120.4 (CHAr), 119.0 (Cq), 113.4 (CHAr), 98.2 (C*), 86.7 (C*), 36.2 (Ad), 33.0 (Ad), 31.8 (Ad), 25.7 (Ad), 25.6 (Ad). HPLC-MS (ESI) $t_r = 22.5$ min; $[\text{M}+\text{H}]^+ = 422.1$ m/z .

Compound 4p: alkene **3p** (17 mg, 0.042 mmol) was photooxygenated following the above-mentioned procedure (Scheme 6.8). The solution was irradiated at $-40\text{ }^{\circ}\text{C}$ for 2 h to give compound **4p** (16 mg, 87%), as a sticky solid. The ^{13}C NMR spectrum showed a partial degradation of the product **4p** into the corresponding ketones **1** and **2p**. ^1H NMR (400 MHz, CDCl_3) δ 8.26 (dd, $J = 7.2, 2.0$ Hz, 2H, Ar), 7.43 (d, $J = 8.2$ Hz, 2H, Ar), 7.21 - 7.11 (m, 6H, Ar), 6.45 (dd, $J =$

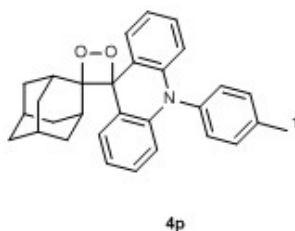


Figure 6.47

8.2, 1.3 Hz, 2H, Ar), 2.50 (s, 3H, H₁), 2.35 (s, 2H, H_α), 1.85 (d, J = 13.6 Hz, 2H, Ad), 1.67 (br s, 1H, Ad), 1.52 - 1.47 (m, 5H, Ad), 1.25 - 1.23 (m, 2H, Ad), 0.88 (br d, J = 11.0 Hz, 2H, Ad). ¹³C NMR (100 MHz, CDCl₃) δ 140.6 (Cq), 138.7 (Cq), 137.2 (Cq), 131.5 (CHAr), 130.4 (CHAr), 128.7 (CHAr), 128.3 (CHAr), 120.3 (CHAr), 119.0 (Cq), 113.5 (CHAr), 98.2 (C*), 86.7 (C*), 36.2 (Ad), 33.02 (Ad), 33.0 (Ad), 31.8 (Ad), 25.7 (Ad), 25.6 (Ad), 21.3 (Ad). **HPLC-MS** (ESI) t_r = 26.9 min; [M+H]⁺ = 436.1 m/z.

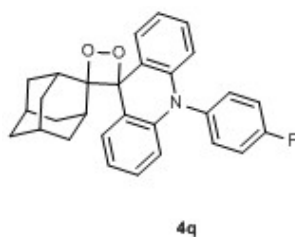


Figure 6.48

Compound 4q: alkene **3q** (19 mg, 0.047 mmol) was photooxygenated following the above-mentioned procedure (Scheme 6.8). The solution was irradiated at -20 °C for 2 h to give compound **4q** (19 mg, 92%), as a sticky solid. ¹H NMR (400 MHz, CDCl₃) δ 8.27 (dd, J = 7.3, 1.9 Hz, 2H, Ar), 7.34 (t, J = 8.5 Hz, 2H, Ar), 7.25 - 7.15 (m, 6H, Ar), 6.40 (dd, J = 7.8, 1.2 Hz, 2H, Ar), 2.34 (s, 2H, H_α), 1.85 (br d, J = 13.2 Hz, 2H, Ad), 1.67 (br s, 1H, Ad), 1.52 - 1.47 (m, 5H, Ad), 1.26 - 1.24 (m, 2H, Ad), 0.85 (br d, J = 12.8 Hz, 2H, Ad). ¹³C NMR (100 MHz, CDCl₃) δ 162.4 (d, J = 247.1 Hz, CF), 140.5 (Cq), 135.7 (Cq), 132.6 (d, J = 8.5 Hz, CHAr), 128.8 (CHAr), 128.5 (CHAr), 120.6 (CHAr), 119.2 (Cq), 118.0 (d, J = 22.4 Hz, CHAr), 113.3 (CHAr), 98.1 (C*), 86.6 (C*), 36.2 (Ad), 33.04 (Ad), 33.0 (Ad), 31.7 (Ad), 25.6 (Ad), 25.57 (Ad). **HPLC-MS** (ESI) t_r = 22.0 min; [M+H]⁺ = 440.1 m/z, [M+Na]⁺ = 462.0 m/z.

Compound 4r: alkene **3r** (25 mg, 0.08 mmol) was photooxygenated following the above-mentioned procedure (Scheme 6.8). The solution was irradiated at -20 °C for 5 h to give compound **4r** (25 mg, 91%), as a white solid. ¹H NMR

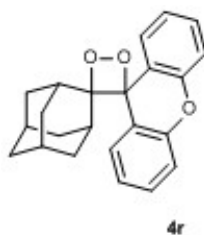


Figure 6.49

(400 MHz, CDCl_3) δ 8.18 (dd, $J = 7.6, 1.6$ Hz, 2H, Ar), 7.43 (dt, $J = 8.0, 1.6$ Hz, 2H, Ar), 7.30 (dt, $J = 7.6, 1.2$ Hz, 2H, Ar), 7.22 (dd, $J = 8.0, 1.2$ Hz, 2H, Ar), 2.43 (br s, 2H, H_α), 1.85 (d, $J = 16.8$ Hz, 2H, Ad), 1.67 (br s, 1H, Ad), 1.50 - 1.45 (m, 5H, Ad), 1.22 (d, $J = 12.7$ Hz, 2H, Ad), 0.69 (d, $J = 15.2$ Hz, 2H, Ad). ^{13}C NMR (100 MHz, CDCl_3) δ 151.2 (Cq), 129.8 (CHAr), 128.3 (CHAr), 123.1 (CHAr), 121.6 (Cq), 116.0 (CHAr), 97.0 (C*), 84.8 (C*), 36.0 (Ad), 33.1 (Ad), 32.8 (Ad), 31.7 (Ad), 25.5 (Ad), 25.3 (Ad). HPLC-MS (ESI) $t_r = 18.9$ min; $[\text{M}+\text{H}]^+ = 347.2$ m/z .

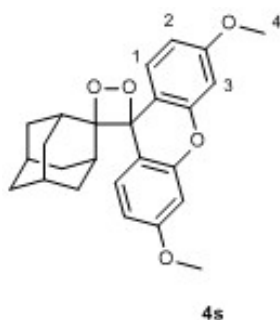


Figure 6.50

Compound 4s: alkene **3s** (19 mg, 0.051 mmol) was photooxygenated following the above-mentioned procedure (Scheme 6.8). The solution was irradiated at -40 °C for 7 h to give compound **4s** (17 mg, 82%), as a sticky solid. ^1H NMR (400 MHz, CDCl_3) δ 8.05 (d, $J = 8.6$ Hz, 2H, H1), 6.86 (dd, $J = 8.6, 2.5$ Hz, 2H, H2), 6.72 (d, $J = 2.5$ Hz, 2H, H3), 3.87 (s, 6H, H4), 2.44 (s, 2H, H_α), 1.84 (d, $J = 12.8$ Hz, 2H, Ad), 1.67 (s, 1H, Ad), 1.51 - 1.47 (m, 5H, Ad), 1.24 (d, $J = 10.8$ Hz, 2H, Ad), 0.70 (d, $J = 13.7$, 2H, Ad). ^{13}C NMR (100 MHz, CDCl_3) δ 160.9 (Cq), 152.3 (Cq), 129.2 (CHAr), 114.2 (Cq), 109.9 (CHAr), 100.7 (CHAr), 97.1 (C*), 84.6 (C*), 55.5 (C4), 36.1 (Ad), 33.17 (Ad), 32.83 (Ad), 31.8 (Ad), 25.55 (Ad), 25.43 (Ad). HPLC-MS (ESI) $t_r = 17.9$ min; $[\text{M}+\text{H}]^+ = 407.1$ m/z , $[\text{M}+\text{Na}]^+ = 429.0$ m/z .

Compound 4t: alkene **3t** (20 mg, 0.067 mmol) was photooxygenated following the above-mentioned procedure (Scheme 6.8). The solution was irradiated at

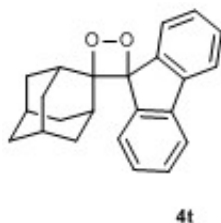


Figure 6.51

-20 °C for 10 h. During the irradiation the 1,2-dioxetane **4t** partially decomposed into the corresponding ketones **1** and **2t**. Compound **4t** was obtained with a 50% yield (11 mg), calculated from the ^1H NMR spectrum of the filtered mixture. ^1H NMR (400 MHz, CDCl_3) δ 8.04 (d, $J = 7.6$ Hz, 2H, Ar), 7.59 (d, $J = 7.6$ Hz, 2H, Ar), 7.42 (t, $J = 7.6$ Hz, 2H, Ar), 7.32 (t, $J = 7.6$ Hz, 2H, Ar), 3.06 (br s, 2H, H_α), 1.75 (br s, 1H, Ad), 1.61 (d, $J = 13.6$ Hz, 4H, Ad), 1.40 (br s, 1H, Ad), 1.34 - 1.31 (m, 4H, Ad), 0.68 (d, $J = 15.2$ Hz, 2H, Ad). ^{13}C NMR (100 MHz, CDCl_3) δ 142.6 (Cq), 140.1 (Cq), 130.2 (CHAR), 127.2 (CHAR), 126.8 (CHAR), 120.1 (CHAR), 97.7 (C*), 94.5 (C*), 36.0 (Ad), 33.7 (Ad), 33.2 (Ad), 31.9 (Ad), 25.5 (Ad), 25.4 (Ad). HPLC-MS (ESI) $t_r = 15.8$ min; $[\text{M}+\text{H}]^+ = 331.1$ m/z , $[\text{M}+\text{K}]^+ = 369.0$ m/z .

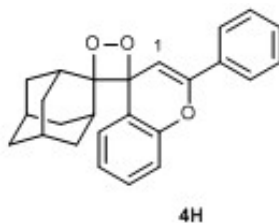


Figure 6.52

Compound 4H: alkene **3H** (20 mg, 0.059 mmol) was photooxygenated following the above-mentioned procedure (Scheme 6.8). The solution was irradiated at -20 °C for 4 h to give compound **4H** (20.9 mg, 95%), as a sticky solid. ^1H NMR (400 MHz, CDCl_3) δ 8.31 (dd, $J = 7.9, 1.5$ Hz, 1H, Ar), 7.81 (dd, $J = 8.0, 2.0$ Hz, 2H, Ar), 7.49 - 7.43 (m, 4H, Ar), 7.32 (t, $J = 8.0$, 1H, Ar), 7.26 (m, 1H, Ar), 6.30 (s, 1H, H1), 2.99 (s, 1H, H_α), 2.53 (s, 1H, H_α), 2.07 (br d, $J = 14.0$ Hz, 2H, Ad), 1.84 (br d, $J = 13.4$ Hz, 1H, Ad), 1.70 - 1.59 (m, 5H, Ad), 1.53 - 1.49 (m, 1H, Ad), 1.30 - 1.25 (m, 2H, Ad), 0.75 (br d, $J = 19.9$ Hz, 1H, Ad). ^{13}C NMR (100 MHz, CDCl_3) δ 151.0 (Cq), 150.9 (Cq), 132.9 (Cq), 129.8 (CHAR), 129.7 (CHAR), 129.3 (CHAR), 128.7 (CHAR), 125.5 (CHAR), 123.5 (CHAR), 119.6 (Cq), 116.2 (CHAR), 98.3 (CHAR), 97.4 (C*), 83.4 (C*), 36.2 (Ad), 33.8 (Ad), 33.77 (Ad), 33.0 (Ad), 32.6 (Ad), 32.4 (Ad), 31.5 (Ad), 25.98 (Ad), 25.84 (Ad).

HPLC-MS (ESI) $t_r = 20.1$ min; $[M+H]^+ = 373.3$ m/z .

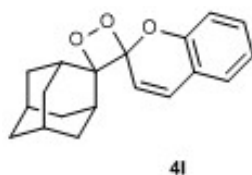


Figure 6.53

Compound 4I: alkene **3I** (25 mg, 0.095 mmol) was photooxygenated following the above-mentioned procedure (Scheme 6.8). The solution was irradiated at -40 °C for 3 h. The product **4I** partially decomposed into the corresponding ketones **1** and **2I** during the photooxygenation. Compound **4I** was obtained with a 78% yield (21.9 mg), calculated from the ^1H NMR spectrum of the filtered mixture. The peaks of the 1,2-dioxetane **4I** are marked with a star in both the ^1H NMR and ^{13}C NMR spectra. ^1H NMR (400 MHz, CDCl_3) δ 7.29 (dt, $J = 8.4, 1.6$ Hz, 1H, Ar), 7.19 - 7.15 (m, 2H, Ar), 7.02 (dt, $J = 7.2, 0.8$ Hz, 1H, Ar), 6.87 (d, $J = 10.0$ Hz, 1H), 6.24 (d, $J = 10.0$ Hz, 1H), 3.16 (s, 1H, H_α), 2.75 (s, 1H, H_α), 1.89 - 1.54 (m, 12H, Ad). ^{13}C NMR (100 MHz, CDCl_3) δ 151.2 (Cq), 130.2, 129.0, 127.0, 122.1, 118.4 (Cq), 116.5, 116.4 (among the last unassigned 6 signals, 4 refer to aromatic CH and 2 refer to alkenyl carbons), 107.2 (C*), 97.2 (C*), 36.2 (Ad), 34.6 (Ad), 33.7 (Ad), 33.0 (Ad), 32.2 (Ad), 31.7 (Ad), 31.1 (Ad), 26.1 (Ad), 26.0 (Ad). **HPLC-MS** (ESI) $t_r = 13.2$ min; $[M+H]^+ = 297.2$ m/z .

6.4 Thermochemiluminescence (TCL) Measurements

TCL imaging experiments were performed with a CCD camera as detector. The heating support consisted of a resistance with a high-resistivity (70-100 Ω). The temperature of the resistance was controlled by varying the applied current and monitored by a copper/constantan thermocouple. Sample was dissolved in acetonitrile and 2 μL of the solution was deposited on the supports. The spot was allowed to dry before the TCL measurement. TCL images were acquired upon heating the support to the desired temperature (70-130 °C, the range was chose properly for each substrates **4**) using different integration times, depending on the compound analyzed and the experimental temperature. Images were then analyzed to measure the TCL signals using the image analysis software provided with the instrument. The kinetic and thermodynamic parameters of the TCL process were obtained by measuring the TCL emission decay kinetics in the temperature range between 70 and 130 °C. For each temperature, the kinetic constant k of the TCL process (*i.e.*, the inverse of the decay time in seconds) was calculated by fitting the decay profile of the TCL emission with the first-order

decay equation (see 6.1), in which $I(t)$ is the intensity of TCL signal during time-acquisition, I_0 is the intensity of TCL signal at zero time.

$$I(t) = (I_0)e^{-kt} \quad (6.1)$$

Then, the activation energy (E_a) and the pre-exponential factor (A) of the TCL process were calculated from the kinetic constants k measured at different temperatures using the logarithmic form of the Arrhenius equation (see 6.2), in which R is the universal gas constant and T is the temperature in Kelvin.

$$\ln K = \ln A - \frac{E_a}{RT} \quad (6.2)$$

The kinetic constants at different temperatures (70 - 100 °C) and the Arrhenius plot for a model compound (**4t**) are reported in Figure 6.54. The values of kinetic constants k are listed in Table 6.2.

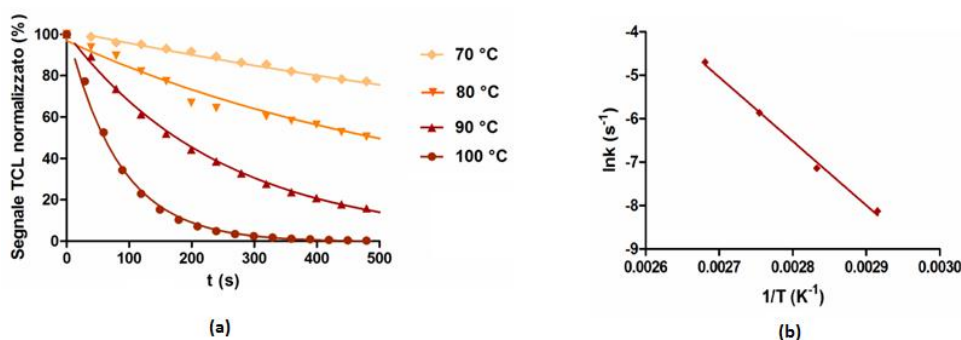


Figure 6.54

Table 6.2: Values of kinetic constants k for compound **4t**.

Temperature (° Celsius)	k (s ⁻¹)
70	$(3.0 \pm 2.1) \times 10^{-4}$
80	$(8.0 \pm 4.1) \times 10^{-4}$
90	$(2.8 \pm 1.6) \times 10^{-3}$
100	$(9.1 \pm 3.7) \times 10^{-3}$

The TCL emission spectrum for a model fluorinated 1,2-dioxetane (**4j**) and the fluorescence emission spectrum of the corresponding ketone **2j** are reported in Figure 6.55. In particular, we chose the most fluorescent dioxetane **4j**. The good overlapping confirms that the light signal recorded during the TCL process is mainly due to the electronic-excited state of the aromatic ketone, which is generated during the thermal decomposition.

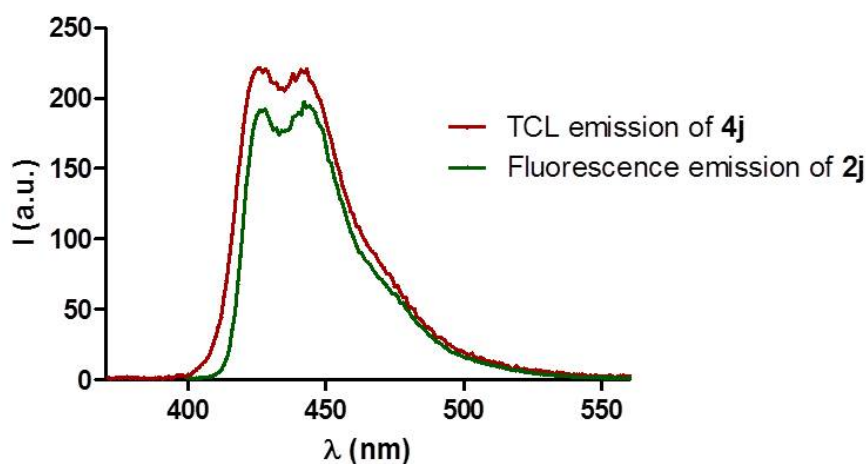


Figure 6.55

6.5 Molecular Descriptors

Table 6.3: Molecular descriptors for alkenes **3a-q**, **3u-y**, and **3F**.

Alkene	HOMO (eV)	LUMO (eV)	Ca-Mul	C9-Mul	Ca-HOMO	C9-HOMO	Ca-LUMO	C9-LUMO	Active
3a	-4.931	-0.592	0.160	-0.071	0.1341	0.0640	0.1969	0.0725	Y
3b	-4.797	-0.489	0.159	-0.070	0.1253	0.0560	0.1977	0.0746	Y
3c	-4.882	-0.551	0.159	-0.069	0.1383	0.0650	0.1956	0.0727	Y
3d	-5.043	-0.515	0.158	-0.085	0.1395	0.0731	0.2107	0.0849	Y
3e	-4.798	-0.549	0.159	-0.071	0.1177	0.0511	0.1963	0.0723	Y
3f	-4.746	-0.490	0.158	-0.071	0.1239	0.0527	0.1967	0.0743	Y
3g	-4.698	-0.433	0.156	-0.069	0.1302	0.0544	0.1974	0.0766	Y
3h	-5.169	-0.712	0.161	-0.070	0.1592	0.0822	0.1939	0.0717	Y
3i	-5.174	-0.687	0.169	-0.049	0.1457	0.0840	0.1841	0.0663	Y
3j	-4.988	-0.839	0.164	-0.069	0.1074	0.0479	0.1925	0.0641	Y
3k	-5.201	-0.925	0.165	-0.071	0.1310	0.0631	0.1901	0.0646	Y
3l	-4.951	-0.550	0.156	-0.066	0.1527	0.0736	0.1945	0.0735	Y
3m	-4.859	-0.527	0.159	-0.071	0.1280	0.0601	0.1973	0.0743	Y
3n	-4.783	-0.436	0.165	-0.076	0.1227	0.0609	0.1897	0.0672	Y
3o	-4.993	-0.753	0.163	-0.081	0.0491	0.0222	0.2046	0.0750	Y
3p	-4.883	-0.717	0.163	-0.080	0.0431	0.0179	0.2033	0.0755	Y
3q	-5.021	-0.810	0.164	-0.083	0.0457	0.0203	0.2036	0.0743	Y
3u	-4.954	-0.473	0.177	-0.095	0.1084	0.0545	0.1926	0.0768	N
3v	-5.041	-0.398	0.171	-0.104	0.1141	0.0609	0.2039	0.0889	N
3w	-4.749	-0.350	0.175	-0.097	0.0944	0.0423	0.1915	0.0797	N
3x	-4.772	-0.373	0.175	-0.097	0.0999	0.0450	0.1918	0.0799	N
3y	-5.072	-0.530	0.177	-0.095	0.1203	0.0629	0.1871	0.0741	N
3F	-5.050	-0.604	0.172	-0.073	0.1261	0.0734	0.1711	0.0596	Y
Mean	-4.937	-0.578	0.165	-0.077	0.116	0.056	0.195	0.074	
St Dev	0.147	0.155	0.007	0.013	0.032	0.018	0.008	0.007	
Var	0.022	0.024	0.00005	0.0001	0.001	0.000	0.0003	0.0001	

Structural descriptors							
Alkene	ϕ_1 (°)	ϕ_2 (°)	d_1 (Å)	d_2 (Å)	d_3 (Å)	d_4 (Å)	Active
3a	131.001	-131.511	3.064	3.065	2.783	2.782	Y
3b	131.397	-131.369	3.058	3.069	2.777	2.785	Y
3c	131.168	-131.770	3.083	3.053	2.794	2.777	Y
3d	131.512	-131.358	3.061	3.096	2.780	2.805	Y
3e	131.523	-131.104	3.056	3.059	2.774	2.776	Y
3f	131.700	-131.091	3.045	3.077	2.769	2.787	Y
3g	132.115	-131.529	3.059	3.064	2.780	2.783	Y
3h	131.812	-131.293	3.062	3.069	2.784	2.788	Y
3i	129.596	-128.890	3.087	3.162	2.786	2.924	Y
3j	131.090	-131.090	3.097	3.097	2.813	2.813	Y
3k	131.330	-131.330	3.097	3.097	2.815	2.815	Y
3l	132.527	-132.319	3.069	3.060	2.791	2.786	Y
3m	131.640	-131.640	3.072	3.072	2.787	2.793	Y
3n	130.868	-130.431	3.080	3.096	2.785	2.793	Y
3o	132.191	-132.191	3.109	3.109	2.803	2.803	Y
3p	131.621	-131.621	3.111	3.111	2.800	2.800	Y
3q	131.533	-131.533	3.113	3.113	2.802	2.802	Y
3u	124.115	-122.085	3.136	2.890	2.794	2.686	N
3v	124.985	-123.570	3.125	2.905	2.792	2.707	N
3w	124.585	-121.797	3.119	2.790	2.784	2.617	N
3x	124.333	-121.650	3.122	2.796	2.787	2.620	N
3y	124.321	-122.075	3.122	2.894	2.790	2.689	N
3F	128.113	-126.708	3.103	3.254	2.788	2.988	Y
Mean	129.786	-129.128	3.089	3.043	2.789	2.779	
St Dev	3.002	3.902	0.027	0.113	0.011	0.081	
Var	9.013	15.225	0.001	0.013	0.0001	0.007	

Table 6.4: Molecular descriptors for alkenes 3a-z and 3A-G.

Electronic descriptors									
Olefin	HOMO (eV)	LUMO (eV)	Ca-Mul	C9-Mul	Ca-HOMO	C9-HOMO	Ca-LUMO	C9-LUMO	Active
3a	-4.931	-0.592	0.160	-0.071	0.1341	0.0640	0.1969	0.0725	Y
3b	-4.797	-0.489	0.159	-0.070	0.1253	0.0560	0.1977	0.0746	Y
3c	-4.882	-0.551	0.159	-0.069	0.1383	0.0650	0.1956	0.0727	Y
3d	-5.043	-0.515	0.158	-0.085	0.1395	0.0731	0.2107	0.0849	Y
3e	-4.798	-0.549	0.159	-0.071	0.1177	0.0511	0.1963	0.0723	Y
3f	-4.746	-0.490	0.158	-0.071	0.1239	0.0527	0.1967	0.0743	Y
3g	-4.698	-0.433	0.156	-0.069	0.1302	0.0544	0.1974	0.0766	Y
3h	-5.169	-0.712	0.161	-0.070	0.1592	0.0822	0.1939	0.0717	Y
3i	-5.174	-0.687	0.169	-0.049	0.1457	0.0840	0.1841	0.0663	Y
3j	-4.988	-0.839	0.164	-0.069	0.1074	0.0479	0.1925	0.0641	Y
3k	-5.201	-0.925	0.165	-0.071	0.1310	0.0631	0.1901	0.0646	Y
3l	-4.951	-0.550	0.156	-0.066	0.1527	0.0736	0.1945	0.0735	Y
3m	-4.859	-0.527	0.159	-0.071	0.1280	0.0601	0.1973	0.0743	Y
3n	-4.783	-0.436	0.165	-0.076	0.1227	0.0609	0.1897	0.0672	Y
3o	-4.993	-0.753	0.163	-0.081	0.0491	0.0222	0.2046	0.0750	Y
3p	-4.883	-0.717	0.163	-0.080	0.0431	0.0179	0.2033	0.0755	Y
3q	-5.021	-0.810	0.164	-0.083	0.0457	0.0203	0.2036	0.0743	Y
3r	-5.365	-0.727	0.161	-0.069	0.1974	0.1272	0.2070	0.0761	Y
3s	-5.052	-0.423	0.153	-0.063	0.2100	0.1132	0.2060	0.0871	Y

3u	-4.954	-0.473	0.177	-0.095	0.1084	0.0545	0.1926	0.0768	N
3v	-5.041	-0.398	0.171	-0.104	0.1141	0.0609	0.2039	0.0889	N
3w	-4.749	-0.350	0.175	-0.097	0.0944	0.0423	0.1915	0.0797	N
3x	-4.772	-0.373	0.175	-0.097	0.0999	0.0450	0.1918	0.0799	N
3y	-5.072	-0.530	0.177	-0.095	0.1203	0.0629	0.1871	0.0741	N
3z	-5.474	-0.703	0.166	-0.146	0.0954	0.0622	0.2001	0.0754	N
3A	-5.955	-1.019	0.168	-0.173	0.0482	0.0280	0.2066	0.0731	N
3B	-6.241	-1.432	0.186	-0.178	0.2251	0.2480	0.1335	0.0331	N
3C	-5.622	-0.603	0.156	-0.132	0.2443	0.1995	0.2127	0.0847	N
3D	-5.141	-1.411	0.157	-0.106	0.1351	0.0730	0.0901	0.0151	N
3E	-4.680	-1.074	0.152	-0.107	0.0298	0.0114	0.0481	0.0125	N
3F	-5.050	-0.604	0.172	-0.073	0.1261	0.0734	0.1711	0.0596	Y
Mean	-5.067	-0.668	0.164	-0.089	0.124	0.069	0.187	0.069	
St Dev	0.354	0.271	0.008	0.031	0.051	0.048	0.035	0.018	
Var	0.125	0.074	0.0001	0.001	0.003	0.002	0.001	0.0003	
3t	-5.643	-1.183	0.134	-0.053	0.2307	0.1670	0.2751	0.0705	SUPP
3G	-5.516	-1.018	0.187	-0.165	0.0816	0.0618	0.0008	0.0001	SUPP

Structural descriptors

Alkene	ϕ_1 (°)	ϕ_2 (°)	d_1 (Å)	d_2 (Å)	d_3 (Å)	d_4 (Å)	Active
3a	131.001	-131.511	3.064	3.065	2.783	2.782	Y
3b	131.397	-131.369	3.058	3.069	2.777	2.785	Y
3c	131.168	-131.770	3.083	3.053	2.794	2.777	Y
3d	131.512	-131.358	3.061	3.096	2.780	2.805	Y
3e	131.523	-131.104	3.056	3.059	2.774	2.776	Y
3f	131.700	-131.091	3.045	3.077	2.769	2.787	Y
3g	132.115	-131.529	3.059	3.064	2.780	2.783	Y
3h	131.812	-131.293	3.062	3.069	2.784	2.788	Y
3i	129.596	-128.890	3.087	3.162	2.786	2.924	Y
3j	131.090	-131.090	3.097	3.097	2.813	2.813	Y
3k	131.330	-131.330	3.097	3.097	2.815	2.815	Y
3l	132.527	-132.319	3.069	3.060	2.791	2.786	Y
3m	131.640	-131.640	3.072	3.072	2.787	2.793	Y
3n	130.868	-130.431	3.080	3.096	2.785	2.793	Y
3o	132.191	-132.191	3.109	3.109	2.803	2.803	Y
3p	131.621	-131.621	3.111	3.111	2.800	2.800	Y
3q	131.533	-131.533	3.113	3.113	2.802	2.802	Y
3r	134.093	-134.093	3.104	3.104	2.827	2.827	Y
3s	135.287	-135.287	3.111	3.111	2.839	2.839	Y
3u	124.115	-122.085	3.136	2.890	2.794	2.686	N
3v	124.985	-123.570	3.125	2.905	2.792	2.707	N
3w	124.585	-121.797	3.119	2.790	2.784	2.617	N
3x	124.333	-121.650	3.122	2.796	2.787	2.620	N
3y	124.321	-122.075	3.122	2.894	2.790	2.689	N
3z	126.277	-126.277	3.078	3.078	2.763	2.763	N
3A	128.748	-128.748	3.105	3.105	2.788	2.788	N
3B	126.853	-126.853	3.096	3.096	2.777	2.777	N
3C	130.538	-130.538	3.088	3.088	2.793	2.793	N
3D	129.521	-132.028	3.064	3.014	2.791	2.761	N
3E	131.871	-131.136	3.057	3.063	2.780	2.777	N
3F	128.113	-126.708	3.103	3.254	2.788	2.988	Y
Mean	129.944	-129.513	3.089	3.053	2.791	2.782	
St Dev	3.018	3.745	0.025	0.099	0.016	0.071	
Var	9.110	14.027	0.001	0.010	0.0003	0.005	
3t	159.802	-159.802	3.243	3.243	3.014	3.014	SUPP
3G	113.280	-113.280	3.111	3.111	2.708	2.708	SUPP

6.6 Multivariate Analyses (PCA and LDA)

PCA analyses were made with the free R software environment for statistical computing and graphics [see Ref. 391], using the FactoMineR package [see Ref. 392].

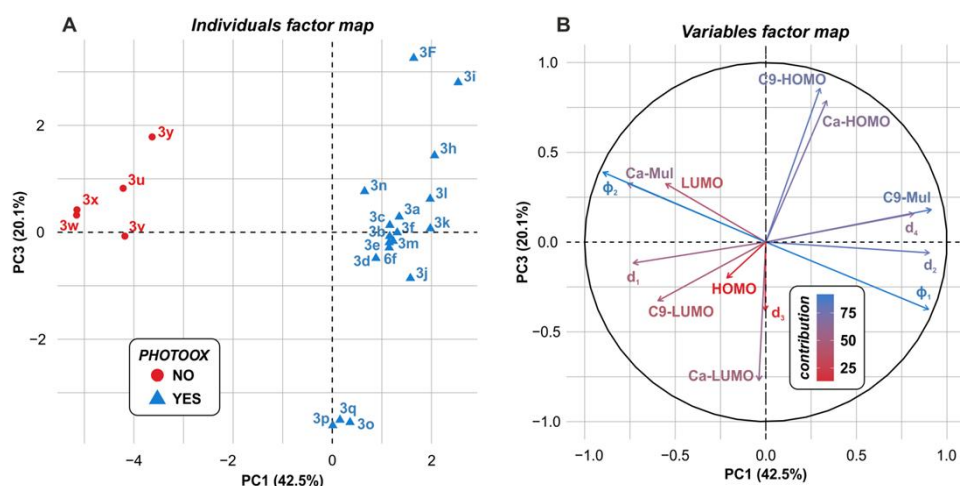


Figure 6.56: PCA results for the data matrix descriptors of olefins **3a-q**, **3u-y**, and **3F**: A) PCA score plot relative to the first and third PCs (blue triangles: reactive compounds; red dots: unreactive compounds); B) PCA loading plot relative to the first and third PCs (variables are colored according to their relative contribution).

As shown in Figure 6.56B, the orbital coefficients **Ca-HOMO**, **C9-HOMO** and **Ca-LUMO** are the main parameters contributing to the third PC ($\cos^2 = 0.621, 0.734$ and 0.594 , respectively). Plotting the data points along the first and the third PCs (Figure 6.56A), it is clear that in this case the olefins **3F** and **3i** are quite apart from the main cluster of the reactive alkenes along the third PC. Their position derives from the presence of a heteroatom in position 1 of the acridan moiety, which confers to these olefins smaller orbital coefficients of the LUMO (**Ca-LUMO** and **C9-LUMO**), without distortion from planarity of the aromatic system as much as the methyl substituent. Also, the N-aryl substituted olefins **3o-q** are clustered together along the negative direction of the third PC, due to the smaller orbital coefficients of the HOMO (**Ca-HOMO** and **C9-HOMO**).

In order to validate the PCA model and to verify its capability to predict the reactivity with singlet oxygen of new compounds, the fluorenyl alkene **3t** (central five-membered ring) and the specially designed new olefin **3G** (central seven-membered ring) were projected in the space defined by the first two PCs (Figure 6.57). The fluorenyl-derived alkene **3t** is positioned in the top-right quadrant of the score plot, farther on the right along the first PC due to an almost completely planar arrangement of the aromatic rings with respect to the plane

that only the starting material was observed in the reaction mixture. Finally, it should be noted that the fluorenyl-derived olefin **3t**, simply considering the energy values of the **HOMO** and **LUMO** orbitals, would have been projected along the negative direction of the PC2 axis, due to the low values of both the **HOMO** (-5.64 eV vs -5.10 eV mean **HOMO** energy) and the **LUMO** (-1.18 eV vs -0.69 eV mean **LUMO** energy) energies. On the other hand, the smaller values of the Mulliken charges on both Ca (0.134 vs 0.164 mean **Ca-Mul** charge) and C9 (-0.053 vs -0.09 mean **C9-Mul** charge), as well as a small but significant contribution of the dihedral angles ϕ_1 and ϕ_2 also on the PC2 axis, overall balance the frontier orbitals electronic effects and move olefin **3t** in the top region of the projection score plot. The experimental findings obtained for the supplementary alkenes **3t** and **3G** validate the developed PCA model, which proves to be able to anticipate the outcome of a photooxygenation reaction carried out on structurally different tetrasubstituted olefins, characterized by the adamantyl unit coupled with a tricyclic aromatic scaffold (regardless of the nature of the central ring).

LDA analyses were made with the free R software environment for statistical computing and graphics [see Ref. 391], using the MASS package and the Deducer plug-in [see Ref. 393].

6.7 Computational Details

MMFF conformational searches were performed with the Spartan suite of programs, using the keywords SEARCHMETHOD=SYSTEMATIC, FINDBOATS and KEEPALL. All the conformers contained in a 8 kcal/mol window were reoptimized at the B3LYP/6-31G(d) DFT level and confirmed as true minima by frequency analysis. DFT calculations were performed with Gaussian 09 [see Ref. 394]. Structural and electronic descriptors were taken from the lowest energy conformation obtained at the DFT level.

Chapter 7

Supporting Information of Chapter 3

7.1 General Remarks

All of the commercial chemicals were purchased from Sigma Aldrich, Alfa Aesar or TCI Chemicals, and used without additional purifications.

- The ^1H and ^{13}C NMR spectra were recorded on a 200 or 400 NMR instrument with a 5 mm probe. All chemical shifts have been quoted relative to deuterated solvent signals; chemical shifts (δ) are reported in ppm, and coupling constants (J) are reported in hertz. Protons and carbons are assigned as follows: (Ar) for aromatic protons, (Ad) for protons and carbons of the adamantyl portion, (H1, H2, H3...) for protons expressly labeled in the molecule picture, ($\text{H}\alpha$) for allylic protons of the adamantyl moiety in the alkenes (the same notation was used for the corresponding 1,2-dioxetanes), (CO) for carbonyl carbons, (COO) for carboxyl carbons, (CF) for carbons bearing a fluorine atom, (CHAr) for aromatic tertiary carbons, (Cq) for quaternary alkenyl and aromatic carbons, (C*) for carbons of the 1,2-dioxetane and (C1, C2, C3...) for carbons expressly labeled in the molecule picture.
- HPLC-MS analyses were performed on an Agilent Technologies HP1100 instrument coupled with an Agilent Technologies MSD1100 single-quadrupole mass spectrometer. A Phenomenex Gemini C18 3 μm (100 x 3 mm) column was employed for the chromatographic separation using the following analytical methods: mobile phase $\text{H}_2\text{O}/\text{CH}_3\text{CN}$, gradient from 30% to 80% of CH_3CN in 8 min, 80% of CH_3CN until 22 min, then up to 90% of CH_3CN in 2 min, stop time at 25 min; flow rate 0.4 mL min^{-1} . Mass spectrometric detection was performed in full-scan mode from m/z 50 to 2500, scan time 0.1 s in positive ion mode, ESI spray voltage 4500 V, nitrogen gas 35 psi, drying gas flow rate 11.5 mL min^{-1} , fragmentor voltage 30 V.
- Flash chromatography purifications were carried out using VWR silica gel (40-63 μm particle size). Thin-layer chromatography was performed on Merck 60 F254 plates.

7.2 Synthetic Procedures and Characterizations

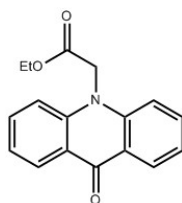


Figure 7.1

Compound 1: Compound **1** was synthesized following the procedure in literature [see Ref. 107]. The reaction was carried out under nitrogen atmosphere. A suspension of 9(10)Acridanone (2g, 10.24 mmol) in dry DMF (9 mL) was added dropwise to a suspension of NaH (492 mg, 12.29 mmol) in anhydrous DMF (35 mL) at 0°C. After 30 min of stirring at room temperature (rt), the reaction was cooled down to 0°C, and Ethyl bromoacetate (1.7 mL, 15.36 mmol) and tetrabutylammonium iodide (Bu₄NI, 40mg, 0.11 mmol) were added. The reaction was stirred at rt overnight. Then, the crude was poured into cold water and the precipitate was filtered through Büchner funnel and dried over MgSO₄. Compound **1** was obtained as pale yellow solid (2.82 g, 98%), and the obtained ¹H NMR and ¹³C NMR were in agreement with the literature data. Product **1** was used directly in the next step, without further purifications.

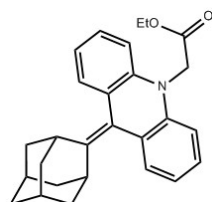


Figure 7.2

Compound 2: Compound **2** was synthesized following the procedure in literature [see Ref. 107]. Under a nitrogen atmosphere, a solution of TiCl₄ (10.85 mL, 1 M in CH₂Cl₂) was added to a suspension of Zn powder (1.55 g, 24.02 mmol) in anhydrous THF (20 mL) at 0°C, and the suspension was stirred for 10 min under reflux. Then, a solution of ketone **1** (500 mg, 1.78 mmol) and 2-adamantanone (267 mg, 1.78 mmol) in anhydrous THF (10 mL) was added dropwise over a period of 30 min. The reaction mixture was refluxed for 45 minutes. Then, it was cooled to room temperature, quenched with water and extracted with AcOEt (3 x 10 mL). The combined organic layers were dried over sodium sulfate and evaporated under vacuum. The chromatographic purification (eluent: cyclohexane/AcOEt = 80:20) provided compound **2** as white solid (642

mg, 90%), and the obtained $^1\text{H NMR}$ and $^{13}\text{C NMR}$ were in agreement with the literature data.

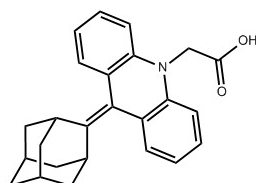


Figure 7.3

Compound 3: Compound **3** was synthesized following the procedure in literature [see Ref. 395]. A solution of NaOH (6 mL, 0.5 M) was added dropwise to a suspension of **2** (200 mg, 0.5 mmol) in EtOH (26 mL) at 0°C . The solution was stirred at 0°C for 1 hour after which the reaction was stirred at rt for additional 58 hours. Then, it was poured into cold water (100 mL) and the acidity of the aqueous solution was adjusted to 4 - 5 pH values, using HCl 6N. The water solution was extracted with AcOEt (3 x 10 mL), and the combined organic layers were dried over sodium sulfate and evaporated under vacuum. Compound **3** was used directly in the next step, without further purifications.

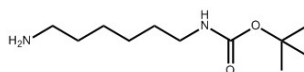


Figure 7.4

Compound 4: Compound **4** was synthesized following the procedure in literature [see Ref. 396]. Under nitrogen atmosphere, a solution of Di-tert-butyl dicarbonate (Boc_2O , 388 mg, 1.78 mmol) in CHCl_3 (9 mL) was added dropwise to a solution of 1,6-hexanediamine (1.03 g, 8.88 mmol) in CHCl_3 (45 mL) at 0°C . The reaction was stirred at rt overnight, after which it was concentrated and purified through flash chromatography on silica gel. The chromatographic purification (eluent: $\text{CH}_2\text{Cl}_2/\text{MeOH} = 90:10$ with 1% of TEA) provided compound **4** as sticky solid (254 mg, 44%), and the obtained $^1\text{H NMR}$ and $^{13}\text{C NMR}$ were in agreement with the literature data [see Ref. 397]. **HPLC-MS** (ESI) $t_r = 10.3$ min; $[\text{M}+\text{H}]^+ = 217.0$, $[\text{M}+\text{Na}]^+ = 239.0$, $[\text{M}+\text{K}]^+ = 255.0$.

Compound 5: Compound **5** was synthesized following the procedure in literature [see Ref. 398]. Under nitrogen atmosphere, COMU coupling reagent (125 mg, 0.29 mmol) was added to a solution of **3** (108 mg, 0.29 mmol), diisopropylamine (DIPEA, 0.1 mL, 0.58 mmol) and **4** (62.88 mg, 0.29 mmol) in anhydrous DMF, at 0°C . The solution was stirred at 0°C for 1 hour after which the reaction was stirred at rt overnight. The crude was washed with a solution of LiCl 5% (3 x 10 mL), and extracted with AcOEt (3x 20 mL). The combined organic layers were

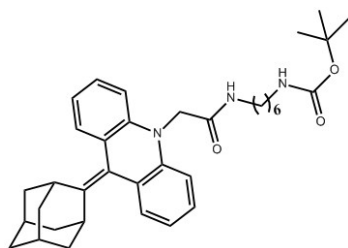


Figure 7.5

dried over sodium sulfate and evaporated under vacuum. The chromatographic purification (eluent: cyclohexane/AcOEt = 95:5) provided compound **5** as pale yellow solid (77.8 mg, 44%). $^1\text{H NMR}$ (400 MHz, CDCl_3) δ 7.28-7.25 (m, 2H), 7.19 (td, $J = 7.6, 1.6$ Hz, 2H), 7.05 (td, $J = 7.2, 0.8$ Hz, 2H), 6.93 (d, $J = 8.4$ Hz, 2H), 5.92 (bs, 1H), 4.57 (s, 2H), 4.45 (bs, 1H), 3.44 (s, 2H), 3.19 (q, $J = 6.4$ Hz, 2H), 3.03 (q, $J = 6.4$ Hz, 2H), 2.18-1.92 (m, 4H), 1.89 (s, 3H), 1.57 (s, 3H), 1.45 (s, 9H), 1.37 – 1.23 (m, 6H), 1.15 (m, 2H), 0.98-1.03 (m, 2H). $^{13}\text{C NMR}$ (100 MHz, CDCl_3) δ 168.5, 155.9, 145.6, 142.8, 127.5, 126.8, 126.5, 121.2, 119.8, 112.5, 79.0, 50.4, 39.1, 36.9, 32.2, 29.2, 28.4, 26.2, 26.2. **HPLC-MS** (ESI) $t_r = 18.3$ min; $[\text{M}+\text{H}]^+ = 570.0$, $[\text{M}+\text{Na}]^+ = 592.0$, $[\text{M}+\text{K}]^+ = 608.0$.

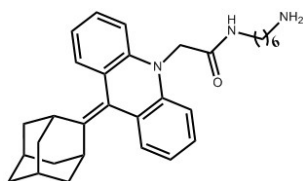


Figure 7.6

Compound 6: Compound **6** was obtained in two different ways: i) after a deprotection step (according to the first strategy) or ii) through a McMurry reductive coupling (following the second synthetic approach).

Approach i): Under nitrogen atmosphere, Trifluoroacetic acid (TFA, 48 μL , 0.63 mmol) was added to a solution of **5** (20 mg, 0.035 mmol) in anhydrous CH_2Cl_2 (0.6 mL), at 0°C . The reaction was stirred at rt for 2 hours; then, it was neutralized adding a saturated solution of NaHCO_3 at 0°C (until pH = 8). The basic aqueous solution was extracted with AcOEt (3 x 2 mL) and CH_2Cl_2 (3 x 2 mL), and the combined organic layers were dried over sodium sulfate and evaporated under vacuum. Product **6** was obtained as yellow solid (12.3 mg, 79%). Compound **6** was used directly in the next step, without further purifications.

Approach ii): Compound **6** was synthesized following the procedure in literature [see Ref. 111]. Under a nitrogen atmosphere, a solution of TiCl_4 (2.9 mL, 1 M in CH_2Cl_2) was added to a suspension of Zn powder (409 mg, 0.47 mmol) in

anhydrous THF (5.5 mL) at 0°C, and the suspension was stirred for 10 min under reflux. Then, a solution of ketone **11** (161 mg, 0.47 mmol) and 2-adamantanone (71 mg, 0.47 mmol) in anhydrous THF (13 mL) was added dropwise over a period of 30 min. The reaction mixture was refluxed for 45 minutes. Then, it was cooled to room temperature, quenched with water and extracted with AcOEt (3 x 10 mL). The aqueous phase was basified using a solution of NaOH (6 N), and it was extracted, a second time, with CH₂Cl₂. The combined organic layers were dried over sodium sulfate and evaporated under vacuum. Compound **6** was used directly in the next step, without further purifications. ¹H NMR (400 MHz, CDCl₃) δ 7.28-7.24 (m, 2H), 7.19 (td, 7.6, 1.2 Hz, 2H), 7.05 (td, J = 7.6, 1.2 Hz, 2H), 6.93 (d, J = 8.2, 2H), 5.93 (s, 1H), 4.57 (s, 2H), 3.44 (s, 2H), 3.19 (q, J = 6.8 Hz, 2H), 2.60 (t, J = 7.2 Hz, 2H), 2.29-1.94 (m, 4H), 1.89 (s, 3H), 1.55-1.37 (m, 4H), 1.35-1.28 (m, 5H), 1.22-1.12 (m, 2H), 1.08-0.98 (m, 2H). ¹³C NMR (100 MHz, CDCl₃) δ 168.5, 145.5, 142.7, 127.4, 126.7, 126.4, 121.1, 119.7, 112.4, 50.4, 41.9, 39.1, 36.9, 33.3, 32.2, 29.2, 26.3, 26.3. HPLC-MS (ESI) t_r = 6.2 min; [M+H]⁺ = 470.0, [M+Na]⁺ = 492.0, [M+K]⁺ = 508.0.

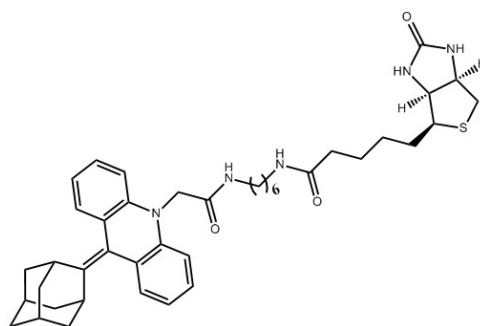


Figure 7.7

Olefin precursor 7: Compound **7** was synthesized following the procedure in literature [see Ref. 398]. Under nitrogen atmosphere, COMU coupling reagent (137 mg, 0.32 mmol) was added to a solution of **6** (150 mg, 150 μmol), diisopropylamine (DIPEA, 0.11 mL, 0.64 mmol) and Biotin (78 mg, 0.32 mmol) in anhydrous DMF (5 mL), at 0°C. The solution was stirred at 0°C for 1 hour after which the reaction was stirred at rt for two more hours. The crude was concentrated under vacuum and the chromatographic purification (eluent: CH₂Cl₂/MeOH = 99:1) provided compound **7** as yellow solid (63 mg, 28%). ¹H NMR (400 MHz, CDCl₃) δ 7.25 (dd, J = 7.6, 1.6 Hz, 2H), 7.19 (td, J=7.6, 1.6, 2H), 7.04 (td, J = 7.2, 0.8 Hz, 2H), 6.92 (d, J = 8.0 Hz, 2H), 5.98 (s, 1H), 5.90 (s, 2H), 5.08 (s, 1H), 4.58 (s, 2H), 4.48 (dd, J = 8.0, 4.8 Hz, 1H), 4.31 (dd, J = 7.6, 4.4 Hz, 1H), 3.43 (s, 2H), 3.22-3.12 (m, 5H), 2.90 (dd, J = 12.8, 4.8 Hz, 1H), 2.72 (d, J = 12.8 Hz, 1H), 2.23-2.17 (m, 5H), 1.89 (s, 3H), 1.79-1.59 (m, 6H), 1.50 – 1.25 (m,

10H), 1.23-1.04 (m, 4H). ^{13}C NMR (100 MHz, CDCl_3) δ 172.9, 168.8, 163.3, 145.7, 142.8, 127.5, 126.8, 126.6, 121.2, 119.7, 112.5, 61.8, 60.1, 55.4, 53.4, 40.5, 39.2, 39.0, 36.9, 35.9, 32.3, 30.9, 29.7, 29.3, 29.2, 28.1, 28.0, 26.1, 26.0, 25.6. **HPLC-MS** (ESI) t_r = 11.6 min; $[\text{M}+\text{H}]^+ = 696.0$, $[\text{M}+\text{K}]^+ = 734.0$.

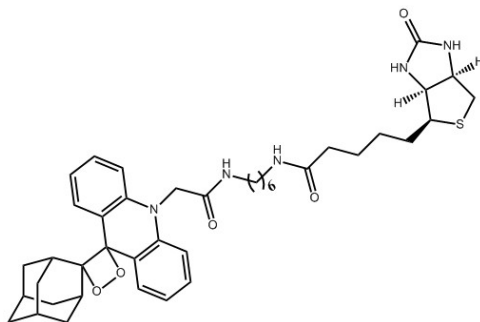


Figure 7.8

TCL-based molecular probe (8): Compound **8** was synthesized following the procedure in literature [see Ref. 111]. Alkene **7** (17 mg, 0.025 mmol) and Methylene Blue (0.60 mg, 0.0015 mmol) were dissolved in CH_2Cl_2 (2 mL). The solution was cooled to -40°C and subjected to an oxygen atmosphere (1 atm, balloon). The solution was stirred at the same temperature under irradiation using a 500 W halogen lamp equipped with a UV cut-off filter (0.5% transmission at 550 nm). The conversion was monitored by ^1H NMR and HPLC-MS. After 5 hours of irradiation, MeOH (0.1 mL) was added to better solubilize the starting material **7**, and the reaction was carried out for further 5 hours. After this time, the irradiation was stopped and the ^1H NMR of crude showed the formation of several by-products (see 3).

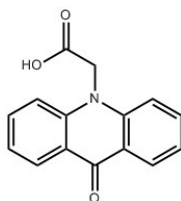


Figure 7.9

Compound 9: Compound **9** was synthesized following the procedure in literature [see Ref. 395]. A solution of NaOH (10 mL, 0.5 M) was added to a suspension of **1** (500 mg, 1.78 mmol) in EtOH (33 mL), at 0°C . The solution was stirred at rt for 4.3 hours and, then, it was poured into cold water (100 mL) and the acidity of the aqueous solution was adjusted to 4 - 5 pH values, using HCl 6N. The water solution was extracted with AcOEt (3 x 10 mL), and the combined organic layers were dried over sodium sulfate and evaporated under

vacuum. Compound **9** was obtained as yellow solid (444 mg, 98%) and the obtained $^1\text{H NMR}$ and $^{13}\text{C NMR}$ were in agreement with the literature data [see Ref. 399].

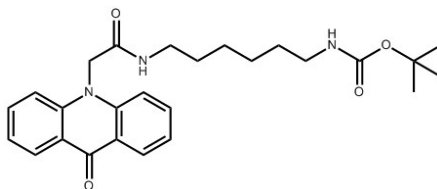


Figure 7.10

Compound 10: Compound **10** was synthesized following the procedure in literature [see Ref. 398]. Under nitrogen atmosphere, COMU coupling reagent (350 mg, 0.82 mmol) was added to a solution of **9** (217 mg, 0.82 mmol), diisopropylamine (DIPEA, 0.29 mL, 1.65 mmol) and **4** (178 mg, 0.82 mmol) in anhydrous DMF (13 mL), at 0°C. The solution was stirred at 0°C for 1 hour after which the reaction was stirred at rt overnight. The crude was washed with a solution of LiCl 5% (3 x 10 mL), and extracted with AcOEt (3x 20 mL). The combined organic layers were dried over sodium sulfate and evaporated under vacuum. The chromatographic purification (eluent: cyclohexane/AcOEt = 50:50) provided compound **10** as yellow solid (332 mg, 91%). $^1\text{H NMR}$ (400 MHz, CDCl_3) δ 8.38 (d, 8.0 Hz, 2H), 7.75 (ddd, $J = 8.8, 6.8, 1.6$ Hz, 2H), 7.38 (d, $J = 8.4$ Hz, 2H), 7.29 (t, $J = 8$ Hz, 2H), 6.61 (s, 1H), 4.99 (s, 2H), 4.47 (s, 1H), 3.29 (q, $J = 6.4$ Hz, 2H), 2.94 (q, $J = 6.4$ Hz, 2H), 1.51 – 1.43 (m, 2H), 1.40-1.31 (m, 11H), 1.24-1.17 (m, 4H). $^{13}\text{C NMR}$ (100 MHz, CDCl_3) δ 177.6, 167.1, 155.9, 142.1, 134.1, 127.2, 122.1, 121.9, 114.3, 78.9, 51.2, 40.0, 39.3, 29.9, 29.0, 28.3, 26.1, 25.9. **HPLC-MS** (ESI) $t_r = 9.0$ min; $[\text{M}+\text{H}]^+ = 452.0$, $[\text{M}+\text{Na}]^+ = 474.0$, $[\text{M}+\text{K}]^+ = 490.0$, $[\text{2M}+\text{K}]^+ = 925.0$.

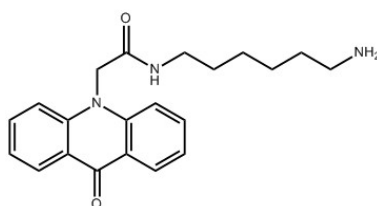


Figure 7.11

N-(6-aminohexyl)-2-(9-oxoacridin-10(9H)-yl)acetamide (11): Under nitrogen atmosphere, Trifluoroacetic acid (TFA, 898 μL , 12 mmol) was added to a solution of **10** (292 mg, 0.65 mmol) in anhydrous CH_2Cl_2 (12 mL), at 0°C. The reaction was stirred at rt for 3 hours; then, the solvent was evaporated under vacuum. The crude was redissolved in H_2O (5 mL) and the aqueous solution was

acidified using HCl 6 N. Once compound **11** was completely dissolved, NaOH 6 N was added dropwise, adjusting the solution pH to 8 -9 values. The aqueous phase was extracted with CH₂Cl₂ (3 x 10 mL) and the combined organic layers were dried over sodium sulfate and evaporated under vacuum. Product **11** was obtained as yellow solid (152 mg, 66%). Compound **11** was used directly in the next step, without further purifications. ¹H NMR (400 MHz, CD₃OD) δ 8.51 (dd, J = 8.4, 2.0 Hz, 2H), 7.77 (ddd, J = 8.4, 6.8, 1.6 Hz, 2H), 7.40-7.33 (m, 4H), 6.13 (s, 1H), 4.98 (s, 2H), 3.29 (q, J = 6.4 Hz, 2H), 2.60 (t, J = 6.8 Hz, 2H), 1.45 – 1.37 (m, 2H), 1.37-1.30 (m, 2H), 1.22- 1.15 (m, 4H). ¹³C NMR (50 MHz, CD₃OD) δ 180.1, 169.7, 144.1, 135.6, 128.1, 123.3, 123.0, 116.5, 54.8, 41.7, 40.4, 31.8, 30.2, 27.5, 27.3. HPLC-MS (ESI) t_r = 1.8 min; [M+H]⁺ = 352.0, [M+Na]⁺ = 374.0, [2M+K]⁺ = 725.0.

Chapter8

Supporting Information of Chapter 4

8.1 General Remarks

All of the commercial chemicals were purchased from Sigma Aldrich and used without additional purifications. Cyano-Polyphenylene vinylene (CN-PPV, MW= 20 - 100 kDa) was purchased from American Dye Source, Inc. while Polystyrene derivatives (PS-COOH, 50 kDa and PS-NH₂, 6.5 kDa) was purchased from Poymer Source, Inc. Biotinylated Mouse IgG (Biotin-IgG) was purchased from abcam, while Anti-IgG magnetic beads were purchased from New England BioLabs, Inc.

Purification of TCL-Pdots-SA was carried out through filtration over a 400 μ m cutoff filter and centrifugation, using a 100 K molecular weight cutoff centrifugal membrane (Amicon Ultra-4, Ultracel - 100K). Then, nanoparticles were further purified by size exclusion chromatography, using Sephacryl S-300 HR resin.

Spectroscopic properties, in terms of absorption and emission spectra were recorded using a UV-Vis spectrophotometer (Varian Cary 50) and a Uv-Vis spectrofluorimeter (Carian Cary Eclipse). The ¹H NMR spectrum of polystyrene functionalized with ketone **2** (PS-NH₂-**2**) was recorded on 400 NMR instrument with a 5 mm probe. Dynamic light scattering (DLS) experiments were conducted using a Malvern Zetasizer NanoZS while TEM images were acquired using a Philips CM100 transmission electron microscope (Philips/FEI Corp., Eindhoven, Holland). Fluorescence images of TCL-Pdots-SA conjugated with Biotin-IgG, before and after the elution step, were obtained using an epi-fluorescence microscope with a 100x, 1.3 oil immersion objective and with a 532 nm diode laser, while the efficiency of FRET mechanism was calculated by Fluorescence Lifetime measurements, using a FluoTime 100 spectrometer (PicoQuant, PicoHarp 300).

TCL signal was acquired using a portable battery-operated CCD camera (model MZ-2PRO, MagZero, Pordenone, Italy) equipped with a thermoelectrically cooled monochrome CCD image sensor and an objective (low distortion wide angle lenses 1/3 in. 1.28 mm, f1.8) obtained from Edmund Optics (Barrington, NJ). TCL images were analyzed using an open source image processing program

(ImageJ). For evaluation of the signal-to-noise (S/N) ratios of the images, signals (S) were calculated by averaging the pixel intensity over the analyzed area, while noise (N) was taken as the standard deviation of the mean pixel intensity in a dark image area.

8.2 Synthesis of Thermochemiluminescent Semiconductive Polymer dots (TCL-Pdots-SA)

1,2-dioxetane **1**-doped Pdots were prepared following a nanoprecipitation method. In a typical procedure a THF solution of CN-PPV (1 mg/mL), PS-COOH (1 mg/mL) and substrate **1** (2 mg/mL) was prepared. Then, a 7 mL aliquot of the mixture was quickly injected into 10 mL of water under vigorous sonication for about 1 minute. For the optimization studies, we prepared different mixed solutions keeping constant the CN-PPV amount and changing the volume of PS-COOH, dioxetane **1** or THF injected. The extra THF was evaporated under nitrogen flow at room temperature and THF-free Pdot solution were filtrated through a 0.4 μm cellulose membrane filter.

TCL-Pdots were bioconjugated to Streptavidin (SA) following a EDC catalyzed codensation reaction between the carboxylic units of polystyrene chains and amino groups of SA enzyme. Specifically, 80 μL of polyethylene glycol (5% w/v PEG, MW 3350) and 80 μL of concentrated HEPES buffer (1 M) were added to a solution of TCL-Pdots (80 ppm in MilliQ water). Then, 120 μL of Streptavidin (2 mg/mL) was added to the solution along with 80 μL of freshly-prepared EDC solution (10 mg/mL in MilliQ water). After 3 hours of stirring at room temperature, BSA (10% (w/v), 80 μL) was added to the Pdots solution and the mixture was stirred for 30 minutes. Lastly, Triton X-100 (2.5% (w/v), 80 μL) was added to the mixture of TCL-Pdots-SA to stabilize the nanoparticles solution. The resulting streptavidinated TCL-Pdots were centrifuged by a 100 K molecular cutoff membrane first, then purified by size exclusion chromatography using Sephacryl HR-300 gel media.

The fully encapsulation of 1,2-dioxetane **1** inside Pdots was confirmed by both the TCL emission from Pdots after bioconjugation and the Uv-vis absorption spectrum (Figure 8.1 b) of the filtrate, which has shown the absence of dioxetane**1**.

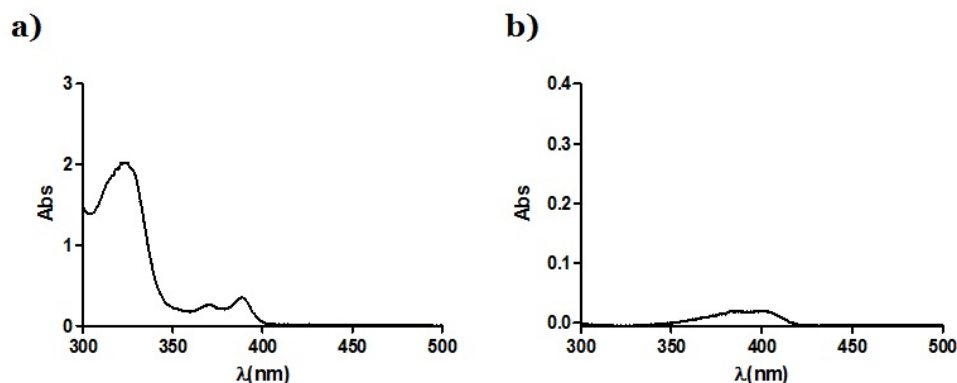


Figure 8.1: a) Uv-vis absorption of 1,2-dioxetane **1** (323 nm) and ketone **2** (387 nm) in THF solution b) Absorption spectrum of the filtrate solution, showing only the presence of a very small amount of ketone **2** (probably generated during the synthesis of TCL-Pdots-SA) in water.

8.3 Photophysical properties of CN-PPV polymer and 1,2-dioxetane **1**

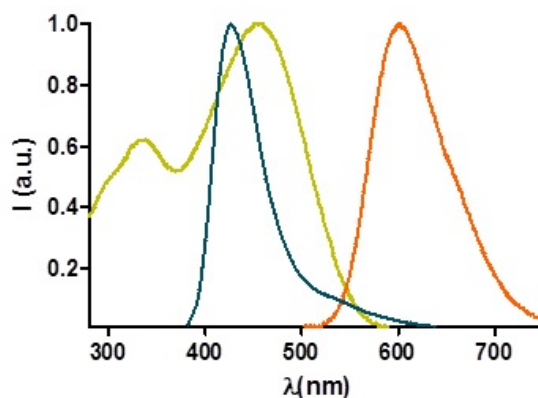


Figure 8.2: Absorption (yellow line) and emission (orange line) of CN-PPV-based Pdots in water solution. The blue line represents the emission of 1,2-dioxetane **1** in THF after thermal decomposition.

8.4 Synthesis of PS-NH₂-**2** derivative and FRET experiments

PS-NH₂-**2** was obtained following a two-steps synthetic strategy. First, the ester functionality of ketone **2** underwent a basic hydrolysis to restore the carboxylic acid unit. Then, a EDC-catalyzed condensation reaction between PS-NH₂ and ketone **2**-COOH yielded the functionalized polymer PS-NH₂-**2**.

According to a previously reported procedure [see Ref. 395], ketone **2** (0.4 mmol) was dissolved in Ethanol (8mL), and the solution was cooled down to

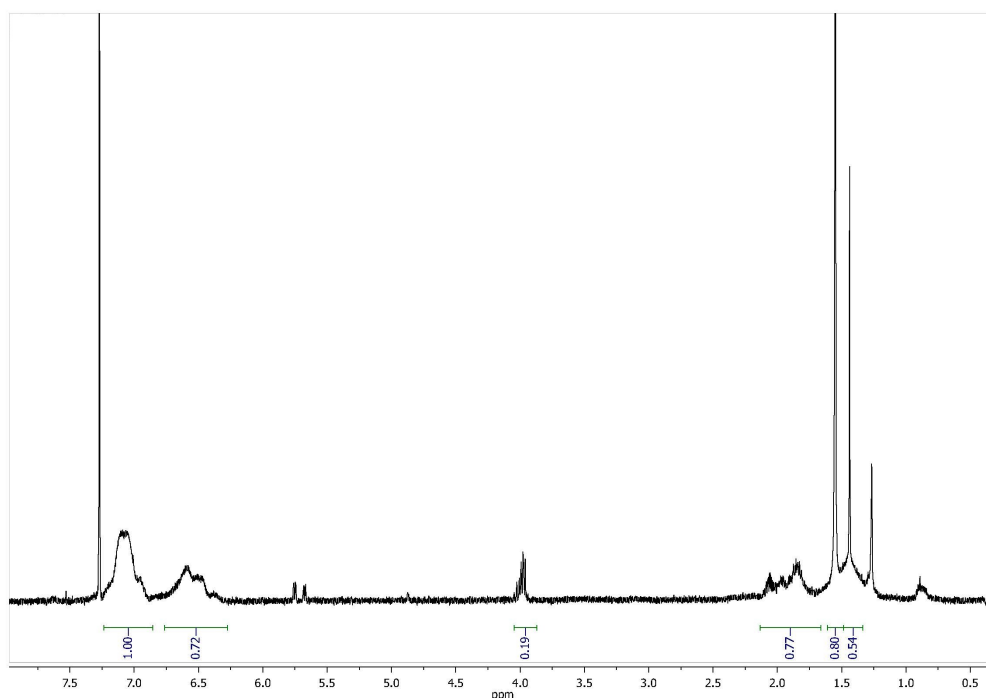


Figure 8.3: ^1H NMR spectrum of the fraction containing the desired product PS-NH₂-2.

0 °C. Then, a solution of NaOH (0.5 M) was added dropwise and the mixture was stirred at room temperature. After 2 hours, the solution was poured into cold water (30 mL) and the pH was adjusted to 4-5 value using HCl (8 M). The precipitate was collected and used in the next step without further purifications.

The condensation reaction was carried out dissolving ketone **2** (0.135 mmol), 1-Ethyl-3-(3-dimethylaminopropyl)carbodiimide (EDC, 1 eq.) and N-Hydroxy-succinimide (NHS, 1 eq.) in DMF (3 mL). After 30 minutes of stirring, PS-NH₂ (0.11 eq.) was added and the mixture was further stirred at room temperature for 16 hours. Then, the solution was poured into cold water (10 mL) and the precipitated was filtered and purified by flash chromatography on silica gel. The fraction containing the desired product (metti grammi e resa) was characterized by both ^1H NMR and Uv-vis absorption spectra (Figure 8.2). The first has shown typical signal of polystyrene hydrogens [see Ref. 400], while the absorption spectrum has confirmed the presence of the ketone **2** (covalently bonded to PS chains).

In order to calculate the efficiency of FRET mechanism, we synthesized two different PS-based nanoparticles, following the above-reported procedure. In particular, PS-NH₂-2 (6 mg/mL) and PS-COOH (1 mg/mL) were mixed together in THF and then, 6 mL aliquot of mixture was dispersed in water under sonication. In a second experiment, CN-PPV (1 mg/mL) was added to the previous THF solution. Both nanoparticle solutions were filtered by a 400 μm cellulose filter, centrifugated using a 100 K molecular weight cutoff centrifugal membrane and

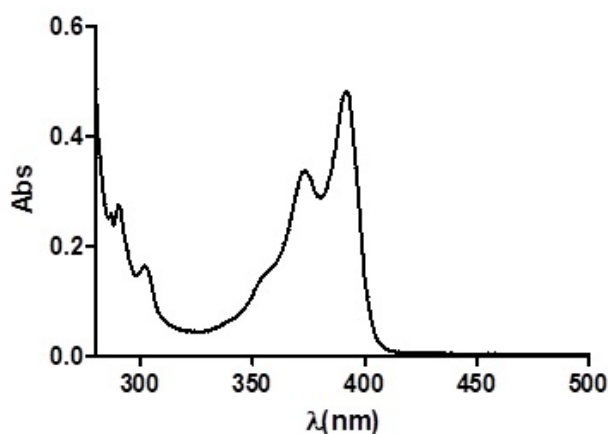


Figure 8.4: Uv-vis absorption spectrum of the fraction containing the desired product PS-NH₂-2.

purified by size exclusion chromatography.

FRET experiments were performed using a FluoTime 100 spectrometer, setting the time resolution of correlated single photon counting system to 32 ps and using a 375 nm laser for excitation of ketone **2**. In order to prevent photons emitted by excited CN-PPV from being collected, a band pass filter (centered at 425 ± 25 nm) was positioned in between the sample and detector. The experimental data were analyzed using the open source software DecayFit.

8.5 Influence of temperature upon the emission of CN-PPV polymer

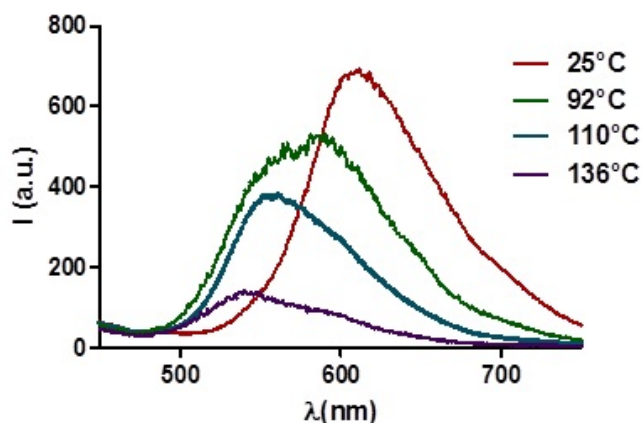


Figure 8.5: Emission spectra of CN-PPV in DMSO, acquired at different temperatures.

Table 8.1: Kinetic constants for the thermal decomposition of dioxetane **1**, occurring at different temperatures.

Temperature (°C)	$\ln k \pm \text{SD}^a$
100	$-7,11 \pm 0,23$
110	$-6,18 \pm 0,29$
120	$-5,81 \pm 0,29$
130	$-4,88 \pm 0,20$

^aMean \pm SD of three independent measurements.

8.6 TCL emission experiment and determination of activation parameters (E_a and $\ln A$)

In order to prove the occurring of FRET process between electronically excited ketone **2** and CN-PPV, a 200 μL solution of 1,2-dioxetane **1** (6 mM) and CN-PPV (0.07 mM) in THF was prepared. The glass vial containing the mixture was positioned onto a mini-heating element (ceramic resistance connected to a power supply) and centered to the spectrofluorimeter's detector. Then, the solution was heated up to 110 °C while acquiring the TCL emission spectrum. Since the low intensity of TCL signal, the emission spectrum was obtained as sum of multiple scans.

Activation parameters of 1,2-dioxetane **1** inside Pdots were calculated measuring the TCL emission decay kinetics at different temperatures. Specifically, 3 μL of TCL-Pdots solution was spotted onto an alluminum foil covering a homemade mini-heater (electrical resistance encapsulated in between two kapton layers) and let evaporating. The spot was allowed to dry, then the foil was heated up to the desired temperature (in the range between 100 and 130 °C), and a sequence of images of TCL emission was acquired, using a CCD camera. For each temperature, the kinetic constant k was calculated by fitting the TCL emission decay profile with the first-order decay equation shown in ??, in which I_{TCL} is the TCL signal at time t and $(I_{TCL})_0$ is the TCL signal at time zero (t_0).

$$I_{TCL} = (I_{TCL})_0 e^{-kt} \quad (8.1)$$

In Table 8.1 are reported the kinetic constants of TCL emission decay, calculated at different temperatures.

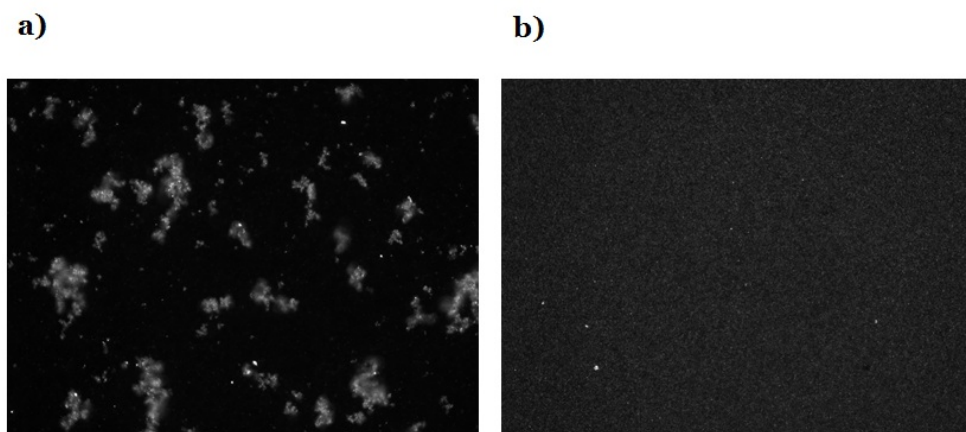


Figure 8.6: Images of TCL-Pdots-SA-Biotin-IgG MBs a) before and b) after the elution step.

8.7 TCL-based non-competitive sandwich-type immunoassay for detection of IgG

For the immunoassay experiments a solution of Goat Anti-Mouse IgG Magnetic Beads (Anti-IgG MBs, 20 mg/mL) and Biotinylated Immunoglobulin G (Biotin-IgG, 0.5 mg/mL) were used. An increasing volume of Biotin-IgG (in the range between 0 and 34 μL) was added to a 100 μL Anti-IgG MBs solution, and the final volume was diluted to 500 μL using a PBS 1X buffer solution (pH = 7.4) with BSA 5% (w/v). Each sample was incubated at 37 °C for 2 hours. Then, MBs were washed three times (washing buffer = PBS 1X with Tween-20 0.1% (v/v)) to remove all the free Biotin-IgG, and 200 μL of TCL-Pdots-SA solution was added along with 300 μL of PBS 1X buffer solution (pH = 7.4) and BSA 5%. Biotin-IgG MBs were let incubating with TCL-Pdots-SA at 37 °C for additional 2 hours, after which MBs were washed three times and dispersed in the elution buffer (50 μL) for 15 minutes, at room temperature. The elution buffer (solution of Glycine, pH = 10) allowed us to effectively recover the TCL-Pdots-SA/Biotin-IgG MBs, as shown in Figure 8.6. In fact, the image taken before the elution step shows the presence of micrometric aggregates (MBs), while after using Glycine buffer, we obtained a well dispersed solution of TCL-Pdots-SA/Biotin-IgG.

The calibration curve was obtained heating 10 μL of the eluted solution up to 110 °C and acquiring the TCL emission by a CCD camera.

AppendixA

License

Following, the reuse license for the published article cited in this work.

**JOHN WILEY AND SONS LICENSE
TERMS AND CONDITIONS**

Oct 24, 2017

This Agreement between Mr. luca andronico ("You") and John Wiley and Sons ("John Wiley and Sons") consists of your license details and the terms and conditions provided by John Wiley and Sons and Copyright Clearance Center.

License Number	4215290071868
License date	Oct 24, 2017
Licensed Content Publisher	John Wiley and Sons
Licensed Content Publication	Chemistry - A European Journal
Licensed Content Title	Synthesis of 1,2-Dioxetanes as Thermochemiluminescent Labels for Ultrasensitive Bioassays: Rational Prediction of Olefin Photooxygenation Outcome by Using a Chemometric Approach
Licensed Content Author	Luca A. Andronico,Arianna Quintavalla,Marco Lombardo,Mara Mirasoli,Massimo Guardigli,Claudio Trombini,Aldo Roda
Licensed Content Date	Oct 31, 2016
Licensed Content Pages	13
Type of use	Dissertation/Thesis
Requestor type	Author of this Wiley article
Format	Print and electronic
Portion	Full article
Will you be translating?	No
Title of your thesis / dissertation	Investigation of the Thermochemiluminescent (TCL) phenomenon as an innovative detection technique for (bio)analytical applications: from the synthesis of new TCL candidates to the realization of TCL-based probes for immunoassays
Expected completion date	Dec 2017
Expected size (number of pages)	200
Requestor Location	Mr. luca andronico via XVI traversa 77 Belpasso, Catania 95032 Italy Attn: Mr. luca andronico
Publisher Tax ID	EU826007151
Billing Type	Invoice
Billing Address	Mr. luca andronico via XVI traversa 77 Belpasso, Italy 95032 Attn: Mr. luca andronico
Total	0.00 EUR
Terms and Conditions	

TERMS AND CONDITIONS

This copyrighted material is owned by or exclusively licensed to John Wiley & Sons, Inc. or one of its group companies (each a "Wiley Company") or handled on behalf of a society with which a Wiley Company has exclusive publishing rights in relation to a particular work (collectively "WILEY"). By clicking "accept" in connection with completing this licensing transaction, you agree that the following terms and conditions apply to this transaction (along with the billing and payment terms and conditions established by the Copyright Clearance Center Inc., ("CCC's Billing and Payment terms and conditions"), at the time that you opened your RightsLink account (these are available at any time at <http://myaccount.copyright.com>).

Terms and Conditions

- The materials you have requested permission to reproduce or reuse (the "Wiley Materials") are protected by copyright.
- You are hereby granted a personal, non-exclusive, non-sub licensable (on a stand-alone basis), non-transferable, worldwide, limited license to reproduce the Wiley Materials for the purpose specified in the licensing process. This license, **and any CONTENT (PDF or image file) purchased as part of your order**, is for a one-time use only and limited to any maximum distribution number specified in the license. The first instance of republication or reuse granted by this license must be completed within two years of the date of the grant of this license (although copies prepared before the end date may be distributed thereafter). The Wiley Materials shall not be used in any other manner or for any other purpose, beyond what is granted in the license. Permission is granted subject to an appropriate acknowledgement given to the author, title of the material/book/journal and the publisher. You shall also duplicate the copyright notice that appears in the Wiley publication in your use of the Wiley Material. Permission is also granted on the understanding that nowhere in the text is a previously published source acknowledged for all or part of this Wiley Material. Any third party content is expressly excluded from this permission.
- With respect to the Wiley Materials, all rights are reserved. Except as expressly granted by the terms of the license, no part of the Wiley Materials may be copied, modified, adapted (except for minor reformatting required by the new Publication), translated, reproduced, transferred or distributed, in any form or by any means, and no derivative works may be made based on the Wiley Materials without the prior permission of the respective copyright owner. **For STM Signatory Publishers clearing permission under the terms of the [STM Permissions Guidelines](#) only, the terms of the license are extended to include subsequent editions and for editions in other languages, provided such editions are for the work as a whole in situ and does not involve the separate exploitation of the permitted figures or extracts**, You may not alter, remove or suppress in any manner any copyright, trademark or other notices displayed by the Wiley Materials. You may not license, rent, sell, loan, lease, pledge, offer as security, transfer or assign the Wiley Materials on a stand-alone basis, or any of the rights granted to you hereunder to any other person.
- The Wiley Materials and all of the intellectual property rights therein shall at all times remain the exclusive property of John Wiley & Sons Inc, the Wiley Companies, or their respective licensors, and your interest therein is only that of having possession of and the right to reproduce the Wiley Materials pursuant to Section 2 herein during the

continuance of this Agreement. You agree that you own no right, title or interest in or to the Wiley Materials or any of the intellectual property rights therein. You shall have no rights hereunder other than the license as provided for above in Section 2. No right, license or interest to any trademark, trade name, service mark or other branding ("Marks") of WILEY or its licensors is granted hereunder, and you agree that you shall not assert any such right, license or interest with respect thereto

- NEITHER WILEY NOR ITS LICENSORS MAKES ANY WARRANTY OR REPRESENTATION OF ANY KIND TO YOU OR ANY THIRD PARTY, EXPRESS, IMPLIED OR STATUTORY, WITH RESPECT TO THE MATERIALS OR THE ACCURACY OF ANY INFORMATION CONTAINED IN THE MATERIALS, INCLUDING, WITHOUT LIMITATION, ANY IMPLIED WARRANTY OF MERCHANTABILITY, ACCURACY, SATISFACTORY QUALITY, FITNESS FOR A PARTICULAR PURPOSE, USABILITY, INTEGRATION OR NON-INFRINGEMENT AND ALL SUCH WARRANTIES ARE HEREBY EXCLUDED BY WILEY AND ITS LICENSORS AND WAIVED BY YOU.
- WILEY shall have the right to terminate this Agreement immediately upon breach of this Agreement by you.
- You shall indemnify, defend and hold harmless WILEY, its Licensors and their respective directors, officers, agents and employees, from and against any actual or threatened claims, demands, causes of action or proceedings arising from any breach of this Agreement by you.
- IN NO EVENT SHALL WILEY OR ITS LICENSORS BE LIABLE TO YOU OR ANY OTHER PARTY OR ANY OTHER PERSON OR ENTITY FOR ANY SPECIAL, CONSEQUENTIAL, INCIDENTAL, INDIRECT, EXEMPLARY OR PUNITIVE DAMAGES, HOWEVER CAUSED, ARISING OUT OF OR IN CONNECTION WITH THE DOWNLOADING, PROVISIONING, VIEWING OR USE OF THE MATERIALS REGARDLESS OF THE FORM OF ACTION, WHETHER FOR BREACH OF CONTRACT, BREACH OF WARRANTY, TORT, NEGLIGENCE, INFRINGEMENT OR OTHERWISE (INCLUDING, WITHOUT LIMITATION, DAMAGES BASED ON LOSS OF PROFITS, DATA, FILES, USE, BUSINESS OPPORTUNITY OR CLAIMS OF THIRD PARTIES), AND WHETHER OR NOT THE PARTY HAS BEEN ADVISED OF THE POSSIBILITY OF SUCH DAMAGES. THIS LIMITATION SHALL APPLY NOTWITHSTANDING ANY FAILURE OF ESSENTIAL PURPOSE OF ANY LIMITED REMEDY PROVIDED HEREIN.
- Should any provision of this Agreement be held by a court of competent jurisdiction to be illegal, invalid, or unenforceable, that provision shall be deemed amended to achieve as nearly as possible the same economic effect as the original provision, and the legality, validity and enforceability of the remaining provisions of this Agreement shall not be affected or impaired thereby.
- The failure of either party to enforce any term or condition of this Agreement shall not constitute a waiver of either party's right to enforce each and every term and condition of this Agreement. No breach under this agreement shall be deemed waived or

excused by either party unless such waiver or consent is in writing signed by the party granting such waiver or consent. The waiver by or consent of a party to a breach of any provision of this Agreement shall not operate or be construed as a waiver of or consent to any other or subsequent breach by such other party.

- This Agreement may not be assigned (including by operation of law or otherwise) by you without WILEY's prior written consent.
- Any fee required for this permission shall be non-refundable after thirty (30) days from receipt by the CCC.
- These terms and conditions together with CCC's Billing and Payment terms and conditions (which are incorporated herein) form the entire agreement between you and WILEY concerning this licensing transaction and (in the absence of fraud) supersedes all prior agreements and representations of the parties, oral or written. This Agreement may not be amended except in writing signed by both parties. This Agreement shall be binding upon and inure to the benefit of the parties' successors, legal representatives, and authorized assigns.
- In the event of any conflict between your obligations established by these terms and conditions and those established by CCC's Billing and Payment terms and conditions, these terms and conditions shall prevail.
- WILEY expressly reserves all rights not specifically granted in the combination of (i) the license details provided by you and accepted in the course of this licensing transaction, (ii) these terms and conditions and (iii) CCC's Billing and Payment terms and conditions.
- This Agreement will be void if the Type of Use, Format, Circulation, or Requestor Type was misrepresented during the licensing process.
- This Agreement shall be governed by and construed in accordance with the laws of the State of New York, USA, without regards to such state's conflict of law rules. Any legal action, suit or proceeding arising out of or relating to these Terms and Conditions or the breach thereof shall be instituted in a court of competent jurisdiction in New York County in the State of New York in the United States of America and each party hereby consents and submits to the personal jurisdiction of such court, waives any objection to venue in such court and consents to service of process by registered or certified mail, return receipt requested, at the last known address of such party.

WILEY OPEN ACCESS TERMS AND CONDITIONS

Wiley Publishes Open Access Articles in fully Open Access Journals and in Subscription journals offering Online Open. Although most of the fully Open Access journals publish open access articles under the terms of the Creative Commons Attribution (CC BY) License only, the subscription journals and a few of the Open Access Journals offer a choice of Creative Commons Licenses. The license type is clearly identified on the article.

The Creative Commons Attribution License

The [Creative Commons Attribution License \(CC-BY\)](#) allows users to copy, distribute and transmit an article, adapt the article and make commercial use of the article. The CC-BY license permits commercial and non-

Creative Commons Attribution Non-Commercial License

The [Creative Commons Attribution Non-Commercial \(CC-BY-NC\) License](#) permits use, distribution and reproduction in any medium, provided the original work is properly cited and is not used for commercial purposes.(see below)

Creative Commons Attribution-Non-Commercial-NoDerivs License

The [Creative Commons Attribution Non-Commercial-NoDerivs License](#) (CC-BY-NC-ND) permits use, distribution and reproduction in any medium, provided the original work is properly cited, is not used for commercial purposes and no modifications or adaptations are made. (see below)

Use by commercial "for-profit" organizations

Use of Wiley Open Access articles for commercial, promotional, or marketing purposes requires further explicit permission from Wiley and will be subject to a fee.

Further details can be found on Wiley Online Library <http://olabout.wiley.com/WileyCDA/Section/id-410895.html>

Other Terms and Conditions:**v1.10 Last updated September 2015**

Questions? customercare@copyright.com or +1-855-239-3415 (toll free in the US) or +1-978-646-2777.

Bibliography

- (1) Atkins P., D. P. J., *Physical Chemistry, 8th Edition*; Freeman W. H. and Co.: Oxford, 2006.
- (2) Turro, N. J.; Lechtken, P.; Schore, N. E.; Schuster, G.; Steinmetzer, H. C.; Yekta, A. *Accounts of Chemical Research* **1974**, 7, 97–105, DOI: [10.1021/ar50076a001](https://doi.org/10.1021/ar50076a001).
- (3) McCapra, F. *Chem. Commun. (London)* **1968**, 155–156, DOI: [10.1039/C19680000155](https://doi.org/10.1039/C19680000155).
- (4) McCapra, F. *Pure Appl. Chem.* **1970**, 611–630, DOI: [10.1351/pac197024030611](https://doi.org/10.1351/pac197024030611).
- (5) Turro, N. J.; Lechtken, P. *Journal of the American Chemical Society* **1973**, 95, 264–266, DOI: [10.1021/ja00782a059](https://doi.org/10.1021/ja00782a059).
- (6) Turro, N. J.; Lechtken, P. *Pure Appl. Chem.* **1973**, 363–388, DOI: [10.1351/pac197333020363](https://doi.org/10.1351/pac197333020363).
- (7) Turro, N. J.; Devaquet, A. *Journal of the American Chemical Society* **1975**, 97, 3859–3862, DOI: [10.1021/ja00846a075](https://doi.org/10.1021/ja00846a075).
- (8) O’Neal, H. E.; Richardson, W. H. *Journal of the American Chemical Society* **1970**, 92, 6553–6557, DOI: [10.1021/ja00725a029](https://doi.org/10.1021/ja00725a029).
- (9) O’Neal, H.; Richardson, W. *Journal of the American Chemical Society* **1971**, 93, 1828–1828, DOI: [10.1021/ja00736a602](https://doi.org/10.1021/ja00736a602).
- (10) Richardson, W. H.; O’Neal, H. E. *Journal of the American Chemical Society* **1972**, 94, 8665–8668, DOI: [10.1021/ja00780a002](https://doi.org/10.1021/ja00780a002).
- (11) Richardson, W. H.; Montgomery, F. C.; Yelvington, M. B.; O’Neal, H. E. *Journal of the American Chemical Society* **1974**, 96, 7525–7532, DOI: [10.1021/ja00831a022](https://doi.org/10.1021/ja00831a022).
- (12) Harding, L. B.; Goddard, W. A. *Journal of the American Chemical Society* **1977**, 99, 4520–4523, DOI: [10.1021/ja00455a061](https://doi.org/10.1021/ja00455a061).
- (13) Dewar, M. J. S.; Kirschner, S. *Journal of the American Chemical Society* **1974**, 96, 7578–7579, DOI: [10.1021/ja00831a046](https://doi.org/10.1021/ja00831a046).

- (14) Dewar, M. J. S.; Kirschner, S.; Kollmar, H. W. *Journal of the American Chemical Society* **1974**, *96*, 7579–7581, DOI: [10.1021/ja00831a047](https://doi.org/10.1021/ja00831a047).
- (15) Evleth, E.; Feler, G. *Chemical Physics Letters* **1973**, *22*, 499–502, DOI: [10.1016/0009-2614\(73\)87016-2](https://doi.org/10.1016/0009-2614(73)87016-2).
- (16) Barnett, G. *Canadian Journal of Chemistry* **1974**, *52*, 3837–3843, DOI: [10.1139/v74-574](https://doi.org/10.1139/v74-574).
- (17) Schmidt, S. P.; Vincent, M. A.; Dykstra, C. E.; Schuster, G. B. *Journal of the American Chemical Society* **1981**, *103*, 1292–1293, DOI: [10.1021/ja00395a084](https://doi.org/10.1021/ja00395a084).
- (18) De Vico, L.; Liu, Y.-J.; Krogh, J. W.; Lindh, R. *The Journal of Physical Chemistry A* **2007**, *111*, 8013–8019, DOI: [10.1021/jp074063g](https://doi.org/10.1021/jp074063g).
- (19) Murphy, S.; Adam, W. *Journal of the American Chemical Society* **1996**, *118*, 12916–12921, DOI: [10.1021/ja9540886](https://doi.org/10.1021/ja9540886).
- (20) Vacher, M.; Brakestad, A.; Karlsson, H. O.; Fdez. Galván, I.; Lindh, R. *Journal of Chemical Theory and Computation* **2017**, *13*, PMID: 28437611, 2448–2457, DOI: [10.1021/acs.jctc.7b00198](https://doi.org/10.1021/acs.jctc.7b00198).
- (21) Schaap, A. P.; Gagnon, S. D. *Journal of the American Chemical Society* **1982**, *104*, 3504–3506, DOI: [10.1021/ja00376a044](https://doi.org/10.1021/ja00376a044).
- (22) Koo, J.-Y.; Schuster, G. B. *Journal of the American Chemical Society* **1977**, *99*, 6107–6109, DOI: [10.1021/ja00460a050](https://doi.org/10.1021/ja00460a050).
- (23) Schmidt, S. P.; Schuster, G. B. *Journal of the American Chemical Society* **1978**, *100*, 1966–1968, DOI: [10.1021/ja00474a074](https://doi.org/10.1021/ja00474a074).
- (24) Koo, J. A.; Schmidt, S. P.; Schuster, G. B. *Proceedings of the National Academy of Sciences* **1978**, *75*, 30–33.
- (25) Schuster, G. B. *Accounts of Chemical Research* **1979**, *12*, 366–373, DOI: [10.1021/ar50142a003](https://doi.org/10.1021/ar50142a003).
- (26) Schmidt, S. P.; Schuster, G. B. *Journal of the American Chemical Society* **1980**, *102*, 306–314, DOI: [10.1021/ja00521a049](https://doi.org/10.1021/ja00521a049).
- (27) Schmidt, S. P.; Schuster, G. B. *Journal of the American Chemical Society* **1980**, *102*, 7100–7103, DOI: [10.1021/ja00543a036](https://doi.org/10.1021/ja00543a036).
- (28) Schuster, G. B.; Schmidt, S. P. In Gold, V., Bethell, D., Eds.; *Advances in Physical Organic Chemistry Supplement C*, Vol. 18; Academic Press: 1982, pp 187–238, DOI: [10.1016/S0065-3160\(08\)60140-9](https://doi.org/10.1016/S0065-3160(08)60140-9).

-
- (29) Edwards, B.; Sparks, A.; Voyta, J. C.; Bronstein, I. *Journal of Bioluminescence and Chemiluminescence* **1990**, *5*, 1–4, DOI: [10.1002/bio.1170050102](https://doi.org/10.1002/bio.1170050102).
- (30) Hoshiya, N.; Fukuda, N.; Maeda, H.; Watanabe, N.; Matsumoto, M. *Tetrahedron* **2006**, *62*, 5808–5820, DOI: [10.1016/j.tet.2006.03.082](https://doi.org/10.1016/j.tet.2006.03.082).
- (31) Hastings, J. W.; Nealson, K. H. *Annual Review of Microbiology* **1977**, *31*, 549–595, DOI: [10.1146/annurev.mi.31.100177.003001](https://doi.org/10.1146/annurev.mi.31.100177.003001).
- (32) Albrecht, H. O. *Zeitschrift für Physikalische Chemie* **2017**, *136U*, 321–330, DOI: [10.1515/zpch-1928-13625](https://doi.org/10.1515/zpch-1928-13625).
- (33) Merényi, G.; Lind, J.; Eriksen, T. E. *Journal of Bioluminescence and Chemiluminescence* **1990**, *5*, 53–56, DOI: [10.1002/bio.1170050111](https://doi.org/10.1002/bio.1170050111).
- (34) Schroeder, H. R.; Yeager, F. M. *Analytical Chemistry* **1978**, *50*, 1114–1120, DOI: [10.1021/ac50030a027](https://doi.org/10.1021/ac50030a027).
- (35) Roswell, D. F.; White, E. H. In *Bioluminescence and Chemiluminescence; Methods in Enzymology Supplement C*, Vol. 57; Academic Press: 1978, pp 409–423, DOI: [doi.org/10.1016/0076-6879\(78\)57038-9](https://doi.org/10.1016/0076-6879(78)57038-9).
- (36) Brundrett, R. B.; White, E. H. *Journal of the American Chemical Society* **1974**, *96*, 7497–7502, DOI: [10.1021/ja00831a018](https://doi.org/10.1021/ja00831a018).
- (37) Stanley, P. E. *Journal of Bioluminescence and Chemiluminescence* **1986**, *1*, 45–46, DOI: [10.1002/bio.1170010109](https://doi.org/10.1002/bio.1170010109).
- (38) Díaz, A. N.; Sánchez, F. G.; González Garcia, J. A. *Journal of Bioluminescence and Chemiluminescence* **1998**, *13*, 75–84, DOI: [10.1002/\(SICI\)1099-1271\(199803/04\)13:2<75::AID-BIO469>3.0.CO;2-7](https://doi.org/10.1002/(SICI)1099-1271(199803/04)13:2<75::AID-BIO469>3.0.CO;2-7).
- (39) Marquette, C. A.; Blum, L. J. *Analytical and Bioanalytical Chemistry* **2006**, *385*, 546–554, DOI: [10.1007/s00216-006-0439-9](https://doi.org/10.1007/s00216-006-0439-9).
- (40) Khan, P.; Idrees, D.; Moxley, M. A.; Corbett, J. A.; Ahmad, F.; von Figura, G.; Sly, W. S.; Waheed, A.; Hassan, M. I. *Applied Biochemistry and Biotechnology* **2014**, *173*, 333–355, DOI: [10.1007/s12010-014-0850-1](https://doi.org/10.1007/s12010-014-0850-1).
- (41) Gleu, K.; Petsch, W. *Angewandte Chemie* **1935**, *48*, 57–59, DOI: [10.1002/ange.19350480302](https://doi.org/10.1002/ange.19350480302).
- (42) McCapra, F.; Richardson, D. *Tetrahedron Letters* **1964**, *5*, 3167–3172, DOI: [10.1016/0040-4039\(64\)83128-2](https://doi.org/10.1016/0040-4039(64)83128-2).
- (43) McCapra, F. *Accounts of Chemical Research* **1976**, *9*, 201–208, DOI: [10.1021/ar50102a001](https://doi.org/10.1021/ar50102a001).
-

- (44) Nakazono, M.; Oshikawa, Y.; Nakamura, M.; Kubota, H.; Nanbu, S. *The Journal of Organic Chemistry* **2017**, *82*, PMID: 28171728, 2450–2461, DOI: [10.1021/acs.joc.6b02748](https://doi.org/10.1021/acs.joc.6b02748).
- (45) Mazumder, A.; Majlessi, M.; Becker, M. M. *Nucleic Acids Research* **1998**, *26*, 1996–2000, DOI: [10.1093/nar/26.8.1996](https://doi.org/10.1093/nar/26.8.1996).
- (46) Brown, R. C.; Li, Z.; Rutter, A. J.; Mu, X.; Weeks, O. H.; Smith, K.; Weeks, I. *Org. Biomol. Chem.* **2009**, *7*, 386–394, DOI: [10.1039/B811947C](https://doi.org/10.1039/B811947C).
- (47) Weeks, I.; Beheshti, I.; McCapra, F.; Campbell, A. K.; Woodhead, J. S. *Clinical Chemistry* **1983**, *29*, 1474–1479.
- (48) Buxton, R. C.; Edwards, B.; Juo, R. R.; Voyta, J. C.; Tisdale, M.; Bethell, R. C. *Analytical Biochemistry* **2000**, *280*, 291–300, DOI: <https://doi.org/10.1006/abio.2000.4517>.
- (49) Beck, S.; Koster, H. *Analytical Chemistry* **1990**, *62*, 2258–2270, DOI: [10.1021/ac00220a003](https://doi.org/10.1021/ac00220a003).
- (50) Adam, W.; Reinhardt, D.; Saha-Moller, C. R. *Analyst* **1996**, *121*, 1527–1531, DOI: [10.1039/AN9962101527](https://doi.org/10.1039/AN9962101527).
- (51) Green, O.; Eilon, T.; Hananya, N.; Gutkin, S.; Bauer, C. R.; Shabat, D. *ACS Central Science* **2017**, *3*, 349–358, DOI: [10.1021/acscentsci.7b00058](https://doi.org/10.1021/acscentsci.7b00058).
- (52) Hori, K.; Charbonneau, H.; Hart, R. C.; Cormier, M. J. *Proceedings of the National Academy of Sciences* **1977**, *74*, 4285–4287.
- (53) Shimomura, O.; Johnson, F. H. *Proceedings of the National Academy of Sciences* **1975**, *72*, 1546–1549.
- (54) Vysotski, E. S.; Lee, J. *Accounts of Chemical Research* **2004**, *37*, 405–415, DOI: [10.1021/ar0400037](https://doi.org/10.1021/ar0400037).
- (55) Hastings, J. *Bulletin of Marine Science* **1983**, *33*, 818–828.
- (56) Shimomura, O.; Teranishi, K. *Luminescence* **2000**, *15*, 51–58, DOI: [10.1002/\(SICI\)1522-7243\(200001/02\)15:1<51::AID-BIO555>3.0.CO;2-J](https://doi.org/10.1002/(SICI)1522-7243(200001/02)15:1<51::AID-BIO555>3.0.CO;2-J).
- (57) Saleh, L.; Plieth, C. *Nature Protocols* **2010**, *5*, 1635–1641, DOI: [10.1038/nprot.2010.121](https://doi.org/10.1038/nprot.2010.121).
- (58) Jiang, T.; Du, L.; Li, M. *Photochem. Photobiol. Sci.* **2016**, *15*, 466–480, DOI: [10.1039/C5PP00456J](https://doi.org/10.1039/C5PP00456J).
- (59) Rauhut, M. M.; Bollyky, L. J.; Roberts, B. G.; Loy, M.; Whitman, R. H.; Iannotta, A. V.; Semsel, A. M.; Clarke, R. A. *Journal of the American Chemical Society* **1967**, *89*, 6515–6522, DOI: [10.1021/ja01001a025](https://doi.org/10.1021/ja01001a025).

-
- (60) Orlovic, M.; Schowen, R. L.; Givens, R. S.; Alvarez, F.; Matuszewski, B.; Parekh, N. *The Journal of Organic Chemistry* **1989**, *54*, 3606–3610, DOI: [10.1021/jo00276a021](https://doi.org/10.1021/jo00276a021).
- (61) Catherall, C. L. R.; Palmer, T. F.; Cundall, R. B. *J. Chem. Soc., Faraday Trans. 2* **1984**, *80*, 823–836, DOI: [10.1039/F29848000823](https://doi.org/10.1039/F29848000823).
- (62) Chokshi, H. P.; Barbush, M.; Carlson, R. G.; Givens, R. S.; Kuwana, T.; Schowen, R. L. *Biomedical Chromatography* **1990**, *4*, 96–99, DOI: [10.1002/bmc.1130040304](https://doi.org/10.1002/bmc.1130040304).
- (63) Imai, K.; Nawa, H.; Tanaka, M.; Ogata, H. *Analyst* **1986**, *111*, 209–211, DOI: [10.1039/AN9861100209](https://doi.org/10.1039/AN9861100209).
- (64) Petre, R.; Zecheru, T. *Journal of Luminescence* **2013**, *135*, 288–294, DOI: <https://doi.org/10.1016/j.jlumin.2012.09.028>.
- (65) M, R. Stabilization of oxalate ester solutions during storage., US Patent 3,718,599, 1973.
- (66) D, L.; VR, E.; M, D.; J, Y.; RM, D.; N, M. *International Journal of Nanomedicine* **2008**, *3*, 471–476, DOI: [10.2147/IJN.S3728](https://doi.org/10.2147/IJN.S3728).
- (67) Omanovic, E.; Kalcher, K. *International Journal of Environmental Analytical Chemistry* **2005**, *85*, 853–860, DOI: [10.1080/14659890500156996](https://doi.org/10.1080/14659890500156996).
- (68) Fitzroy, R.; King, P.; Darwin, C., *Journal and remarks, 1832-1836. By Charles Darwin. (Part of maps in pockets)*; Narrative of the Surveying Voyages of His Majesty's Ships Adventure and Beagle, Between the Years 1826 and 1836: Describing Their Examination of the Southern Shores of South America, and the Beagle's Circumnavigation of the Globe; H. Colburn: 1839.
- (69) Harvey, E., *The Nature of Animal Light*; Monographs on experimental biology and general physiology; J.P. Lippincott Company: 1920.
- (70) Harvey, E. N., *The Evolution of Bioluminescence and Its Relation to Cell Respiration*; 4; American Philosophical Society: 1932; Vol. 71, pp 135–141.
- (71) Seliger, H. H. *NAVAL RESEARCH REVIEWS* **1993**, *45*.
- (72) Rees, J. F.; de Wergifosse, B.; Noiset, O.; Dubuisson, M.; Janssens, B.; Thompson, E. M. *Journal of Experimental Biology* **1998**, *201*, 1211–1221.
- (73) S., A.; M.B., D.; E., L.; J.C., P.; Vallerga, S., *Adaptive Mechanisms in the Ecology of Vision*; Springer Netherlands: 1999.
-

- (74) Haddock, S. H.; Moline, M. A.; Case, J. F. *Annual Review of Marine Science* **2010**, *2*, PMID: 21141672, 443–493, DOI: [10.1146/annurev-marine-120308-081028](https://doi.org/10.1146/annurev-marine-120308-081028).
- (75) Hastings, J. *Gene* **1996**, *173*, Fluorescent Proteins and Applications, 5–11, DOI: [https://doi.org/10.1016/0378-1119\(95\)00676-1](https://doi.org/10.1016/0378-1119(95)00676-1).
- (76) McElroy, W. D.; Ballentine, R. *Proceedings of the National Academy of Sciences of the United States of America* **1944**, *30*, 377–382.
- (77) Santaniello, E.; Meroni, G. *Minerva Biotechnologica* **2009**, *21*, 77–86.
- (78) Branchini, B. R.; Ablamsky, D. M.; Rosenberg, J. C. *Bioconjugate Chemistry* **2010**, *21*, PMID: 20936788, 2023–2030, DOI: [10.1021/bc100256d](https://doi.org/10.1021/bc100256d).
- (79) Paley, M. A.; Prescher, J. A. *Med. Chem. Commun.* **2014**, *5*, 255–267, DOI: [10.1039/C3MD00288H](https://doi.org/10.1039/C3MD00288H).
- (80) Steinberg, S. M.; Poziomek, E. J.; Engelmann, W. H.; Rogers, K. R. *Chemosphere* **1995**, *30*, 2155–2197, DOI: [https://doi.org/10.1016/0045-6535\(95\)00087-O](https://doi.org/10.1016/0045-6535(95)00087-O).
- (81) Badr, C. E.; Tannous, B. A. *Trends in Biotechnology* **2011**, *29*, 624–633, DOI: [10.1016/j.tibtech.2011.06.010](https://doi.org/10.1016/j.tibtech.2011.06.010).
- (82) Söling, A.; Rainov, N. G. *Expert Opinion on Biological Therapy* **2003**, *3*, 1163–1172, DOI: [10.1517/14712598.3.7.1163](https://doi.org/10.1517/14712598.3.7.1163).
- (83) Staples, R. F.; Office., U. S. N. O., *The distribution and characteristics of surface bioluminescence in the oceans*; Washington :Naval Oceanographic Office, p 62.
- (84) KH, N.; JW, H. *Microbiological Reviews* **1979**, *43*, 496–518.
- (85) Ruby, E. G.; Morin, J. G. *Applied and Environmental Microbiology* **1979**, *38*, 406–411.
- (86) Nunes-Halldorson, V. d. S.; Duran, N. L.-c. *Brazilian Journal of Microbiology* **2003**, *34*, 91–96, DOI: [10.1590/S1517-83822003000200001](https://doi.org/10.1590/S1517-83822003000200001).
- (87) JW, H.; C, B.; CL, P.; P, D. *Proceedings of the National Academy of Sciences of the United States of America* **1973**, *70*, 3468–3472.
- (88) Tinikul, R.; Chaiyen, P., *Structure, Mechanism, and Mutation of Bacterial Luciferase*; Thouand, G., Marks, R., Eds.; Springer International Publishing: Cham, 2016, pp 47–74, DOI: [10.1007/10_2014_281](https://doi.org/10.1007/10_2014_281).
- (89) Girotti, S.; Ferri, E. N.; Fumo, M. G.; Maiolini, E. *Analytica Chimica Acta* **2008**, *608*, 2–29, DOI: <https://doi.org/10.1016/j.aca.2007.12.008>.

-
- (90) Robinson, G. M.; Tonks, K. M.; Thorn, R. M. S.; Reynolds, D. M. *Antimicrobial Agents and Chemotherapy* **2011**, *55*, 5214–5219, DOI: [10.1128/AAC.00489-11](https://doi.org/10.1128/AAC.00489-11).
- (91) Alloush, H. M.; Lewis, R. J.; Salisbury, V. C. *Analytical Letters* **2006**, *39*, 1517–1526, DOI: [10.1080/00032710600713172](https://doi.org/10.1080/00032710600713172).
- (92) Chatterjee, J.; Meighen, E. A. *Photochemistry and Photobiology* **1995**, *62*, 641–650, DOI: [10.1111/j.1751-1097.1995.tb08711.x](https://doi.org/10.1111/j.1751-1097.1995.tb08711.x).
- (93) Hoffmann, K., *Environmental Physiology and Biochemistry of Insects*; Springer Berlin Heidelberg: 2012.
- (94) H, S. H.; B, B. J.; G, F. W.; D, M. W. *The Journal of General Physiology* **1964**, *48*, 95–104.
- (95) Biggley WH Lloyd JE, S. H. *The Journal of General Physiology* **1967**, *50*, 1681–1692.
- (96) Marques, S. M.; Esteves da Silva, J. C. G. *IUBMB Life* **2009**, *61*, 6–17, DOI: [10.1002/iub.134](https://doi.org/10.1002/iub.134).
- (97) Fraga, H. *Photochem. Photobiol. Sci.* **2008**, *7*, 146–158, DOI: [10.1039/B719181B](https://doi.org/10.1039/B719181B).
- (98) Li, J.; Chen, L.; Du, L.; Li, M. *Chem. Soc. Rev.* **2013**, *42*, 662–676, DOI: [10.1039/C2CS35249D](https://doi.org/10.1039/C2CS35249D).
- (99) Roda, A.; Guardigli, M.; Michelini, E.; Mirasoli, M. *TrAC Trends in Analytical Chemistry* **2009**, *28*, 307–322, DOI: [10.1016/j.trac.2008.11.015](https://doi.org/10.1016/j.trac.2008.11.015).
- (100) KR, O.; RM, E. *Assay Drug Dev Technol.* **2007**, *5*, 137–144, DOI: [10.1089/adt.2006.052](https://doi.org/10.1089/adt.2006.052).
- (101) Steinberg, S. M.; Poziomek, E. J.; Engelmann, W. H.; Rogers, K. R. *Chemosphere* **1995**, *30*, 2155–2197, DOI: [10.1016/0045-6535\(95\)00087-O](https://doi.org/10.1016/0045-6535(95)00087-O).
- (102) Wieringa, J.; Strating, J.; Wynberg, H.; Adam, W. *Tetrahedron Letters* **1972**, *13*, 169–172, DOI: [10.1016/S0040-4039\(01\)84269-6](https://doi.org/10.1016/S0040-4039(01)84269-6).
- (103) Luijder, T. M.; Hummelen, J. C.; Oudman, D.; Wynberg, H., *Thermochemiluminescence Immunoassay for hCG*; University of Groningen, Stratingh Institute for Chemistry: 1990.
- (104) Hara, K.; Schuster, G. B.; Drickamer, H. *Chemical Physics Letters* **1977**, *47*, 462–465, DOI: [10.1016/0009-2614\(77\)85016-1](https://doi.org/10.1016/0009-2614(77)85016-1).
-

- (105) O'Sullivan, M. P.; Testa, A. C. *Journal of the American Chemical Society* **1970**, *92*, 5842–5844, DOI: [10.1021/ja00723a005](https://doi.org/10.1021/ja00723a005).
- (106) Hummelen, J. C.; Luider, T. M.; Wynberg, H. In *Bioluminescence and Chemiluminescence Part B; Methods in Enzymology Supplement C*, Vol. 133; Academic Press: 1986, pp 531–557, DOI: [10.1016/0076-6879\(86\)33088-X](https://doi.org/10.1016/0076-6879(86)33088-X).
- (107) Roda, A.; Di Fusco, M.; Quintavalla, A.; Guardigli, M.; Mirasoli, M.; Lombardo, M.; Trombini, C. *Analytical Chemistry* **2012**, *84*, 9913–9919, DOI: [10.1021/ac302306u](https://doi.org/10.1021/ac302306u).
- (108) DI, F.; Guardigli, M.; Lombardo, M.; MIRASOLI, M.; Quintavalla, A.; Roda, A.; Trombini, C. Method for the production of thermochemiluminescent silica nanoparticles and their use as markers in bioanalytic methods., WO Patent App. PCT/IB2013/056,340, 2014.
- (109) Di Fusco, M.; Quintavalla, A.; Lombardo, M.; Guardigli, M.; Mirasoli, M.; Trombini, C.; Roda, A. *Analytical and Bioanalytical Chemistry* **2015**, *407*, 1567–1576, DOI: [10.1007/s00216-014-8406-3](https://doi.org/10.1007/s00216-014-8406-3).
- (110) Di Fusco, M.; Quintavalla, A.; Trombini, C.; Lombardo, M.; Roda, A.; Guardigli, M.; Mirasoli, M. *The Journal of Organic Chemistry* **2013**, *78*, 11238–11246, DOI: [10.1021/jo401683r](https://doi.org/10.1021/jo401683r).
- (111) Andronico, L. A.; Quintavalla, A.; Lombardo, M.; Mirasoli, M.; Guardigli, M.; Trombini, C.; Roda, A. *Chemistry – A European Journal* **2016**, *22*, 18156–18168, DOI: [10.1002/chem.201603765](https://doi.org/10.1002/chem.201603765).
- (112) Lee, C.; Singer, L. A. *Journal of the American Chemical Society* **1980**, *102*, 3823–3829, DOI: [10.1021/ja00531a026](https://doi.org/10.1021/ja00531a026).
- (113) Ciscato, L. F. M. L.; Bartoloni, F. H.; Weiss, D.; Beckert, R.; Baader, W. J. *The Journal of Organic Chemistry* **2010**, *75*, 6574–6580, DOI: [10.1021/jo1013405](https://doi.org/10.1021/jo1013405).
- (114) Ciscato, L. F. M. L.; Weiss, D.; Beckert, R.; Bastos, E. L.; Bartoloni, F. H.; Baader, W. J. *New J. Chem.* **2011**, *35*, 773–775, DOI: [10.1039/C0NJ00843E](https://doi.org/10.1039/C0NJ00843E).
- (115) Chen, Y.; Spiering, A. J. H.; Karthikeyan, S.; Peters, G. W. M.; Meijer, E. W.; Sijbesma, R. P. *Nature Chemistry* **2012**, *4*, 559–562, DOI: [doi: 10.1038/nchem.1358](https://doi.org/10.1038/nchem.1358).
- (116) P. D. Bartlett, M. E. L. In; Academic Press, New York: 1979, pp 243–286.
- (117) In *Peroxides 1983*; John Wiley & Sons: 2010, pp 829–920, DOI: [10.1002/9780470771730.ch24](https://doi.org/10.1002/9780470771730.ch24).

-
- (118) Adam, W. In; Wiley, New York: 1986, pp 351–429.
- (119) Adam, W.; Heil, M.; Mosandl, T.; Saha-Moller, C. R., *"Organic Peroxides"*; Wiley: New York, 1992.
- (120) C. R. Saha-Möller, W. A. In; Pergamon, New York: 1996, pp 1041–1082.
- (121) W. Adam, A. V. T. In; Wiley, New York: 2006, pp 1171–1209.
- (122) Masakatsu, M.; Nobuko, W. *Bulletin of the Chemical Society of Japan* **2005**, 78, 1899–1920, DOI: [10.1246/bcsj.78.1899](https://doi.org/10.1246/bcsj.78.1899).
- (123) Matsumoto, M. *Journal of Photochemistry and Photobiology C: Photochemistry Reviews* **2004**, 5, 27–53, DOI: <https://doi.org/10.1016/j.jphotochemrev.2004.02.001>.
- (124) W. J. Baader C. V. Stevani, E. L. B. In; Wiley & Sons, Chichester: 2006, pp 1211–1278.
- (125) Shimomura O Goto T, J. F. *Proceedings of the National Academy of Sciences of the United States of America* **1977**, 74, 2799–2802.
- (126) Kean, Z. S.; Hawk, J. L.; Lin, S.; Zhao, X.; Sijbesma, R. P.; Craig, S. L. *Advanced Materials* **2014**, 26, 6013–6018, DOI: [10.1002/adma.201401570](https://doi.org/10.1002/adma.201401570).
- (127) Chen, Y.; Sijbesma, R. P. *Macromolecules* **2014**, 47, 3797–3805, DOI: [10.1021/ma500598t](https://doi.org/10.1021/ma500598t).
- (128) Mayer, A.; Neuenhofer, S. *Angewandte Chemie International Edition in English* **1994**, 33, 1044–1072, DOI: [10.1002/anie.199410441](https://doi.org/10.1002/anie.199410441).
- (129) Mayer, A.; Neuenhofer, S. *Angewandte Chemie* **1994**, 106, 1097–1126, DOI: [10.1002/ange.19941061005](https://doi.org/10.1002/ange.19941061005).
- (130) Hummelen, J. C.; Luider, T. M.; Wynberg, H. In; John Wiley & Sons, Chichester: 1988.
- (131) Luider, T. M.; Hummelen, J. C.; Koek, J. N.; Oudman, D.; Wynberg, H., *Luminescence Immunoassay and Molecular Applications*; CRC Press: Boca Raton, 1990.
- (132) Bronstein, I.; Edwards, B.; Voyta, J. C. *Journal of Bioluminescence and Chemiluminescence* **1989**, 4, 99–111, DOI: [10.1002/bio.1170040116](https://doi.org/10.1002/bio.1170040116).
- (133) Sabelle, S.; Renard, P.-Y.; Pecorella, K.; de Suzzoni-Dézard, S.; Créminon, C.; Grassi, J.; Mioskowski, C. *Journal of the American Chemical Society* **2002**, 124, PMID: 11971738, 4874–4880, DOI: [10.1021/ja0171299](https://doi.org/10.1021/ja0171299).
- (134) Edwards, " Sparks, A.; Voyta, J. C.; Bronstein, I., *Bioluminescence and Chemiluminescence, Fundamentals and Applied Aspects*; Wiley: Chichester, 1994.
-

- (135) Bronstein, I.; Voyta, J. C.; Thorpe, G. H.; Kricka, L. J.; Armstrong, G. *Clinical Chemistry* **1989**, *35*, 1441–1446.
- (136) Thorpe, G. H.; Bronstein, I.; Kricka, L. J.; Edwards, B.; Voyta, J. C. *Clinical Chemistry* **1989**, *35*, 2319–2321.
- (137) Bronstein, I.; Voyta, J. C.; Edwards, B. *Analytical Biochemistry* **1989**, *180*, 95–98, DOI: [https://doi.org/10.1016/0003-2697\(89\)90093-6](https://doi.org/10.1016/0003-2697(89)90093-6).
- (138) Tizard, R.; Cate, R. L.; Ramachandran, K. L.; Wysk, M.; Voyta, J. C.; Murphy, O. J.; Bronstein, I. *Proceedings of the National Academy of Sciences* **1990**, *87*, 4514–4518, DOI: [10.1073/pnas.87.12.4514](https://doi.org/10.1073/pnas.87.12.4514).
- (139) Gilbert, M.; Zakharova, V.; Ramenda, A.; Jebsen, C.; Schulze, B.; Wilhelm, C. *Tetrahedron* **2012**, *68*, 6765–6771, DOI: <https://doi.org/10.1016/j.tet.2012.05.100>.
- (140) Kong, H.; Wang, H.; Zhang, S.; Zhang, X. *Analyst* **2011**, *136*, 3643–3648, DOI: [10.1039/C1AN15382J](https://doi.org/10.1039/C1AN15382J).
- (141) Wiener-Megnazi, Z.; Shiloh, H.; Avraham, L.; Lahav-Baratz, S.; Koifman, M.; Reznick, A. Z.; Auslender, R.; Dirnfeld, M. *Fertility and Sterility* **2011**, *95*, 979–984, DOI: <https://doi.org/10.1016/j.fertnstert.2010.10.019>.
- (142) Kong, H.; Liu, D.; Zhang, S.; Zhang, X. *Analytical Chemistry* **2011**, *83*, 1867–1870, DOI: [10.1021/ac200076c](https://doi.org/10.1021/ac200076c).
- (143) Amir, O.; Yamin, C.; Sagiv, M.; Eynon, N.; Shnizer, S.; Kagan, T.; Reznick, A. Z.; Sagiv, M.; Amir, R. E. *J. Sports Med. Phys. Fitness* **2009**, *49*, 105–111.
- (144) Amir, O.; Paz, H.; Rogowski, O.; Barshai, M.; Sagiv, M.; Shnizer, S.; Reznick, A. Z.; Amir, R. E. *Clinical Cardiology* **2009**, *32*, 199–203, DOI: [10.1002/clc.20317](https://doi.org/10.1002/clc.20317).
- (145) Igor, S.; Vera, B.; Michael, L.; A., R. M.; Sergei, S.; Nitza, L.; G., M. J.; Haim, B. *Critical Care Medicine* **2009**, *37*, 1054–1061, DOI: [10.1097/CCM.0b013e31819d0f5c](https://doi.org/10.1097/CCM.0b013e31819d0f5c).
- (146) Wiener-Megnazi, Z.; Vardi, L.; Lissak, A.; Shnizer, S.; Reznick, A. Z.; Ishai, D.; Lahav-Baratz, S.; Shiloh, H.; Koifman, M.; Dirnfeld, M. *Fertility and Sterility* **2004**, *82*, 1171–1176, DOI: <https://doi.org/10.1016/j.fertnstert.2004.06.013>.
- (147) Shnizer, S.; Kagan, T.; Lanir, A.; Maor, I.; Reznick, A. Z. *Luminescence* **2003**, *18*, 90–96, DOI: [10.1002/bio.699](https://doi.org/10.1002/bio.699).
- (148) Shnizer, S.; Resnik, A.; Lanir, A.; Piuk, V., WO 9919728A1 19990422, 1999.

- (149) Kiel, J. L.; Alls, J. L.; Holwitt, E. A.; Stribling, L. J.; Parker, J. E. *Bioelectrochemistry and Bioenergetics* **1998**, *47*, 253–257, DOI: [https://doi.org/10.1016/S0302-4598\(98\)00196-2](https://doi.org/10.1016/S0302-4598(98)00196-2).
- (150) Hummelen, J.; Wynberg, H. Chemiluminescent labeled organic reagents and their use in analysis of organic compounds., WO Patent App. PCT/US1985/000,684, 1985.
- (151) Hummelen, J.; Luider, T.; Wynberg, H. *Pure and Applied Chemistry* **1987**, *59*, 639–650, DOI: [10.1351/pac198759050639](https://doi.org/10.1351/pac198759050639).
- (152) Luider, T.; Hummelen, J. C.; Koek, J. N.; Wynberg, H., EP 261719A2 19880330, 1988.
- (153) Imanishi, T.; Ueda, Y.; Tainaka, R.; Miyashita, K.; Hoshino, N. *Tetrahedron Letters* **1997**, *38*, 841–844, DOI: [https://doi.org/10.1016/S0040-4039\(96\)02463-X](https://doi.org/10.1016/S0040-4039(96)02463-X).
- (154) H., W. E.; Nobutaka, S.; H., H. W. *Chemistry Letters* **1979**, *8*, 1491–1494, DOI: [10.1246/cl.1979.1491](https://doi.org/10.1246/cl.1979.1491).
- (155) Suzuki, N.; Kazui, Y.; Izawa, Y. *Tetrahedron Letters* **1982**, *23*, 95–96, DOI: [https://doi.org/10.1016/S0040-4039\(00\)97542-7](https://doi.org/10.1016/S0040-4039(00)97542-7).
- (156) Adam, W.; Reinhardt, D. *Liebigs Annalen* **1997**, *1997*, 1359–1364, DOI: [10.1002/jlac.199719970712](https://doi.org/10.1002/jlac.199719970712).
- (157) Adam, W.; Reinhardt, D. *J. Chem. Soc., Perkin Trans. 2* **1997**, 1453–1464, DOI: [10.1039/A701189J](https://doi.org/10.1039/A701189J).
- (158) Imanishi, T.; Ueda, Y.; Tainaka, R.; Kuni, N.; Minagawa, M.; Hoshino, N.; Miyashita, K. *Heterocycles* **1998**, *47*, 829–838, DOI: [10.3987/COM-97-S\(N\)85](https://doi.org/10.3987/COM-97-S(N)85).
- (159) Choudhary, P.; Sharma, V.; Om, H.; Devi, P. *American Journal of Chemistry* **2013**, *3*, 115–125, DOI: [10.5923/j.chemistry.20130305.01](https://doi.org/10.5923/j.chemistry.20130305.01).
- (160) In *Organic Reactions*; John Wiley & Sons, Inc.: 2004, DOI: [10.1002/0471264180.or082.01](https://doi.org/10.1002/0471264180.or082.01).
- (161) Heravi, M. M.; Faghihi, Z. *Current Organic Chemistry* **2012**, *16*, 2097–2123, DOI: [10.2174/138527212803532404](https://doi.org/10.2174/138527212803532404).
- (162) Bodwell, G. J.; Nandaluru, P. R. *Israel Journal of Chemistry* **2012**, *52*, 105–138, DOI: [10.1002/ijch.201200003](https://doi.org/10.1002/ijch.201200003).
- (163) Iyoda, M. *Pure and Applied Chemistry* **2010**, *82*, 831–841, DOI: [doi: 10.1351/PAC-CON-09-11-01](https://doi.org/10.1351/PAC-CON-09-11-01).
- (164) T. Takeda, A. T. *Sci. Synth.* **2010**, *47a*, 247–325.

- (165) Li, J.; Corey, E., *Name Reactions for Homologation*; Comprehensive Name Reactions pt. 1; Wiley: 2009.
- (166) M M Krayushkin M A Kalik, V. A. M. *Russian Chemical Reviews* **2009**, 78, 329–336.
- (167) Ladipo, F. T. *Current Organic Chemistry* **2006**, 10, 965–980, DOI: [10.2174/138527206777435526](https://doi.org/10.2174/138527206777435526).
- (168) Takeda, T., *Modern Carbonyl Olefination, Methods and Applications*; Wiley: 2006.
- (169) Matthias Beller, C. B., *Transition Metals for Organic Synthesis: Building Blocks and Fine Chemicals, 2nd Revised and Enlarged Edition, 2-Volume Set*; Wiley: 2004.
- (170) McMurry, J. E. *Chemical Reviews* **1989**, 89, 1513–1524, DOI: [10.1021/cr00097a007](https://doi.org/10.1021/cr00097a007).
- (171) Ashen-Garry, D.; Selke, M. *Photochemistry and Photobiology* **2014**, 90, 257–274, DOI: [10.1111/php.12211](https://doi.org/10.1111/php.12211).
- (172) Knipe, A., *Organic Reaction Mechanisms 2012: An annual survey covering the literature dated January to December 2012*; Organic Reaction Mechanisms Series; Wiley: 2015.
- (173) In *Encyclopedia of Radicals in Chemistry, Biology and Materials*; John Wiley & Sons, Ltd: 2012, DOI: [10.1002/9781119953678.rad063](https://doi.org/10.1002/9781119953678.rad063).
- (174) Flavio Cermola, M. R. I. In; Boca Raton, CRC Press: 2012.
- (175) Lacombe, S.; Pigot, T. In *Photochemistry: Volume 38*; The Royal Society of Chemistry: 2010; Vol. 38, pp 307–329, DOI: [10.1039/9781849730860-00307](https://doi.org/10.1039/9781849730860-00307).
- (176) In *Handbook of Synthetic Photochemistry*; Wiley-VCH Verlag GmbH & Co. KGaA: 2010, pp 353–386, DOI: [10.1002/9783527628193.ch11](https://doi.org/10.1002/9783527628193.ch11).
- (177) Iesce, M. R.; Cermola, F.; Rubino, M. *Current Organic Chemistry* **2007**, 11, 1053–1075, DOI: [10.2174/138527207781369254](https://doi.org/10.2174/138527207781369254).
- (178) Clennan, E. L.; Pace, A. *Tetrahedron* **2005**, 61, 6665–6691, DOI: [10.1016/j.tet.2005.04.017](https://doi.org/10.1016/j.tet.2005.04.017).
- (179) Stratakis, M. *Current Organic Synthesis* **2005**, 2, 281–299, DOI: [10.2174/1570179053545387](https://doi.org/10.2174/1570179053545387).
- (180) Foote, C.; Valentine, J.; Greenberg, A.; Liebman, J., *Active Oxygen in Chemistry*; Structure Energetics and Reactivity in Chemistry Series; Springer Netherlands: 1995.

- (181) Jefford, C. W. *Chem. Soc. Rev.* **1993**, 22, 59–66, DOI: [10.1039/CS9932200059](https://doi.org/10.1039/CS9932200059).
- (182) Jiang, Z.-Q. *Research on Chemical Intermediates* **1990**, 14, 185–207, DOI: [10.1163/156856790X00256](https://doi.org/10.1163/156856790X00256).
- (183) Lopez, L. In *Photoinduced Electron Transfer I*, Mattay, J., Ed.; Springer Berlin Heidelberg: Berlin, Heidelberg, 1990, pp 117–166, DOI: [10.1007/3-540-52379-0_5](https://doi.org/10.1007/3-540-52379-0_5).
- (184) Frimer, A. In *Singlet Oxygen, Volume 2*; CRC Press, Boca Raton: 1985.
- (185) McCapra, F.; Beheshti, I.; Burford, A.; Hann, R. A.; Zaklika, K. A. *J. Chem. Soc., Chem. Commun.* **1977**, 944–946, DOI: [10.1039/C39770000944](https://doi.org/10.1039/C39770000944).
- (186) Lechtken, P.; Reissenweber, G.; Grubmüller, P. *Tetrahedron Letters* **1977**, 18, 2881–2884, DOI: [10.1016/S0040-4039\(01\)83100-2](https://doi.org/10.1016/S0040-4039(01)83100-2).
- (187) Matsumoto, M.; Suganuma, H.; Katao, Y.; Mutoh, H. *J. Chem. Soc., Chem. Commun.* **1995**, 431–432, DOI: [10.1039/C39950000431](https://doi.org/10.1039/C39950000431).
- (188) Ciscato, L. F. M.; Weiss, D.; Beckert, R.; Baader, W. J. *Journal of Photochemistry and Photobiology A: Chemistry* **2011**, 218, 41–47, DOI: [10.1016/j.jphotochem.2010.12.001](https://doi.org/10.1016/j.jphotochem.2010.12.001).
- (189) Brouwer, A.; Hummelen, J. C.; Luidier, T.; van Bolhuis, P.; Wynberg, H. *Tetrahedron Letters* **1988**, 29, 3137–3140, DOI: [10.1016/0040-4039\(88\)85106-2](https://doi.org/10.1016/0040-4039(88)85106-2).
- (190) Schaap, A.; Sandison, M. D.; Handley, R. S. *Tetrahedron Letters* **1987**, 28, 1159–1162, DOI: [10.1016/S0040-4039\(00\)95314-0](https://doi.org/10.1016/S0040-4039(00)95314-0).
- (191) Richardson, W. H.; Thomson, S. A. *The Journal of Organic Chemistry* **1985**, 50, 1803–1810, DOI: [10.1021/jo00211a003](https://doi.org/10.1021/jo00211a003).
- (192) Adam, W.; Encarnación, L. A. A. *Chemische Berichte* **1982**, 115, 2592–2605, DOI: [10.1002/cber.19821150722](https://doi.org/10.1002/cber.19821150722).
- (193) Schuster, G. B.; Turro, N. J.; Steinmetzer, H. C.; Schaap, A. P.; Faler, G.; Adam, W.; Liu, J. C. *Journal of the American Chemical Society* **1975**, 97, 7110–7118, DOI: [10.1021/ja00857a024](https://doi.org/10.1021/ja00857a024).
- (194) Kazakov, V. P.; Voloshin, A. I.; Ostakhov, S. S.; Ableeva, N. S. *High Energy Chem.* **1997**, 31, 109–112.
- (195) Matsumoto, M.; Hiroshima, T.; Chiba, S.; Isobe, R.; Watanabe, N.; Kobayashi, H. *Luminescence* **1999**, 14, 345–348, DOI: [10.1002/\(SICI\)1522-7243\(199911/12\)14:6<345::AID-BIO559>3.0.CO;2-T](https://doi.org/10.1002/(SICI)1522-7243(199911/12)14:6<345::AID-BIO559>3.0.CO;2-T).

- (196) Yu, T.; Tsunaki, T.; Hiroshi, I.; Yasunori, Y.; Kizashi, Y.; Isao, S. *Bulletin of the Chemical Society of Japan* **1999**, *72*, 213–225, DOI: [10.1246/bcsj.72.213](https://doi.org/10.1246/bcsj.72.213).
- (197) Isobe, H.; Takano, Y.; Okumura, M.; Kuramitsu, S.; Yamaguchi, K. *Journal of the American Chemical Society* **2005**, *127*, PMID: 15954772, 8667–8679, DOI: [10.1021/ja043295f](https://doi.org/10.1021/ja043295f).
- (198) Yue, L.; Liu, Y.-J. *Journal of Chemical Theory and Computation* **2013**, *9*, PMID: 26583723, 2300–2312, DOI: [10.1021/ct400206k](https://doi.org/10.1021/ct400206k).
- (199) Bronstein, I.; Edwards, B.; Sparks, A. Chemiluminescent 1,2-dioxetanes., US Patent 5,538,847, 1996.
- (200) Giri, B. Chemiluminescent 1,2-dioxetanes., WO Patent App. PCT/US1999/020,590, 2000.
- (201) Matsumoto, M.; Mizuno, T.; Watanabe, N. *Chem. Commun.* **2003**, 482–483, DOI: [10.1039/B210857G](https://doi.org/10.1039/B210857G).
- (202) Dagli, D.; Giri, B. Deuterium-based chemiluminescent 1,2-dioxetanes., WO Patent App. PCT/US2002/022,828, 2004.
- (203) Watanabe, N.; Mizuno, T.; Matsumoto, M. *Tetrahedron* **2005**, *61*, 9569–9585, DOI: [10.1016/j.tet.2005.07.081](https://doi.org/10.1016/j.tet.2005.07.081).
- (204) Edwards, B.; Juo, R.; Sparks, A. Intermediate compounds and methods for synthesizing chemiluminescent dioxetane substrates., US Patent App. 11/210,967, 2006.
- (205) Huang, Z.-E.; Liang, X.-G.; Leung, H.-K.; Chan, Y.-Y. *Chinese Journal of Chemistry* **1991**, *9*, 506–511, DOI: [10.1002/cjoc.19910090605](https://doi.org/10.1002/cjoc.19910090605).
- (206) Bronstein, I.; Edwards, B.; Voyta, J.; Kricka, L. Dioxetanes for use in assays., WO Patent App. PCT/US1989/000,015, 1989.
- (207) Nijegorodov, N.; Vasilenko, V.; Monowe, P.; Masale, M. *Spectrochimica Acta Part A: Molecular and Biomolecular Spectroscopy* **2009**, *74*, 188–194, DOI: [10.1016/j.saa.2009.06.003](https://doi.org/10.1016/j.saa.2009.06.003).
- (208) Watanabe, N.; Kikuchi, M.; Maniwa, Y.; Ijuin, H. K.; Matsumoto, M. *The Journal of Organic Chemistry* **2010**, *75*, PMID: 20073481, 879–884, DOI: [10.1021/jo902477n](https://doi.org/10.1021/jo902477n).
- (209) Watanabe, N.; Sano, Y.; Suzuki, H.; Tanimura, M.; Ijuin, H. K.; Matsumoto, M. *The Journal of Organic Chemistry* **2010**, *75*, PMID: 20681740, 5920–5926, DOI: [10.1021/jo101114b](https://doi.org/10.1021/jo101114b).
- (210) Matsumoto, M.; Nasu, S.; Takeda, M.; Murakami, H.; Watanabe, N. *Chem. Commun.* **2000**, 821–822, DOI: [10.1039/B002161J](https://doi.org/10.1039/B002161J).

- (211) Matsumoto, M.; Watanabe, N.; Kasuga, N. C.; Hamada, F.; Tadokoro, K. *Tetrahedron Letters* **1997**, *38*, 2863–2866, DOI: [10.1016/S0040-4039\(97\)00483-8](https://doi.org/10.1016/S0040-4039(97)00483-8).
- (212) Schaap, A.; Handley, R. S.; Giri, B. P. *Tetrahedron Letters* **1987**, *28*, 935–938, DOI: [10.1016/S0040-4039\(00\)95878-7](https://doi.org/10.1016/S0040-4039(00)95878-7).
- (213) Schaap, A.; Chen, T.-S.; Handley, R. S.; DeSilva, R.; Giri, B. P. *Tetrahedron Letters* **1987**, *28*, 1155–1158, DOI: [10.1016/S0040-4039\(00\)95313-9](https://doi.org/10.1016/S0040-4039(00)95313-9).
- (214) Clennan, E. L. In; Boca Raton, CRC Press: 2012.
- (215) Clennan, E. L.; Hightower, S. E. *The Journal of Organic Chemistry* **2006**, *71*, PMID: 16438547, 1247–1250, DOI: [10.1021/jo052269c](https://doi.org/10.1021/jo052269c).
- (216) Adam, W.; Kumar, A. S.; Saha-Möller, C. R. *Tetrahedron Letters* **1995**, *36*, 7853–7854, DOI: [10.1016/0040-4039\(95\)01669-9](https://doi.org/10.1016/0040-4039(95)01669-9).
- (217) Cermola, F.; Iesce, M. R. *The Journal of Organic Chemistry* **2002**, *67*, PMID: 12098308, 4937–4944, DOI: [10.1021/jo020008m](https://doi.org/10.1021/jo020008m).
- (218) Gompper, R. *Angewandte Chemie International Edition in English* **1969**, *8*, 312–327, DOI: [10.1002/anie.196903121](https://doi.org/10.1002/anie.196903121).
- (219) Gompper, R. *Angewandte Chemie* **1969**, *81*, 348–363, DOI: [10.1002/ange.19690811003](https://doi.org/10.1002/ange.19690811003).
- (220) Hoffmann, R. W. *Angewandte Chemie International Edition in English* **1968**, *7*, 754–765, DOI: [10.1002/anie.196807541](https://doi.org/10.1002/anie.196807541).
- (221) Hoffmann, R. W. *Angewandte Chemie* **1968**, *80*, 823–835, DOI: [10.1002/ange.19680802003](https://doi.org/10.1002/ange.19680802003).
- (222) Foote, C. S.; Dzakpasu, A. A.; Lin, J. H.-P. *Tetrahedron Letters* **1975**, *16*, 1247–1250, DOI: [10.1016/S0040-4039\(00\)72109-5](https://doi.org/10.1016/S0040-4039(00)72109-5).
- (223) Bartlett, P. D.; Schaap, A. P. *Journal of the American Chemical Society* **1970**, *92*, 3223–3225, DOI: [10.1021/ja00713a072](https://doi.org/10.1021/ja00713a072).
- (224) Mazur, S.; Foote, C. S. *Journal of the American Chemical Society* **1970**, *92*, 3225–3226, DOI: [10.1021/ja00713a073](https://doi.org/10.1021/ja00713a073).
- (225) Schaap, A. P.; Bartlett, P. D. *Journal of the American Chemical Society* **1970**, *92*, 6055–6057, DOI: [10.1021/ja00723a041](https://doi.org/10.1021/ja00723a041).
- (226) Clennan, E. L.; Nagraba, K. *Journal of the American Chemical Society* **1988**, *110*, 4312–4318, DOI: [10.1021/ja00221a034](https://doi.org/10.1021/ja00221a034).
- (227) Ohkubo, K.; Nanjo, T.; Fukuzumi, S. *Organic Letters* **2005**, *7*, 4265–4268, DOI: [10.1021/ol051696a001](https://doi.org/10.1021/ol051696a001).

- (228) Kotani, H.; Ohkubo, K.; Fukuzumi, S. *Journal of the American Chemical Society* **2004**, *126*, PMID: 15584734, 15999–16006, DOI: [10.1021/ja048353b](https://doi.org/10.1021/ja048353b).
- (229) Yasunori, Y.; Satoru, Y.; Takashi, K.; Masamichi, N.; Kizashi, Y.; Isao, S. *Bulletin of the Chemical Society of Japan* **1996**, *69*, 2683–2699, DOI: [10.1246/bcsj.69.2683](https://doi.org/10.1246/bcsj.69.2683).
- (230) Adam, W.; Saha-Möller, C. R.; Schambony, S. B. *Journal of the American Chemical Society* **1999**, *121*, 1834–1838, DOI: [10.1021/ja9835077](https://doi.org/10.1021/ja9835077).
- (231) Matsumoto, M.; Kobayashi, H.; Matsubara, J.; Watanabe, N.; Yamashita, S.; Oguma, D.; Kitano, Y.; Ikawa, H. *Tetrahedron Letters* **1996**, *37*, 397–400, DOI: [10.1016/0040-4039\(95\)02185-X](https://doi.org/10.1016/0040-4039(95)02185-X).
- (232) Matsumoto, M.; Kitano, Y.; Kobayashi, H.; Ikawa, H. *Tetrahedron Letters* **1996**, *37*, 8191–8194, DOI: [10.1016/0040-4039\(96\)01858-8](https://doi.org/10.1016/0040-4039(96)01858-8).
- (233) Adam, W.; Bosio, S. G.; Turro, N. J. *Journal of the American Chemical Society* **2002**, *124*, 8814–8815, DOI: [10.1021/ja026815k](https://doi.org/10.1021/ja026815k).
- (234) Poon, T.; Sivaguru, J.; Franz, R.; Jockusch, S.; Martinez, C.; Washington, I.; Adam, W.; Inoue, Y.; Turro, N. J. *Journal of the American Chemical Society* **2004**, *126*, PMID: 15327281, 10498–10499, DOI: [10.1021/ja048438c](https://doi.org/10.1021/ja048438c).
- (235) Wu, W.; An, F.; Geng, Z.; Zhang, R.; Jiang, Z. *Letters in Organic Chemistry* **2013**, *10*, 223–227, DOI: [10.2174/1570178611310030015](https://doi.org/10.2174/1570178611310030015).
- (236) Yamaguchi, K.; Yabushita, S.; Fueno, T.; Houk, K. N. *Journal of the American Chemical Society* **1981**, *103*, 5043–5046, DOI: [10.1021/ja00407a013](https://doi.org/10.1021/ja00407a013).
- (237) Kojima, M.; Nakajoh, M.; Matsubara, C.; Hashimoto, S. *J. Chem. Soc., Perkin Trans. 2* **2002**, 1894–1901, DOI: [10.1039/B205672K](https://doi.org/10.1039/B205672K).
- (238) Maranzana, A.; Ghigo, G.; Tonachini, G. *Journal of the American Chemical Society* **2000**, *122*, 1414–1423, DOI: [10.1021/ja990805a](https://doi.org/10.1021/ja990805a).
- (239) Bobrowski, M.; Liwo, A.; Ołdziej, S.; Jeziorek, D.; Ossowski, T. *Journal of the American Chemical Society* **2000**, *122*, 8112–8119, DOI: [10.1021/ja001185c](https://doi.org/10.1021/ja001185c).
- (240) Sevin, F.; McKee, M. L. *Journal of the American Chemical Society* **2001**, *123*, PMID: 11457246, 4591–4600, DOI: [10.1021/ja010138x](https://doi.org/10.1021/ja010138x).
- (241) Ferre, N.; Guihery, N.; Malrieu, J.-P. *Phys. Chem. Chem. Phys.* **2015**, *17*, 14375–14382, DOI: [10.1039/C4CP05531D](https://doi.org/10.1039/C4CP05531D).

- (242) Yamaguchi, K.; Yamanaka, S.; Shimada, J.; Isobe, H.; Saito, T.; Shoji, M.; Kitagawa, Y.; Okumura, M. *International Journal of Quantum Chemistry* **2009**, *109*, 3745–3766, DOI: [10.1002/qua.22388](https://doi.org/10.1002/qua.22388).
- (243) Rajeev, R.; Sunoj, R. B. *The Journal of Organic Chemistry* **2012**, *77*, PMID: 22324308, 2474–2485, DOI: [10.1021/jo3001707](https://doi.org/10.1021/jo3001707).
- (244) Bro, R.; Smilde, A. K. *Anal. Methods* **2014**, *6*, 2812–2831, DOI: [10.1039/C3AY41907J](https://doi.org/10.1039/C3AY41907J).
- (245) Abdi, H.; Williams, L. J. *Wiley Interdisciplinary Reviews: Computational Statistics* **2010**, *2*, 433–459, DOI: [10.1002/wics.101](https://doi.org/10.1002/wics.101).
- (246) Afifi, A.; May, S.; Clark, V., *Practical Multivariate Analysis, Fifth Edition*; Chapman & Hall/CRC Texts in Statistical Science; Taylor & Francis: 2011.
- (247) Varmuza, K.; Filzmoser, P., *Introduction to Multivariate Statistical Analysis in Chemometrics*; CRC Press: 2016.
- (248) Eriksson, L.; Verhaar, H. J. M.; Hermens, J. L. M. *Environmental Toxicology and Chemistry* **1994**, *13*, 683–691, DOI: [10.1002/etc.5620130502](https://doi.org/10.1002/etc.5620130502).
- (249) Mousavi-Kamazani, M.; Salavati-Niasari, M.; Goudarzi, M.; Gharehbaii, A. *Journal of Inorganic and Organometallic Polymers and Materials* **2016**, *26*, 259–263, DOI: [10.1007/s10904-015-0300-8](https://doi.org/10.1007/s10904-015-0300-8).
- (250) Chen, W.; Luo, H.; Liu, X.; Foley, J. W.; Song, X. *Analytical Chemistry* **2016**, *88*, 3638–3646, DOI: [10.1021/acs.analchem.5b04333](https://doi.org/10.1021/acs.analchem.5b04333).
- (251) Vandekar, V. D. *Journal of Natural Product and Plant Resources* **2015**, *5*, 43–52.
- (252) Megala, M.; Rajkumar, B. J. M. *Journal of Computational Electronics* **2016**, *15*, 557–568, DOI: [10.1007/s10825-016-0791-8](https://doi.org/10.1007/s10825-016-0791-8).
- (253) Traven, V. F.; Manaev, A. V.; Bochkov, A. Y.; Chibisova, T. A.; Ivanov, I. V. *Russian Chemical Bulletin* **2012**, *61*, 1342–1362, DOI: [10.1007/s11172-012-0179-2](https://doi.org/10.1007/s11172-012-0179-2).
- (254) Han, K.; Zhao, G., *Hydrogen Bonding and Transfer in the Excited State*; Wiley: 2011.
- (255) Fery-Forgues, S.; Fournier-Noël, C., *Organic Fluorescent Nanofibers and Sub-Micrometer Rods, Nanofibers*; InTech: 2010.
- (256) Musa, M. A.; Cooperwood, J. S.; Khan, M. O. F. *Current Medicinal Chemistry* **2008**, *15*, 2664–2679, DOI: [10.2174/092986708786242877](https://doi.org/10.2174/092986708786242877).
- (257) Sekar, N. *Colourage*, *52*, 71–73.

- (258) Goddard, J.-P.; Reymond, J.-L. *Trends in Biotechnology* **2004**, *22*, 363–370, DOI: <https://doi.org/10.1016/j.tibtech.2004.04.005>.
- (259) R., H. B.; P., S. M.; K., K. V. *PharmaChem* **2003**, *2*, 50–52.
- (260) Cormier, M.; Hercules, D.; Lee, J., *Chemiluminescence and Bioluminescence*; Plenum Press: 1973.
- (261) Adam, W.; Heil, M. *Journal of the American Chemical Society* **1992**, *114*, 5591–5598, DOI: [10.1021/ja00040a017](https://doi.org/10.1021/ja00040a017).
- (262) Zaklika, K. A.; Burns, P. A.; Schaap, A. P. *Journal of the American Chemical Society* **1978**, *100*, 318–320, DOI: [10.1021/ja00469a072](https://doi.org/10.1021/ja00469a072).
- (263) Cauda, V.; Schlossbauer, A.; Bein, T. *Microporous and Mesoporous Materials* **2010**, *132*, 60–71, DOI: <https://doi.org/10.1016/j.micromeso.2009.11.015>.
- (264) Yamada, H.; Urata, C.; Aoyama, Y.; Osada, S.; Yamauchi, Y.; Kuroda, K. *Chemistry of Materials* **2012**, *24*, 1462–1471, DOI: [10.1021/cm3001688](https://doi.org/10.1021/cm3001688).
- (265) He, Q.; Zhang, J.; Shi, J.; Zhu, Z.; Zhang, L.; Bu, W.; Guo, L.; Chen, Y. *Biomaterials* **2010**, *31*, 1085–1092, DOI: <https://doi.org/10.1016/j.biomaterials.2009.10.046>.
- (266) Bagwe, R. P.; Hilliard, L. R.; Tan, W. *Langmuir* **2006**, *22*, 4357–4362, DOI: [10.1021/la052797j](https://doi.org/10.1021/la052797j).
- (267) Diamandis, E. P.; Christopoulos, T. K. *Clinical Chemistry* **1991**, *37*, 625–636.
- (268) Lakshmipriya, T.; Gopinath, S. C.; Hashim, U.; Tang, T.-H. *Journal of Taibah University Medical Sciences* **2016**, *11*, 432–438, DOI: <https://doi.org/10.1016/j.jtumed.2016.05.010>.
- (269) Hermanson, G., *Bioconjugate Techniques*; Elsevier Science: 2010.
- (270) Liu, F.-T.; Leonard, N. J. *Journal of the American Chemical Society* **1979**, *101*, 996–1005, DOI: [10.1021/ja00498a034](https://doi.org/10.1021/ja00498a034).
- (271) El-Faham, A.; Albericio, F. *Journal of Peptide Science* **2010**, *16*, 6–9, DOI: [10.1002/psc.1204](https://doi.org/10.1002/psc.1204).
- (272) McNaught, A. D.; Wilkinson, A., *IUPAC. Compendium of Chemical Terminology, 2nd ed. (the Gold Book)*; Blackwell Scientific Publications, Oxford: 1997.
- (273) Clark, L. C.; Lyons, C. *Annals of the New York Academy of Sciences* **1962**, *102*, 29–45, DOI: [10.1111/j.1749-6632.1962.tb13623.x](https://doi.org/10.1111/j.1749-6632.1962.tb13623.x).

- (274) Turner, A. P. F. *Chem. Soc. Rev.* **2013**, *42*, 3184–3196, DOI: [10.1039/C3CS35528D](https://doi.org/10.1039/C3CS35528D).
- (275) S, V.; CC, S.; B, S.; H, P. *Frontiers in Bioengineering and Biotechnology* **2016**, *4*, DOI: [doi:10.3389/fbioe.2016.00011](https://doi.org/10.3389/fbioe.2016.00011).
- (276) P, M. *Journal of Oral Biology and Craniofacial Research* **2016**, *6*, 153–159, DOI: [doi:10.1016/j.jobcr.2015.12.002](https://doi.org/10.1016/j.jobcr.2015.12.002).
- (277) Buerk, D., *Biosensors: Theory and Applications*; Taylor & Francis: 1995.
- (278) Strianese, M.; Staiano, M.; Ruggiero, G.; Labella, T.; Pellecchia, C.; D’Auria, S. In *Spectroscopic Methods of Analysis: Methods and Protocols*, Bujalowski, W. M., Ed.; Humana Press: Totowa, NJ, 2012, pp 193–216, DOI: [10.1007/978-1-61779-806-1_9](https://doi.org/10.1007/978-1-61779-806-1_9).
- (279) Hemmilä, I., *Applications of Fluorescence in Immunoassays*; A Wiley-Interscience publication; Wiley: 1991.
- (280) Goldys, E., *Fluorescence Applications in Biotechnology and Life Sciences*; Wiley: 2009.
- (281) Hemmilä, I. *Clinical Chemistry* **1985**, *31*, 359–370.
- (282) Visor, G. C.; Schulman, S. G. *Journal of Pharmaceutical Sciences* **1981**, *70*, 469–475, DOI: [10.1002/jps.2600700502](https://doi.org/10.1002/jps.2600700502).
- (283) Maragos, C. *Toxins* **2009**, *1*, 196–207, DOI: [10.3390/toxins1020196](https://doi.org/10.3390/toxins1020196).
- (284) Geddes, C., *Reviews in Fluorescence 2016*; Reviews in Fluorescence; Springer International Publishing: 2017.
- (285) Zhang, W. H.; Hu, X. X.; Zhang, X. *Nanomaterials* **2016**, *6*, 81, DOI: [10.3390/nano6050081](https://doi.org/10.3390/nano6050081).
- (286) Wolfbeis, O. S. *Chem. Soc. Rev.* **2015**, *44*, 4743–4768, DOI: [10.1039/C4CS00392F](https://doi.org/10.1039/C4CS00392F).
- (287) Sakamoto, S.; Shoyama, Y.; Tanaka, H.; Morimoto, S. *Advances in Bio-science and Biotechnology* **2014**, *5*, 557–563, DOI: [doi:10.4236/abb.2014.56065](https://doi.org/10.4236/abb.2014.56065).
- (288) Gong, X.; Cai, J.; Zhang, B.; Zhao, Q.; Piao, J.; Peng, W.; Gao, W.; Zhou, D.; Zhao, M.; Chang, J. *J. Mater. Chem. B* **2017**, *5*, 5079–5091, DOI: [10.1039/C7TB01049D](https://doi.org/10.1039/C7TB01049D).
- (289) Smith, D. S.; Al-Hakiem, M. H. H.; Landon, J. *Annals of Clinical Bio-chemistry: International Journal of Laboratory Medicine* **1981**, *18*, 253–274.

- (290) Devlin, R.; Dandliker, W.; Arrhenius, P. Fluorescence immunoassays using fluorescent dyes free of aggregation and serum binding., US Patent 5,846,703, 1998.
- (291) Diamandis, E. P. *Clinical Biochemistry* **1988**, *21*, 139–150, DOI: [https://doi.org/10.1016/0009-9120\(88\)90001-X](https://doi.org/10.1016/0009-9120(88)90001-X).
- (292) Diamandis, E. P. *Clinical Chemistry* **2001**, *47*, 380–381.
- (293) AK, H.; T, Z. *Analytical and Bioanalytical Chemistry* **2011**, *400*, 2847–2864, DOI: [10.1007/s00216-011-5047-7](https://doi.org/10.1007/s00216-011-5047-7).
- (294) Zhang, Z.; Zhang, S.; Zhang, X. *Analytica Chimica Acta* **2005**, *541*, Liquid Phase Chemiluminescence, 37–46, DOI: <https://doi.org/10.1016/j.aca.2004.11.069>.
- (295) Zhang, L.; Hu, J.; Lv, Y.; Hou, X. *Applied Spectroscopy Reviews* **2010**, *45*, 474–489, DOI: [10.1080/05704928.2010.503527](https://doi.org/10.1080/05704928.2010.503527).
- (296) Cinquanta, L.; Fontana, D. E.; Bizzaro, N. *Auto-Immunity Highlights* **2017**, *8*, 9, DOI: [10.1007/s13317-017-0097-2](https://doi.org/10.1007/s13317-017-0097-2).
- (297) Iranifam, M. *TrAC Trends in Analytical Chemistry* **2014**, *59*, 156–183, DOI: <https://doi.org/10.1016/j.trac.2014.03.010>.
- (298) Lara, F. J.; Airado-Rodríguez, D.; Moreno-González, D.; Huertas-Pérez, J. F.; García-Campaña, A. M. *Analytica Chimica Acta* **2016**, *913*, 22–40, DOI: <https://doi.org/10.1016/j.aca.2016.01.046>.
- (299) Roda, A.; Mirasoli, M.; Michelini, E.; Fusco, M. D.; Zangheri, M.; Cevenini, L.; Roda, B.; Simoni, P. *Biosensors and Bioelectronics* **2016**, *76*, 30th Anniversary Issue, 164–179, DOI: <https://doi.org/10.1016/j.bios.2015.06.017>.
- (300) Xing, C.; Jing, X.; Zhang, X.; Yuan, J. *Food and Agricultural Immunology* **2017**, *28*, 1269–1282, DOI: [10.1080/09540105.2016.1272550](https://doi.org/10.1080/09540105.2016.1272550).
- (301) Zhao, L.; Sun, L.; Chu, X. *TrAC Trends in Analytical Chemistry* **2009**, *28*, 404–415, DOI: <https://doi.org/10.1016/j.trac.2008.12.006>.
- (302) Park, J. Y.; Kricka, L. J. *Analytical and Bioanalytical Chemistry* **2014**, *406*, 5631–5637, DOI: [10.1007/s00216-014-7697-8](https://doi.org/10.1007/s00216-014-7697-8).
- (303) Mirasoli, M.; Guardigli, M.; Michelini, E.; Roda, A. *Journal of Pharmaceutical and Biomedical Analysis* **2014**, *87*, Review Papers on Pharmaceutical and Biomedical Analysis 2013, 36–52, DOI: <https://doi.org/10.1016/j.jpba.2013.07.008>.
- (304) Ugarova, N. N.; Lebedeva, O. V. *Applied Biochemistry and Biotechnology* **1987**, *15*, 35–51, DOI: [10.1007/BF02798505](https://doi.org/10.1007/BF02798505).

-
- (305) Eed, H. R.; Abdel-Kader, N. S.; Tahan, M. H. E.; Dai, T.; Amin, R. *Journal of Sensors* **2016**, DOI: [10.1155/2016/1492467](https://doi.org/10.1155/2016/1492467).
- (306) JW, L.; D, H.; J, L.; SK, L.; T, K. *Frontiers in Bioengineering and Biotechnology* **2015**, 3, 61, DOI: [10.3389/fbioe.2015.00061](https://doi.org/10.3389/fbioe.2015.00061).
- (307) Zourob, M.; Elwary, S.; Turner, A., *Principles of Bacterial Detection: Biosensors, Recognition Receptors and Microsystems*; Springer New York: 2008.
- (308) Hole, S.; DS, D. *Journal of Biotechnology & Biomaterials* **2011**, 1, DOI: [10.4172/2155-952X.1000118](https://doi.org/10.4172/2155-952X.1000118).
- (309) Hattori, M.; Ozawa, T. *RSC Adv.* **2015**, 5, 12655–12663, DOI: [10.1039/C4RA14979C](https://doi.org/10.1039/C4RA14979C).
- (310) Sato, A.; Klaunberg, B.; Tolwani, R. *Comparative Medicine* **2004**, 54, 631–634.
- (311) Cai, D.; Marques, M. A. L.; Nogueira, F. *The Journal of Physical Chemistry B* **2013**, 117, 13725–13730, DOI: [10.1021/jp405665v](https://doi.org/10.1021/jp405665v).
- (312) Kim, D.-S.; Choi, J.-R.; Ko, J.-A.; Kim, K. *Current Protein & Peptide Science* **2017**, 18, 1–6, DOI: [10.2174/1389203718666161122104530](https://doi.org/10.2174/1389203718666161122104530).
- (313) Wood, K. V. *Proc.SPIE* **2004**, 5328, 5328–5328, DOI: [10.1117/12.528447](https://doi.org/10.1117/12.528447).
- (314) Nakajima, Y.; Ohmiya, Y. *Expert Opinion on Drug Discovery* **2010**, 5, PMID: 22823259, 835–849, DOI: [10.1517/17460441.2010.506213](https://doi.org/10.1517/17460441.2010.506213).
- (315) Coutant, E. P.; Janin, Y. L. *Chemistry – A European Journal* **2015**, 21, 17158–17171, DOI: [10.1002/chem.201501531](https://doi.org/10.1002/chem.201501531).
- (316) Badr, C. E. In *Bioluminescent Imaging: Methods and Protocols*, Badr, C. E., Ed.; Humana Press: Totowa, NJ, 2014, pp 1–18, DOI: [10.1007/978-1-62703-718-1_1](https://doi.org/10.1007/978-1-62703-718-1_1).
- (317) Ravalli, A.; Voccia, D.; Palchetti, I.; Marrazza, G. *Biosensors* **2016**, 6, 39, DOI: [10.3390/bios6030039](https://doi.org/10.3390/bios6030039).
- (318) Kirschbaum, S. E. K.; Baeumner, A. J. *Analytical and Bioanalytical Chemistry* **2015**, 407, 3911–3926, DOI: [10.1007/s00216-015-8557-x](https://doi.org/10.1007/s00216-015-8557-x).
- (319) Blackburn, G. F.; Shah, H. P.; Kenten, J. H.; Leland, J.; Kamin, R. A.; Link, J.; Peterman, J.; Powell, M. J.; Shah, A.; Talley, D. B. *Clinical Chemistry* **1991**, 37, 1534–1539.
- (320) Gross, E. M.; Maddipati, S. S.; Snyder, S. M. *Bioanalysis* **2016**, 8, 2071–2089, DOI: [10.4155/bio-2016-0178](https://doi.org/10.4155/bio-2016-0178).
-

- (321) Liu, Y.; Zhu, D.; Cao, Y.; Ma, W.; Yu, Y.; Guo, M.; Xing, X. *Electrochemistry Communications* **2017**, *85*, 11–14, DOI: <https://doi.org/10.1016/j.elecom.2017.10.012>.
- (322) Richter, M. M. *Chemical Reviews* **2004**, *104*, 3003–3036, DOI: [10.1021/cr020373d](https://doi.org/10.1021/cr020373d).
- (323) Zho, X.; Zhu, D.; Liao, Y.; Liu, W.; Liu, H.; Ma, Z.; Xing, D. *Nature Protocols* **2014**, *9*, 1146–1159, DOI: [doi:10.1038/nprot.2014.060](https://doi.org/10.1038/nprot.2014.060).
- (324) Kenten, J. H. In *Nonradioactive Analysis of Biomolecules*, Kessler, C., Ed.; Springer Berlin Heidelberg: Berlin, Heidelberg, 2000, pp 271–275, DOI: [10.1007/978-3-642-57206-7_20](https://doi.org/10.1007/978-3-642-57206-7_20).
- (325) Zhai, Q.; Li, J.; Wang, E. *ChemElectroChem* **2017**, *4*, 1639–1650, DOI: [10.1002/celec.201600898](https://doi.org/10.1002/celec.201600898).
- (326) Hu, L.; Xu, G. *Chem. Soc. Rev.* **2010**, *39*, 3275–3304, DOI: [10.1039/B923679C](https://doi.org/10.1039/B923679C).
- (327) Sun, K.; Tang, Y.; Li, Q.; Yin, S.; Qin, W.; Yu, J.; Chiu, D. T.; Liu, Y.; Yuan, Z.; Zhang, X.; Wu, C. *ACS Nano* **2016**, *10*, PMID: 27303785, 6769–6781, DOI: [10.1021/acsnano.6b02386](https://doi.org/10.1021/acsnano.6b02386).
- (328) Wu, X.; Wu, L.; Wu, I.-C.; Chiu, D. T. *RSC Advances* **2016**, *6*, 103618–103621, DOI: [10.1039/C6RA20439B](https://doi.org/10.1039/C6RA20439B).
- (329) Wu, L.; Wu, I.-C.; DuFort, C. C.; Carlson, M. A.; Wu, X.; Chen, L.; Kuo, C.-T.; Qin, Y.; Yu, J.; Hingorani, S. R.; Chiu, D. T. *Journal of the American Chemical Society* **2017**, *139*, PMID: 28459559, 6911–6918, DOI: [10.1021/jacs.7b01545](https://doi.org/10.1021/jacs.7b01545).
- (330) T, K. C.; AM, T.; et al., G. M. *Nature Communications* **2016**, *7*, 11468, DOI: [10.1038/ncomms11468](https://doi.org/10.1038/ncomms11468).
- (331) Chen, X.; Li, R.; Liu, Z.; Sun, K.; Sun, Z.; Chen, D.; Xu, G.; Xi, P.; Wu, C.; Sun, Y. *Advanced Materials* **2017**, *29*, 1604850, DOI: [10.1002/adma.201604850](https://doi.org/10.1002/adma.201604850).
- (332) Sun, W.; Yu, J.; Deng, R.; Rong, Y.; Fujimoto, B.; Wu, C.; Zhang, H.; Chiu, D. T. *Angewandte Chemie International Edition* **2013**, *52*, 11294–11297, DOI: [10.1002/anie.201304822](https://doi.org/10.1002/anie.201304822).
- (333) Wu, C.; Jin, Y.; Schneider, T.; Burnham, D. R.; Smith, P. B.; Chiu, D. T. *Angewandte Chemie International Edition* **2010**, *49*, 9436–9440, DOI: [10.1002/anie.201004260](https://doi.org/10.1002/anie.201004260).
- (334) Wu, C.; Chiu, D. T. *Angewandte Chemie International Edition* **2013**, *52*, 3086–3109, DOI: [10.1002/anie.201205133](https://doi.org/10.1002/anie.201205133).

- (335) Yu, J.; Rong, Y.; Kuo, C.-T.; Zhou, X.-H.; Chiu, D. T. *Analytical Chemistry* **2017**, *89*, PMID: 28105818, 42–56, DOI: [10.1021/acs.analchem.6b04672](https://doi.org/10.1021/acs.analchem.6b04672).
- (336) Liou, S.-Y.; Ke, C.-S.; Chen, J.-H.; Luo, Y.-W.; Kuo, S.-Y.; Chen, Y.-H.; Fang, C.-C.; Wu, C.-Y.; Chiang, C.-M.; Chan, Y.-H. *ACS Macro Letters* **2016**, *5*, 154–157, DOI: [10.1021/acsmacrolett.5b00842](https://doi.org/10.1021/acsmacrolett.5b00842).
- (337) Rong, Y.; Wu, C.; Yu, J.; Zhang, X.; Ye, F.; Zeigler, M.; Gallina, M. E.; Wu, I.-C.; Zhang, Y.; Chan, Y.-H.; Sun, W.; Uvdal, K.; Chiu, D. T. *ACS Nano* **2013**, *7*, PMID: 23282278, 376–384, DOI: [10.1021/nn304376z](https://doi.org/10.1021/nn304376z).
- (338) Wu, I.-C.; Yu, J.; Ye, F.; Rong, Y.; Gallina, M. E.; Fujimoto, B. S.; Zhang, Y.; Chan, Y.-H.; Sun, W.; Zhou, X.-H.; Wu, C.; Chiu, D. T. *Journal of the American Chemical Society* **2015**, *137*, PMID: 25494172, 173–178, DOI: [10.1021/ja5123045](https://doi.org/10.1021/ja5123045).
- (339) Rong, Y.; Yu, J.; Zhang, X.; Sun, W.; Ye, F.; Wu, I.-C.; Zhang, Y.; Hayden, S.; Zhang, Y.; Wu, C.; Chiu, D. T. *ACS Macro Letters* **2014**, *3*, PMID: 25419486, 1051–1054, DOI: [10.1021/mz500383c](https://doi.org/10.1021/mz500383c).
- (340) Chen, D.; Wu, I.-C.; Liu, Z.; Tang, Y.; Chen, H.; Yu, J.; Wu, C.; Chiu, D. T. *Chem. Sci.* **2017**, *8*, 3390–3398, DOI: [10.1039/C7SC00441A](https://doi.org/10.1039/C7SC00441A).
- (341) Zhang, X.; Yu, J.; Rong, Y.; Ye, F.; Chiu, D. T.; Uvdal, K. *Chem. Sci.* **2013**, *4*, 2143–2151, DOI: [10.1039/C3SC50222H](https://doi.org/10.1039/C3SC50222H).
- (342) Wu, C.; Peng, H.; Jiang, Y.; McNeill, J. *The Journal of Physical Chemistry B* **2006**, *110*, PMID: 16854113, 14148–14154, DOI: [10.1021/jp0618126](https://doi.org/10.1021/jp0618126).
- (343) F, Y.; C, W.; Y, J.; et al. *Chemical communications* **2012**, *48*, 1778–1780, DOI: [10.1039/c2cc16486h](https://doi.org/10.1039/c2cc16486h).
- (344) Sun, W.; Ye, F.; Gallina, M. E.; Yu, J.; Wu, C.; Chiu, D. T. *Analytical Chemistry* **2013**, *85*, PMID: 23600767, 4316–4320, DOI: [10.1021/ac4007123](https://doi.org/10.1021/ac4007123).
- (345) Owens, D. E.; Jian, Y.; Fang, J. E.; Slaughter, B. V.; Chen, Y.-H.; Peppas, N. A. *Macromolecules* **2007**, *40*, 7306–7310, DOI: [10.1021/ma071089x](https://doi.org/10.1021/ma071089x).
- (346) Gandhi, A.; Paul, A.; Sen, S. O.; Sen, K. K. *Asian Journal of Pharmaceutical Sciences* **2015**, *10*, 99–107, DOI: [10.1016/j.ajps.2014.08.010](https://doi.org/10.1016/j.ajps.2014.08.010).
- (347) Wu, C.; McNeill, J. *Langmuir, The ACS Journal of Surfaces and Colloids* **2008**, *24*, 5855–5861, DOI: [10.1021/la8000762](https://doi.org/10.1021/la8000762).
- (348) Jin, Y.; Ye, F.; Zeigler, M.; Wu, C.; Chiu, D. T. *ACS Nano* **2011**, *5*, PMID: 21280613, 1468–1475, DOI: [10.1021/nn103304m](https://doi.org/10.1021/nn103304m).
- (349) Lakowicz, J., *Principles of Fluorescence Spectroscopy*; Springer US: 2007.

- (350) Hananya, N.; Eldar Boock, A.; Bauer, C. R.; Satchi-Fainaro, R.; Shabat, D. *Journal of the American Chemical Society* **2016**, *138*, PMID: 27652602, 13438–13446, DOI: [10.1021/jacs.6b09173](https://doi.org/10.1021/jacs.6b09173).
- (351) Hersh, W.; Jacko, J.; Greenes, R.; Tan, J.; Janies, D.; Embi, P.; Payne, P. *Nature* **2011**, *470*, 327–329, DOI: [10.1038/470327a](https://doi.org/10.1038/470327a).
- (352) Bercich, R.; Bernhard, J.; Larson, K.; Lindsey, J. *IEEE Transactions on Biomedical Engineering* **2011**, *58*, 759–762, DOI: [10.1109/TBME.2010.2095419](https://doi.org/10.1109/TBME.2010.2095419).
- (353) Pollock, N. R.; Rolland, J. P.; Kumar, S.; Beattie, P. D.; Jain, S.; Noubary, F.; Wong, V. L.; Pohlmann, R. A.; Ryan, U. S.; Whitesides, G. M. *Science Translational Medicine* **2012**, *4*, 152ra129–152ra129, DOI: [10.1126/scitranslmed.3003981](https://doi.org/10.1126/scitranslmed.3003981).
- (354) Wang, E.; Meier, D.; Sandoval, R.; Von Hendy-Willson, V.; Pressler, B.; Bunch, R.; Alloosh, M.; Sturek, M.; Schwartz, G.; Molitoris, B. *Kidney International* **2012**, *81*, 112–117, DOI: [10.1038/ki.2011.294](https://doi.org/10.1038/ki.2011.294).
- (355) Myers, F. B.; Lee, L. P. *Lab Chip* **2008**, *8*, 2015–2031, DOI: [10.1039/B812343H](https://doi.org/10.1039/B812343H).
- (356) Ahn, C. H.; Choi, J.-W.; Beaucage, G.; Nevin, J. H.; Lee, J.-B.; Puntambekar, A.; Lee, J. Y. *Proceedings of the IEEE* **2004**, *92*, 154–173, DOI: [10.1109/JPROC.2003.820548](https://doi.org/10.1109/JPROC.2003.820548).
- (357) Kazmierczak, S. C. *Clinical Chemistry* **2011**, *57*, 1219–1220, DOI: [10.1373/clinchem.2011.171538](https://doi.org/10.1373/clinchem.2011.171538).
- (358) Wei, Q.; Nagi, R.; Sadeghi, K.; Feng, S.; Yan, E.; Ki, S. J.; Caire, R.; Tseng, D.; Ozcan, A. *ACS Nano* **2014**, *8*, PMID: 24437470, 1121–1129, DOI: [10.1021/nm406571t](https://doi.org/10.1021/nm406571t).
- (359) Lu, Y.; Shi, W.; Jiang, L.; Qin, J.; Lin, B. *ELECTROPHORESIS* **2009**, *30*, 1497–1500, DOI: [10.1002/elps.200800563](https://doi.org/10.1002/elps.200800563).
- (360) Reinhard, E.; Khan, E. A.; Akyz, A. O.; Johnson, G. M., *Color Imaging: Fundamentals and Applications*; A. K. Peters, Ltd.: Natick, MA, USA, 2008.
- (361) Gamal, A. E.; Eltoukhy, H. *IEEE Circuits and Devices Magazine* **2005**, *21*, 6–20, DOI: [10.1109/MCD.2005.1438751](https://doi.org/10.1109/MCD.2005.1438751).
- (362) Martinez, A. W.; Phillips, S. T.; Whitesides, G. M.; Carrilho, E. *Analytical Chemistry* **2010**, *82*, PMID: 20000334, 3–10, DOI: [10.1021/ac9013989](https://doi.org/10.1021/ac9013989).
- (363) *Lab Chip* **2008**, *8*, 1988–1991, DOI: [10.1039/B814043J](https://doi.org/10.1039/B814043J).

- (364) Hossain, S. M. Z.; Luckham, R. E.; Smith, A. M.; Lebert, J. M.; Davies, L. M.; Pelton, R. H.; Filipe, C. D. M.; Brennan, J. D. *Analytical Chemistry* **2009**, *81*, PMID: 19492815, 5474–5483, DOI: [10.1021/ac900660p](https://doi.org/10.1021/ac900660p).
- (365) Martinez, A. W.; Phillips, S. T.; Butte, M. J.; Whitesides, G. M. *Angewandte Chemie International Edition* **2007**, *46*, 1318–1320, DOI: [10.1002/anie.200603817](https://doi.org/10.1002/anie.200603817).
- (366) Bruzewicz, D. A.; Reches, M.; Whitesides, G. M. *Analytical Chemistry* **2008**, *80*, PMID: 18333627, 3387–3392, DOI: [10.1021/ac702605a](https://doi.org/10.1021/ac702605a).
- (367) Khan, M. S.; Fon, D.; Li, X.; Tian, J.; Forsythe, J.; Garnier, G.; Shen, W. *Colloids and Surfaces B: Biointerfaces* **2010**, *75*, 441–447, DOI: <https://doi.org/10.1016/j.colsurfb.2009.09.032>.
- (368) Abe, K.; Suzuki, K.; Citterio, D. *Analytical Chemistry* **2008**, *80*, PMID: 18698798, 6928–6934, DOI: [10.1021/ac800604v](https://doi.org/10.1021/ac800604v).
- (369) Li, X.; Tian, J.; Shen, W. *Cellulose* **2010**, *17*, 649–659, DOI: [10.1007/s10570-010-9401-2](https://doi.org/10.1007/s10570-010-9401-2).
- (370) Fenton, E. M.; Mascarenas, M. R.; López, G. P.; Sibbett, S. S. *ACS Applied Materials & Interfaces* **2009**, *1*, PMID: 20355763, 124–129, DOI: [10.1021/am800043z](https://doi.org/10.1021/am800043z).
- (371) Olkkonen, J.; Lehtinen, K.; Erho, T. *Analytical Chemistry* **2010**, *82*, PMID: 21090744, 10246–10250, DOI: [10.1021/ac1027066](https://doi.org/10.1021/ac1027066).
- (372) Dungchai, W.; Chailapakul, O.; Henry, C. S. *Analyst* **2011**, *136*, 77–82, DOI: [10.1039/C0AN00406E](https://doi.org/10.1039/C0AN00406E).
- (373) Chitnis, G.; Ding, Z.; Chang, C.-L.; Savran, C. A.; Ziaie, B. *Lab Chip* **2011**, *11*, 1161–1165, DOI: [10.1039/C0LC00512F](https://doi.org/10.1039/C0LC00512F).
- (374) Birks, J. B., *Photophysics of aromatic molecules*, Includes bibliographical references; London ; New York : Wiley-Interscience: 1970.
- (375) Moreno, D. R. R.; Giorgi, G.; Salas, C. O.; Tapia, R. A. *Molecules* **2013**, *18*, 14797–14806, DOI: [10.3390/molecules181214797](https://doi.org/10.3390/molecules181214797).
- (376) Geng, W.; Wang, H.; Wang, Z.; Zhang, S.; Zhang, W.-X.; Xi, Z. *Tetrahedron* **2012**, *68*, Tetrahedron Young Investigator Award 2012 Advances in Metal-Mediated Organic Synthesis Zhang-Jie Shi, 5283–5289, DOI: <https://doi.org/10.1016/j.tet.2012.01.088>.
- (377) Seo, J. W.; Kim, H. J.; Lee, B. S.; Katzenellenbogen, J. A.; Chi, D. Y. *The Journal of Organic Chemistry* **2008**, *73*, PMID: 18088140, 715–718, DOI: [10.1021/jo701850u](https://doi.org/10.1021/jo701850u).

- (378) Duan, X.-F.; Zeng, J.; Zhang, Z.-B.; Zi, G.-F. *The Journal of Organic Chemistry* **2007**, *72*, PMID: 18027967, 10283–10286, DOI: [10.1021/jo7019652](https://doi.org/10.1021/jo7019652).
- (379) Gauthier, S.; Mailhot, J.; Labrie, F. *The Journal of Organic Chemistry* **1996**, *61*, PMID: 11667248, 3890–3893, DOI: [10.1021/jo952279l](https://doi.org/10.1021/jo952279l).
- (380) Dams, R.; Malinowski, M.; Westdorp, I.; Geise, H. *The Journal of Organic Chemistry* **1982**, *47*, 248–259, DOI: [10.1021/jo00341a014](https://doi.org/10.1021/jo00341a014).
- (381) Zhou, W.; Yang, Y.; Liu, Y.; Deng, G.-J. *Green Chem.* **2013**, *15*, 76–80, DOI: [10.1039/C2GC36502B](https://doi.org/10.1039/C2GC36502B).
- (382) Maegawa, Y.; Mizoshita, N.; Tani, T.; Inagaki, S. *J. Mater. Chem.* **2010**, *20*, 4399–4403, DOI: [10.1039/C0JM00275E](https://doi.org/10.1039/C0JM00275E).
- (383) Vezzu, D. A. K.; Deaton, J. C.; Shayeghi, M.; Li, Y.; Huo, S. *Organic Letters* **2009**, *11*, PMID: 19711945, 4310–4313, DOI: [10.1021/ol901584g](https://doi.org/10.1021/ol901584g).
- (384) Huang, P.-C.; Parthasarathy, K.; Cheng, C.-H. *Chemistry – A European Journal* **2013**, *19*, 460–464, DOI: [10.1002/chem.201203859](https://doi.org/10.1002/chem.201203859).
- (385) Zhou, W.; Liu, Y.; Yang, Y.; Deng, G.-J. *Chem. Commun.* **2012**, *48*, 10678–10680, DOI: [10.1039/C2CC35425J](https://doi.org/10.1039/C2CC35425J).
- (386) Cui, J.; Jin, J.; Hsieh, Y.-H.; Yang, H.; Ke, B.; Damera, K.; Tai, P. C.; Wang, B. *ChemMedChem* **2013**, *8*, 1384–1393, DOI: [10.1002/cmdc.201300216](https://doi.org/10.1002/cmdc.201300216).
- (387) Bahrami, K. *Tetrahedron Letters* **2006**, *47*, 2009–2012, DOI: <https://doi.org/10.1016/j.tetlet.2006.01.051>.
- (388) Amriou, S.; Wang, C.; Batsanov, A. S.; Bryce, M. R.; Perepichka, D. F.; Ortí, E.; Viruela, R.; Vidal-Gancedo, J.; Rovira, C. *Chemistry – A European Journal* **2006**, *12*, 3389–3400, DOI: [10.1002/chem.200501326](https://doi.org/10.1002/chem.200501326).
- (389) Akhavan-Tafti, H.; Eickholt, R.; Lauwers, K.; Handley, R. Signalling compounds and methods for detecting hydrogen peroxide., US Patent App. 10/371,053, 2004.
- (390) Miyashita, K.; Minagawa, M.; Ueda, Y.; Tada, Y.; Hoshino, N.; Imanishi, T. *Tetrahedron* **2001**, *57*, 3361–3367, DOI: [https://doi.org/10.1016/S0040-4020\(01\)00216-2](https://doi.org/10.1016/S0040-4020(01)00216-2).
- (391) R Core Team R: A Language and Environment for Statistical Computing.; R Foundation for Statistical Computing, Vienna, Austria, 2016.
- (392) Le, S.; Josse, J.; Husson, F. *Journal of Statistical Software* **2008**, *25*, 1–18.

-
- (393) <http://www.deducer.org/pmwiki/pmwiki.php?n=Main.DeducerManual> (accessed).
- (394) <http://gaussian.com/g09citation/> (accessed).
- (395) David-Cordonnier, M.-H.; Hildebrand, M.-P.; Baldeyrou, B.; Lansiaux, A.; Keuser, C.; Benzsawel, K.; Lemster, T.; Pindur, U. *European Journal of Medicinal Chemistry* **2007**, *42*, 752–771, DOI: <https://doi.org/10.1016/j.ejmech.2006.12.039>.
- (396) Cinelli, M. A.; Cordero, B.; Dexheimer, T. S.; Pommier, Y.; Cushman, M. *Bioorganic & Medicinal Chemistry* **2009**, *17*, 7145–7155, DOI: <https://doi.org/10.1016/j.bmc.2009.08.066>.
- (397) Yamaguchi, T.; Asanuma, M.; Nakanishi, S.; Saito, Y.; Okazaki, M.; Dodo, K.; Sodeoka, M. *Chem. Sci.* **2014**, *5*, 1021–1029, DOI: [10.1039/C3SC52704B](https://doi.org/10.1039/C3SC52704B).
- (398) El-Faham, A.; Albericio, F. *Journal of Peptide Science* **2010**, *16*, 6–9, DOI: [10.1002/psc.1204](https://doi.org/10.1002/psc.1204).
- (399) Kumar, R.; Bahia, M. S.; Silakari, O. *Medicinal Chemistry Research* **2015**, *24*, 921–933, DOI: [10.1007/s00044-014-1156-0](https://doi.org/10.1007/s00044-014-1156-0).
- (400) Bevington, J.; Huckerby, T. *European Polymer Journal* **2006**, *42*, 1433–1436, DOI: <https://doi.org/10.1016/j.eurpolymj.2005.12.011>.

